

Fall 2011

Experimental and numerical evaluation of cured in place pipe lining system for high temperature applications in sewer pipes

Shaurav Z. Alam
Louisiana Tech University

Follow this and additional works at: <https://digitalcommons.latech.edu/dissertations>



Part of the [Civil Engineering Commons](#)

Recommended Citation

Alam, Shaurav Z., "" (2011). *Dissertation*. 361.
<https://digitalcommons.latech.edu/dissertations/361>

This Dissertation is brought to you for free and open access by the Graduate School at Louisiana Tech Digital Commons. It has been accepted for inclusion in Doctoral Dissertations by an authorized administrator of Louisiana Tech Digital Commons. For more information, please contact digitalcommons@latech.edu.

**EXPERIMENTAL AND NUMERICAL EVALUATION OF CURED IN
PLACE PIPE LINING SYSTEM FOR HIGH TEMPERATURE
APPLICATIONS IN SEWER PIPES**

by

Shaurav Z. Alam, M.S.

A Dissertation Presented in Partial Fulfillment
of the Requirements for the Degree
Doctor of Philosophy

COLLEGE OF ENGINEERING AND SCIENCE
LOUISIANA TECH UNIVERSITY

November 2011

UMI Number: 3492483

All rights reserved

INFORMATION TO ALL USERS

The quality of this reproduction is dependent upon the quality of the copy submitted.

In the unlikely event that the author did not send a complete manuscript and there are missing pages, these will be noted. Also, if material had to be removed, a note will indicate the deletion.



UMI 3492483

Copyright 2012 by ProQuest LLC.

All rights reserved. This edition of the work is protected against unauthorized copying under Title 17, United States Code.



ProQuest LLC
789 East Eisenhower Parkway
P.O. Box 1346
Ann Arbor, MI 48106-1346

LOUISIANA TECH UNIVERSITY

THE GRADUATE SCHOOL

09.27.2011

Date

We hereby recommend that the dissertation prepared under our supervision
by SHAURAV Z. ALAM

entitled Experimental and Numerical Evaluation of Cured In Place Pipe Lining System
For High Temperature Applications In Sewer Pipes

be accepted in partial fulfillment of the requirements for the Degree of
Doctor of Philosophy in Engineering

enezallouche
Supervisor of Dissertation Research

enezallouche
Head of Department

Department

Recommendation concurred in:

[Signature]

[Signature]

[Signature]

[Signature]

Advisory Committee

Approved:

[Signature]

Director of Graduate Studies

Approved:

[Signature]

Dean of the Graduate School

[Signature]

Dean of the College

ABSTRACT

Some of the older cities across North America and Europe had been using steam driven HVAC systems since beginning of the last century. Consolidated Edison (Con Ed.) of New York operates the New York City steam system, the largest commercial district heating system in the world, with more than 100 miles of transmission and distribution pipes serving Manhattan Island. Other steam district systems exist in San Francisco, Harrisburg, Minneapolis, Pittsburgh, San Diego, and Detroit, some dating back to 1903. In those cities the sewer pipes are used as venues for discharging the waste steam condensate from the HVAC system.

The city of New York is considering the rehabilitation of the Time Square, including the near-by sewer pipes which pass beneath the subway station and/or along the concrete wall. Rehabilitation of these sewer pipes requires trenchless technique, installation of CIPP liners. Therefore, in the event of a malfunction of the aging steam system and failed steam trap, the sewer pipes lined with CIPP liners might be subjected to direct steam injection and the temperature may soar as high as 212° F. The presence of steam and the associated elevated temperature inside the lined pipe could result in an environment, incompatible with standard CIPP lining products.

The main objective achieved within the first phase of the research was to experimentally determine the thermal effects on the aging of resin used in CIPP liner. Therefore, the resins expected to perform well under prolonged exposure to elevated

temperature (up to 212° F) were identified first. Total 1890 specimens (ASTM D638 and ASTM D790) were prepared using epoxy, vinyl ester and polyester resin which were subjected to cyclic thermal loading (maximum 540 cycles intermittently changing between 90° F and 212° F). Next the specimens were tested to obtain the modulus of elasticity value and stress-strain curve; thus to identify the best resin to serve at elevated cyclic temperature. Raman spectroscopy, a technique used for studying the chemical composition and chemical bonds of materials, was also used to provide more fundamental understanding of the degradation of the resin materials at the molecular level. It was found that vinyl ester and epoxy resin performs better at elevated temperature application than polyester resin, although polyester resin is used in more than 90 percent of the CIPP projects as it is economical.

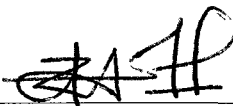
Another objective completed at the second phase was to evaluate the stresses generated due to the thermal strain on the full scale specimens. At this phase CIPP liners were impregnated using the best two resin types performed at elevated cyclic temperature in the phase one and full scale specimens were prepared by lining steel host pipe. The full scale specimens were kept inside custom built oven and cyclic thermal load was applied. Stresses generated on the specimen due to thermal loading were observed by analyzing strain gage data. It was found that stresses developed in the liners impregnated with vinyl ester resin were significantly lower in comparison to the liners impregnated with the epoxy resin.

In the third phase, numerical simulation of the effect of high temperature on a CIPP liner was performed and parametric study was carried out to compare and validate the results obtained in the second phase.

APPROVAL FOR SCHOLARLY DISSEMINATION

The author grants to the Prescott Memorial Library of Louisiana Tech University the right to reproduce, by appropriate methods, upon request, any or all portions of this Dissertation. It is understood that "proper request" consists of the agreement, on the part of the requesting party, that said reproduction is for his personal use and that subsequent reproduction will not occur without written approval of the author of this Dissertation. Further, any portions of the Dissertation used in books, papers, and other works must be appropriately referenced to this Dissertation.

Finally, the author of this Dissertation reserves the right to publish freely, in the literature, at any time, any or all portions of this Dissertation.

Author 

Date 11.02.2011

TABLE OF CONTENTS

ABSTRACT	iii
LIST OF TABLES	xiii
LIST OF FIGURES.....	xvi
LIST OF EQUATIONS	xxvi
LIST OF SYMBOLS AND ABBREVIATIONS.....	xxvii
ACKNOWLEDGEMENTS	xxx
CHAPTER 1 INTRODUCTION	32
1.1 General Introduction	32
1.2 Interaction between Sewer Pipe and CIPP Liner	36
1.3 Objectives.....	38
1.4 Scope of Work.....	39
CHAPTER 2 LITERATURE REVIEW	40
2.1 Introduction.....	40
2.2 Background History	41
2.3 Effect of Thermal Strain.....	42
2.4 Pipe Rehabilitation Methods	43
2.5 Components of CIPP	43
2.6 CIPP Method.....	44
2.7 Vendors of High Temperature CIPP Liner Components	45
2.7.1 Reichhold Chemicals, Inc.	45

2.7.1.1 DION 382-20.....	45
2.7.1.2 DION 9800-20.....	45
2.7.2 Neopoxy International, Inc.	47
2.7.3 Noveon, Inc.....	48
2.7.4 Belzona, Inc.	48
2.7.5 AOC LLC	48
2.8 Related Work and Theories.....	50
2.8.1 Introduction.....	50
2.8.2 Behavior of Close-fit Lining Subjected to External Pressure.....	52
2.8.3 Mechanisms of Restrained Hydrostatic Buckling	54
2.9 The Basic Formulas.....	57
2.9.1 Imperfections	57
2.9.2 ASTM F1216	58
2.9.3 Formula of Hall (TTC, LA Tech, USA).....	59
2.9.4 Formula of Boot (University of Bradford, UK).....	59
2.9.5 Formula of ATV-M 127-2 (Germany)	60
2.9.6 Formula of Moore (Queen’s University, Canada).....	60
2.9.7 Formula of Thépot (RERAU National Project, France).....	60
2.9.8 Conclusion	61
2.10 Effect of External Hydrostatic Pressure.....	61
2.11 Effect of Soil and Traffic Load	61
2.12 Force and Moment Causing Stresses on a Circular Pipe-Liner Section.....	62

2.12.1 Axial Stress.....	62
2.12.2 Bending Stress	62
2.12.3 Stresses Due to Uneven Settlement	63
2.13 Strain Gage Thermal Output and Gage Factor Variation.....	63
2.14 Elastic and Plastic Strain.....	64
2.15 Summary	64
CHAPTER 3 BENCH SCALE TESTING.....	66
3.1 Introduction.....	66
3.2 Preparation of Specimens.....	66
3.3 Testing Program - ASTM D638 and ASTM D790	71
3.4 Results of ASTM D638 and ASTM D790.....	76
3.4.1 ASTM D638	76
3.4.2 ASTM D790	83
3.5 Creep Test – ASTM D2990	90
3.6 Results of Creep Test	91
3.7 Microscopy and Raman Spectroscopy	93
3.7.1 Microscopy	93
3.7.2 Raman Spectroscopy	94
3.8 Results of Microscopy and Raman Spectroscopy.....	97
3.8.1 Results of Microscopy	97
3.8.2 Results of Raman Spectroscopy	100
3.9 Conclusion	102

CHAPTER 4 FULL SCALE TESTING	105
4.1 Introduction	105
4.2 Testing Program	105
4.2.1 Building the Custom Built Ovens	106
4.2.1.1 Structure of the oven	106
4.2.1.2 Placing of heating elements inside the oven	108
4.2.1.3 Electrical circuit of the heating element	109
4.2.2 Preparation of the Full-Scale Specimens	112
4.2.3 Profile Plot of the Specimens Before Thermal Loading	114
4.2.4 Placing of the Full Scale Specimens Inside the Oven	117
4.2.5 Discussion of Strain Results	118
4.2.6 Discussion of Profile Plot Results	128
4.3 Conclusion	130
CHAPTER 5 NUMERICAL SIMULATION	133
5.1 Introduction	133
5.2 Elements Used	133
5.3 Sample Simulation with Solid Block	135
5.4 Steel Host Pipe and Liner – Uniform Thermal Load	140
5.5 Comparison between Actual and Numerical Simulation	149
5.6 Steel Host Pipe and Liner – Non-uniform Thermal Load	151
5.7 Case Study - Gap between Liner and Host-Pipe	159
5.8 Parametric Study – Liner Thickness	162
5.9 Numerical Simulation – Projected Condition	167

5.10 Conclusion	170
CHAPTER 6 CONCLUSIONS, RECOMMENDATIONS AND FUTURE WORK	171
6.1 Conclusions	171
6.2 Recommendations	172
6.3 Future Work	172
APPENDIX A TENSILE AND BENDING MODULUS ELASTICITY OF EACH DURATION SPECIMEN MADE OF FOUR RESIN TYPES	174
A.1 Resin Type-A; Test Specimen; ASTM D638	175
A.2 Resin Type-B; Test Specimen; ASTM D638.....	184
A.3 Resin Type-C; Test Specimen; ASTM D638.....	202
A.4 Resin Type-D; Test Specimen; ASTM D638	220
A.5 Resin Type-A; Test Specimen; ASTM D790	238
A.6 Resin Type-B; Test Specimen; ASTM D790.....	247
A.7 Resin Type-C; Test Specimen; ASTM D790.....	265
A.8 Resin Type-D; Test Specimen; ASTM D790	283
APPENDIX B CAD DRAWING OF THE OVEN FRAMES AND POWER SUPPLY CIRCUIT DIAGRAMS TO THE OVENS.....	301
B.1 Front View and Rear View of Custom Built Oven	302
B.2 Side Views of Custom Built Oven	303
B.3 View of Frame of Custom Built Oven	304
B.4 Top View and Side View of Frame of Custom Built Oven	305
B.5 View of Rear Frame and Front Frame of Custom Built Oven	306

B.6 View of Middle Frame of Custom Built Oven.....	307
B.7 Power Circuit Diagram of the Oven.....	308
APPENDIX C LABEL OF THE STRAIN GAGES AND STRAIN ROSETTES FOR EACH OVEN	309
C.1 Oven 1 – Resin Type A – Full Scale Sample # 1	310
C.2 Oven 1 – Resin Type C – Full Scale Sample # 3	311
C.3 Oven 1 – Temperature Sensor	312
C.4 Oven 2 – Resin Type A – Full Scale Sample # 3	313
C.5 Oven 2 – Resin Type C – Full Scale Sample # 2	314
C.6 Oven 2 – Temperature Sensor	315
C.7 Oven 3 – Resin Type A – Full Scale Sample # 4	316
C.8 Oven 3 – Resin Type A – Full Scale Sample # 2	317
C.9 Oven 3 – Resin Type C – Full Scale Sample # 4	318
C.10 Oven 3 – Resin Type C – Full Scale Sample # 1	319
C.11 Oven 3 – Temperature Sensor	320
APPENDIX D ANALYTICAL CALCULATION OF THE SAMPLE SOLID BLOCK.....	321
D.1 Temperature Change Calculation at the Interface.....	322
D.2 Deflection Calculation due to Temperature	323
D.3 Calculation for Elongation of Steel.....	324
D.4 Calculation for Elongation of Aluminum	325
APPENDIX E LONGITUDINAL AND CIRCUMFERENTIAL STRESS AT 53, 79, 181 AND 241 DAYS.....	326
E.1 Oven 1.....	327

E.2 Oven 2.....	331
E.3 Oven 3.....	337
REFERENCES	343

LIST OF TABLES

Table 1:	Segments of Sewer Affected by Steam Discharge within Project Limits (modified after Ng, 2008).....	34
Table 2:	Steam Pipe and Water Main Blast in NY in 1989.....	41
Table 3:	Typical Properties of DION 9800-20 at Elevated Temperatures	46
Table 4:	Typical Laminate Properties of DION® 382-20 at Elevated Temperatures	47
Table 5:	List of Potentially Suitable Resins	49
Table 6:	Number of ASTM D638 Specimens Prepared for Test.....	70
Table 7:	Number of ASTM D790 Specimens Prepared for Test.....	70
Table 8:	Thermal Treatment Schedule for Oven – 1	72
Table 9:	Thermal Treatment Schedule for Oven – 2	73
Table 10:	Summary of ASTM D638 Test on Neat Resin Type-A	80
Table 11:	Summary of ASTM D638 Test on Neat Resin Type-B	81
Table 12:	Summary of ASTM D638 Test on Neat Resin Type-C	82
Table 13:	Summary of ASTM D638 Test on Neat Resin Type-D	83
Table 14:	Summary of ASTM D790 Test on Neat Resin Type-A	86
Table 15:	Summary of ASTM D790 Test on Neat Resin Type-B	87
Table 16:	Summary of ASTM D790 Test on Neat Resin Type-C	88
Table 17:	Summary of ASTM D790 Test on Neat Resin Type-D	89
Table 18:	Summary of Raman Spectroscopy Test Program.....	95
Table 19:	Test Program for Phase II.....	106

Table 20:	Stress on Resin: Type-C at Different Days	127
Table 21:	Stress on Resin: Type-A at Different Days	128
Table 22:	Material Properties of Steel and Aluminum	136
Table 23:	Comparison of Results - FE Analysis and Analytical Solution.....	139
Table 24:	Mechanical Properties of Steel Host Pipe, Type-A and Type-C Resin.....	140
Table 25:	Thermal Properties of Steel Host Pipe, Type-A and Type-C Resin.....	141
Table 26:	List of the Nodes	143
Table 27:	Von-Mises Stress (Equivalent Stress) in CIPP liner Containing Type-A.....	144
Table 28:	Von-Mises Stress (Equivalent Stress) in CIPP liner Containing Type-C	145
Table 29:	Thermal Stress on Resin Caused by Different Temperature.....	149
Table 30:	Von-Mises Stress (Equivalent Stress) at Selected Nodes in CIPP Liner Impregnated with Resin Type-A.....	154
Table 31:	Von-Mises Strain (Equivalent Strain) at Selected Nodes in CIPP Liner Containing Type-A.....	155
Table 32:	Von-Mises Stress (Equivalent Stress) at Selected Nodes in CIPP Liner Containing Type-C.....	158
Table 33:	Von-Mises Strain (Equivalent Strain) at Selected Nodes in CIPP Liner Containing Type-C.....	159
Table 34:	Material Properties of Brick Host Pipe	163
Table 35:	Physical Properties of Brick Host Pipe	163
Table 36:	Change in Von-Mises Stress Caused by Temperature for Different Liner Thickness (Resin: Type-A).....	164
Table 37:	Change in Von-Mises Stress Caused by Temperature for Different Liner Thickness (Resin: Type-C).....	165

Table 38: Temperature Value on the Three Segments of a Lined with Resin Type-A Brick Pipe	168
Table A. 39: Mechanical Properties of Steel and Aluminum.....	323
Table A. 40: Thermal Properties of Steel and Aluminum	323

LIST OF FIGURES

Figure 1:	An Egg-shaped Sewer Located Underneath the Subway Platform at 7th Avenue Roadway (modified after Dino Ng, 2008).....	33
Figure 2:	Schematic Diagram of Manhattan’s Steam Distribution System (modified after Dino Ng, 2008).....	36
Figure 3:	Change in Depth of Flow Due to Daily Fluctuations and Locations of Temperature Gradients.....	37
Figure 4:	Relative Movement in CIPP Liner Due to Changes in Thermal Energy.....	38
Figure 5:	Steam Pipe Blast in the City of NY (modified after The New York Times, 2007).....	42
Figure 6:	Close-fit Lining in an Oval Shaped Sewer.....	51
Figure 7:	Horse-shoe Type Sewer (after WRc)	52
Figure 8:	Critical Condition - Deformation Lob is Localized	54
Figure 9:	Sub-critical Condition - Lob Extends Over Entire Height of the Liner	54
Figure 10:	Steps in Nonlinear Hydrostatic Buckling of Circular Pipe	55
Figure 11:	Liner Deformations Implicit in Current ASTM Design Formula w/ Enhancement Factor K and Ovality Factor C	57
Figure 12:	Water Jet Cutter.....	67
Figure 13:	ASTM D638 Specimens Cut From a Panel Using the Water Jet Cutter.....	67
Figure 14:	Toggle Press (left) and ASTM D638 and D790 Dies (right).....	68
Figure 15:	Sample Prepared by Pouring Resin in Rubber Mold	68
Figure 16:	ASTM D638 Specimens on Aluminum Foil.....	69

Figure 17: ASTM D790 Specimens on Aluminum Foil.....	69
Figure 18: ASTM D638 Specimens Immersed in Heat Transfer Medium	71
Figure 19: Programmable Oven.....	72
Figure 20: ADMET eXperT 2611 Universal Testing Machine.....	74
Figure 21: Pneumatic Grip for ASTM D638 Test	74
Figure 22: ASTM D638 Test Setup.....	75
Figure 23: ASTM D790 Test Setup.....	75
Figure 24: Tensile Modulus of Elasticity, E_T , Vs. Time Cycles for Resin Type-A	76
Figure 25: Tensile Modulus of Elasticity, E_T , Vs. Time Cycles for Resin Type-B.....	77
Figure 26: Tensile Modulus of Elasticity, E_T , Vs. Time Cycles for Resin Type-C.....	77
Figure 27: Tensile Modulus of Elasticity, E_T , Vs. Time Cycles for Resin Type-D	78
Figure 28: Bending Modulus of Elasticity, E_B , Vs. Time Cycles for Resin Type-A	84
Figure 29: Bending Modulus of Elasticity, E_B , Vs. Time Cycles for Resin Type-B.....	84
Figure 30: Bending Modulus of Elasticity, E_B , Vs. Time Cycles for Resin Type-C.....	85
Figure 31: Bending Modulus of Elasticity, E_B , Vs. Time Cycles for Resin Type-D	85
Figure 32: ASTM D2990 – Flexure Creep Test	90
Figure 33: ASTM D2990 – Tensile Creep Test.....	91
Figure 34: ASTM D2990 – Flexure Creep Data.....	92
Figure 35: ASTM D2990 – Tensile Creep Data	92

Figure 36: Nikon EPIPHOT 200	93
Figure 37: Laboratory Polisher	94
Figure 38: Specimens Inside the Oven	96
Figure 39: Raman Spectrometer	97
Figure 40: Images of Specimens – Before Commencement of Thermal Loading Resin Type – A.....	98
Figure 41: Images of Specimens – Following 270 Cycles of Thermal Loading.....	98
Figure 42: Images of Specimens – Before Commencement of Thermal Loading Resin Type – C	99
Figure 43: Images of Specimens – Following 270 Cycles of Thermal Loading.....	99
Figure 44: Raman Spectra of Type-A Resin.....	100
Figure 45: Raman Spectra of Type-C Resin	101
Figure 46: Percent Deviation of Tensile Modulus of Elasticity	103
Figure 47: Percent Deviation of Bending Modulus of Elasticity.....	103
Figure 48: Steel Frame of a Custom Built Oven	106
Figure 49: Front Side of Custom Built Oven.....	107
Figure 50: Rear Side of Custom Built Oven.....	108
Figure 51: Uncovered Heating Elements inside the Oven.....	109
Figure 52: Covered Heating Element and Exhaust inside the Oven.....	109
Figure 53: Power Supply Box and Two Thermostats on the Rear Wall of the Oven	110
Figure 54: Thermostat Sensor and Thermocouple inside the Oven.....	111
Figure 55: Test Run of the Oven for One Cycle.....	112
Figure 56: Strain Vs. Time	112

Figure 57: Liner Wet Out Process at the TTC Research Facility	113
Figure 58: Inversion of the Liner inside a PVC Mold	114
Figure 59: The Finished Product - Cured CIPP Liner	114
Figure 60: Profile Plotter	115
Figure 61: Profile Plotting of a Full-scale Sample	116
Figure 62: Profile Plotter Inside a Full-scale Sample	116
Figure 63: A Circumferential Plot Showing Ovality Due to a Stitch and Uneven Surface in the CIPP Liner	117
Figure 64: Strain Gauge at the Spring-line and Strain Rosette at the Invert	118
Figure 65: Longitudinal Strain Cycle at the Spring Line due to Temperature Change at Day 1 (Temperature Range 110° F-260° F).....	119
Figure 66: Longitudinal Strain Cycle at the Crown due to Temperature Change at Day 1 (Temperature Range 110° F-260° F).....	120
Figure 67: Circumferential Strain Cycle at the Crown due to Temperature Change at Day 1 (Temperature Range 110° F-260° F).....	120
Figure 68: Longitudinal Strain Cycle at the Crown due to Temperature Change at Day 1 (Temperature Range 110° F-260° F).....	121
Figure 69: Circumferential Strain Cycle at the Invert due to Temperature Change at Day 1 (Temperature Range 110° F-260° F).....	121
Figure 70: Initial Strain on Resin Type-C (Temperature Range 110° F-260° F).....	122
Figure 71: Creep Due to Temperature Cycle of 341 days for Resin Type-C (Temperature Range 110° F-260° F)	123

Figure 72: Initial Strain on Resin Type-A (Temperature Range 110° F-260° F).....	124
Figure 73: Creep Due to Temperature Cycle of 341 days for Resin Type-A (Temperature Range 110° F-260° F).....	124
Figure 74: Longitudinal and Hoop Stress Due to Thermal Loading on Day 1 for Resin Type-C (Temperature Range 110° F-260° F).....	125
Figure 75: Longitudinal and Hoop Stress Due to Thermal Loading on Day 341 for Resin Type-C (Temperature Range 110° F-260° F).....	126
Figure 76: Longitudinal and Hoop Stress Due to Thermal Loading on Day 1 for Type-A (Temperature Range 110° F-260° F).....	126
Figure 77: Longitudinal and Hoop Stress Due to Thermal Loading on Day 341 for Resin Type-A (Temperature Range 110° F-260° F).....	127
Figure 78: Profile Plot after Thermal Loading of 110° F - 260° F for Type-C Day 79	129
Figure 79: Profile Plot after Thermal Loading of 110° F - 260° F for Type-A Day 79.....	130
Figure 80: Stress (psi) Due to Thermal Loading on Day 341 on Type-A Resin	131
Figure 81: Stress (psi) Due to Thermal Loading on Day 341 on Type-C Resin.....	132
Figure 82: SOLID69 Element (Left) (Modified after ANSYS 11.0 Manual)	134
Figure 83: CONTA174 Element (Right) (Modified after ANSYS 11.0 Manual)	135
Figure 84: FE Simulation of a Block Model – Before Modeling	136
Figure 85: Restrained Condition of the Test Model	137
Figure 86: FE Analysis – Temperature Distribution	138
Figure 87: FE Analysis – Displacement	138

Figure 88: Thermal Gradient for the Complete Length	139
Figure 89: Thermal Gradient at the Vicinity of the Contact Surface.....	140
Figure 90: Stress – Strain Curve for Steel used in the FE Analysis	142
Figure 91: Stress – Strain Curve for Resins used in the FE Analysis.....	142
Figure 92: Location of Nodes on Spring Line	143
Figure 93: Change in Stress of Type-A and Type-C Resins Due to Thermal Loading	146
Figure 94: Change in Strains of Type-A and Type-C Resins Due to Thermal Loading	147
Figure 95: Contour Plot of Von-Mises Stress – Type-A Resin	148
Figure 96: Contour Plot of Von-Mises Stress – Type-C Resin	148
Figure 97: Thermal Stress on Resin Type-A Sample	150
Figure 98: Thermal Stress on Resin Type-C Sample.....	150
Figure 99: Thermal Gradient And Location Of The Investigated Nodes.....	151
Figure 100: Thermal Stress on Liner Impregnated with Resin Type-A	152
Figure 101: Thermal Strain on Liner Impregnated with Resin Type-A	153
Figure 102: Thermal Stress on Liner Impregnated with Resin Type-C.....	156
Figure 103: Thermal Strain on Liner Impregnated with Resin Type-C.....	157
Figure 104: Change in Deformation Magnitude and Condition w/ Annular Space	160
Figure 105: Change in Deformation Magnitude and Condition w/o Annular Space	161
Figure 106: Maximum Deformation of the Resin at 212° F	162
Figure 107: Temperature Distribution on the Liner.....	166
Figure 108: Von-Mises Stress Distribution on the Liner.....	166

Figure 109:	Temperature Distribution on the Three Segment Brick Pipe.....	167
Figure 110:	Selected Nodes on the Crown of the Three Segment Brick Pipe.....	168
Figure 111:	Von-Mises Stress along the Plotted Path on the Segments of Brick Host Pipe	169
Figure 112:	Von-Mises Strain along the Plotted Path on the Segments of Brick Host Pipe	170
Figure 113:	Proposed Installation of Distributed Thermal Sensors in the Vicinity of a Stream Trap.....	173
Figure A. 114:	Oven Front View.....	302
Figure A. 115:	Oven Rear View.....	302
Figure A. 116:	Left Side View	303
Figure A. 117:	Right Side View	303
Figure A. 118:	Front View of Door Frame.....	304
Figure A. 119:	Bottom View of Frame.....	304
Figure A. 120:	Top View of Frame	305
Figure A. 121:	Side View of Frame	305
Figure A. 122:	View of Rear Frame	306
Figure A. 123:	View of Front Frame.....	306
Figure A. 124:	View of Middle Frame	307
Figure A. 125:	Power Circuit Diagram	308
Figure A. 126:	Temperature Gradient on the Steel and Aluminum Block	322
Figure A. 127:	Longitudinal and Hoop Stress Due to Thermal Loading on Day 53 for Resin Type-A (Temperature Range 110° F-260° F)	327

Figure A. 128: Longitudinal and Hoop Stress Due to Thermal Loading on Day 53 for Resin Type-C (Temperature Range 110° F-260° F).....	327
Figure A. 129: Longitudinal and Hoop Stress Due to Thermal Loading on Day 79 for Resin Type-A (Temperature Range 110° F-260° F).....	328
Figure A. 130: Longitudinal and Hoop Stress Due to Thermal Loading on Day 79 for Resin Type-C (Temperature Range 110° F-260° F).....	328
Figure A. 131: Longitudinal and Hoop Stress Due to Thermal Loading on Day 181 for Resin Type-A (Temperature Range 110° F-260° F).....	329
Figure A. 132: Longitudinal and Hoop Stress Due to Thermal Loading on Day 181 for Resin Type-C (Temperature Range 110° F-260° F).....	329
Figure A. 133: Longitudinal and Hoop Stress Due to Thermal Loading on Day 241 for Resin Type-A (Temperature Range 110° F-260° F).....	330
Figure A. 134: Longitudinal and Hoop Stress Due to Thermal Loading on Day 241 for Resin Type-C (Temperature Range 110° F-260° F).....	330
Figure A. 135: Longitudinal and Hoop Stress Due to Thermal Loading on Day 1 for Resin Type-A (Temperature Range 90° F-210° F).....	331
Figure A. 136: Longitudinal and Hoop Stress Due to Thermal Loading on Day 1 for Resin Type-C (Temperature Range 90° F-210° F).....	331
Figure A. 137: Longitudinal and Hoop Stress Due to Thermal Loading on Day 53 for Resin Type-A (Temperature Range 90° F-210° F).....	332
Figure A. 138: Longitudinal and Hoop Stress Due to Thermal Loading on Day 53 for Resin Type-C (Temperature Range 90° F-210° F).....	332

Figure A. 139: Longitudinal and Hoop Stress Due to Thermal Loading on Day 79 for Resin Type-A (Temperature Range 90° F-210° F).....	333
Figure A. 140: Longitudinal and Hoop Stress Due to Thermal Loading on Day 79 for Resin Type-C (Temperature Range 90° F-210° F).....	333
Figure A. 141: Longitudinal and Hoop Stress Due to Thermal Loading on Day 181 for Resin Type-A (Temperature Range 90° F-210° F).....	334
Figure A. 142: Longitudinal and Hoop Stress Due to Thermal Loading on Day 181 for Resin Type-C (Temperature Range 90° F-210° F).....	334
Figure A. 143: Longitudinal and Hoop Stress Due to Thermal Loading on Day 241 for Resin Type-A (Temperature Range 90° F-210° F).....	335
Figure A. 144: Longitudinal and Hoop Stress Due to Thermal Loading on Day 241 for Resin Type-C (Temperature Range 90° F-210° F).....	335
Figure A. 145: Longitudinal and Hoop Stress Due to Thermal Loading on Day 341 for Resin Type-A (Temperature Range 90° F-210° F).....	336
Figure A. 146: Longitudinal and Hoop Stress Due to Thermal Loading on Day 341 for Resin Type-C (Temperature Range 90° F-210° F).....	336
Figure A. 147: Longitudinal and Hoop Stress Due to Thermal Loading on Day 1 for Resin Type-A (Temperature Range 100° F-150° F)	337
Figure A. 148: Longitudinal and Hoop Stress Due to Thermal Loading on Day 1 for Resin Type-C (Temperature Range 100° F-150° F)	337
Figure A. 149: Longitudinal and Hoop Stress Due to Thermal Loading on Day 53 for Resin Type-A (Temperature Range 100° F-150° F)	338

Figure A. 150: Longitudinal and Hoop Stress Due to Thermal Loading on Day 53 for Resin Type-C (Temperature Range 100° F-150° F)	338
Figure A. 151: Longitudinal and Hoop Stress Due to Thermal Loading on Day 79 for Resin Type-A (Temperature Range 100° F-150° F).....	339
Figure A. 152: Longitudinal and Hoop Stress Due to Thermal Loading on Day 79 for Resin Type-C (Temperature Range 100° F-150° F).....	339
Figure A. 153: Longitudinal and Hoop Stress Due to Thermal Loading on Day 181 for Resin Type-A (Temperature Range 100° F-150° F).....	340
Figure A. 154: Longitudinal and Hoop Stress Due to Thermal Loading on Day 181 for Resin Type-C (Temperature Range 100° F-150° F).....	340
Figure A. 155: Longitudinal and Hoop Stress Due to Thermal Loading on Day 241 for Resin Type-A (Temperature Range 100° F-150° F).....	341
Figure A. 156: Longitudinal and Hoop Stress Due to Thermal Loading on Day 241 for Resin Type-C (Temperature Range 100° F-150° F).....	341
Figure A. 157: Longitudinal and Hoop Stress Due to Thermal Loading on Day 341 for Resin Type-A (Temperature Range 100° F-150° F).....	342
Figure A. 158: Longitudinal and Hoop Stress Due to Thermal Loading on Day 341 for Resin Type-C (Temperature Range 100° F-150° F).....	342

LIST OF EQUATIONS

Equation (1)	Timoshenko's equation.....	57
Equation (2)	Glock's equation.....	57
Equation (3)	Ovality equation by Moore.....	58
Equation (4)	Average radius of liner or host-pipe.....	58
Equation (5)	Diameter of host-pipe given by Hall.....	58
Equation (6)	ASTM F1216 equation.....	58
Equation (7)	Reduction factor for ovality.....	58
Equation (8)	Equation given by Hall.....	59
Equation (9)	Equation given by Boot.....	59
Equation (10)	Equation of ATV-M 127-2.....	60
Equation (11)	Equation of buckling factor.....	60
Equation (12)	Equation of flexural stiffness of liner.....	60
Equation (13)	Equation of Moore.....	60
Equation (14)	Equation of Thépot.....	60
Equation (15)	Equation of shear stresses.....	62
Equation (16)	Equation of first moment.....	63
Equation (17)	Equation of correction for thermal output.....	63
Equation (18)	Equation of correction for gage factor.....	63
Equation (19)	Equation of Combination of Thermal Output and Gage Factor.....	64

LIST OF SYMBOLS AND ABBREVIATIONS

B	:	Thickness of the cross-section
C	:	Reduction factor for ovality
<i>CIPP</i>	:	Cured in place pipe
<i>Circum.</i>	:	Circumferential direction
D	:	Average diameter
D_h	:	Horizontal diameter
D_v	:	Vertical diameter
E	:	Modulus of elasticity of the liner
E_L	:	Long-term modulus of elasticity of the liner
F^*	:	Initial gage factor
<i>FE</i>	:	Finite element
$F(T_I)$:	Gage factor at the test temperature
<i>HVAC</i>	:	Heat, ventilation and air-conditioning
I	:	Moment of inertia of area
K	:	Enhancement factor
<i>Long.</i>	:	Longitudinal direction
N	:	Safety coefficient

P_{cr}	:	Critical load
Q	:	First moment
R	:	Average radius
R_d	:	Reduction factor due to annular gap
R_q	:	Reduction factor due to the ovality
R_d	:	Reduction factor due to local intrusion
SDR	:	Standard dimension ratio
V	:	Shear stress
b	:	Thickness of the cross-section
p	:	Allowable stress
q	:	Influencing in ovality from Moore's definition
r_L	:	Radius of the liner wall's middle axis
s_L	:	Flexural stiffness of the liner
t	:	Thickness of the liner
w_g	:	Amplitude of the liner's ovality
α_D	:	Buckling factor
β_k	:	Buckling factor in a simplified form
$\dot{\epsilon}_1$:	Corrected strain for thermal output only
$\ddot{\epsilon}_1$:	Initial strain uncorrected for thermal out

$\varepsilon_{T/O}(T_1)$:	Thermal output at temperature T_1
ν	:	Poisson's ratio
$\Gamma_{p,g}$:	Buckling factor in a simplified form
$\Gamma_{p,h}$:	Reduction factor for ovality
$K_{GR,\nu}$:	Reduction factor due to the ovality
K_s	:	Reduction factor due to annular gap
K_ν	:	Reduction factor due to the local intrusion

ACKNOWLEDGEMENTS

The information presented in this dissertation required support and dedication from many organizations and people. First, the Louisiana Tech University Board of Regents and the Louisiana Tech College of Engineering and Science provided the financial support as well as permission to use space and equipment to perform the experimentation. The researchers would like to acknowledge the financial support provided by the City of New York, Department of Design and Construction (Infrastructure Division) and Consolidated Edison, Inc. for this research. The researchers would also like to thank Insituform Technologies, Inc., AOC L.L.C., Pipe Lining Supply, Inc., GEBR. RÖDERS AG, and Applied Felts, Inc. for providing the resins and felts required for the testing program.

Individuals who require special acknowledgement are:

- Dr. Raymond Sterling, Dr. Jay Wang, Dr. David Hall, and Dr. Sven Eklund for their guidance, encouragement, and support throughout this process.
- Dr. Mike Baumert for his support at the very beginning.
- Dr. Robert Mckim is highly appreciable for his time to time advice.
- Fellow Graduate Students and friends Dr. John Matthews, Dr. Ivan Diaz, Dr. Eric Steward, Abdullah Al-Masud, Md. Rashedul Islam, and Rajesh Dulam for their continued support and helpful advice.

- Mr. Nathan Pettit, Ex-TTC Lab Technician for his immeasurable help to setup the physical experimentation.
- Above them Dr. Erez Allouche had provided continuous guidance, encouragement, and financial support throughout this process. He presented to me the original ideas that blossomed into this dissertation, all the while allowing me the freedom to explore new ideas.

Most importantly, I would like to thank my wife, Nazifa, our daughter Arisha, my parents, mother-in-law, brother and sisters for their continued support and sacrifice during these years.

CHAPTER 1

INTRODUCTION

1.1 General Introduction

The City of New York operates 6,375 miles of storm, sanitary and combined sewers, ranging from 6" to 90" in diameter. Over 65% of the current system was built prior to 1940, and suffers from varying degrees of deterioration. The city is currently considering the reconstruction of Times Square, a world famous tourist site in downtown Manhattan. The project limits are 7th Avenue 42nd Street to 48th Street, and Broadway 42nd Street to 49th Street. As part of the proposed construction program, selected sewer pipes within the project limits were identified as candidates for rehabilitation or replacement. Seven of these sewer segments are known to be subjected to intermittent steam condensation discharge. These pipe sections vary from circular 12" pipes to 5'-7" x 3'-6" egg-shaped pipes. In most cases, these pipe segments are placed beneath subway platforms or tracks, or are attached to the tunnel wall (Figure 1). The locations and characteristics of these segments are summarized in Table 1. Thus, replacement of these pipe-segments using the cut-and-cover construction method is not a viable option. However, having been exposed to steam injection for nearly 75 years, these pipes require rehabilitation.

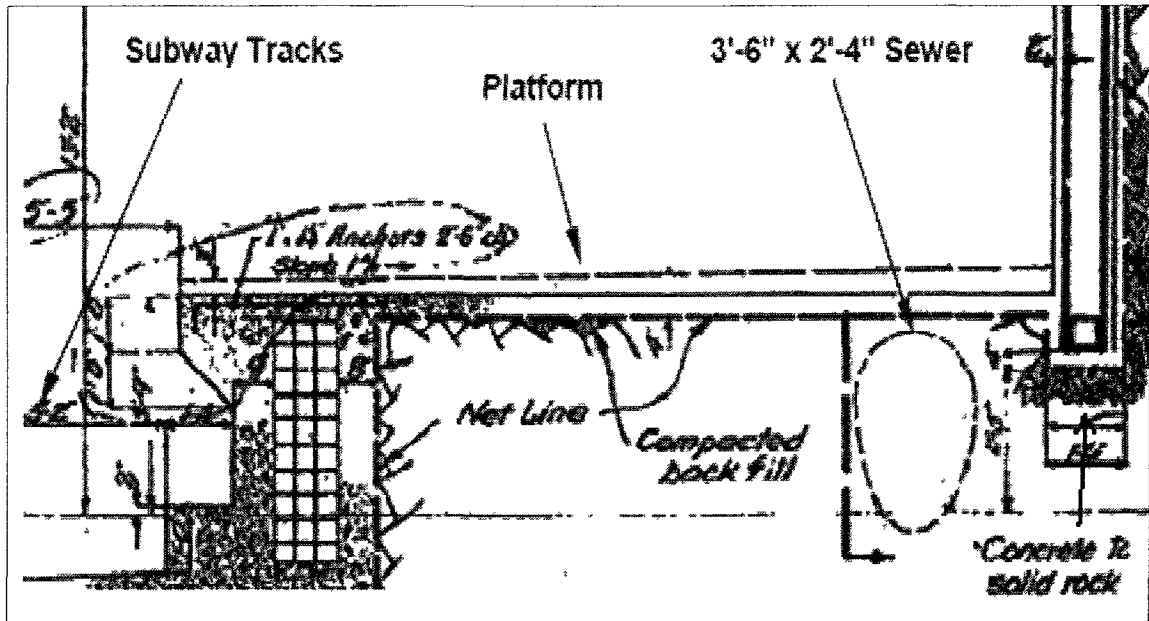


Figure 1: An Egg-shaped Sewer Located Underneath the Subway Platform at 7th Avenue Roadway (modified after Dino Ng, 2008)

**Table 1: Segments of Sewer Affected by Steam Discharge within Project Limits
(modified after Ng, 2008)**

Street	From	To	M#	M#	Size	Comments
W. 43 rd Street	Broadway	East	51	52	12"	
			52	53	4' × 2'-8"	
W. 45 th Street	7 th Avenue	West	68	15	36" (2 pipes)	Located beneath the base of a subway rail bed.
W. 47 th Street	Broadway	7 th Avenue	Tee	85	3'-6" × 2'-4"	Located under subway a platform.
			85	87	4' × 2'-8"	Located under subway a platform.
W. 49 th St	7 th Avenue	West	1	2	18"	Sewer is attached to a tunnel wall.
Broadway	W. 45 th Street	W. 46 th Street	68A	63	5'-7" × 3'-6"	Located under subway rail at 30'-0" depth.

Manhattan is the largest steam system district in the US, with its roots going back to the New York Steam Company, which opened for business in 1892. Con Edison purchased the NY Steam Company in 1936, and presently operates 104 miles of main and services, which serve 1811 customers. In FY 2004, sales were 26 billion pounds of steam and revenues were estimated at US \$531 M. The steam is generated at the B.N.Y.C.P. power plant and distributed via a network of transmission and distribution mains. The transmission mains range between 24" and 30" in diameter and operate at 400 PSIG and

475° F (total of 12 miles). The distribution mains range between 6” and 30” in diameter and operate at 200 PSIG and 413° F (total length 80 miles). The remainder of the system consists of service lines.

A schematic diagram of the steam distribution system is given in Figure 2. The distribution system delivers the steam to hundreds of buildings between Battery Park and 96th Street powering air-conditioning compressors or passing through a series of pressure reducing valves, allowing it to be used directly in heating systems. The steam condensation is then discharged into the sewer system. At the outlet of the steam trap, the temperature of the condensate is at a minimum of 212° F. The discharge temperature could be higher if backpressure develops in the drainpipes. Under normal operation conditions, the condensate spends considerable time in a cooling chamber and gets down to 150° F before it is discharged into the sewer. Malfunctioning of the steam trap could result in condensate discharged into the sewer system at temperatures as high as 212° F.

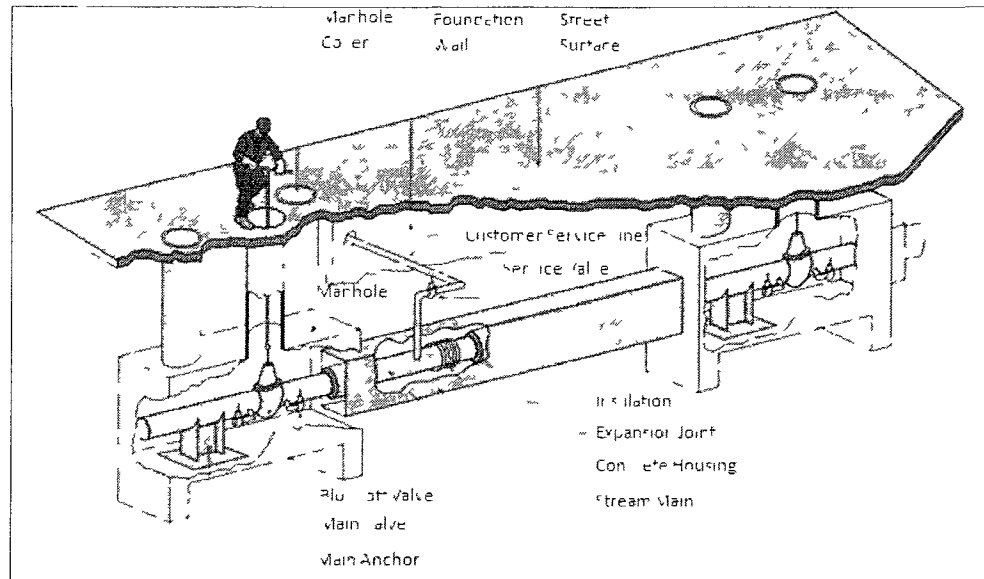


Figure 2: Schematic Diagram of Manhattan's Steam Distribution System (modified after Dino Ng, 2008)

1.2 Interaction between Sewer Pipe and CIPP Liner

The depth of the flow in gravity sewers changes due to daily fluctuations in water use. As shown in Figure 3, around 7:00 AM sewer flow is considerably higher compared with 3:00 AM. The head space and hydraulic perimeter inside the sewer changes with the depth of the flow. When a high temperature steam condensate enters the sewer, it releases latent heat, causing an uneven temperature distribution at the surface of the liner (i.e., much higher temperature above the water level than beneath it). If the temperature of the waste water stream and the host pipe wall is significantly lower than that of the steam condensate, strains (both circumferential and longitudinal) induced by the steep temperature gradient might develop across the liner. The magnitude of these strains will fluctuate with the volume of the head space and the temperature difference between the steam and that of the waste water stream.

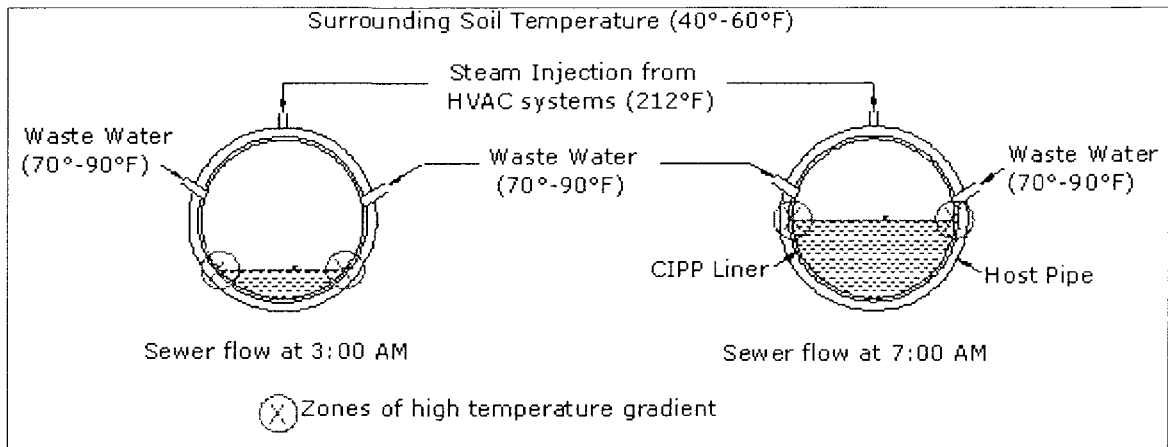


Figure 3: Change in Depth of Flow Due to Daily Fluctuations and Locations of Temperature Gradients

Current design practices assume little or no bonding between the host pipe and the CIPP liner. Thus, the liner might experience localized relative movements due to changes in thermal energy, as shown in Figure 4. This relative movement may take place in either the longitudinal or the circumferential directions, or simultaneously in both directions. The impact of these thermally induced strains could be amplified by geometrical imperfections such as folds, annular gaps, interior bulges and sags, causing the formation of localized high stress zones.

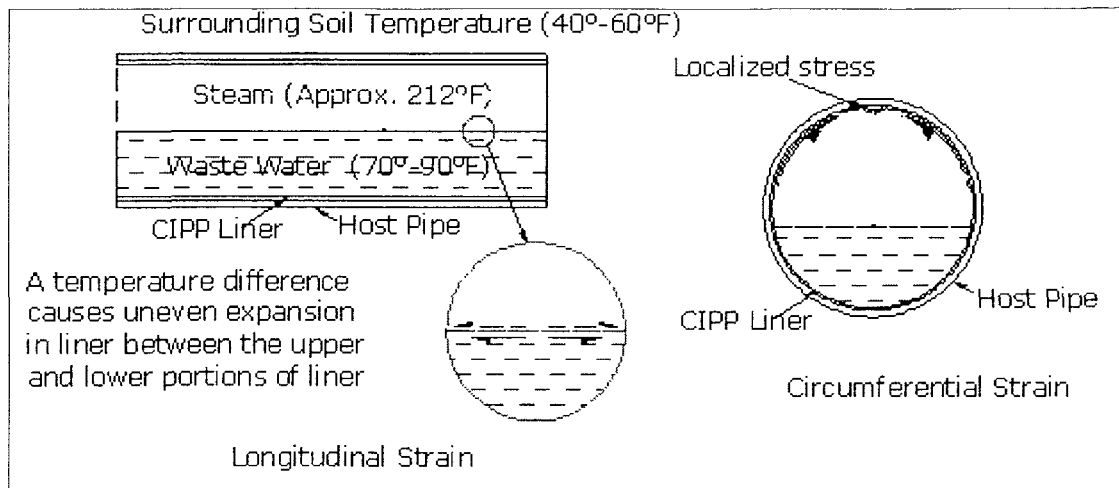


Figure 4: Relative Movement in CIPP Liner Due to Changes in Thermal Energy
1.3 Objectives

The main objective of this research was to identify resin-liner combinations that are expected to perform well under prolonged exposure to elevated temperature (up to 212° F). In addition to this quite broad goal, a number of lesser goals were identified which are listed below:

- Estimate the magnitude of the resulting thermally induced strains in the case of the Times Square project.
- Determine if any modifications to current design procedures are needed.
- Evaluate the resulting stresses from thermally induced in-plane shear strains and to examine ways in which these strains could be accounted for by current design procedures.

1.4 Scope of Work

The research described herein investigates the effect of elevated temperature on CIPP liner over a prolonged period of time. Inspired by a research project funded by the City of New York, Department of Design and Construction (Infrastructure Division) and Consolidated Edison, Inc., it was quickly determined that the resin was playing the key role to withstand elevated temperature. Therefore, the research was mainly divided into three phases, namely:

- Phase – I: Material characterization and bench scale testing of resin-felt candidate systems. The bench scale testing program was developed and performed for one year on different resins to determine the type of resin suitable for elevated temperature application.
- Phase – II: Full scale testing of lined host pipes under cyclic temperature loading. The full scale testing was performed on lined specimens for more than 1080 temperature cycles (three cycles per day) and thermally induced strains and corresponding stresses were measured.
- Phase – III: Next a third phase was added where it was planned to perform 3-D numerical simulation of liner-pipe interaction systems with and without annular gap between the host-pipe and liner under thermal loading condition.

CHAPTER 2

LITERATURE REVIEW

2.1 Introduction

This dissertation presents the interim's findings of a State of Technology assessment through industry survey and experimental testing of the suitability of purpose-developed cure-in-place pipe (CIPP) resin-felt systems for the relining of sewer pipes in the Manhattan area, which must tolerate elevated temperatures due to discharge of steam condensate. The study was undertaken with the recognition that most commercially available resins used in CIPP lining systems are not intended to perform at temperatures as high as 212° F. Furthermore, the current design methods and practices do not account for stress conditions that could be induced due to combined hydrostatic pressure and cyclic thermal loads. A literature review revealed that little information is available in the public domain regarding the installation of CIPP rehabilitation systems in pipes subjected to elevated temperatures. Nevertheless, there are several resins products that claim to be suitable for such applications.

2.2 Background History

In 2007, a 24-in. steam pipe that was laid in 1924 exploded in Midtown near Grand Central Terminal. Investigator found that apparently cold water got into the steam pipe, producing a change in pressure which caused the blast. In August 19, 1989, people had to evacuate from their homes in Manhattan due to a steam pipe blast. Several related accidents occurred in NY in a small time span reported by Ms. Laurie Goodstein in the Washington Post, and published in the Star Tribune November 24, 1989 are listed in Table 2.

Table 2: Steam Pipe and Water Main Blast in NY in 1989

Date	Description
Sept. 3	In Midtown Manhattan a water pipe burst.
Sept. 6	In upper west side steam pipe exploded.
Sept. 25	Steam pipe exploded six blocks from the united nations office.
Oct. 6	30-ft section 6 th Avenue collapsed due to a broken water main.
Oct. 10	8 th Avenue Subway station was closed due to a burst water main.

Although only a handful of steam pipes have exploded in the past decade, the threat remains because the 105 miles of steam mains and service pipes that pump steam beneath the streets of Manhattan are near other utilities, including gas and electrical

equipment. Therefore, problems with one system can often affect the others. Aftermath of a steam pipe blast is shown in Figure 5.



Figure 5: Steam Pipe Blast in the City of NY (modified after The New York Times, 2007)

Rehabilitation of these old pipes is difficult but not impossible, and again closing traffic for several weeks will incur enormous financial loss for a city like New York. So, little to no digging trenchless method is preferable to the traditional "dig and replace" methods.

2.3 Effect of Thermal Strain

Recently, a paper was published notifying the thermal aspects of designing a CIPP liner during and after the installation (McKim et al., 2010). ASTM F1216 assumes some structural support from the host pipe by including the "K" (Enhancement Factor) and does not consider any mechanical or chemical bonding between the liner and the host-pipe. But there is a contradiction that the thermal strain experienced by the liner as it cools off from

the installation temperatures depends on the host pipe and when the host pipe fails to restrain the liner's thermal strain, the liner can fail under tension.

2.4 Pipe Rehabilitation Methods

Trenchless technology refers to family of methods and equipment used for the installation of new or replacement or rehabilitation of existing underground infrastructure with minimal disruption to surface traffic and other surface activities. Cured-in-place pipe (CIPP) technology consists of protecting/sealing/reinforcing the inner wall of the host pipe with a thermosetting composite liner that is cured in place. It is a system in which a thin flexible tube of polymer or glass fiber fabric is impregnated with resin and forced to harden the material. Once inserted into the pipe, the tube is expanded with hot air or hot water to make it assume the shape of the inner wall of the pipe and cured under elevated temperature (Wood E. 1977, and Bruzzone et al., 1987).

2.5 Components of CIPP

The basic components of CIPP include a flexible fabric tube and a thermosetting resin system. The fabric tube is made up of woven or non-woven material, mainly felt, glass fiber composite cloth, and impermeable plastic. The tube should be strong enough to withstand installation stresses. Impermeable plastic coatings are used on the interior or the exterior of the tube to protect the resin during installation. The major function of the tube is to carry and support the resin until it is placed within the existing pipe and cured. Primary resin systems used include polyester (filled and unfilled), vinyl ester and epoxy. Polyester resins have high water resistance and are the most economic among the three. Styrene is added to reduce the viscosity of polyester resins. Styrene also helps in the curing of the resins by cross-linking of the molecular chains of polyester. The major

application of polyester resins is in the municipal sewage system. Vinyl ester and epoxy resins are tougher and more resilient than polyester resins. They are used for industrial and pressure pipeline applications where their enhanced corrosion and solvent resistance properties are required. The epoxy resins are the most costly of these three resin types and are used in drinking water pipelines (Robert et al., 1995).

2.6 CIPP Method

The existing pipe is first inspected to assess the extent of damage to the pipe. It is then cleaned of roots, sediments, and debris and the flow is bypassed. A flexible tube impregnated with thermosetting resin is then inserted into the pipe through an entry point. The installation is done by winching mechanically or by inverting it under air or water pressure. In the inversion process, the tube is cuffed back and clamped to an inversion ring at the entry point. It is then fed into the pipe through the ring with the tube being turned inside out. Water or air pressure is then applied to turn the tube inside out and to push it inside the pipe. The pressure keeps the tube expanded against the pipe wall as it inverts along the installation length. In the winching technique, the tube is pulled through the pipe length. An inflation bladder is then inverted through the tube to expand it against the wall of the host pipe.

After the tube is inserted and expanded, heated water or steam is circulated through the pipe to initiate the curing of the resin. After the curing cycle is complete, the CIPP is cooled. The ends of the cured pipe are then trimmed. At the service connections and laterals, dimples are created owing to the pressure. In big pipelines where personnel entry is possible, a cutting device is used to reopen the connections. In small pipelines,

robots and closed-circuit television (CCTV) cameras are used to locate the dimples and reopen the connections (Robert et al., 1995).

2.7 Vendors of High Temperature CIPP Liner Components

An extensive literature review was undertaken to identify commercially available CIPP products that are expected to perform well in elevated temperature environments. Chemical resistance of CIPP liners depends on the type of resin used. Unsaturated polyester resins provide good chemical resistance to municipal sewerage; however, vinyl ester resins and epoxy resins provide further increased chemical resistance where special corrosion and higher temperature performance is needed.

2.7.1 Reichhold Chemicals, Inc.

The Composites Division manufactures two resins that can be used at elevated temperatures.

2.7.1.1 DION 382-20

This is polyester-based (bisphenol-A fumarate) resin. This is a highly corrosion-resistant resin with over 30 years history of good performance at high temperatures. It has been converted for use in CIPP liners and the customers include Novel Pipe, Inliner, etc.

2.7.1.2 DION 9800-20

Formerly known as ATLAC® 580-20, this vinyl ester resin has been specifically designed for CIPP applications requiring the high degree of chemical and temperature resistance. This vinyl ester is urethane modified. Urethane-modification creates a tough, resilient polymer that combines outstanding corrosion-resistance and high-temperature performance with excellent laminating characteristics. The resin wet-outs really well and has good wetting characteristics with carbon and ARAMID fibers, as well as conventional

glass fibers. The resin can be thickened using regular (not hydrophobic) grades of fumed silica, and will not foam when used with standard MEKP initiators. Until a few years ago, Insituform was the main customer, but now, this resin is mostly sold to several smaller customers such as Improved Technologies in Knoxville, TN.

The mechanical properties of the DION 9820-20 and DION 382-20 resins have not been tested at elevated temperature for the application of CIPP liners but have been tested in laminates and listed in Table 3 and Table 4.

Table 3: Typical Properties of DION 9800-20 at Elevated Temperatures

Temp.	Tensile Strength		Flexural Strength		Flexural Modulus	
	° F	psi	MPa	psi	MPa	Psi
77	19,500	134	26,300	181	1,010,000	6,960
150	19,500	134	25,600	176	870,000	5,995
200	19,500	134	23,100	159	740,000	5,100
250	13,000	90	19,200	132	580,000	4,000
300	9,000	62	7,400	51	320,000	2,205

Table 4: Typical Laminate Properties of DION® 382-20 at Elevated Temperatures

Temp.	Flexural Strength	Flexural Modulus	Tensile Strength	Tensile Modulus
° F	psi	×10 ⁶ psi	psi	×10 ⁶ psi
77	25,500	1.21	18,000	1.45
150	27,000	1.10	21,500	1.40
200	23,500	1.00	21,500	1.35
250	17,500	0.88	20,000	1.20

2.7.2 Neopoxy International, Inc.

The company manufactures high heat resistant epoxy named NPR-1571. This epoxy resin is designed for medium and large diameter CIPP structural liners having an operating temperature of over 300° F. For application in smaller diameters and/or different operating temperatures, NPR-1571 can be further modified to meet specific needs. NPR-1571 is a slow curing resin, with initial cure at ambient temperature and post cure at 70° F (higher better) in duration on several hours (e.g. 2-3 hrs) to provide improved heat resistance and chemical resistance. One known case history involves the lining of a pipe 18” in diameter and 110-ft long conveying chemicals at elevated temperatures at the Shell Deer Park Refinery, approximately 20 miles east of downtown Houston, TX. The contact person was Mr. Ron Soots, BEI Engineering, 3741, Red Bluff Road, Ste 200, Pasadena, TX. 77503. Tel.: (713) 246-7314.

2.7.3 Noveon, Inc.

Noveon, Inc., an integral part of the Lubrizol Corporation, offers Estane® thermoplastic polyurethanes (TPUs). Estane TPU is a coating used in felt that is impregnated with a resin and is built for toughness and durability and provides a combination of heat, chemical and abrasion resistance. High melting point (~145° C / 293° F) allows the use of hot water and steam across a wide range of pipe thicknesses and can be used in combination with a wide range of thermosetting resin matrix systems.

2.7.4 Belzona, Inc.

Belzona, Inc. manufactures several ceramic coatings; however, they are too viscous to be poured and are not suitable as resins for CIPP application. This can only be applied with a brush or spray.

2.7.5 AOC LLC

AOC is a leading global supplier of resins, gel coats, colorants, additives, and synergistic systems for composites and cast polymers. They are the North American leader in resins for corrosion resistant applications and produces Vipel F085 resin in ISO 9001:2000-certified facilities that use proprietary process control technology for ensuring batch-to-batch consistency. Vipel® resins have excellent process ability and high levels of consistency. It has high organic solvent resistance with improved high temperature properties. Pipelines totaling 5,044 ft. in length with diameters ranging from 15 to 48 in. were rehabilitated in the city of Columbus, Ohio using Vipel F085 products. The city of Pittsburgh, Pennsylvania rehabilitated 1,372 ft of 54 in. diameter pipe. The Orange County, Florida used Vipel F085 to rehabilitate 18.9 miles of pipes with diameters of up to 72 in.

A list of potentially suitable resins for high temperature CIPP applications is given in Table 5.

Table 5: List of Potentially Suitable Resins

Product	Characteristics
CoREZYN VE8738	A vinyl ester resin suitable for highly corrosive and elevated temperature applications.
CORVE 8190	A vinyl ester resin for sewer applications.
DION 9800-20	Vinyl ester resin specifically designed for CIPP applications that require higher degree of chemical and temperature resistance.
Quik PE	A polyester resin featuring polymer composition that prevents degradation in corrosive environments.
Quik POX	A modified cycloaliphatic hardener featuring high strength and high heat distortion temperature (HDT) post cure.
Vipel F085	F085 series is an epoxy novolac vinyl ester resin dissolved in styrene.

2.8 Related Work and Theories

2.8.1 Introduction

Linings are used for the rehabilitation of sewers to restore hydraulic integrity and extend the structural life duration. Lining takes the shape of the existing sewer. Therefore, the shape can be oval (Figure 6), horse-shoe or circular. Cured in place linings closely match the inside shapes of the sewers. The lining system is designed to act as a flexible pipe within the old deteriorated rigid host, with the soil providing the necessary support to maintain stability (WRc/WAA 1994). No bond is required between the liner and host pipe. From the mechanical standpoint, lining can be affected by deformations of the host structure or by internal or external hydrostatic pressures when the pipe is below groundwater table. Deformations of buried structures are generally small, and the resulting stresses produced in the liner are almost negligible. Conversely, external pressure due to groundwater can cause lining failure by geometric instability or material breakdown. Therefore, a lining must be designed to resist the action of external hydrostatic pressure and this is the only loading case having any major probability of occurring (Trenchless Technology Research Colloquium, 2000). Thus, failure may take place in the form of buckling due to excessive compressive forces. Therefore, a properly designed sewer must comply with the deflection limit and buckling criteria. The stress-limit criterion is defined so that the maximum buckling stress developed under hydrostatic pressure must not exceed the allowable bending stress of the lining material.

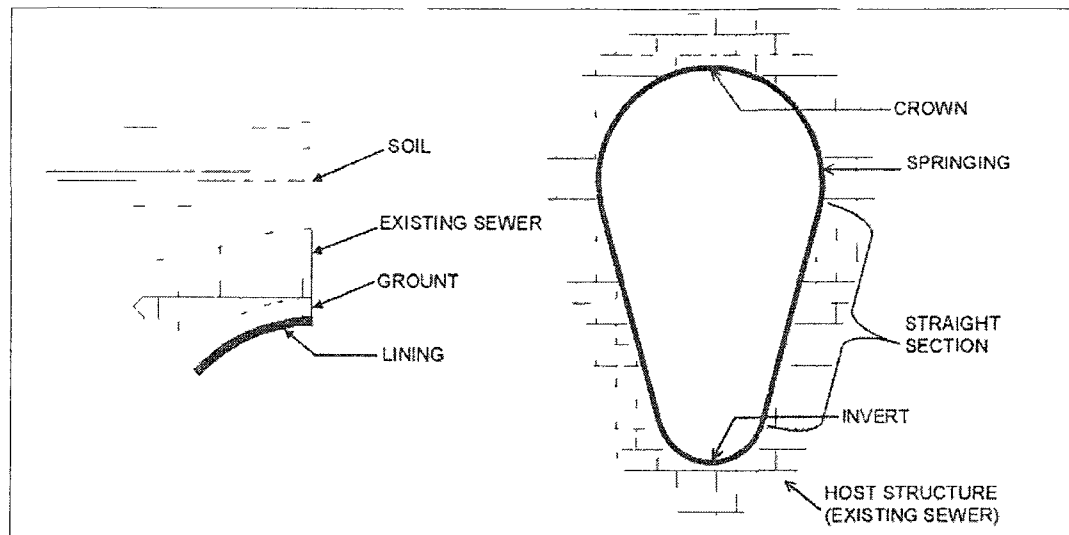


Figure 6: Close-fit Lining in an Oval Shaped Sewer

For deflection-limit criteria, a maximum allowable deflection in the liner should not exceed 3% of the width of the liner (Oliver, 2001). With buckling criteria, the lining must be designed such that failure is not triggered by buckling due to large hoop compression. There are many design methods for circular linings and an equal number of published experimental data (Oliver, 2004, Falter, 1996, and Boot et al., 1996). Conversely, there is far less information, both in terms of theoretical and experimental results, for non-circular linings (especially egg-shaped and oval-shaped linings). Currently, only the WRc recommendations (WRc/WAA 1994) offer a design method for non-circular linings (see Figure 7), but the calculation model is linear and does not allow for the risk of buckling under hydrostatic pressure.

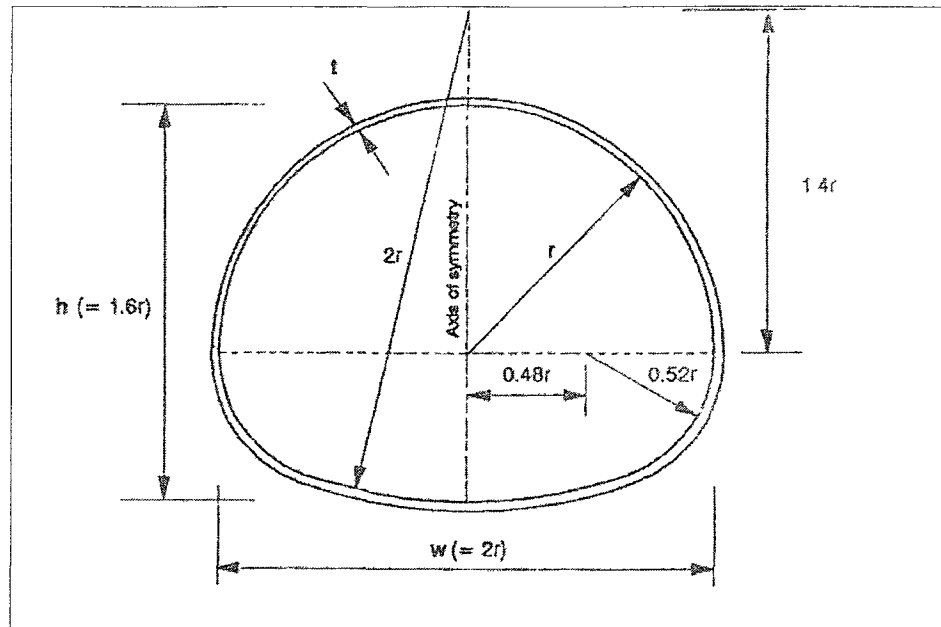


Figure 7: Horse-shoe Type Sewer (after WRc)

2.8.2 Behavior of Close-fit Lining Subjected to External Pressure

The load cases on the sewer pipes are hydrostatic pressure and earth and traffic loads. Sustained hydrostatic pressure is due to groundwater acting in the annular space between the liner and the host pipe. Since gravity sewers in need of renovation invariably leak, this load case applies regardless of the host pipe's condition or whether the aim of the rehabilitation is primarily structural or simply to provide a barrier against internal corrosion or ex-filtration. Even where the permanent groundwater table is below the pipe's invert level, the liner must generally be designed to resist a short-term hydrostatic head which could arise under storm conditions.

The second load case assumes that earth and traffic loads will, in due course, be transferred from the existing pipe-soil structure to the liner. The likelihood of this occurring is assumed to be a function of the condition of the sewer at the time of lining. In the great majority of practical situations, however, little or no such load transfer ever takes

place because the existing equilibrium, of even quite badly deteriorated sewer structures, is effectively and permanently secured by the lining process. So far this fact is recognized explicitly only in the UK design procedure (WRc/WAA, 1994), and with few exceptions the treatment of the soil load transfer case in other design methods is over-conservative (Gumbel, 1997).

Because linings restore hydraulic integrity and because the bond between the liner and the host cannot be relied on in the long-term, it is necessary to consider the effects of external water pressure acting on the lining. Groundwater may percolate through the cracks and act at the interface between the lining and the host. External pressure applied to an egg-shaped lining cause formation of a gap at the section of maximum radius. The similar phenomena take place at the location of the straight section for an oval-shaped lining (Figure 8). Pressure in the gap pushes the liner against the host structure and a blister forms over the gap (Seraj et al., 1999). When the pressure builds up, two possible behaviors of the blister might take place depending on the curvature of the section where the gap forms. If the curvature is sufficient, the blister remains localized (i.e., contained by the curvature) and the blister angle decreases (Figure 8), but a critical buckling pressure develops. If the curvature is too small, for instance in the case of an oval- or an egg-shape with straight sides (Figure 9), the blister extends continuously over the entire liner (the blister angle increases) and a critical buckling pressure does not develop. The first behavior is termed “critical” while the second is termed “sub-critical”. Deflections of the liner subjected to sub-critical conditions under external pressure are larger than the liners subjected to critical conditions. Critical linings are more likely to buckle under external pressure, but deflections (before buckling) are relatively small.

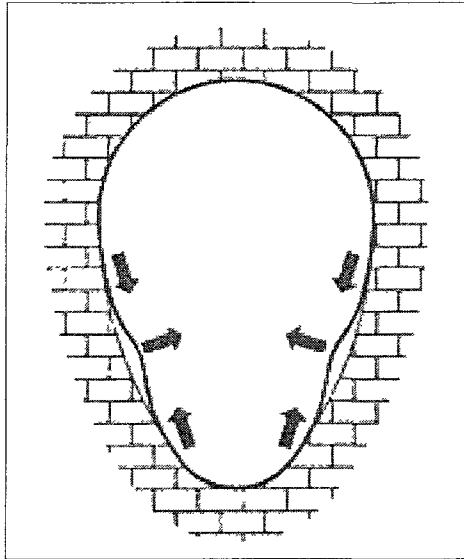


Figure 8: Critical Condition - Deformation Lob is Localized

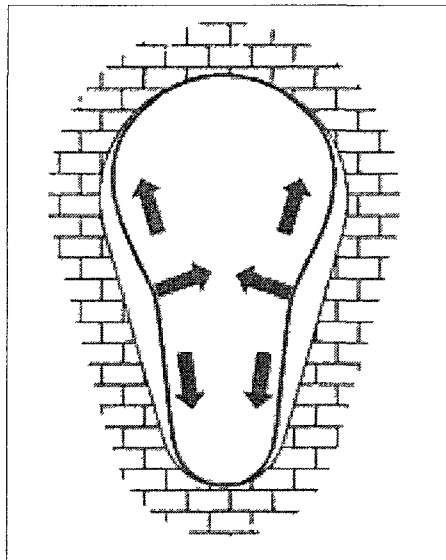


Figure 9: Sub-critical Condition - Lob Extends Over Entire Height of the Liner

2.8.3 Mechanisms of Restrained Hydrostatic Buckling

Figure 10 illustrates the steps leading to buckling failure of an encased circular liner pipe subject to external hydrostatic pressure, as observed in numerous laboratory experiments in the US and UK (e.g. Guice et al., 1994; Boot et al., 1996, and Boot, 1997).

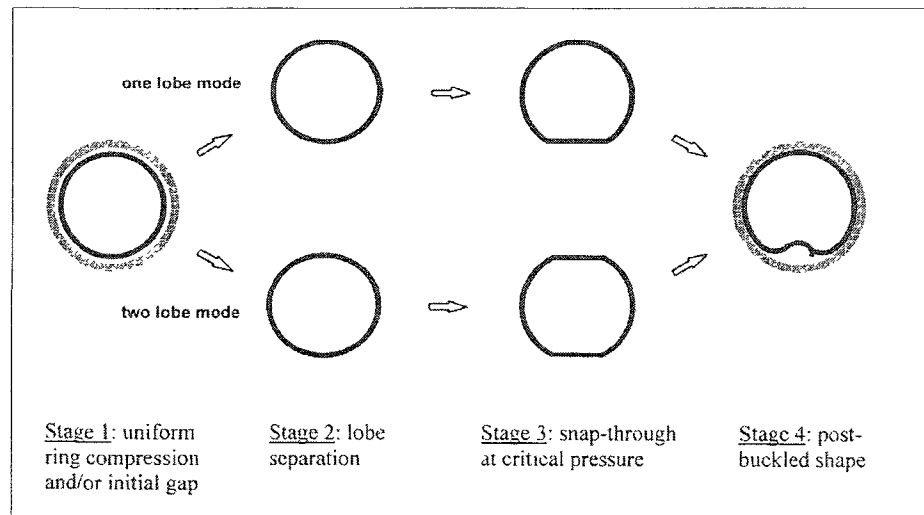


Figure 10: Steps in Nonlinear Hydrostatic Buckling of Circular Pipe

If the unloaded liner is a tight fit to the host pipe, it can initially deform only by uniform hoop compression (Step 1). The resulting slack in the system allows the liner to lift away from the host pipe in either an asymmetric (one-lobe) or symmetric (two-lobe) mode (Step 2). As pressure further increases, the inward deformation of the lifted lobe or lobes is accompanied by a shortening of lobe length and an increase in the ring compressive strain. Eventual snap-through (Step 3) is in essence a form of geometric instability, in which the buckling pressure is associated with the critical lobe length at failure. The critical lobe length increases as a result of the initial annular gap, and both elastic and creep compressive strains contribute to further reduction in liner perimeter under pressure. This controlling influence of hoop compressive strains is what distinguishes the buckling mode as essentially non-linear.

The pre-buckling deformations leading to instability are not generally noticeable to the naked eye, and regardless of whether one or two lobes develop, snap-through can only occur at a single point because the associated release of strain energy instantly stabilizes

any other incipient points of failure. The resulting manifestation of post-buckling deformation (Step 4) as apparently single lobe should not therefore be confused with the buckling mode itself.

The non-linear theory was originally developed by Glock in 1977, assuming a single lobe mode associated with initially perfect circular geometry. However, as soon as some initial gap is introduced, the liner pipe will tend to deform elliptically while taking up the slack as if unrestrained (Figure 11a), following the symmetrical two-lobe mode up to failure. For nominally close-fitting liners, this tendency has been confirmed in the great majority of cases where pre-buckling deformation measurements have been made. A contradiction was expected for a relatively loose-fitting liner tested horizontally and pressurized by water would tend to float and create an asymmetrical initial gap favoring the one-lobe mode (Moore, 1998). In the additional presence of even the modest initial ovality (Figure 11b), for example the typical 2% tolerance on diameter associated with manufacture of new concrete and vitrified clay pipes, the liner will be even more strongly predisposed to follow a symmetrical deformation mode. Two-lobe deformation has been observed in nearly all appropriately monitored buckling experiments in horizontally aligned, ovalized casings to date (Seeman et al., 2001). In view of their important influence on the qualitative as well as quantitative buckling response of restrained liner pipe, any design theory must take explicit account of geometrical imperfections.

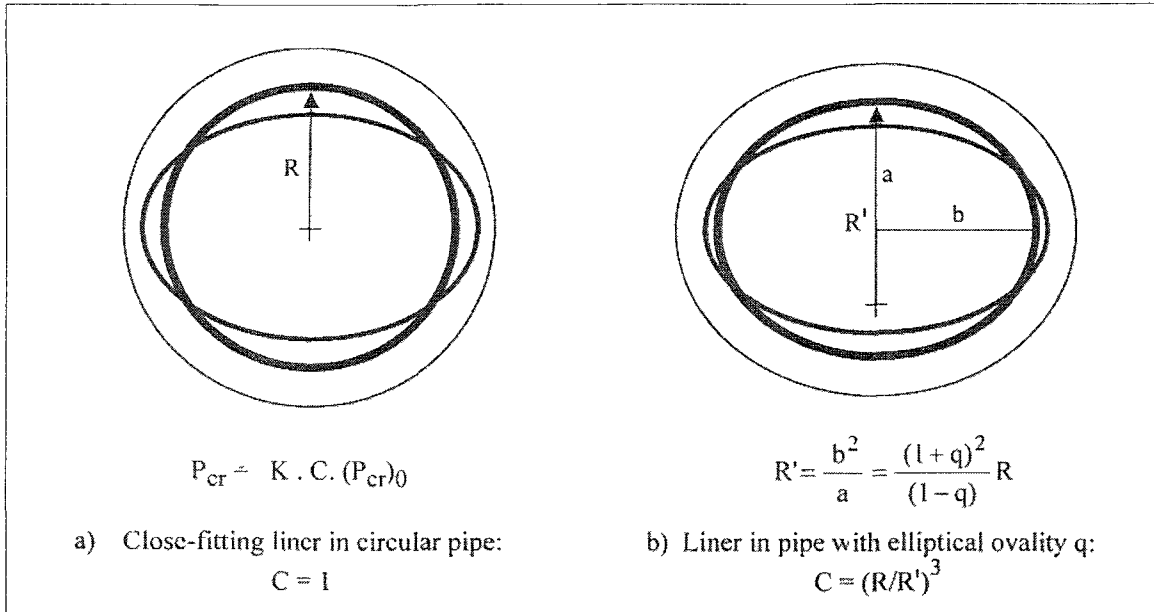


Figure 11: Liner Deformations Implicit in Current ASTM Design Formula w/ Enhancement Factor K and Ovality Factor C

2.9 The Basic Formulas

According to the derivation source design, formulas can be divided into two categories –

Derivation based on Timoshenko's formula:

$$P_{er} = \frac{3EI}{R^3} \cdot \quad (1)$$

Derivations based on Glock's formula:

$$P_{er} = E \left(\frac{t}{D} \right)^{2.2} \cdot \quad (2)$$

2.9.1 Imperfections

Ovality imperfection is considered during calculation of the critical stress, and is viewed as the elliptical deformation of a rigid pipe with longitudinal cracks. The estimation of oval imperfection is fairly variable. Certain authors like to measure ovality

directly on the photograph of the pipe. The estimation of ovality varies from 3% to 9%.

Ovality was defined by Moore (Moore et al., 1996) as follows:

$$q(\%) = 100 \frac{D_h - D_v}{D_h + D_v}. \quad (3)$$

The annular gap is assumed to be uniform and characterized by its amplitude. As for ovality, a percentage of the radius of the diameter is typically used. One practice is to divide the amplitude by the average radius of the liner or the host pipe:

$$g(\%) = 100 \frac{w_g}{R}. \quad (4)$$

Others, such as Hall (Hall D.E. et al, 2001), use the diameter of the host pipe:

$$g(\%) = 100 \frac{w_g}{D}. \quad (5)$$

Longitudinal intrusion is characterized by its angular extension and its maximum amplitude.

2.9.2 ASTM F1216

The following formula, derived based on Timoshenko (Timoshenko et al., 1961), is the most frequently used. The critical buckling pressure is multiplied by a casing factor K equal to 7.0 for liners:

$$\frac{P_{cr}}{N} = p = \frac{2KE_L}{(1-\nu^2)} \frac{1}{(SDR-1)} \frac{C}{N} \quad (6)$$

$$C = \left[\frac{1-q}{(1+q)^2} \right]^3. \quad (7)$$

In ASTM 1216, the equation includes a safety factor and directly yields the admissible pressures as a function of SDR, or the inverse. Its validity depends mostly on the value of K used.

2.9.3 Formula of Hall (TTC, LA Tech, USA)

Hall uses a one-lobe Glock formula with variable coefficients corrected for three imperfections:

$$P = \frac{aE_L}{(1-\nu^2)} \frac{1}{(SDR-1)^m} \frac{1}{N}. \quad (8)$$

The definitions of N , EL , SDR , and ν are already mentioned. The three imperfections are annular gap (x), ovality (y), and local intrusion (z). The coefficients take the following forms:

$$a = b_{ijk} x_i y_j z_k$$

$$m = c_{ijk} x_i y_j z_k.$$

These are polynomials with three variables whose 27 coefficients have been adjusted based on results of FE calculations. For, $x=y=z=0$, the value of $m = 2.25$ and $a = 1.06$, effectively resulting in Glock solution for the one-lobe mode.

2.9.4 Formula of Boot (University of Bradford, UK)

Boot uses a two-lobe Glock formula with variable coefficients corrected for two imperfections:

$$\log_{10} \left(\frac{P_{cr}}{E} \right) = m \cdot \log_{10} \left(\frac{D}{t} \right) + \log_{10} c. \quad (9)$$

Here, m and c depend on ovality and the annular gap and are obtained by interpolating the results from FE analysis or by directly solving the Glock equation.

2.9.5 Formula of ATV-M 127-2 (Germany)

The ATV-M 127-2 formula written below is a one-lobe Glock formula with reduction factors corrected for three imperfections:

$$p_{cr} = \kappa_{\nu} \kappa_{GR,\nu} \kappa_s \alpha_D S_L \quad (10)$$

$$\alpha_D = 2.62 \left(\frac{r_L}{S_L} \right)^{0.8} \quad (11)$$

$$S_L = \frac{(EI)_L}{r_L^3} \quad (12)$$

2.9.6 Formula of Moore (Queen's University, Canada)

The following equation given by Moore (Moore, 1998) used a one-lobe Glock (Glock, 1977) formula with reduction factors corrected for three imperfections:

$$p_{cr} = \frac{E_L}{(1-\nu)^2} \left(\frac{t}{D} \right)^{2.2} R_q R_{\Delta} R_d \quad (13)$$

2.9.7 Formula of Thépot (RERAU National Project, France)

Thépot also used a Glock formula of one-lobe or two-lobe type with reduction factors corrected for two imperfections. The formula is mentioned below:

$$p_{cr} = \Gamma_{p,h} \cdot \Gamma_{p,g} \cdot \beta_k \frac{EI_L}{R^3} \quad (14)$$

where,

$$\beta_k = 2.62 k^{0.4} \left(\frac{R}{t} \right)^{0.8} \quad .$$

There also exists a global reduction factor which combines the two imperfections.

2.9.8 Conclusion

Existing design formulas for calculating the buckling pressure of a CIPP liner can be classified as derivatives of either Timoshenko's or Glock's equations. In Timoshenko's equation, the influence of the different imperfections, with the exception of ovality, is taken into consideration via a single, constant enhancement factor (K) which was determined experimentally. In the case of Glock's equation, imperfections are treated individually using reduction factors or variable coefficients. Therefore, precise definitions of imperfections are of limited importance for Timoshenko's derived formulas where the safety factor is concentrated in a global coefficient, but they are very important for Glock's derived formulas where the safety factor is distributed over a group of coefficients.

2.10 Effect of External Hydrostatic Pressure

Different authors deal with the effect of external hydrostatic pressure in different ways. It is obvious that local stresses due to hydrostatic pressure loading are very sensitive to geometric imperfections. For certain combinations of imperfections, it is possible that the limit state of the liner material rupture will be reached before the limit state for the stability of liner geometry.

2.11 Effect of Soil and Traffic Load

In cases where the host pipe is separated by at least four longitudinal cracks, or if its mechanical characteristics are very weak, possible movements of the wall must be considered because the pipe becomes a quasi-mechanism in the interaction with soil embedment. This particular state is considered "fully deteriorated" in ASTM 1216 or

"stage III" in ATV-M 127-2. In this case, the existing host pipe is neglected and stresses and displacements are calculated as if the liner were placed directly in the soil.

2.12 Force and Moment Causing Stresses on a Circular Pipe-Liner Section

A pipe-liner can face stresses caused by forces and moment due to axial tension or compression, bending, and uneven settlement of the host pipe.

2.12.1 Axial Stress

In the case of a tensile, loading pipe-liner will be elongated in the axial direction and the resulting tensile stress will be normal to the cross-section of the pipe-liner and will be uniformly distributed.

2.12.2 Bending Stress

If the pipe-liner is supported at the ends and load is applied at a point between the supports (for simplicity say center), bending, or flexural action, will be occurring. Depending upon the load direction and point of applied loading, there will be one compressive and one tensile stress components which are typically of the same magnitude but in opposite directions. Both of these stresses will be acting perpendicular to the cross-section of the liner. All these are true as long as the centroid is exactly at the center of the pipe. However, a deviation of the centroidal location may lead to some unequal magnitude of the compressive and tensile stress.

In the case of bending, shear stresses may develop along the spring lines of the liner. Shear stress in a circular cylinder can be expressed as:

$$\tau = \frac{VQ}{Ib} \quad (15)$$

Here the first moment, Q can be written as:

$$Q = \sum_{i=1}^N A_i d_i + \sum_{i=1}^N A_i (y_i - \bar{y}). \quad (16)$$

2.12.3 Stresses Due to Uneven Settlement

This situation may arise when one of the supports settles. This will result in moments on the support, which will lead to forces perpendicular to the neutral axis at the support for equilibrium. As the force is acting perpendicular to the neutral axis, it can be designated as a shear force and will result in shear stresses.

2.13 Strain Gage Thermal Output and Gage Factor Variation

The electrical resistance of strain gage varies not only with strain but also with temperature. In addition to that, the gage factor of the strain gage varies with temperature. These deviations can cause significant errors when properly not addressed.

The first correction that needs to be addressed is the correction for thermal output. The gage factor setting of the strain indicator coincides with the strain gage used in measuring the thermal output. Therefore, the thermal output correction can be made by direct subtraction of the thermal output from the indicated strain and is shown in Equation (17):

$$\dot{\varepsilon}_1 = \ddot{\varepsilon}_1 - \varepsilon_{T/O}(T_1). \quad (17)$$

Next, the correction is made for the gage factor variation with temperature. First, the strain measurement was made at an initial gage factor setting, and then correction to the gage factor at the test temperature is performed using Equation (18):

$$\varepsilon_1 = \dot{\varepsilon}_1 \frac{F^*}{F(T_1)}. \quad (18)$$

The correction for thermal output and gage factor is obtained combining Equation (17) and Equation (18) and written as Equation (19):

$$\varepsilon_1 = [\ddot{\varepsilon}_1 - \varepsilon_{T/o}(T_1)] \frac{F^*}{F(T_1)} . \quad (19)$$

When the zero balance temperature and the conditions for the gage factor meet, the strain obtained from Equation (19) is the actual strain induced by the mechanical and thermal stresses.

2.14 Elastic and Plastic Strain

When enough loads are applied to a structural material, they cause the material to change shape. This change in shape is called deformation, and as this deformation is compared to its original length, the strain value is obtained. A temporary shape change which is self-reversing after the force is removed is called elastic deformation. When the stress is sufficient to deform the material permanently, it is called plastic deformation. The summation of elastic and plastic deformation is total deformation. The strains related to elastic, plastic and total deformation is named as elastic, plastic, and total strain, respectively. The elastic strain can be calculated by subtracting the plastic strain value from the total strain. There, it is expected to see more or less constant stress value (strain multiplied with modulus of elasticity) after the specimens reach plastic stage.

2.15 Summary

Designing a liner is a difficult mechanical problem which combines several non-linear effects: contact, displacement and material behavior. Liners are thin, deformable structures subject to significant creep and in variable contact with a rigid host pipe structure. Sometimes the host pipe is broken into segments that interact with the elasto-

plastic soil material. Furthermore, the geometrical and mechanical characteristics of the problems are generally difficult to implement in most designs, with some estimated while others are treated as default values. The three imperfections are not always measurable, and default values were defined based on experimental results and numerical evaluation.

It was found from the literature review that none of the design standards included the effect of elevated temperature on the liner.

While obtaining thermal strain data, the correction for thermal output and gage factor are required to perform as the strain gage itself is sensitive to temperature and can lead to poor quality data.

CHAPTER 3

BENCH SCALE TESTING

3.1 Introduction

While the felt component in a CIPP liner conforms to the shape of the host pipe and serves as a carrier medium for the resin, it is the resin that provides the stiffness to the cured CIPP liner. Thus, the experimental program in this research focused on the ability of the cured resin to retain its mechanical properties in the presence of cyclic thermal loading. The mechanical properties of the resins were tested in accordance with ASTM D638, which measures the tensile elastic modulus and ASTM D790, which measures the flexural elastic modulus of the resin material.

ASTM standards require a minimum of five specimens per data point for statistical significance. In this research, a significantly greater number of specimens were prepared from the available panels and resin materials as no similar research work was conducted before.

3.2 Preparation of Specimens

Specimens for testing in accordance with ASTM D638 and ASTM D790 were prepared following two processes. In one way, specimens of resin Type-A were made by cutting 1/8" thick panels of neat (pure) resin using a computer-controlled water-jet cutter (see Figure 12 and Figure 13). The use of the water-jet cutter minimized the thermal effect at the cutting edges. These panels were supplied by a participating vendor.

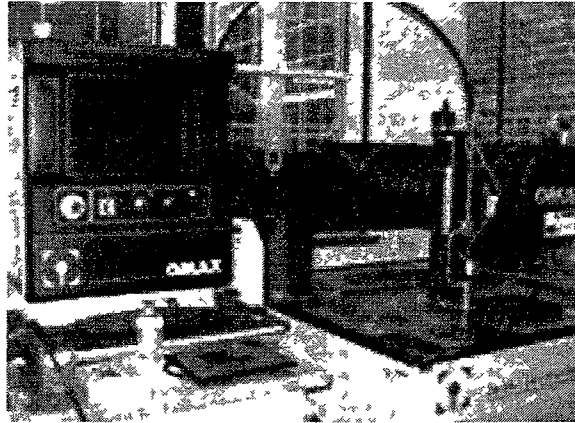


Figure 12: Water Jet Cutter

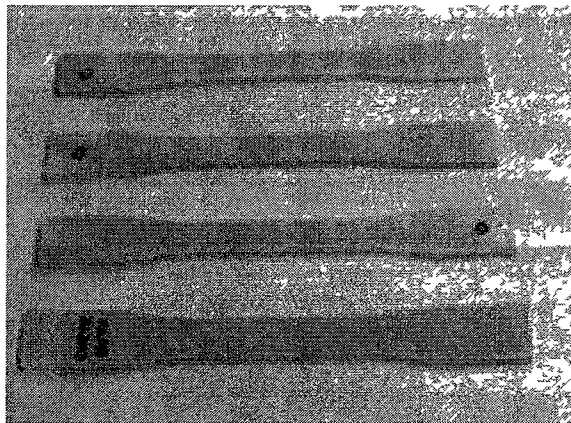


Figure 13: ASTM D638 Specimens Cut From a Panel Using the Water Jet Cutter

In the second process, specimens of other resin types were prepared by pouring the resin into rubber molds. The molds were made from 2" wide and 1/8" thick rubber strips that were cut using standard ASTM D638 and ASTM D790 dies. Later, the rubber molds were glued on a wax paper which was stuck on a Plexiglas, (thus making a Plexiglas-wax-paper system) and next filled with neat resin, and cured (see Figure 14 and Figure 15)

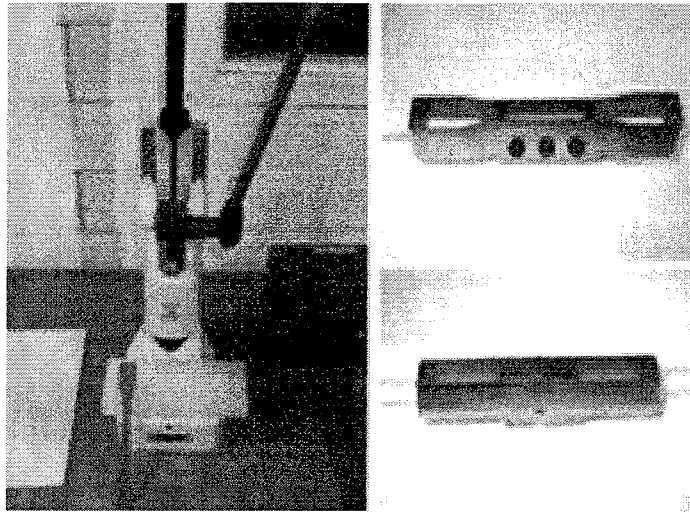


Figure 14: Toggle Press (left) and ASTM D638 and D790 Dies (right)

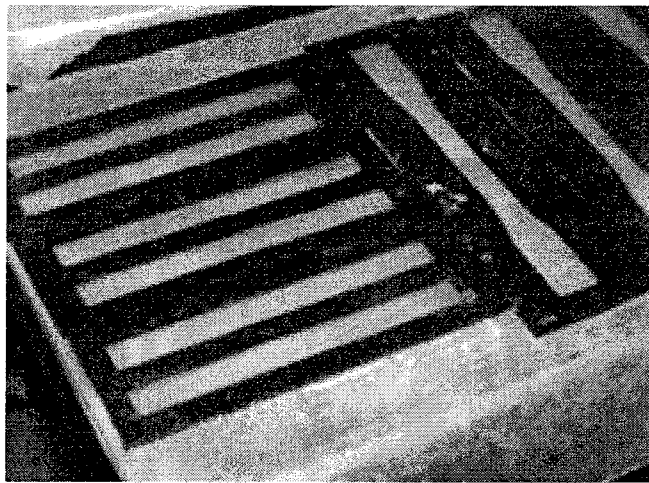


Figure 15: Sample Prepared by Pouring Resin in Rubber Mold

All specimens were kept at room temperature (77° F) for 24 hours for initial setting. When hardened to a point where dimensional stability was achieved, the specimens were removed from the wax paper and placed on aluminum foil for fifteen (15) days to achieve full cure (see Figure 16 and Figure 17).

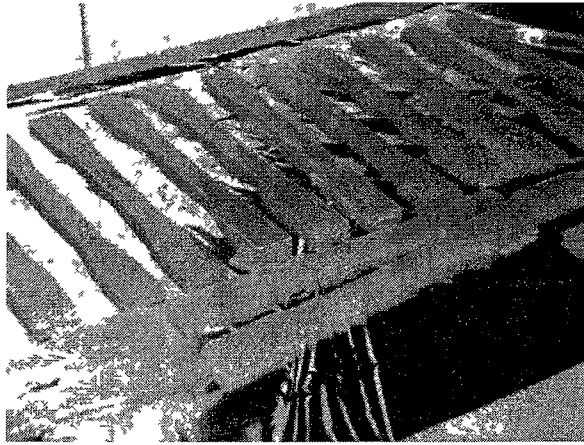


Figure 16: ASTM D638 Specimens on Aluminum Foil

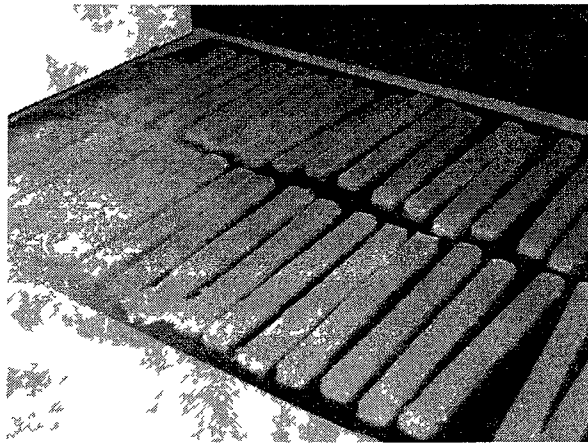


Figure 17: ASTM D790 Specimens on Aluminum Foil

Following the mentioned procedures, a total of 1,890 specimens were prepared as part of Phase I of the research program. Of these, 1,680 specimens were subjected to thermal cyclic loading and the remaining 210 specimens were used as controls (i.e., provide baseline strength values at room temperature). Table 6 and Table 7 list the total number of specimens prepared for ASTM D638 and ASTM D790 respectively for each resin type along with the test duration and number of thermal load cycles.

Table 6: Number of ASTM D638 Specimens Prepared for Test

Product	Thermal treatment period, number of loading cycles and number of specimens for each test period									Number of Specimens	
	0-d*	7-d	14-d	28-d	2-m	3-m	4-m	5-m	6-m		
	0	21	42	84	180	270	360	450	540		
Type-A**	14	14	14	14	14	14	14	14	14	14	126
Type-B	30	30	30	30	30	30	30	30	30	30	270
Type-C	30	30	30	30	30	30	30	30	30	30	270
Type-D	30	30	30	30	30	30	30	30	30	30	270
Total										936	

Table 7: Number of ASTM D790 Specimens Prepared for Test

Product	Thermal treatment period, number of loading cycles and number of specimens for each test period									Number of Specimens	
	0-d*	7-d	14-d	28-d	2-m	3-m	4-m	5-m	6-m		
	0	21	42	84	180	270	360	450	540		
Type-A**	16	16	16	16	16	16	16	16	16	16	144
Type-B	30	30	30	30	30	30	30	30	30	30	270
Type-C	30	30	30	30	30	30	30	30	30	30	270
Type-D	30	30	30	30	30	30	30	30	30	30	270
Total										954	

* The specimens were kept in room temperature;

** Limited numbers of panels were available.

3.3 Testing Program - ASTM D638 and ASTM D790

Following the curing stage, the specimens were immersed in an inert heat transfer medium (peanut oil), in a manner such that they were isolated from each other as well as from the walls of the pan (see Figure 18). Peanut oil was selected as a heat transfer medium due to its high boiling temperature (440° F), which eliminates evaporation related issues, and the fact that it does not interact with the resins.

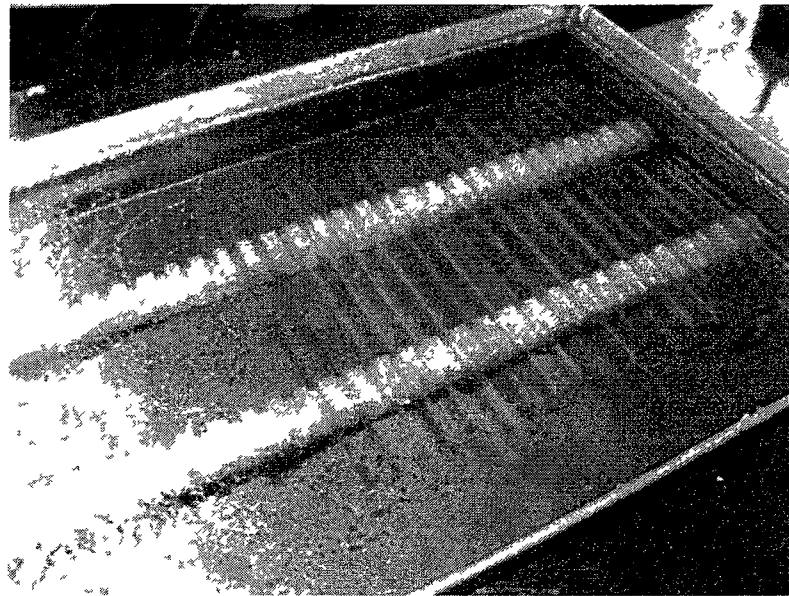


Figure 18: ASTM D638 Specimens Immersed in Heat Transfer Medium

The cyclic thermal loading was applied by placing the pans in two 7.0 cft programmable ovens (see Figure 19), each capable of accommodating eight pans at a time, each pan containing 30 specimens. The ovens were programmed to follow a uniform temperature cycle, where a 4-hour period at a temperature of 212° F was followed by a 4-hour period at 90° F, and vice versa. Thus, the specimens were thermally treated following the schedule given in Table 8 and Table 9.

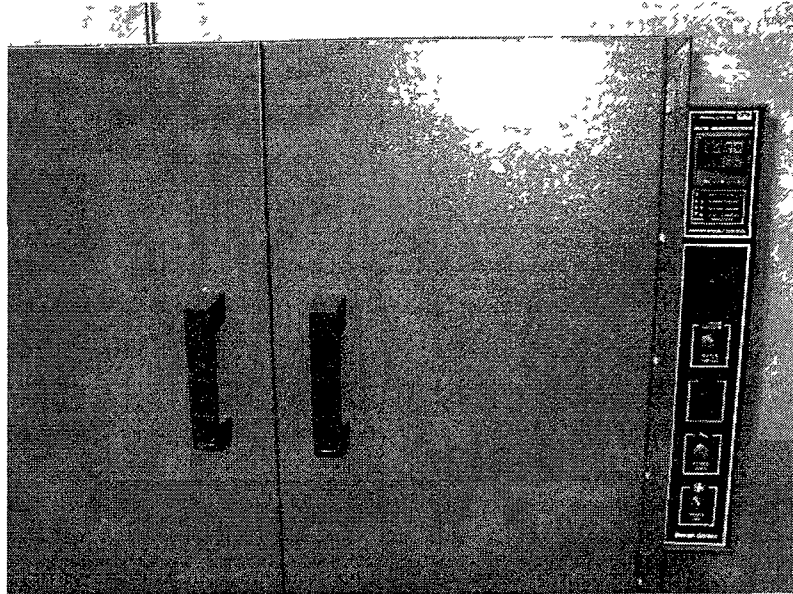


Figure 19: Programmable Oven

Table 8: Thermal Treatment Schedule for Oven – 1

OVEN 1											
Start	Type - A		Type - B		Type - C		Type-D		Total	End	Period
	638	790	638	790	638	790	638	790			
11/12/08	14	16	15	15	15	15	15	15	120	11/19/08	7-d
11/12/08	14	16	15	15	15	15	15	15	120	11/26/08	14-d
11/19/08	14	16	15	15	15	15	15	15	120	5/19/09	6-m
11/26/08	14	16	15	15	15	15	15	15	120	4/26/09	5-m
4/27/09			15	15	15	15	15	15	90	5/4/09	7-d
5/4/09			15	15	15	15	15	15	90	5/18/09	14-d
5/19/09			15	15	15	15	15	15	90	11/19/09	6-m
5/19/09			15	15	15	15	15	15	90	10/19/09	5-m
Total									840		

Table 9: Thermal Treatment Schedule for Oven – 2

OVEN 2											
Start	Type - A		Type - B		Type - C		Type-D		Total	End	Period
	638	790	638	790	638	790	638	790			
12/12/08	14	16	15	15	15	15	15	15	120	3/12/09	3-m
12/12/08	14	16	15	15	15	15	15	15	120	4/12/09	4-m
3/12/09	14	16	15	15	15	15	15	15	120	4/12/09	28-d
4/12/09	14	16	15	15	15	15	15	15	120	6/12/09	2-m
5/12/09			15	15	15	15	15	15	90	9/12/09	4-m
6/12/09			15	15	15	15	15	15	90	8/12/09	2-m
8/12/09			15	15	15	15	15	15	90	11/12/09	3-m
8/12/09			15	15	15	15	15	15	90	9/12/09	28-d
Total									840		

After the thermal treatment, the specimens were kept at room temperature for a minimum of 24 hrs before being subjected to testing as per ASTM D638 and ASTM D790. Tests were conducted using a 2,500 lb capacity universal testing machine (ADMET eXperT 2611) equipped with servo-control and pneumatic grips (see Figure 20 and Figure 21). The testing unit is accurate to $\pm 1\%$ of the peak load. Pneumatic grips were used to prevent slippage of the specimens during the uniaxial tensile (ASTM D638) test. ASTM D638 and ASTM D790 support conditions are shown in Figure 22 and Figure 23. Based on the measured values, the moduli of elasticity (tensile or bending, depending on the test conducted) were calculated for each specimen.

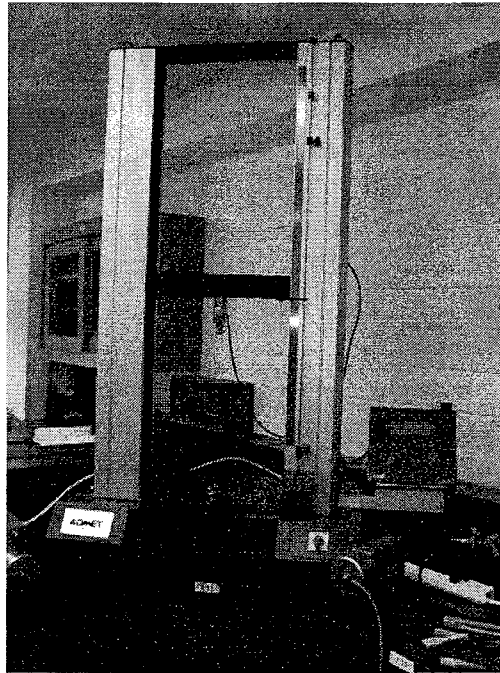


Figure 20: ADMET eXperT 2611 Universal Testing Machine

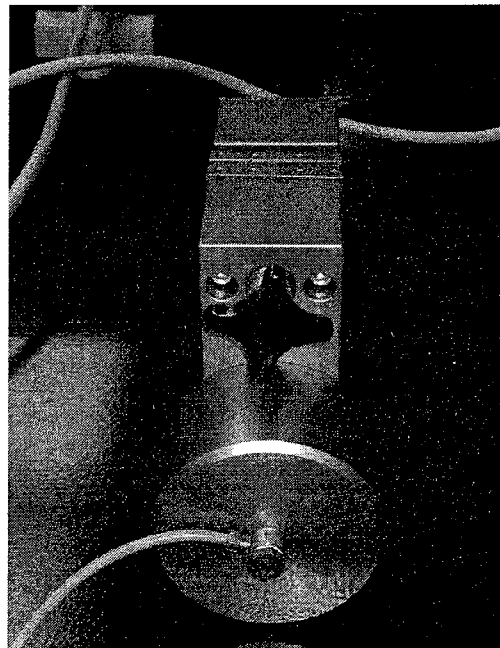


Figure 21: Pneumatic Grip for ASTM D638 Test

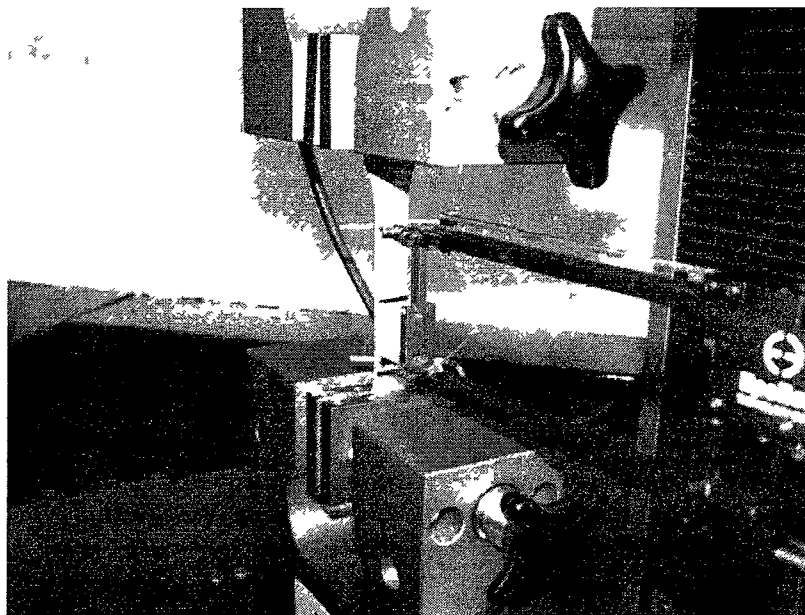


Figure 22: ASTM D638 Test Setup

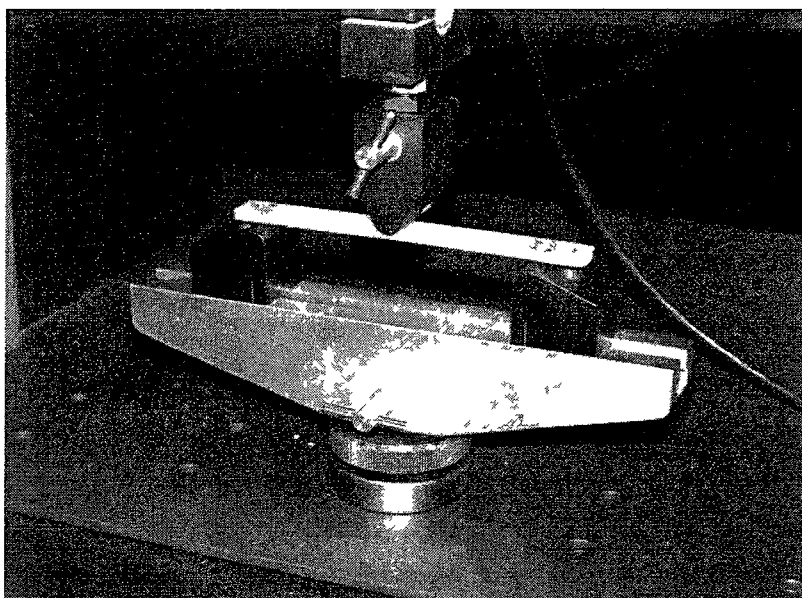


Figure 23: ASTM D790 Test Setup

3.4 Results of ASTM D638 and ASTM D790

3.4.1 ASTM D638

The measured tensile modulus of elasticity, E_T , was plotted for each resin type as a function of the number of thermal loading cycles (each cycle lasted 8 hours: 4 hours at 90° F and 4 hours at 212° F). In total, 3,894 thermal loading cycles were implemented, with individual specimens subjected to up to 540 thermal loading cycles over a six month period. The tensile modulus of elasticity, E_T , as a function of the number of thermal loading cycles for the various neat resins, are shown from Figure 24 to Figure 27.

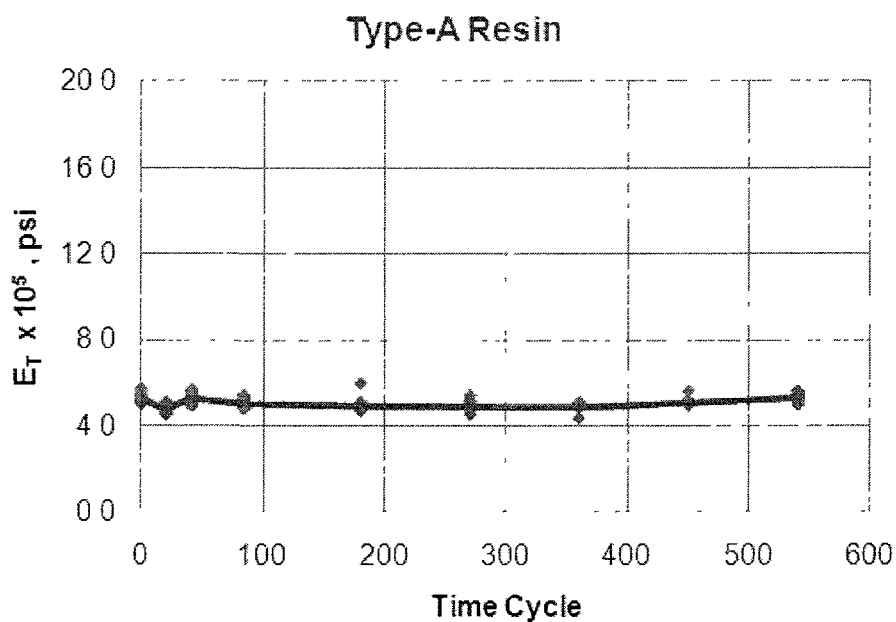


Figure 24: Tensile Modulus of Elasticity, E_T , Vs. Time Cycles for Resin Type-A

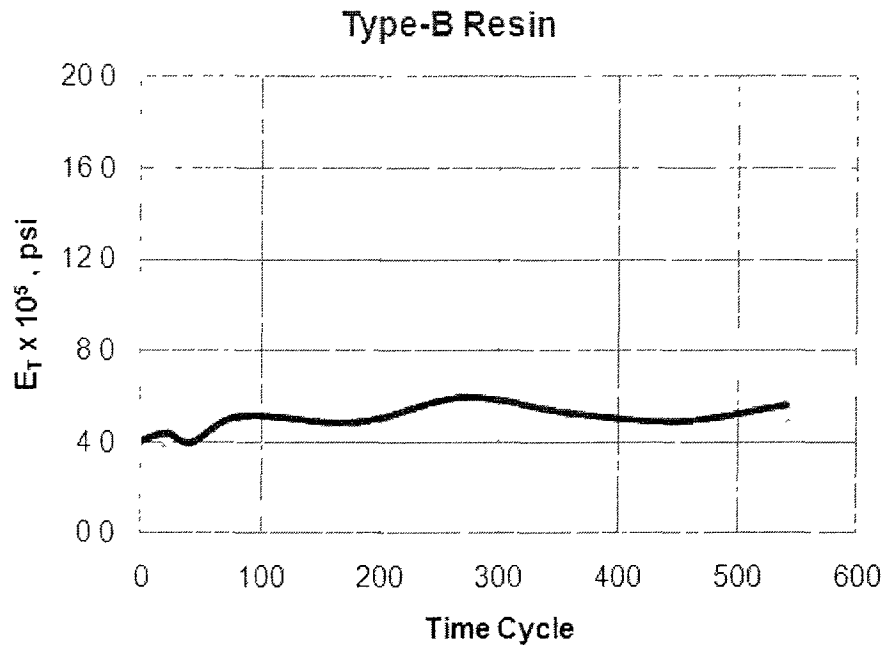


Figure 25: Tensile Modulus of Elasticity, E_T , Vs. Time Cycles for Resin Type-B

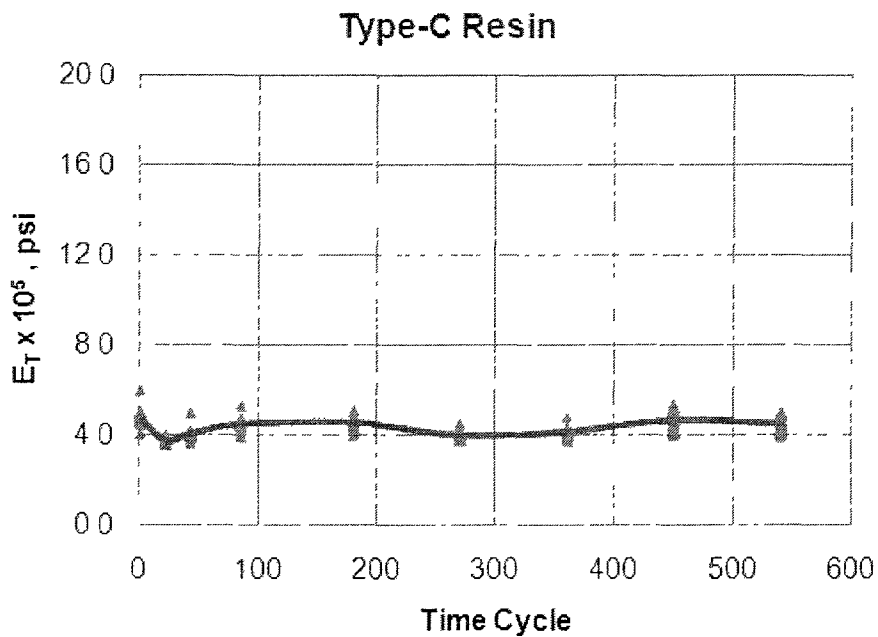


Figure 26: Tensile Modulus of Elasticity, E_T , Vs. Time Cycles for Resin Type-C

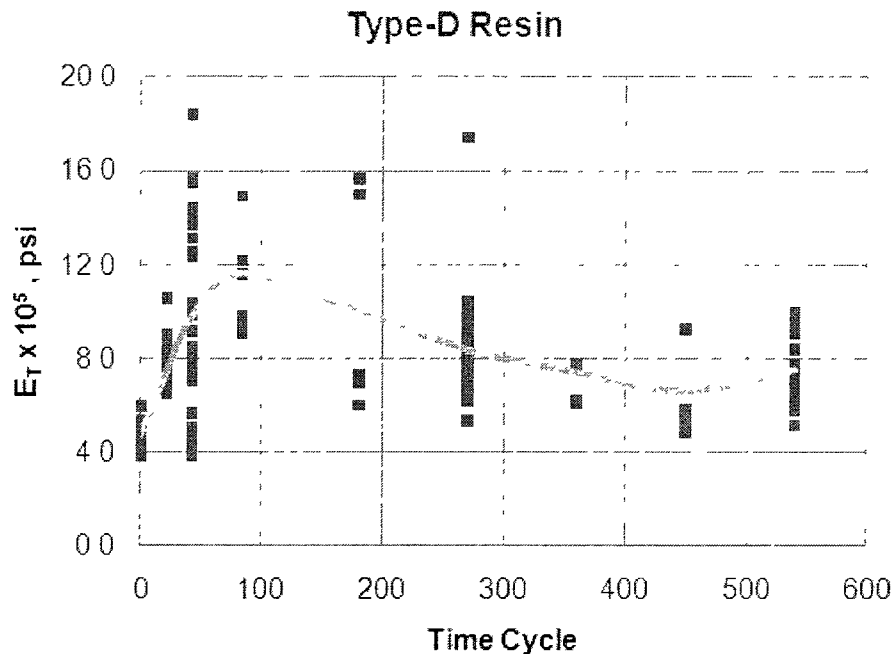


Figure 27: Tensile Modulus of Elasticity, E_T , Vs. Time Cycles for Resin Type-D

It can be seen that the tensile modulus of elasticity of Type-A resin is nearly unaffected by the repetitive exposure to elevated temperature. The test data for Type-B are somewhat scattered, indicating changes in the mechanical characteristics of Type-B resin with increased exposure to cyclic thermal loading. The results for Type-C resin show overall the tensile elastic modulus (or ‘stiffness’) of the material to be nearly independent of the number of thermal cyclic loads, suggesting that the mechanical characteristic of Type-C resin are not altered significantly when exposed to intermittent elevated temperature. Type-D resin data suggest that the tensile modulus of elasticity of this resin changes dramatically upon exposure to as little as 25 thermal load cycles. When subjected to 180 or more thermal load cycles, the neat resin becomes highly brittle. As many as 30 specimens were tested at each testing mile stone for each resin, giving significant statistical credibility to the results presented in Figure 25 and Figure 27. The tensile

modulus of elasticity for Type-A appears to be independent of the number of thermal load cycles, demonstrating high resistance to thermal loading. Type-D becomes highly brittle, resulting in a significant increase in the value of modulus of elasticity. Type-B and Type-C resins exhibited similar performance; however, the elastic modulus values for Type-C appear to fluctuate less over the duration of the test, implying a slightly higher stability under cyclic thermal loads.

A summary of ASTM D638 test data for all four resin materials is given in Table 10 to Table 13. For each series of tests, arithmetic mean, standard deviation, and percent deviation (standard deviation divided by the arithmetic mean) were calculated. Consistency in the performance of the resin material under elevated temperature is reciprocal to the percent deviation. It can be seen that for resin Type-A, percent deviation values are consistently around 4%. On the other hand, percent deviation values computed for Type-D are as high as 48%, indicating the unstable behavior of the material.

Table 10: Summary of ASTM D638 Test on Neat Resin Type-A

Time Cycle	Mean Tensile Modulus of Elasticity, E_T psi	Standard Deviation	% Deviation
0	532410.2	23380.5	4.4
21	481418.7	19942.8	4.1
42	525857.5	25315.2	4.8
84	506111.9	18876.2	3.7
180	494374.7	31552.0	6.4
270	491033.1	24254.5	4.9
360	488398.6	17524.6	3.6
450	509595.9	16436.8	3.2
540	533725.8	21956.5	4.1

Table 11: Summary of ASTM D638 Test on Neat Resin Type-B

Time Cycle	Mean Tensile Modulus of Elasticity, E_T psi	Standard Deviation	% Deviation
0	402956.1	29170.5	7.2
21	437253.0	30162.8	6.9
42	395780.2	29067.7	7.3
84	515078.9	46689.7	9.1
180	485223.9	34230.9	7.1
270	598368.1	35664.0	5.9
360	527451.6	34766.2	6.6
450	489945.4	39425.7	8.1
540	562231.5	37353.1	6.6

Table 12: Summary of ASTM D638 Test on Neat Resin Type-C

Time Cycle	Mean Tensile Modulus of Elasticity, E_T psi	Standard Deviation	% Deviation
0	479267.6	33968.1	7.1
21	380228.9	12637.9	3.3
42	408747.9	20391.4	5.0
84	451631.9	24487.9	5.4
180	458793.1	23410.4	5.1
270	404410.1	11050.9	2.7
360	418886.9	17561.3	4.2
450	468788.3	45481.6	9.7
540	452174.4	34792.9	7.7

Table 13: Summary of ASTM D638 Test on Neat Resin Type-D

Time Cycle	Mean Tensile Modulus of Elasticity, E_T psi	Standard Deviation	% Deviation
0	471636.7	46383.3	9.8
21	750811.5	95342.1	12.7
42	985136.2	379179.4	38.5
84	1169573.9	247588.4	21.2
180	1004284.4	488556.8	48.6
270	837080.4	233949.5	27.9
360	738445.5	153632.0	20.8
450	661045.0	184827.7	27.9
540	753785.6	153228.1	20.3

3.4.2 ASTM D790

The bending modulus of elasticity, E_B , as a function of the number of thermal loading cycles for the various neat resins is shown from Figure 28 to Figure 31. Summary of the test results are presented from Table 14 to Table 17. For each series of test, the arithmetic mean, standard deviation, and percent deviation were calculated as before.

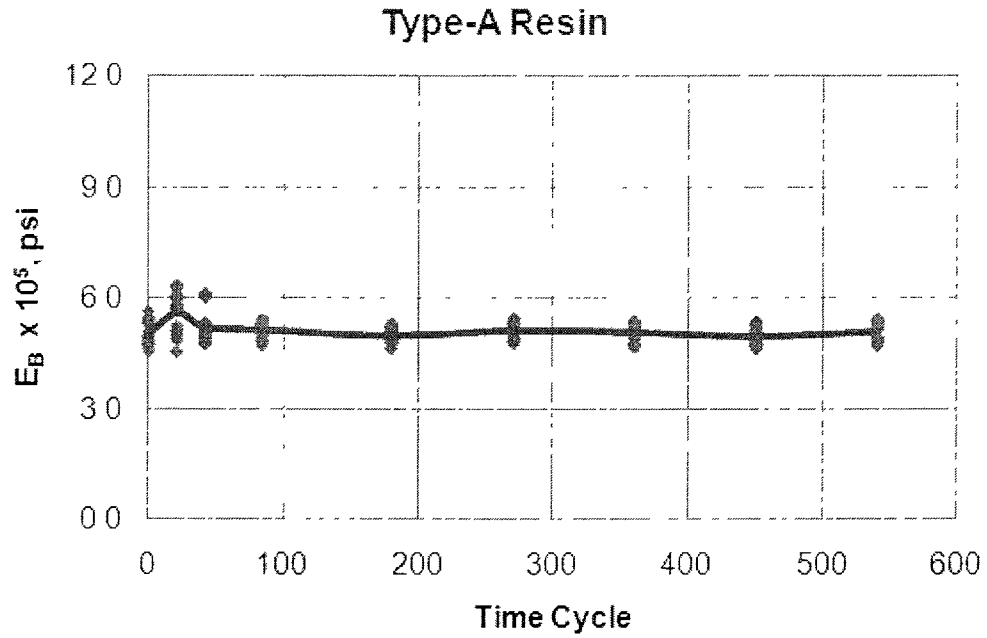


Figure 28: Bending Modulus of Elasticity, E_B , Vs. Time Cycles for Resin Type-A

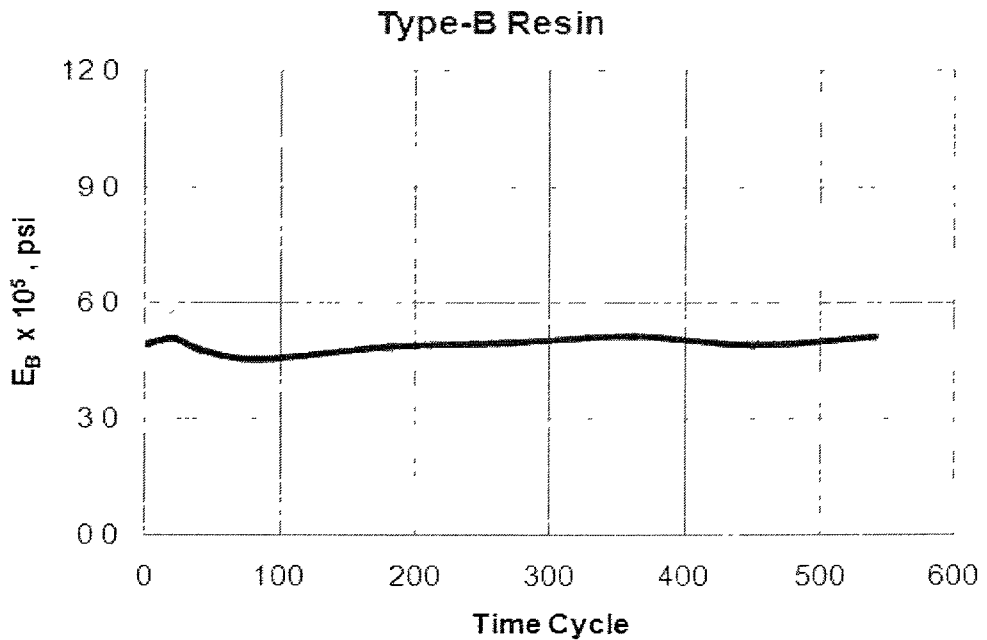


Figure 29: Bending Modulus of Elasticity, E_B , Vs. Time Cycles for Resin Type-B

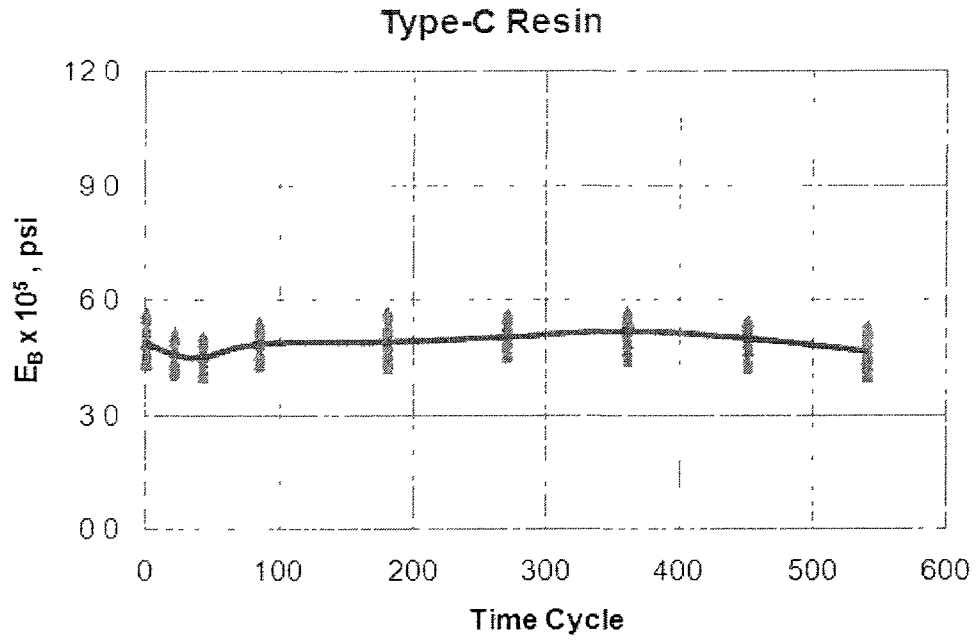


Figure 30: Bending Modulus of Elasticity, E_B , Vs. Time Cycles for Resin Type-C

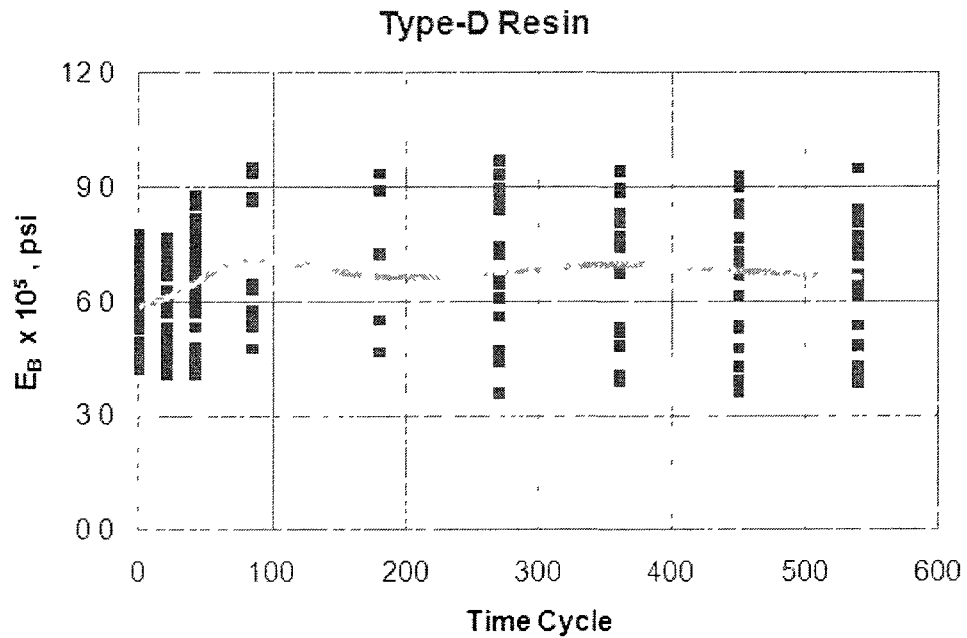


Figure 31: Bending Modulus of Elasticity, E_B , Vs. Time Cycles for Resin Type-D

Table 14: Summary of ASTM D790 Test on Neat Resin Type-A

Time Cycle	Mean Bending Modulus of Elasticity, E_T psi	Standard Deviation	% Deviation
0	505028.3	33531.4	6.6
21	562495.4	56753.5	10.1
42	522083.2	47135.7	9.0
84	515212.7	22825.9	4.4
180	499314.6	20580.1	4.1
270	513692.9	21836.2	4.3
360	508507.7	24737.0	4.9
450	496895.7	26556.5	5.3
540	510594.9	26307.6	5.2

Table 15: Summary of ASTM D790 Test on Neat Resin Type-B

Time Cycle	Mean Bending Modulus of Elasticity, E_T psi	Standard Deviation	% Deviation
0	491252.7	21211.7	4.3
21	406941.6	52414.6	10.3
42	475767.9	35465.4	7.5
84	452163.0	35803.9	7.9
180	485224.0	34230.9	7.1
270	495661.9	38745.6	7.8
360	512961.3	41803.8	8.2
450	489945.4	39425.7	8.1
540	511385.4	39047.6	7.6

Table 16: Summary of ASTM D790 Test on Neat Resin Type-C

Time Cycle	Mean Bending Modulus of Elasticity, E_T psi	Standard Deviation	% Deviation
0	491743.1	44445.5	9.0
21	458659.0	37768.0	8.2
42	451653.8	38782.4	8.6
84	487929.4	36821.3	7.6
180	492962.3	43992.0	8.9
270	505871.6	36269.7	7.2
360	522758.2	38454.1	7.3
450	502613.8	42348.1	8.4
540	467968.0	44352.9	9.5

Table 17: Summary of ASTM D790 Test on Neat Resin Type-D

Time Cycle	Mean Bending Modulus of Elasticity, E_T psi	Standard Deviation	% Deviation
0	585721.4	114887.2	19.6
21	610793.6	117161.9	19.2
42	649367.1	116096.2	17.9
84	715207.0	174549.3	24.4
180	664295.6	179445.3	27.0
270	675294.9	207085.9	30.7
360	697908.6	176256.6	25.3
450	679504.7	175866.3	25.9
540	661807.1	151095.5	22.8

The results for Type-A were found to be nearly independent of the number of cyclic thermal loads, suggesting high stability of the resin when exposed to intermittent elevated temperature over a prolonged period of time. For both Type-B and Type-C, some variability was noticed when the resins were exposed to elevated temperature. As for Type-D, the measured values of the bending modulus of elasticity became highly inconsistent, with variations of nearly 100% in the measured values of E_B within the same batch.

3.5 Creep Test – ASTM D2990

Both tensile and flexural creep test was performed on specimen prepared using resin Type-A and Type-C. For both resins, ASTM D790 and ASTM D638 samples were prepared by cutting the panels using the water jet cutter. For resin Type-A, the panel was supplied by the vendor where as for the other resin type the panel was prepared from raw resin. There were two apparatus: one for tensile creep and the other for flexure creep. Next, the ASTM D790 and ASTM D638 samples were placed inside the testing equipment and the temperature inside the equipment was set to 160° F.

The loading on the ASTM D790 and ASTM D638 samples were such that it does not exceed 500 psi, which is less than or around 30% of the bending stress tested under normal laboratory temperature (77° F) condition. The time schedule was 1 and 30 sec; 1, 6, 12, and 30 min; 1, 2, 5, 20, 50, 100, 200, 500, 700, and 1000 hr.

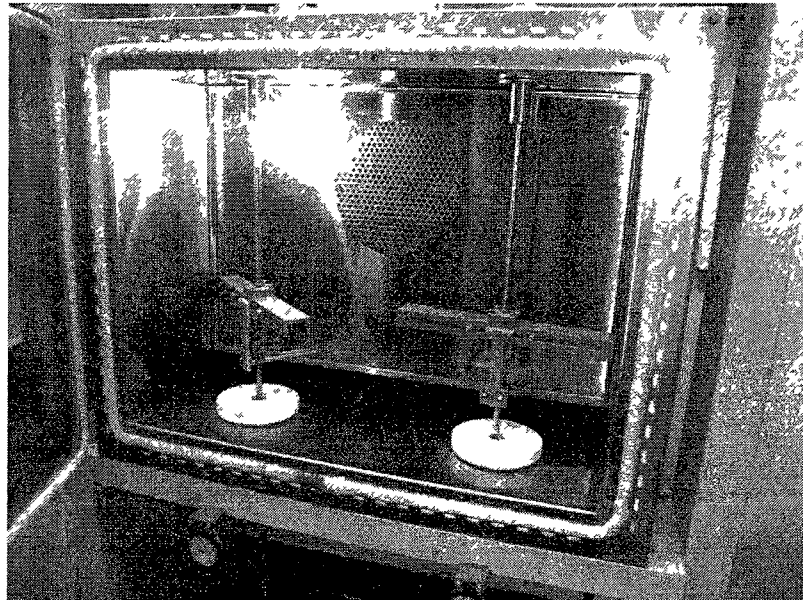


Figure 32: ASTM D2990 – Flexure Creep Test

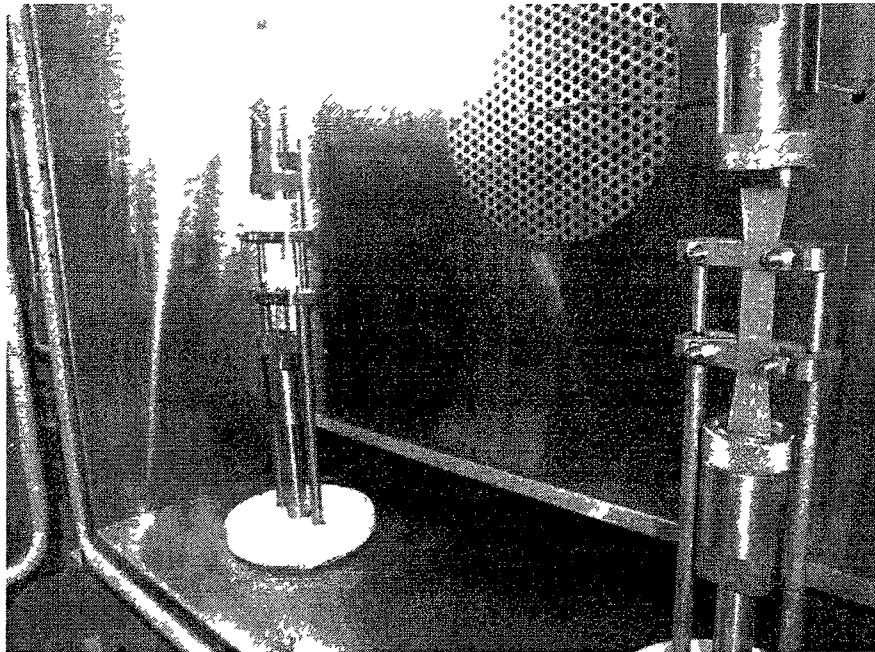


Figure 33: ASTM D2990 – Tensile Creep Test

3.6 Results of Creep Test

Creep data was collected until 100 hr. Resin Type-C failed while performing the flexural creep in around 3 minutes and displayed a maximum deflection of 0.42 in. Flexure creep plot of Type-A resin is shown in Figure 34. It was found that primary creep value for resin Type-A was around 0.16 in/in. Figure 35 shows the tensile creep plot of resin Type-A and Type-C. It was found that tensile creep of resin Type-C was more than nine times of that of resin Type-A.

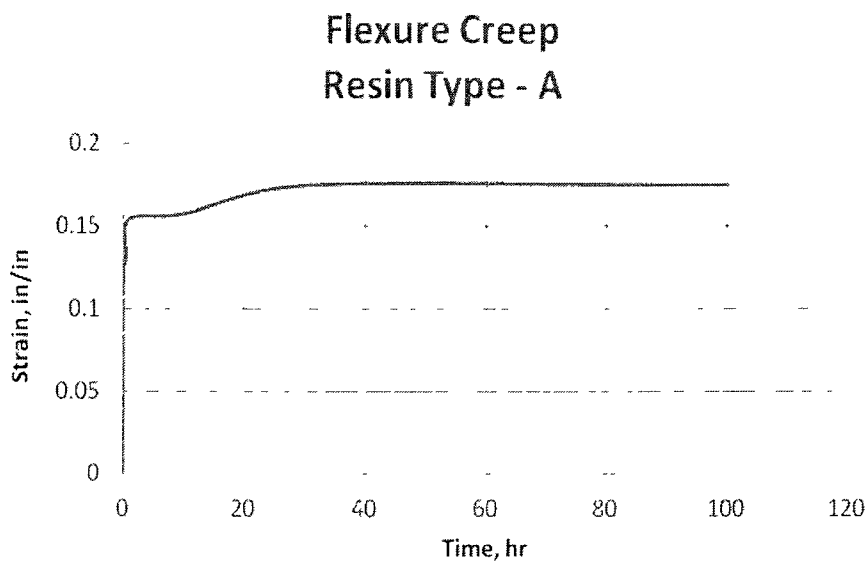


Figure 34: ASTM D2990 – Flexure Creep Data

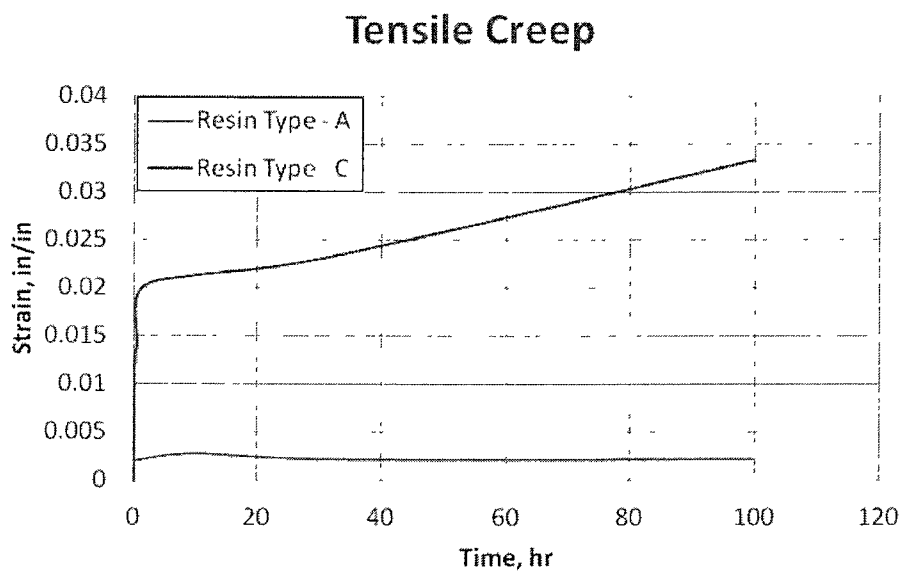


Figure 35: ASTM D2990 – Tensile Creep Data

3.7 Microscopy and Raman Spectroscopy

The utilization of microscopic and vibration-based studies is a new arena in the evaluation of CIPP liner technology, which is currently being pioneered by the researchers at LTU.

3.7.1 Microscopy

An inverted-light microscope Nikon EPIPHOT 200 (see Figure 36) was used to examine the strains in the neat resin specimens. Prior to the microscopy study, the specimens were polished using a mechanical polisher (Figure 37) to ensure a uniform surface, as well as to remove any loose particles from the surface of the specimens.

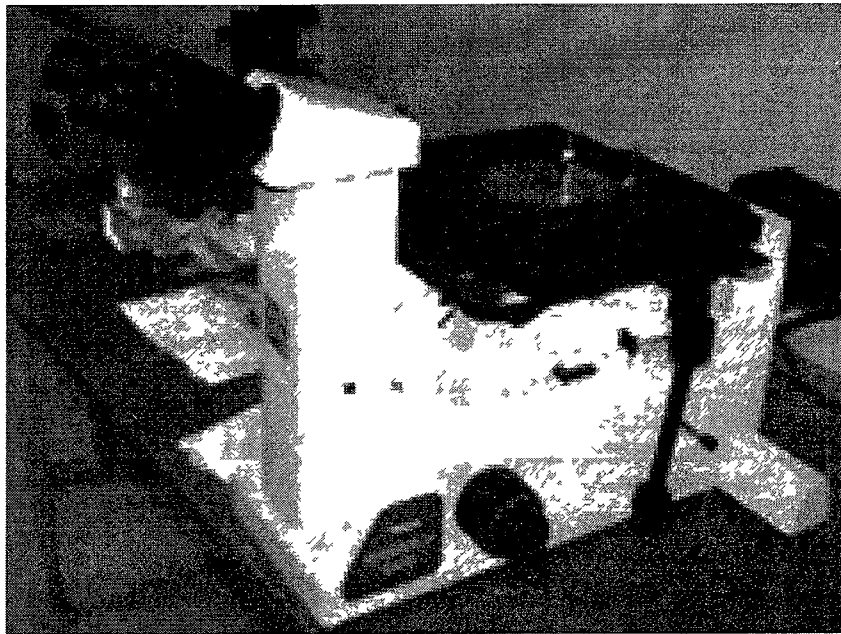


Figure 36: Nikon EPIPHOT 200

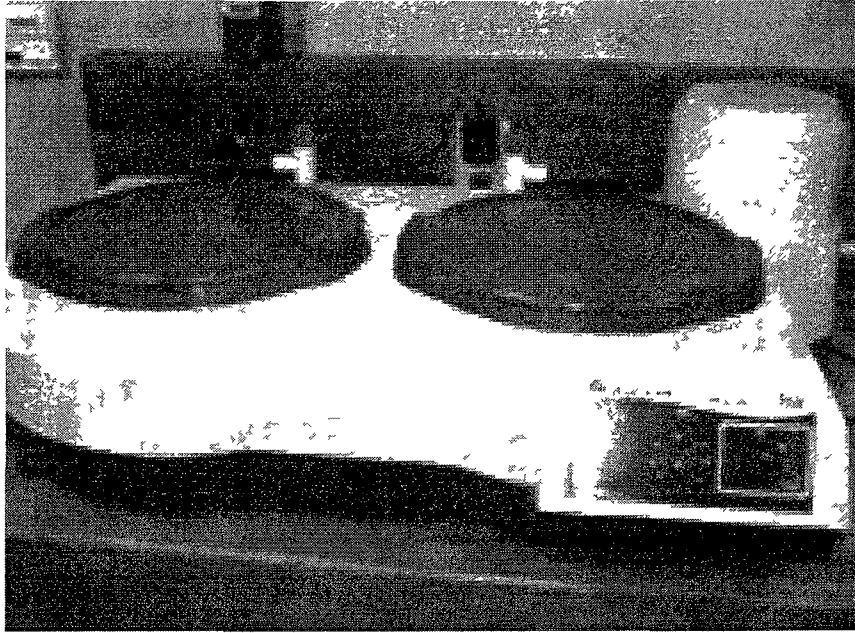


Figure 37: Laboratory Polisher

3.7.2 Raman Spectroscopy

Raman Spectroscopy is a technique based on inelastic scattering of monochromatic light, usually from a laser source. Inelastic scattering refers to change in the frequency of photons in the monochromatic light upon interaction with a sample. Photons of the laser light are absorbed by the sample and then reemitted. The frequency of the reemitted photons is shifted in comparison with the original monochromatic frequency, and a phenomenon is known as Raman Effect. This shift provides information about vibration, rotational and other low frequency transitions in the molecules, which are indicators of degradation and breakdown of the resin at its most fundamental (molecular) level.

Raman spectroscopy was used to assess the material degradation of the four resin types tested. Raman spectra can be collected from a very small surface area of the sample, so the specimens used were $\frac{1}{2}'' \times \frac{1}{2}''$. The specimens were polished using a mechanical

polisher, cleaned with distilled water and then subjected to thermal loading inside the oven in a humid environment as per the test program listed in Table 18 (see Figure 38).

Table 18: Summary of Raman Spectroscopy Test Program

Product	Thermal treatment period, number of loading cycles and number of specimens for each test period									Number of Specimens
	0-d*	7-d	14-d	28-d	2-m	3-m	4-m	5-m	6-m	
	0	21	42	84	180	270	360	450	540	
Type-A	5	5	5	5	5	5	5	5	5	45
Type-B	5	5	5	5	5	5	5	5	5	45
Type-C	5	5	5	5	5	5	5	5	5	45
Type-D	5	5	5	5	5	5	5	5	5	45
Total										180

* The specimens were kept in room temperature.



Figure 38: Specimens Inside the Oven

The thermal loading cycles lasted 8 hours each (4 hours at 90° F followed by 4 hours at 212° F). Next, the specimens were removed from the oven and placed under the Raman spectrometer as shown in Figure 39. Spectra from 200 to 2100 cm^{-1} were collected using R-3000 HR Raman spectrometer utilizing a 785 nm diode laser operating at 290 mW via a fiber optic probe. Integration time was 30 seconds.

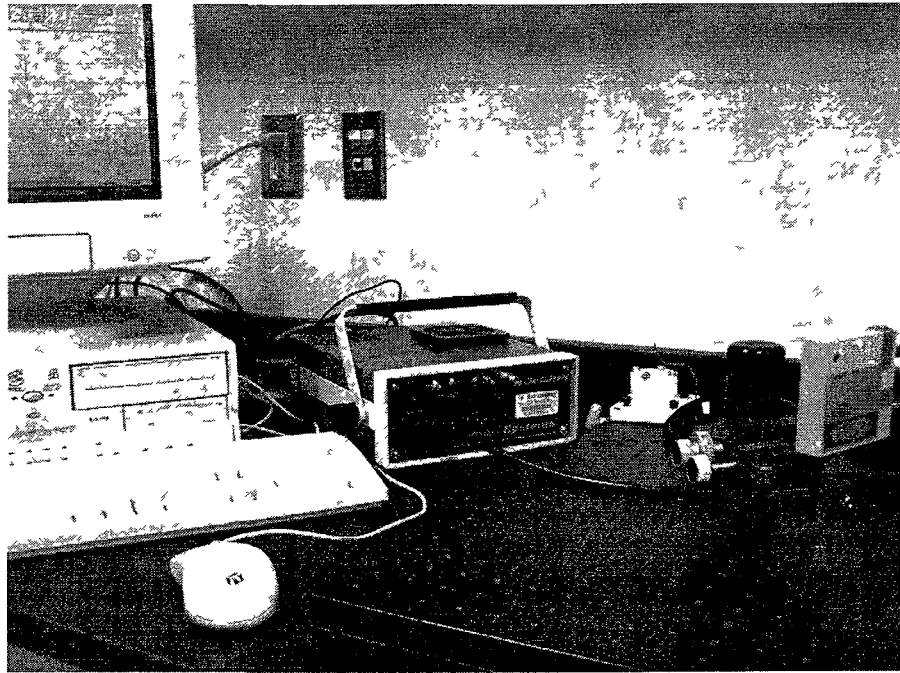
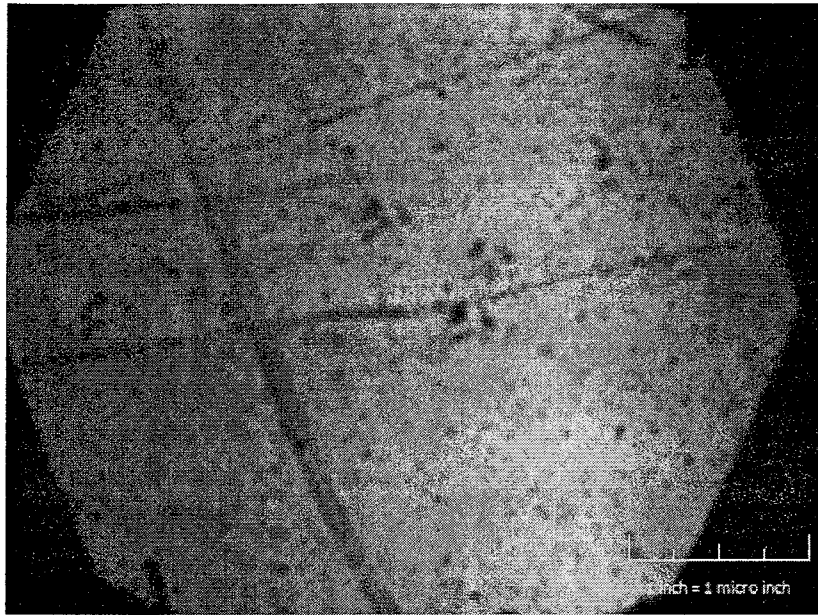


Figure 39: Raman Spectrometer

3.8 Results of Microscopy and Raman Spectroscopy

3.8.1 Results of Microscopy

Following exposure to 270 thermal load cycles, the samples were removed from the neat resin specimens and subjected to a microscopic examination. Virgin and heat-exposed resin samples were compared (Figure 40 to Figure 43). Strains induced within the resin matrix due to the thermal loading were visible in the form of stretch marks and a rougher surface. While definite conclusions could not be made due to the relatively small number of specimens examined, this was believed to be an effective qualitative approach for evaluating physical changes in the neat resin matrix due to the presence of adverse environmental loads.



**Figure 40: Images of Specimens – Before Commencement of Thermal Loading
Resin Type – A**

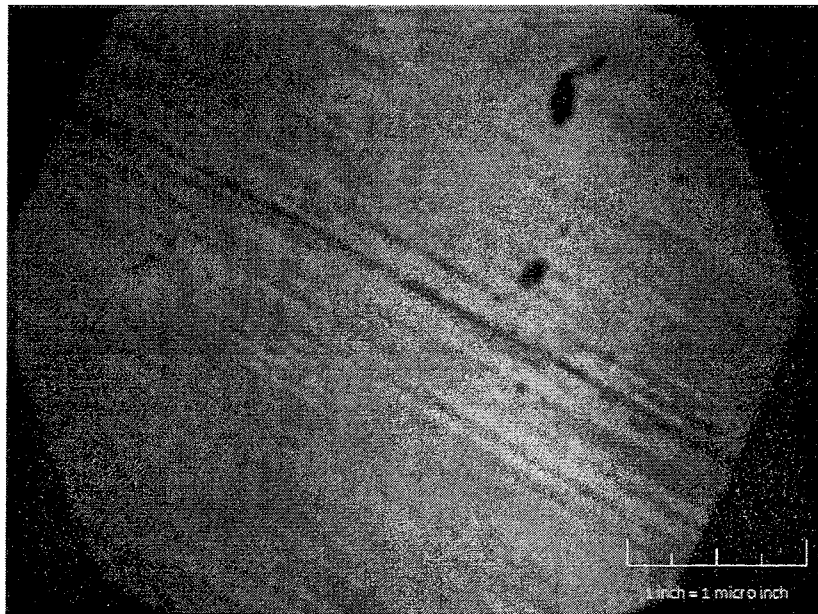


**Figure 41: Images of Specimens – Following 270 Cycles of Thermal Loading
Resin Type – A**

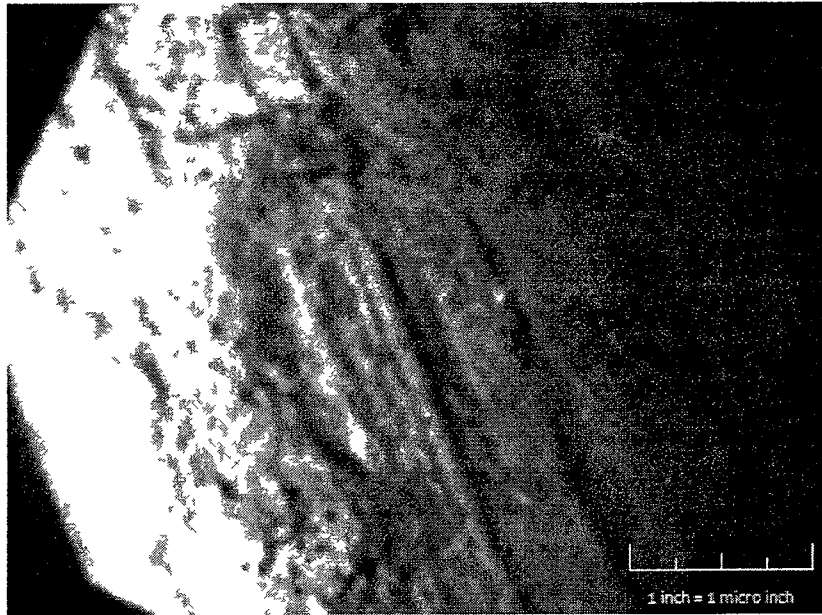


**Figure 42: Images of Specimens – Before Commencement of Thermal Loading
Resin Type – C**

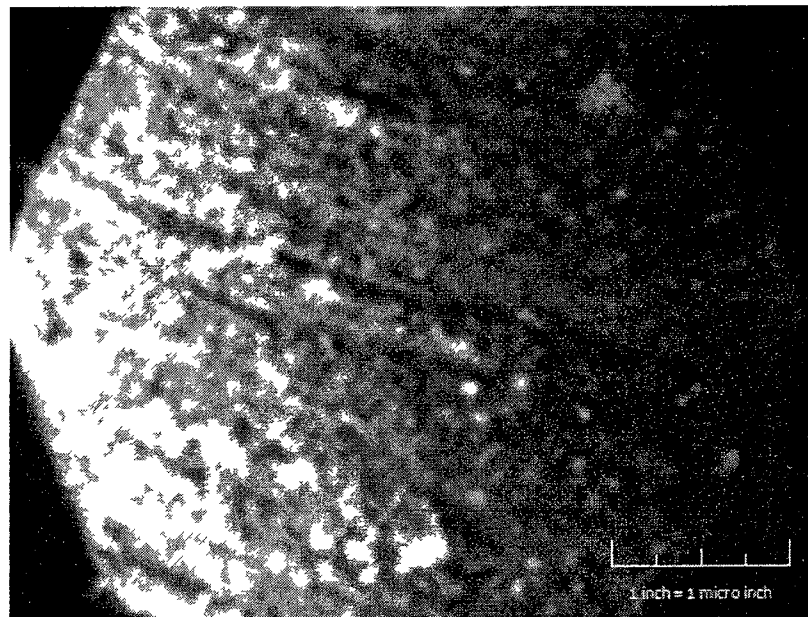


**Figure 43: Images of Specimens – Following 270 Cycles of Thermal Loading
Resin Type – C**

3.8.2 Results of Raman Spectroscopy

The measured intensity of the Raman signal in arbitrary units (a.u.) is plotted on the y-axis, while the wave length in cm^{-1} is plotted on the x-axis. The results of Raman spectroscopy (see Figure 44 and Figure 45) obtained from the specimens subjected to cyclic thermal loading over a period of four months. The last two months results were not obtained because unfortunately the specimens got mixed up.

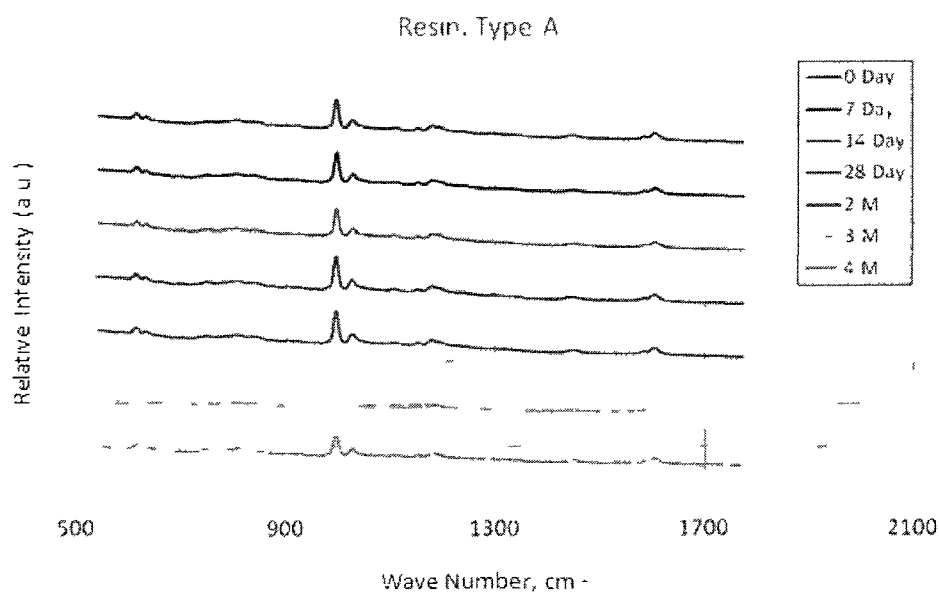


Figure 44: Raman Spectra of Type-A Resin

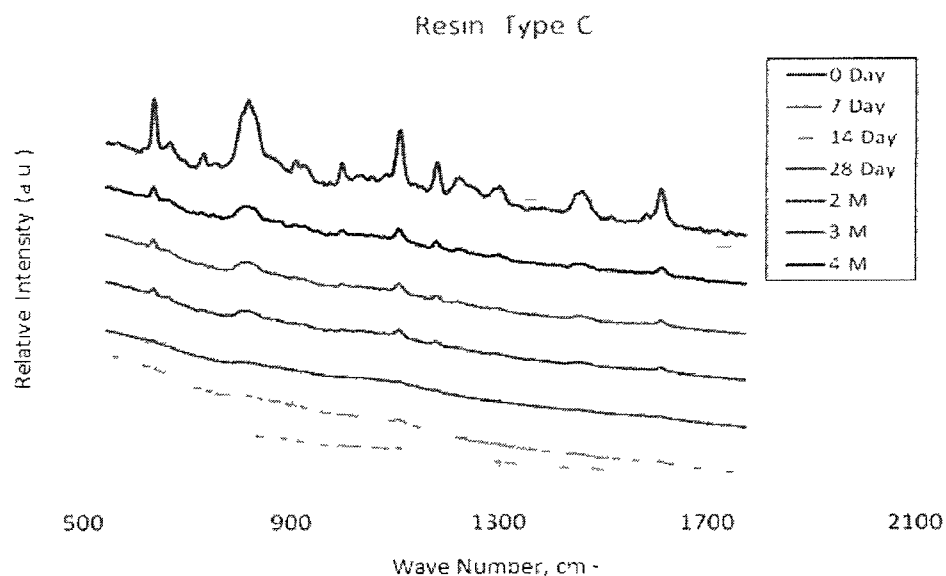


Figure 45: Raman Spectra of Type-C Resin

Overall, it was found that Type-A exhibited high chemical stability with little to no changes in the Raman signature over the testing period. Some degradation of the chemical signature of Type-C was observed over the course of the 4-month testing period. The chemical signature means that the intensity of Raman bands decreased due to degradation of polymer.

The Raman band peak intensities for Type-C resin which show a decrease under the action of cyclic elevated temperature treatment; indicating degradation of the polymer material. This phenomenon was found to be more pronounced for resin Type-B (also a vinyl ester resin but does not have high temperature application properties) and Type-D and therefore, were discontinued after 28-days.

3.9 Conclusion

The percent deviation of the moduli of elasticity (tensile and bending, determined in accordance with ASTM D638 and D790, respectively) is shown in Figure 46 and Figure 47 for the four resin types tested. It can be seen that the measured values for the Type-D resin specimens exhibited significant variations, which would suggest that the mechanical performance of this resin type deteriorates rapidly and in an uneven manner when the resin is exposed to elevated temperatures changing in an intermittent fashion between 90° F and 212° F at a frequency equal to 4 hours. These variations were attributed to the instability of the resin material when exposed to elevated temperature, leading to brittleness and premature failure. Also, higher brittleness implies higher likelihood of the resin cracking under vibration. The development of a network of micro cracks within the resin matrix can facilitate migration of water through the liner barrier (infiltration/ex-filtration) and ultimately shorten the useful service life of the liner. The other three resin types exhibited a relatively narrow band in terms of percent deviation of their tensile and bending moduli of elasticity, ranging between 5% and 10%. Thus, it might be concluded that the effect of thermal load on the mechanical properties of these resins was minimal to moderate.

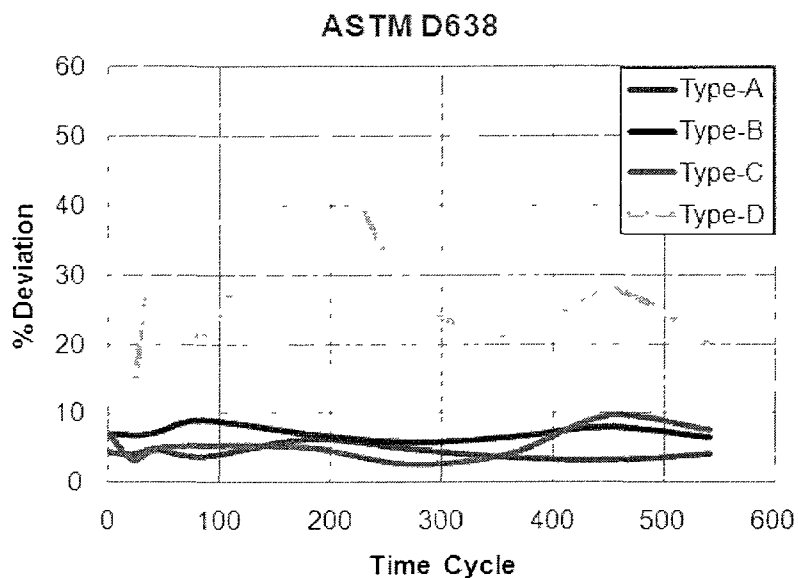


Figure 46: Percent Deviation of Tensile Modulus of Elasticity

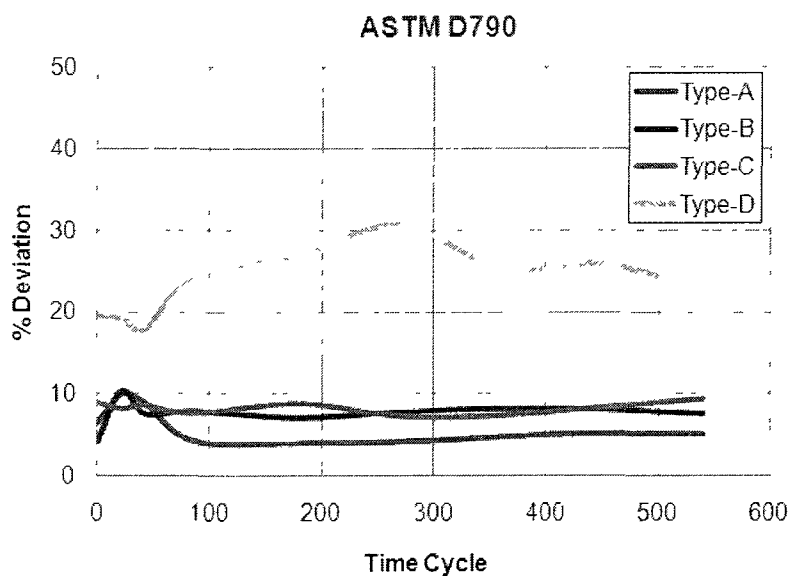


Figure 47: Percent Deviation of Bending Modulus of Elasticity

The tensile and flexural creep result also revealed that elevated temperature accelerated the degradation of the resin which is not designed for high temperature application.

Raman spectroscopy results in the context of the degradation of a neat organic polymer under the action of cyclic thermal loading. However, the fact that a correlation exists between the mechanical test results and the Raman spectroscopy test results is a positive indication that Raman spectroscopy can provide a useful insight, and potentially serves as a quantification method, for capturing the deterioration of resin materials at the molecular level under chemical or thermal loadings. The utilization of vibration-based testing could provide the engineering community with an additional insight into the deterioration mechanisms of thermosetting liners and spray-on coating systems, beyond that provided solely by destructive mechanical tests.

CHAPTER 4

FULL SCALE TESTING

4.1 Introduction

Based on the results of Phase I (Bench Scale Tests), Type-A and Type-C resins were chosen for Phase II of the testing plan. Both Type-A and Type-B are vinyl ester resins; however, the performance of Type-A was found to be slightly better. Also, Type-B and Type-C are provided by the same vendor (Pipe Lining Supply), and having products from different vendors for the final testing Phase (AOC LLC and Pipe Lining Supply) was preferred.

4.2 Testing Program

The objective of Phase II was a long-term experimental testing of full scale specimens (under three ranges of cyclic thermal loading) to assess the resistance of the CIPP liner material to thermal and buckling failure. The testing program for Phase II is summarized in Table 19.

Table 19: Test Program for Phase II

Resin Type	Number of Specimen Tubes	Temperature Cycle	Duration	Remarks
Type – A	4 – 2 for each type	110° F - 260° F	12-months	High Range
and	2 – 1 for each type	90° F - 210° F	12-months	Target Range
Type - C	2 – 1 for each type	100° F - 150° F	12-months	Control Specimen

4.2.1 Building the Custom Built Ovens

4.2.1.1 Structure of the oven

Three ovens ($L \times W \times H = 6 \text{ ft } 2 \text{ in.} \times 3 \text{ ft } 4 \text{ in.} \times 4 \text{ ft } 9 \text{ in.}$) were custom designed and built. First, the structural skeleton was designed by the researcher in the TTC, LA Tech (Appendix B). Next, based on the given design, the structural frame for each oven was built by Sabre Machining in West Monroe, LA (see Figure 48).

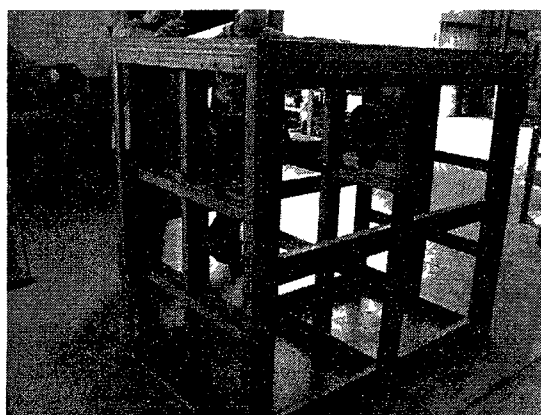


Figure 48: Steel Frame of a Custom Built Oven

Eighteen (18) gauge thick galvanized sheets were riveted on all inner sides of the frame. Fiber glass wool was then placed on the galvanized sheet and between the metal

frames. Next, the outer sides were covered with similar size galvanized sheet riveted on the steel frame. A 10" × 10" fan was attached at the top corner to ensure proper circulation of hot air inside the oven. Three ovens without electrical connections are shown in Figure 49 and Figure 50.

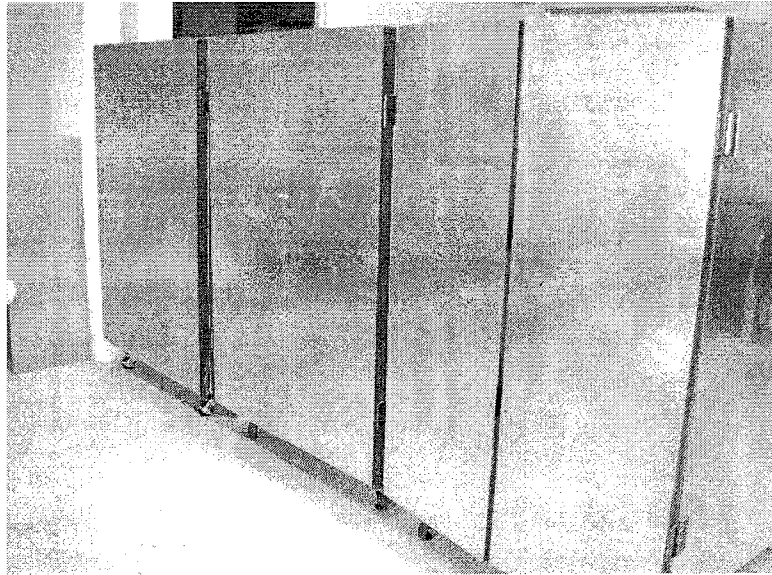


Figure 49: Front Side of Custom Built Oven

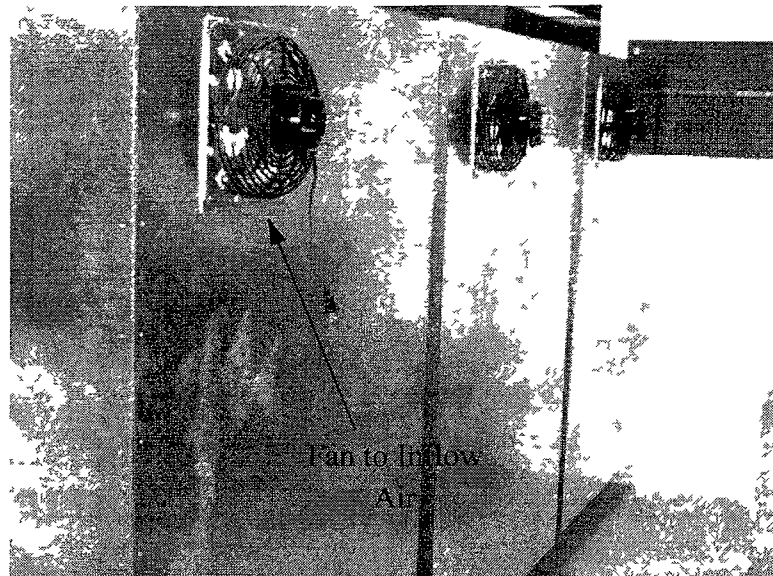


Figure 50: Rear Side of Custom Built Oven

4.2.1.2 Placing of heating elements inside the oven

Each oven was equipped with four electrical heating elements placed along the opposite diagonals on each side wall (see Figure 51). Fiberglass blankets were glued to metal sheets to form heat shields that covered the bare heating elements. This would mitigate from developing the localize heat spots on areas of the specimens adjacent to the heating elements. As hot air is lighter than the cool air and stays above the cool air, two exhaust holes were made on the rear wall of the oven at the other corner along the diagonal to circulate and force the hot air flow through the bottom part of the oven (see Figure 52).



Figure 51: Uncovered Heating Elements inside the Oven

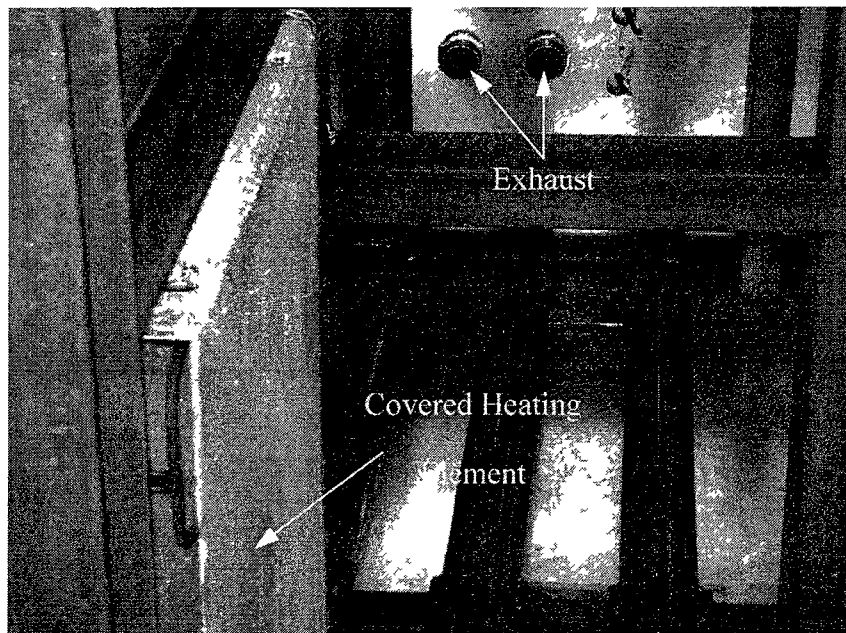


Figure 52: Covered Heating Element and Exhaust inside the Oven

4.2.1.3 Electrical circuit of the heating element

Two thermostats, connected to an electronic timer, and two relays were housed in a 12" × 12" PVC made control box (see Figure 53). The detail power circuit diagram is

given in Appendix B. The control box was mounted on the outside rear wall of the oven and thermostat sensors were placed close to the exhaust at the bottom part on each oven. The thermostats were used to establish the high and low temperature bounds for the oven. One thermostat terminated power to the heating elements when temperature exceeded the upper limit, while the second thermostat powered the heating elements when temperature in the oven dropped below a pre-set level. To monitor the temperature inside the oven, thermocouples were installed at several places inside the oven (see Figure 54).

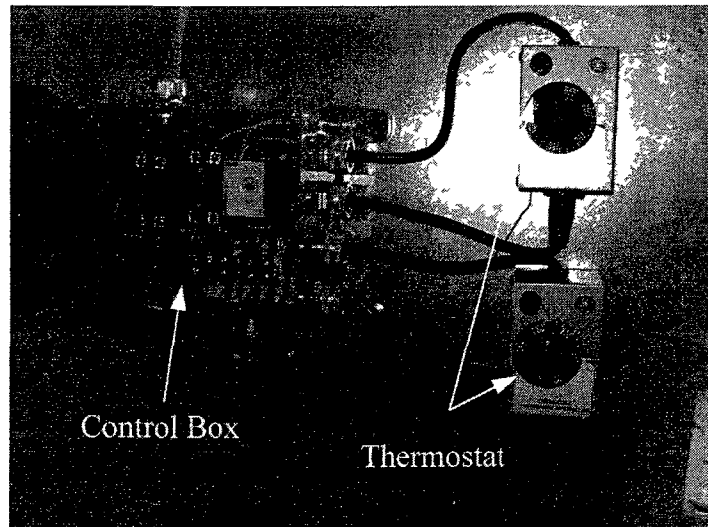


Figure 53: Power Supply Box and Two Thermostats on the Rear Wall of the Oven

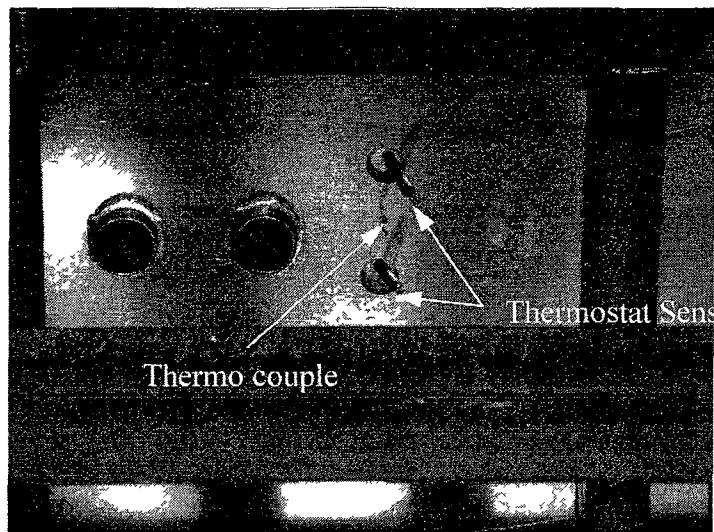


Figure 54: Thermostat Sensor and Thermocouple inside the Oven

The ovens were built in a manner that none of the full-scale specimens was adjacent to the heating elements along its entire length. Therefore, there was a temperature gradient within the pipe. This simulated the steam injection inside the sewer, where the liner section nearest to the steam injection lateral experienced higher temperature compared with the location further away, resulting in an uneven distribution of temperature along the liner. A test run was conducted to evaluate the temperature distribution inside the oven and the resulting strain gradient in the CIPP liner. Strain rosettes were installed on the crown and invert of each CIPP liner specimen, while longitudinal strain gages were installed on the liner's spring lines. The measured Temperature vs. Time and Strain vs. Time are presented in Figure 55 and Figure 56, respectively.

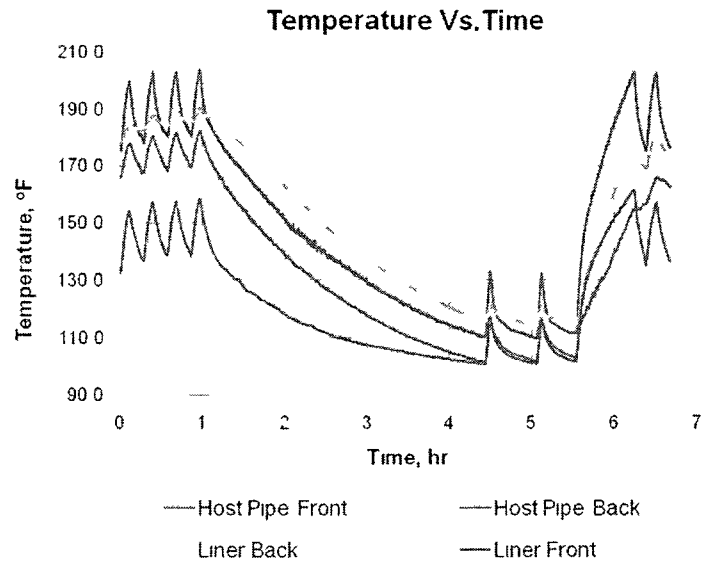


Figure 55: Test Run of the Oven for One Cycle

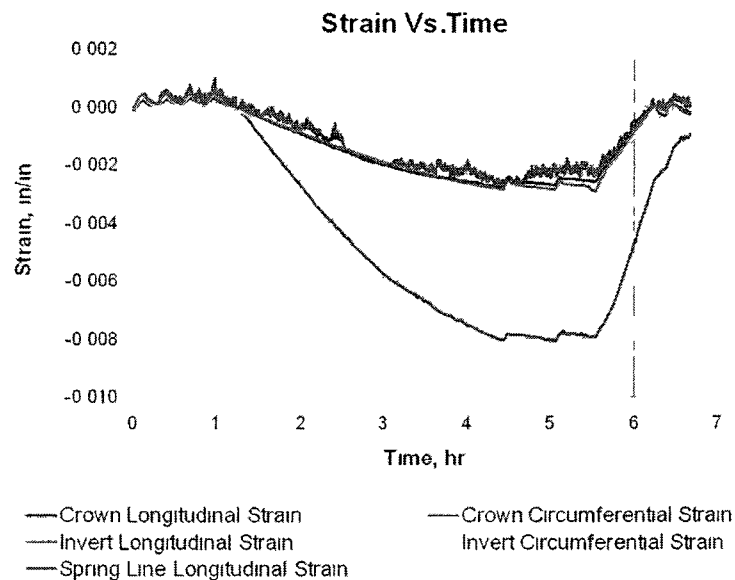


Figure 56: Strain Vs. Time

4.2.2 Preparation of the Full-Scale Specimens

Eight felt socks, each 6 ft long, 8 in. diameter, 7 mm thick, were impregnated with resin (see Figure 57 through Figure 59). Four specimens were impregnated using Type-A resin and four specimens were prepared using Type-C resin. The liners containing Type-A

resin were wetted out at the Insituform facility in McGregor, TX, while the liners containing the Type-C resin were wetted out at the TTC facility in Ruston, Louisiana, under the supervision of Mr. James Gaithner from Pipe Lining Supply, Inc., California. All liners were inverted in a mold and cured utilizing a “torpedo” inversion chamber located at the TTC research facility in Ruston, Louisiana, using hot water. The inversion and curing of the CIPP liners were performed in compliance with relevant ASTM standards. A pre-liner was used to ensure easy separation of the liner from the mold.

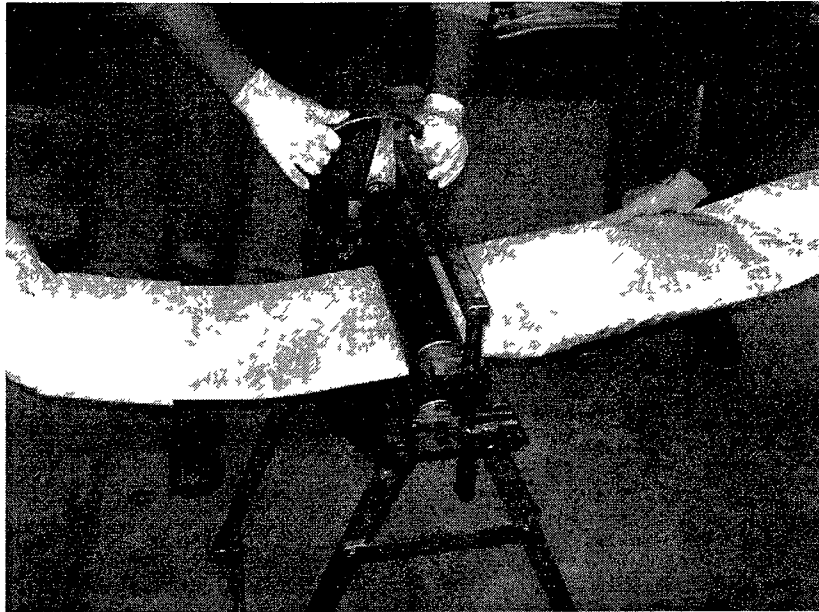


Figure 57: Liner Wet Out Process at the TTC Research Facility

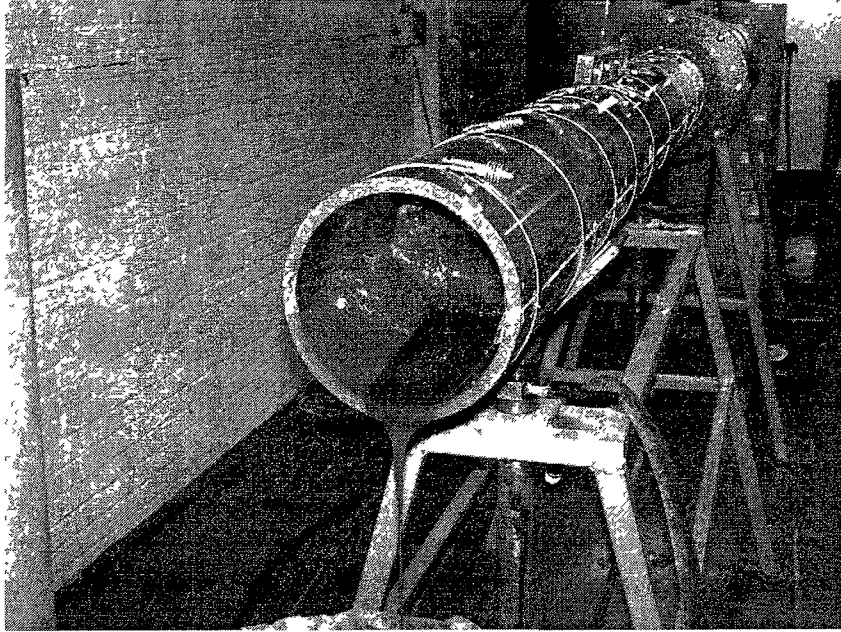


Figure 58: Inversion of the Liner inside a PVC Mold



Figure 59: The Finished Product - Cured CIPP Liner

4.2.3 Profile Plot of the Specimens Before Thermal Loading

A profile plotter (Figure 60) was developed to map any deformation accurately inside the liner due to circumferential strains and subsequent buckling. The system was

equipped with a 4” long linear variable displacement transducer (LVDT) connected to a motor-gear system that travel around the inner circumference of the liner in one minute. An HP34970A Data Acquisition system was connected to get the readings of the LVDT. Each time the LVDT reads the radial displacement the data is then converted to the Cartesian co-ordinate system, and plotted, and thus provided position information regarding the location around the pipe at which the data was taken. The starting point is always the crown and the LVDT rotates in a clock-wise direction.

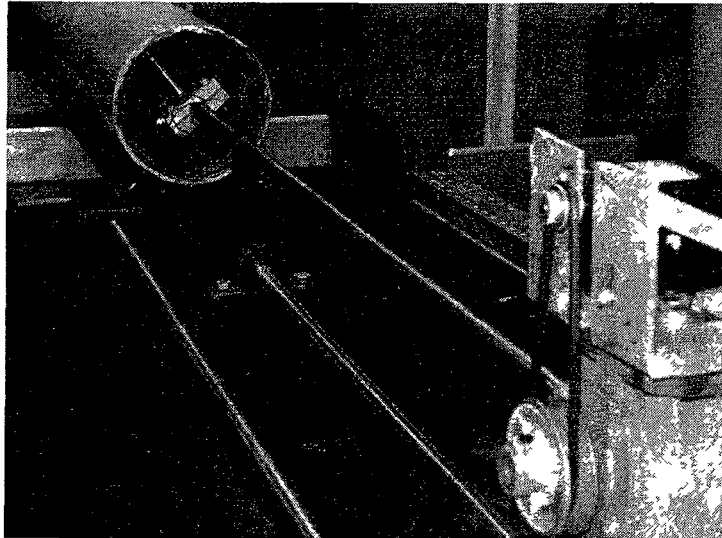


Figure 60: Profile Plotter

Detail profiling system is shown in Figure 61 and Figure 62. Readings from the LVDT were communicated to a laptop computer where they were plotted using a graphical software package, as seen in Figure 63. The term ‘Engineering-profile’ in Figure 63 refers to a perfectly circular profile, while ‘True-profile’ refers to actual inner profile of the CIPP liner. The research plan called for measuring the inner profile (‘True-profile’) of each specimen at their pre-determined locations – at center and 2” apart from center, prior

to and following the thermal cyclic load test, thus monitoring the deformation of the liner over time under thermal loadings.

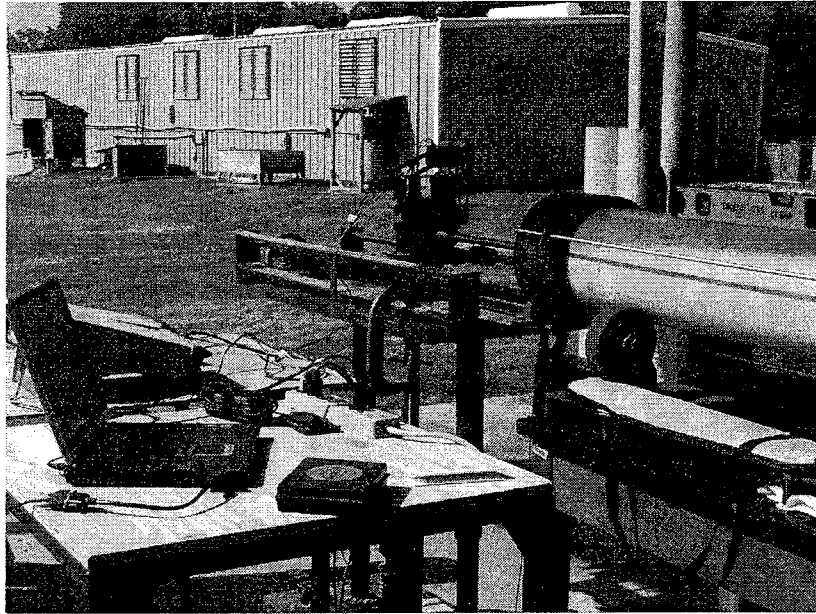


Figure 61: Profile Plotting of a Full-scale Sample

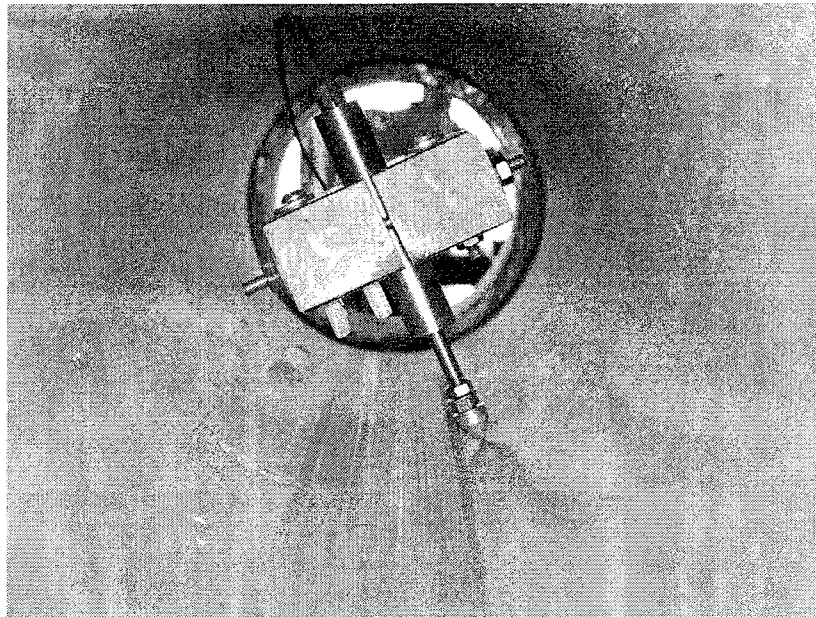


Figure 62: Profile Plotter Inside a Full-scale Sample

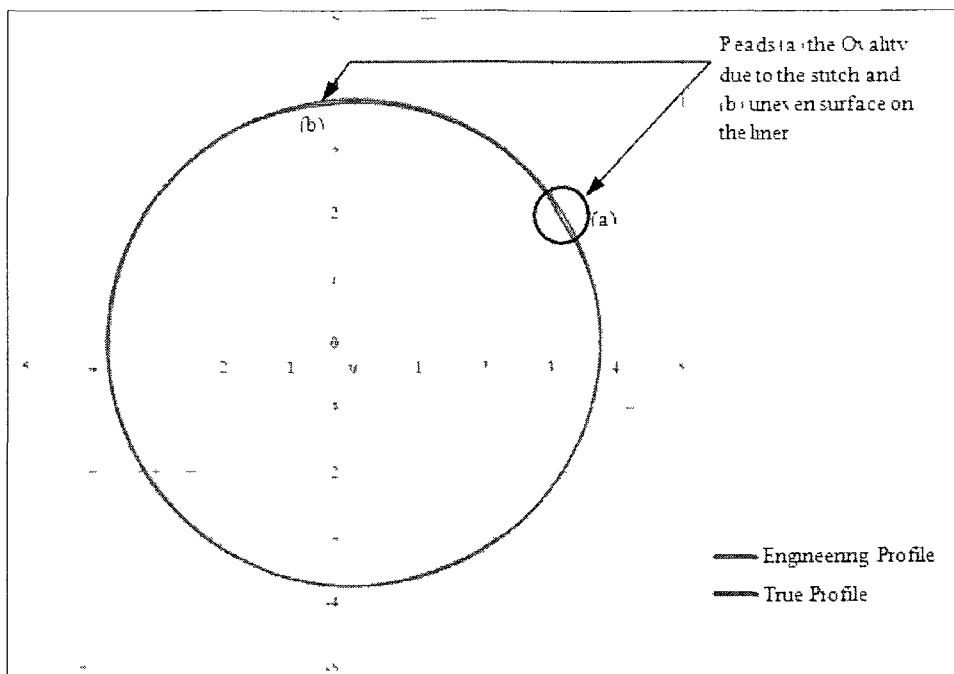


Figure 63: A Circumferential Plot Showing Ovality Due to a Stitch and Uneven Surface in the CIPP Liner

4.2.4 Placing of the Full Scale Specimens Inside the Oven

Each oven was capable of housing minimum four full-scale specimens. Two high range specimens, one target range specimen and one control specimen of each resin were kept in each individual oven. Provision of manual entrance as and when required was kept in each oven. The first category of host-pipes each lined with the liner which was impregnated with resin Type-A was marked as 1 and the second set impregnated with resin Type-C was marked as 2. There were four full scale samples under each category of liner. Strain gauge was attached at the front part (the part close to the door of the oven) spring-line location of each liner. Two 90° strain rosettes were also glued on the liner: one at the front part invert and the other at the rear part crown location. To minimize the thermal effect, each strain gauge and strain rosette was covered by insulation foam as shown in Figure 64.

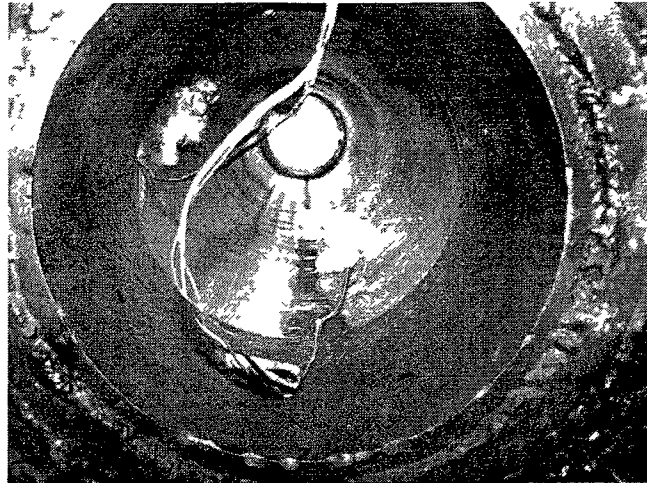


Figure 64: Strain Gauge at the Spring-line and Strain Rosette at the Invert

Two thermocouples – one at the front and one at the rear side of the oven – were installed. Careful measurements were taken to mark the strain gauge, strain rosette, and thermocouple connections to the data acquisition system and are shown in Appendix C.

4.2.5 Discussion of Strain Results

After all the specimens were prepared and placed inside the ovens on June 17, 2010, the ovens were turned on. For almost eleven months, strain data were collected using HP3497A data acquisition system. Correction relating to thermal output and gage factor of strain gage glued under elevated temperature environment was performed.

In total, nearly 5 million data points were collected from all ovens and analyzed by the TTC research team. Strain data was collected from five locations in each liner, resulting in five graphs per day for each specimen and more than 900 plots were to be prepared showing the strain versus corresponding temperature cycle on each liner specimen. The ovens are still running and this dissertation work includes processed data for up to 341 days (approximately 11.50 months).

Figure 65 to Figure 69 display the longitudinal strain and circumferential strain cycles at the spring-line, crown and invert of the CIPP liners prepared with Type-A resin and Type-C resin, on Day 1 of the long-term test. The temperature range was 110° F to 260° F. It can be seen that both liners exhibited linear elastic behavior, with the strain increasing as the temperature increased. Upon cooling of the specimens, the strain returned to its original level, displaying nearly a full recovery.

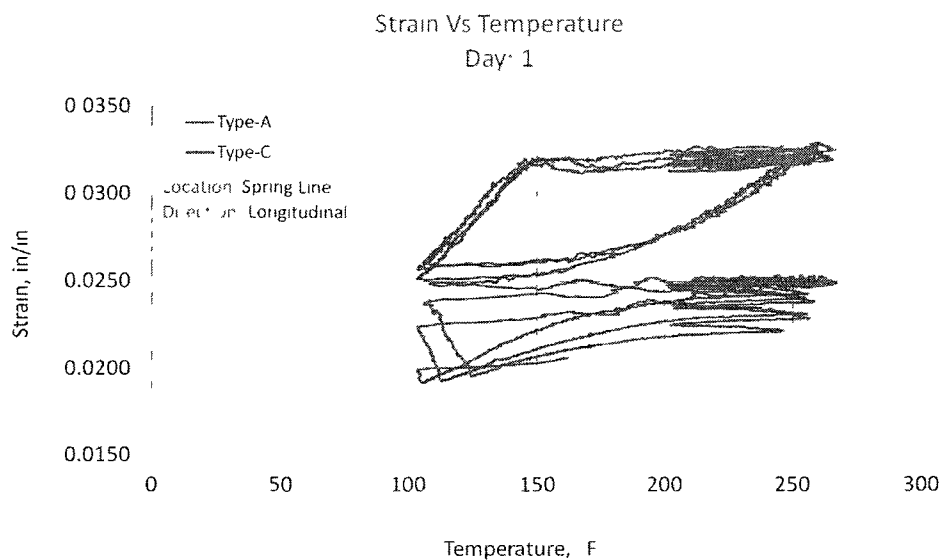


Figure 65: Longitudinal Strain Cycle at the Spring Line due to Temperature Change at Day 1 (Temperature Range 110° F-260° F)

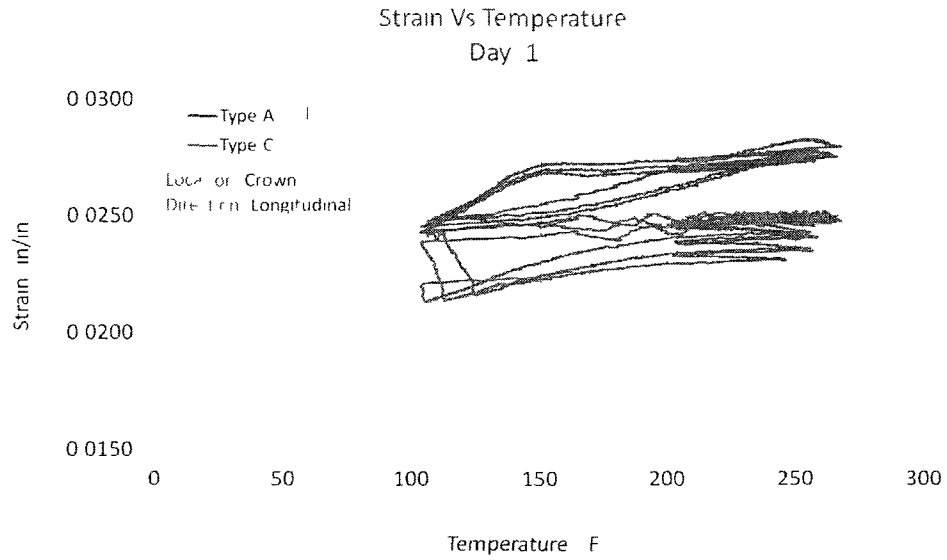


Figure 66: Longitudinal Strain Cycle at the Crown due to Temperature Change at Day 1 (Temperature Range 110° F-260° F)

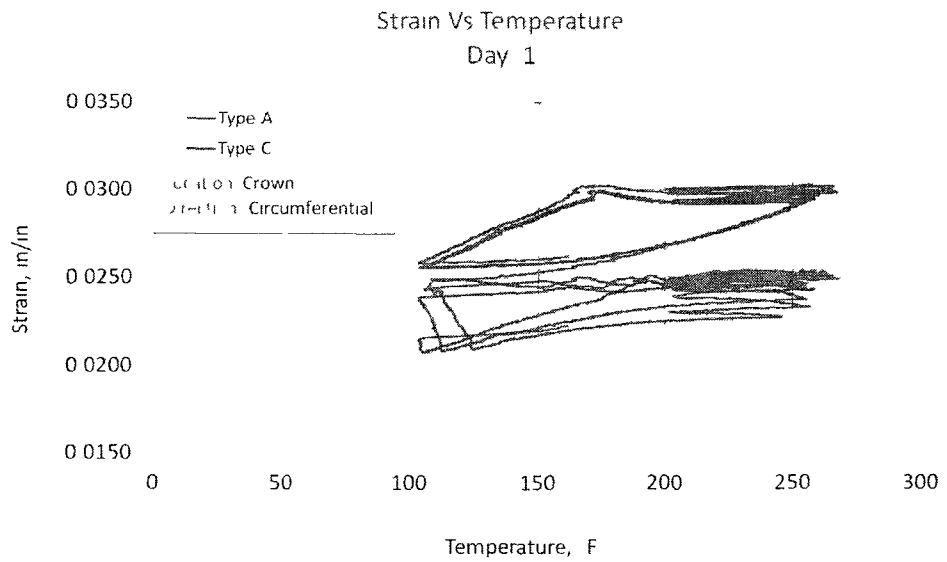


Figure 67: Circumferential Strain Cycle at the Crown due to Temperature Change at Day 1 (Temperature Range 110° F-260° F)

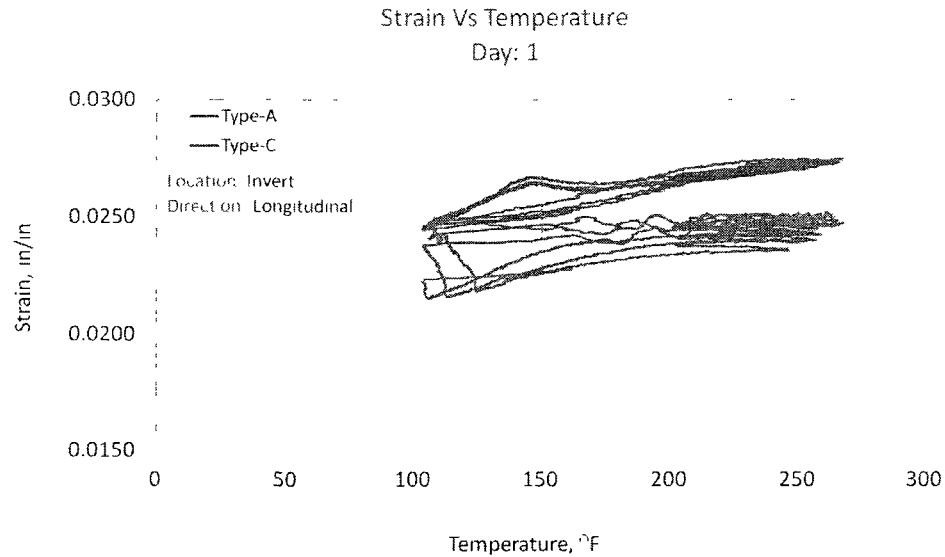


Figure 68: Longitudinal Strain Cycle at the Crown due to Temperature Change at Day 1 (Temperature Range 110° F-260° F)

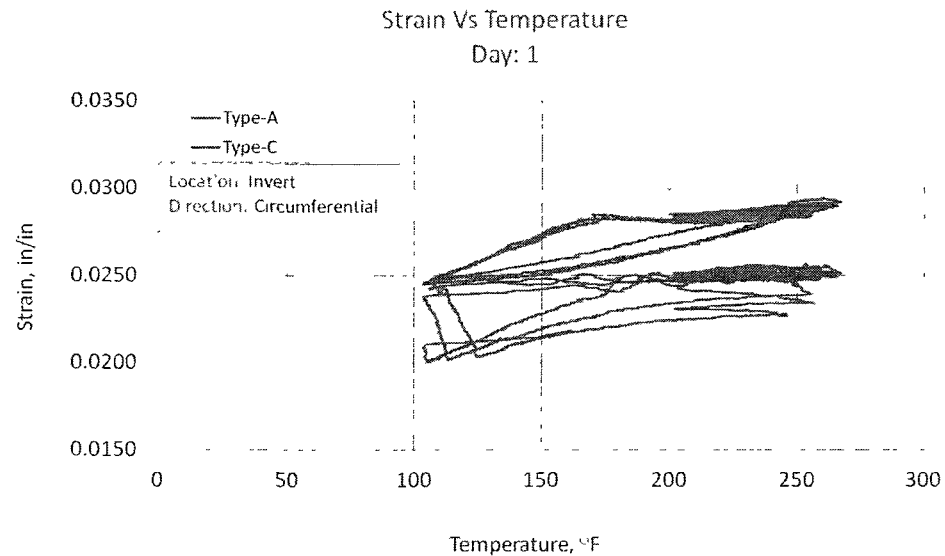


Figure 69: Circumferential Strain Cycle at the Invert due to Temperature Change at Day 1 (Temperature Range 110° F-260° F)

Figure 70 shows the initial strain on resin Type-C. It was found that the maximum strain of around 0.0018 in/in occurred at the spring line in the longitudinal direction. After 27 days of elevated temperature load, the strain went to plastic. Detailed explanation is

shown in Figure 71 which presents the creep curve at each of these five locations over the duration of the testing period for Type-C impregnated liner specimens. It can be seen that the increase in the resulting strain for a fixed change in temperature followed characteristics of creep curve with an initial (primary) creep, a rate (secondary) stage and a steep increase resulting in brittleness and ultimately failure over the 341-day test data reported herein (~1,000 thermal loading cycles). The measured strain increased by 11 folds, quickly approaching the mechanical limits of the material. One contributing factor to the rapid increase in strain was the development of relatively large plastic strains (i.e., permanent deformation) within in the liner material.

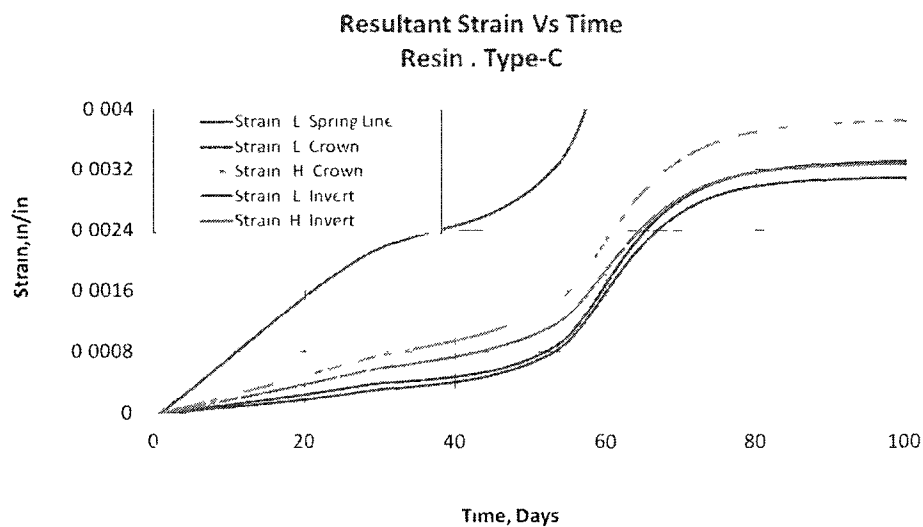
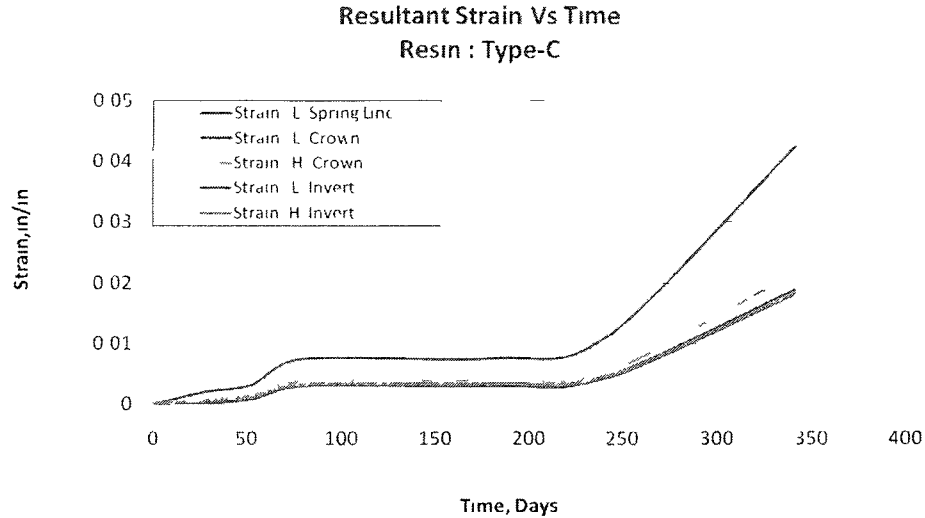


Figure 70: Initial Strain on Resin Type-C (Temperature Range 110° F-260° F)



**Figure 71: Creep Due to Temperature Cycle of 341 days for Resin Type-C
(Temperature Range 110° F-260° F)**

Figure 72 shows the initial strain on resin Type-A. The maximum strain at around 20 days was found approximately 0.001 in/in, which was 80% less than that of resin Type-C. After 20 days of thermal load, resin Type-A reached to plastic region. Figure 73 presents the net change in the strain at each of these five locations over the duration of the testing period for Type-A resin impregnated liner specimens. It can be seen that the increase in the resulting strain for a fixed change in temperature exhibited an initial increase before leveling off after approximately 35 days (~100 cycles), with little changes in the resulting strain for a fixed change in temperature for the remaining measurement period. The results suggest that after an initial primary (or transient) creep took place, the secondary creep progressed at a very slow rate, indicating high chemical stability of the resin in an elevated temperature environment. Also, the residual strain (i.e., permanent deformation) in the liner was relatively small even after 1,000 thermal loading cycles.

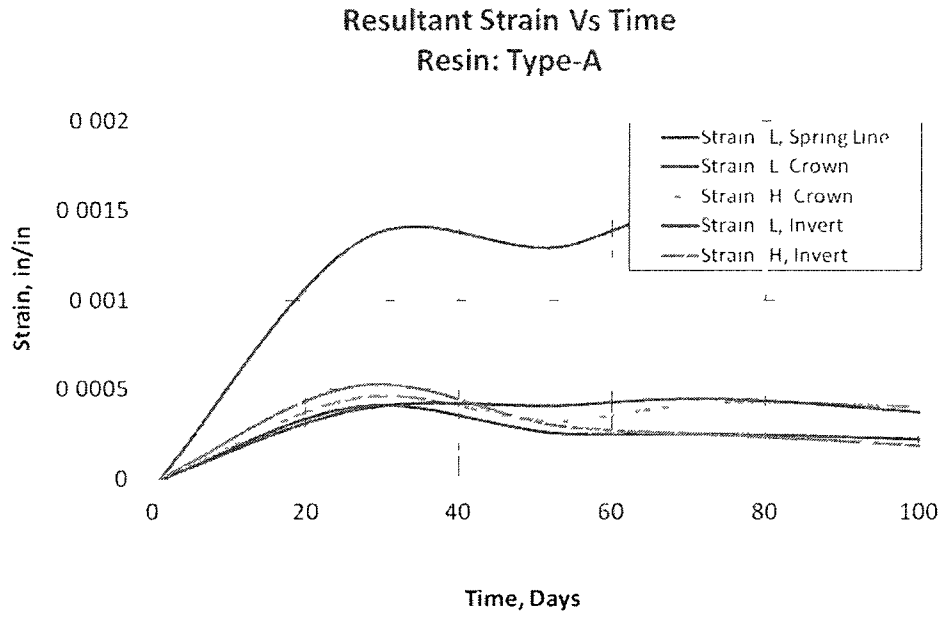


Figure 72: Initial Strain on Resin Type-A (Temperature Range 110° F-260° F)

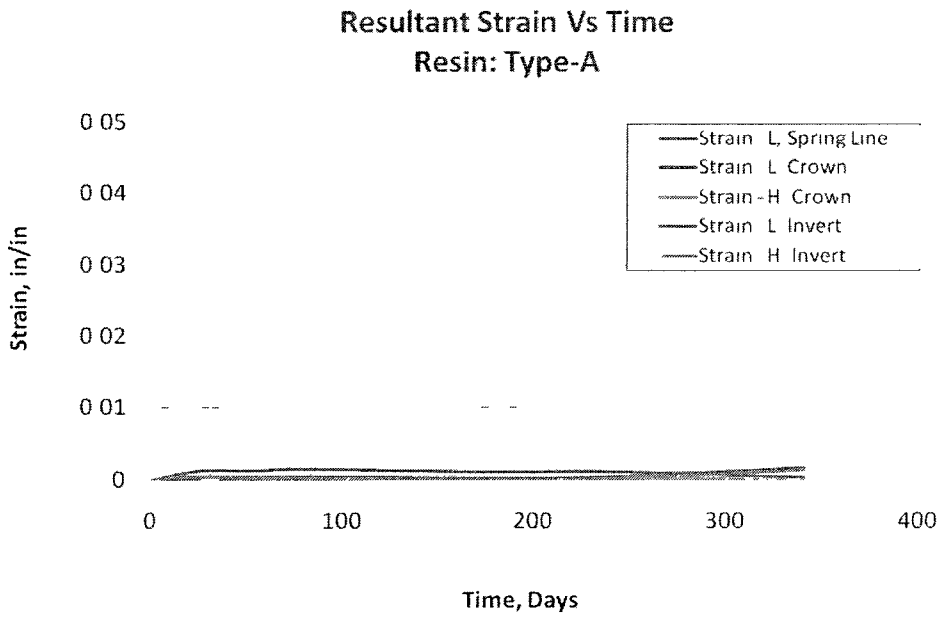


Figure 73: Creep Due to Temperature Cycle of 341 days for Resin Type-A (Temperature Range 110° F-260° F)

Figure 74 through Figure 77 display the stress values for Type-C and Type-A resin impregnated liner specimens on Day 1 and Day 341. On Day 1 the stress value was low as the liner was inside the elastic region, but after around 27 days the liner became plastic. The stress value was calculated by deducting the permanent strain or plastic strain from the total strain and then multiplying the experimentally obtained modulus of elasticity value. Additional graphs displaying the minimum and maximum stress values on days 53, 79, 181, and 241 are given in Appendix E. Table 20 and Table 21 summarize the stress values recorded in each of the five points of measurement (i.e., longitudinal stress at spring line, invert and crown; hoop stress at invert and crown) on days 1, 53, 79, 181, 241, and 341, for Type-C and Type-A resin impregnated liner specimens, respectively.

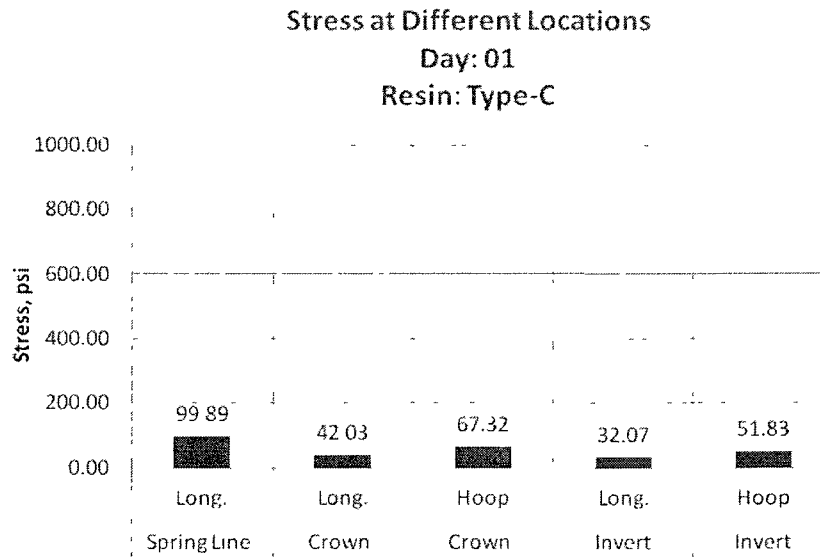


Figure 74: Longitudinal and Hoop Stress Due to Thermal Loading on Day 1 for Resin Type-C (Temperature Range 110° F-260° F)

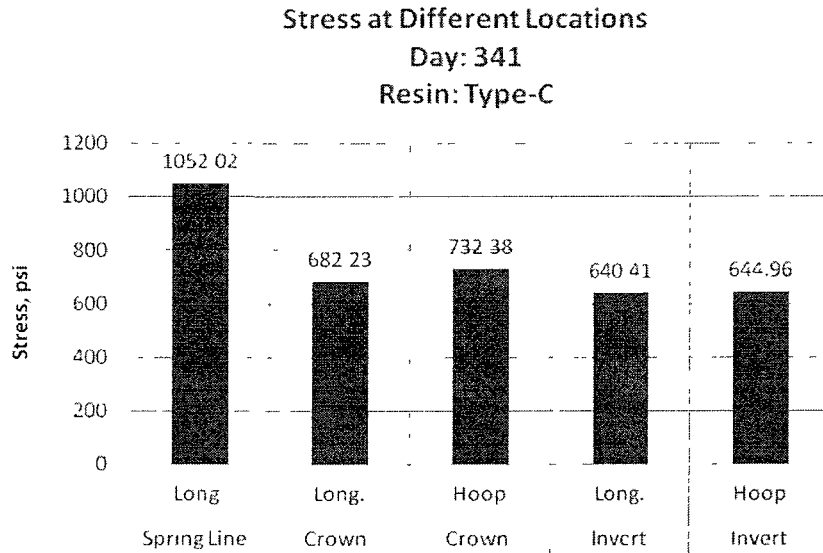


Figure 75: Longitudinal and Hoop Stress Due to Thermal Loading on Day 341 for Resin Type-C (Temperature Range 110° F-260° F)

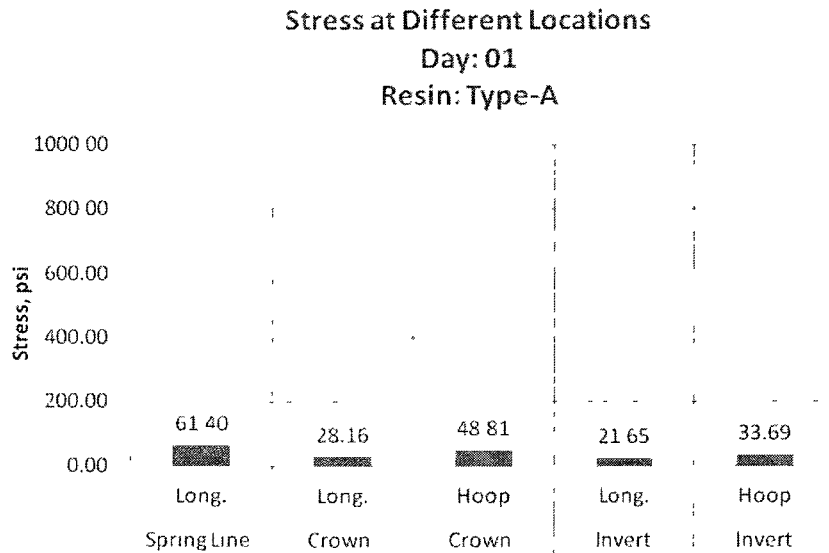


Figure 76: Longitudinal and Hoop Stress Due to Thermal Loading on Day 1 for Type-A (Temperature Range 110° F-260° F)

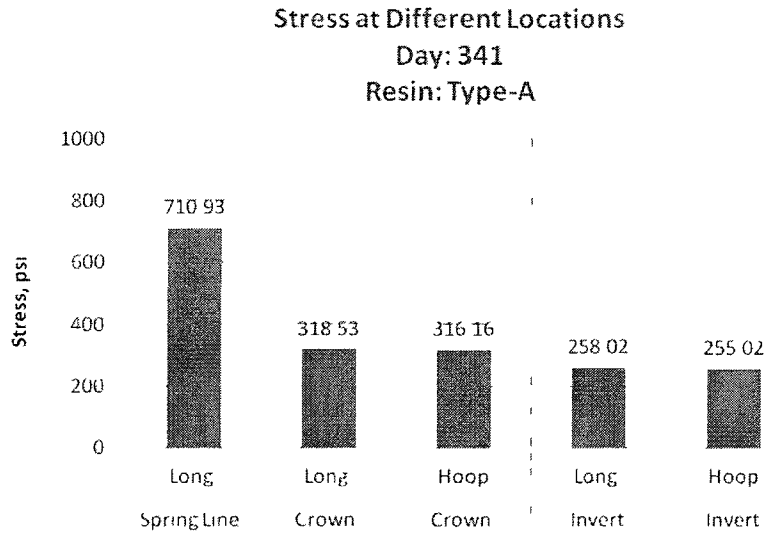


Figure 77: Longitudinal and Hoop Stress Due to Thermal Loading on Day 341 for Resin Type-A (Temperature Range 110° F-260° F)

Table 20: Stress on Resin: Type-C at Different Days

Direction	Location	Day (Temperature Range 110° F-260° F)					
		1	53	79	181	241	341
Spring Line	Long.	99.89	792.83	792.84	792.55	807.61	802.91
Crown	Long.	42.03	787.68	783.25	793.88	808.32	782.69
Crown	Hoop	67.32	793.26	793.91	797.34	782.73	807.77
Invert	Long.	32.07	783.31	791.29	804.98	803.36	809.86
Invert	Hoop	51.83	798.09	791.71	805.22	787.04	792.44

Table 21: Stress on Resin: Type-A at Different Days

Direction	Location	Day (Temperature Range 110° F-260° F)					
		1	53	79	181	241	341
Spring Line	Long.	61.40	793.28	738.23	768.50	726.74	793.60
Crown	Long.	28.16	768.51	703.41	703.83	794.74	718.06
Crown	Hoop	48.81	708.57	700.42	707.81	771.22	732.45
Invert	Long.	21.65	765.10	798.88	776.06	771.25	745.29
Invert	Hoop	33.69	755.83	782.49	793.58	726.15	787.18

4.2.6 Discussion of Profile Plot Results

A profile plot was performed to investigate the deformation due to thermal loading. It was very difficult to remove the full scale specimens from the oven and reinstate them. Therefore, profile plot was taken only twice: once before the specimens were placed inside the oven and at an intermediate period – Day 79. On average, deformation on the liner impregnated with Type-C resin was found to be greater than the deformation on the liner impregnated with resin Type-A (see Figure 78 and Figure 79).

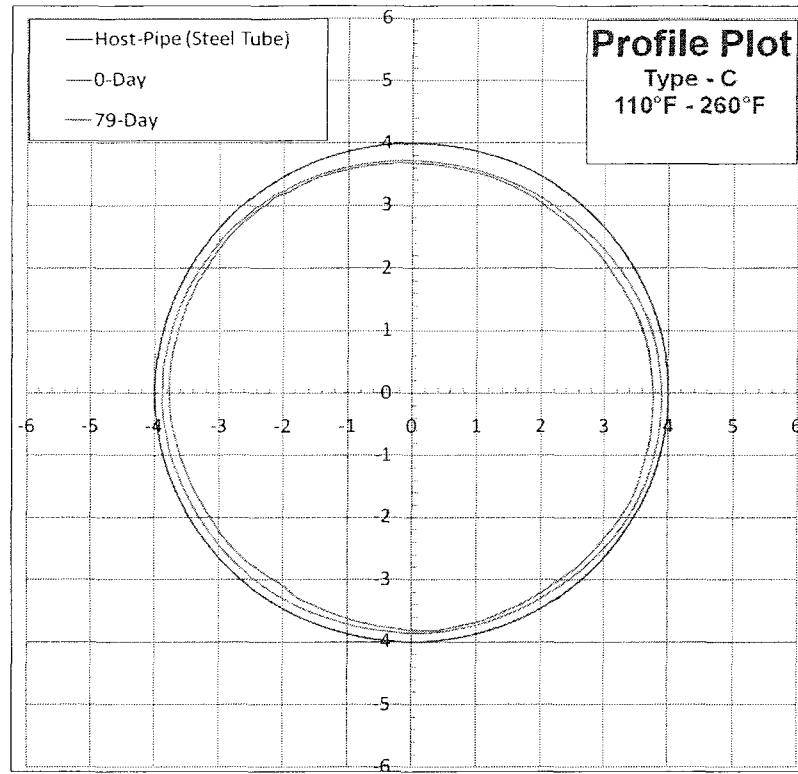


Figure 78: Profile Plot after Thermal Loading of 110° F - 260° F for Type-C Day 79

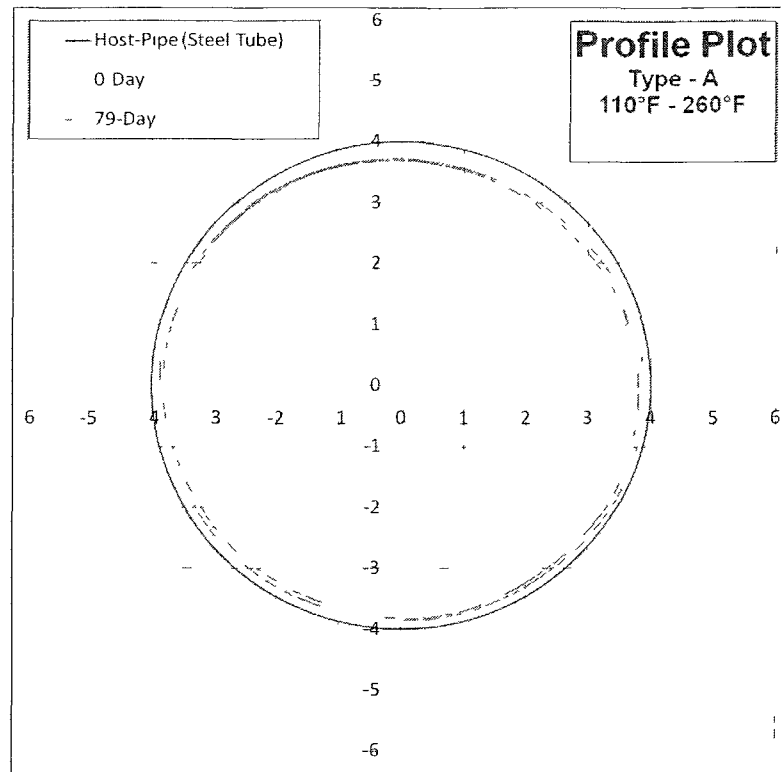


Figure 79: Profile Plot after Thermal Loading of 110° F - 260° F for Type-A Day 79

4.3 Conclusion

Data collected after 330 days of cyclic thermal loading of the full scale specimens (three loading-unloading cycles per day for a total of ~1,000 cycles) revealed that Type-A resin was able to handle the cyclic thermal load the best, accumulating the least residual strain and exhibiting the lowest peak stress for the three temperature ranges, as shown in Figure 80.

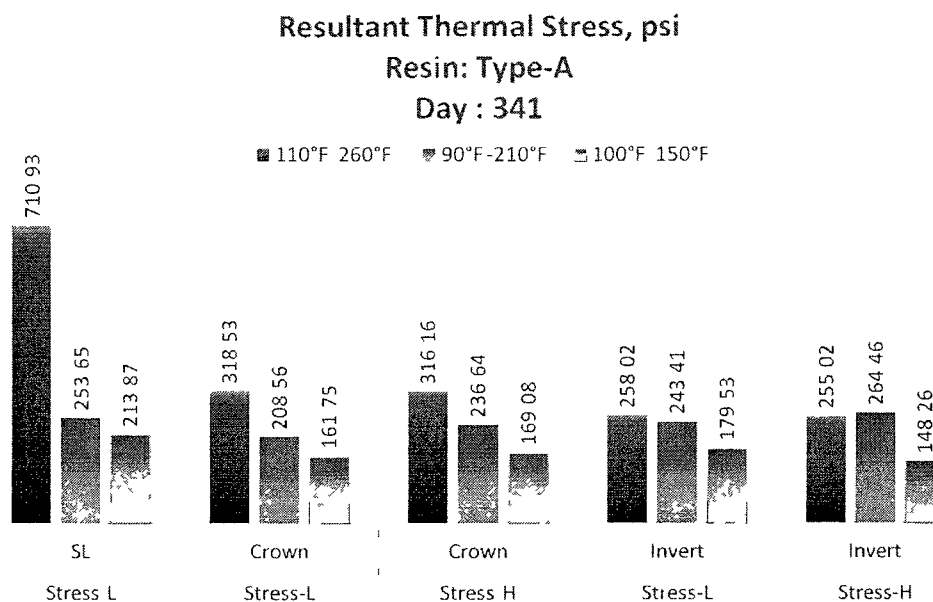


Figure 80: Stress (psi) Due to Thermal Loading on Day 341 on Type-A Resin

As for the Type-C resin (see Figure 81), after 11 months of cyclic testing between 110° F to 260° F, one of the two specimens containing Type-C resin experienced a buckling failure due the cumulative plastic strains in the hoop direction, without the presence of external pressure. It should be noted the ~1,000 cycles of 110° F to 260° F, which brought about these high plastic strains and buckling failure, represent an extreme loading condition which is significantly more severe than these anticipated in the application under consideration.

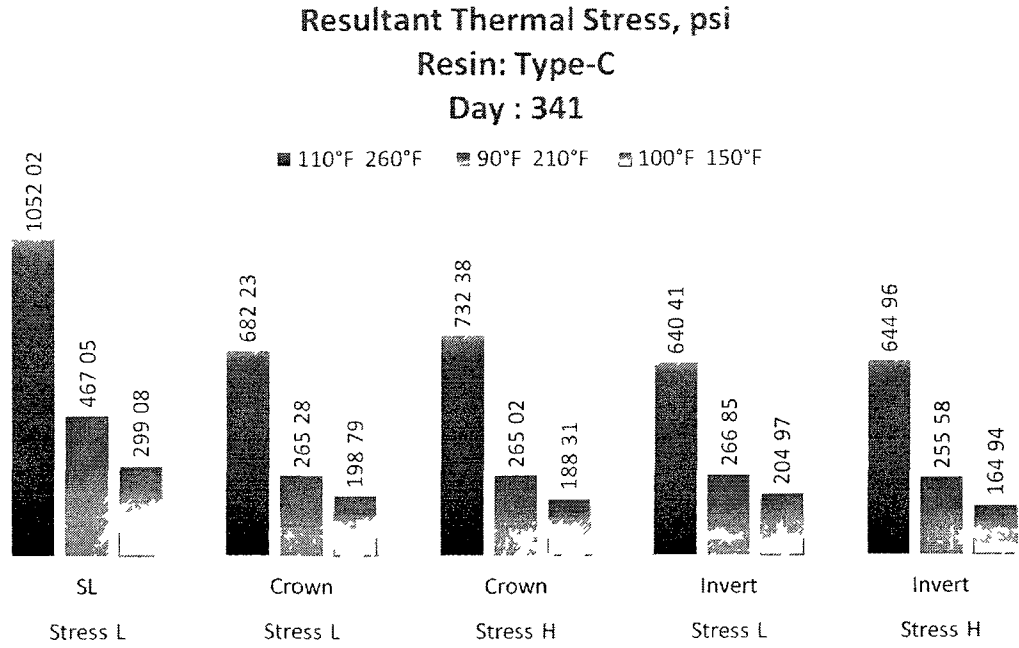


Figure 81: Stress (psi) Due to Thermal Loading on Day 341 on Type-C Resin

CHAPTER 5

NUMERICAL SIMULATION

5.1 Introduction

A 3-D finite element (FE) model of a CIPP lined brick sewer pipe, which is partially filled with water and contains steam in the head space, was developed. The model was subjected to an extensive validation effort, comparing its predictions with close form analytical solutions and experimentally measured data.

5.2 Elements Used

The following elements were used in the finite element analysis performed using ANSYS:

- SOLID69 thermal element representing the two materials (steel host pipe and CIPP liner) and an equivalent structural element SOLID45, used in “solid block analysis”.
- CONTA174 and TARGE170 elements for both heat and stress transfer between the host pipe and liner.

SOLID69 has three-dimensional thermal conduction capability as well as electrical conduction capability (in this analysis, the later was turned off using the built-in key-options facilities in ANSYS). The element has eight nodes with two degrees of freedom, one of which is temperature at each node. This solid element is suitable for a three-dimensional, steady-state or transient thermal analysis. The SOLID69 element (see Figure

82) does not have any real constants and requires an iterative solution to include the Joule heating effect in the thermal solution.

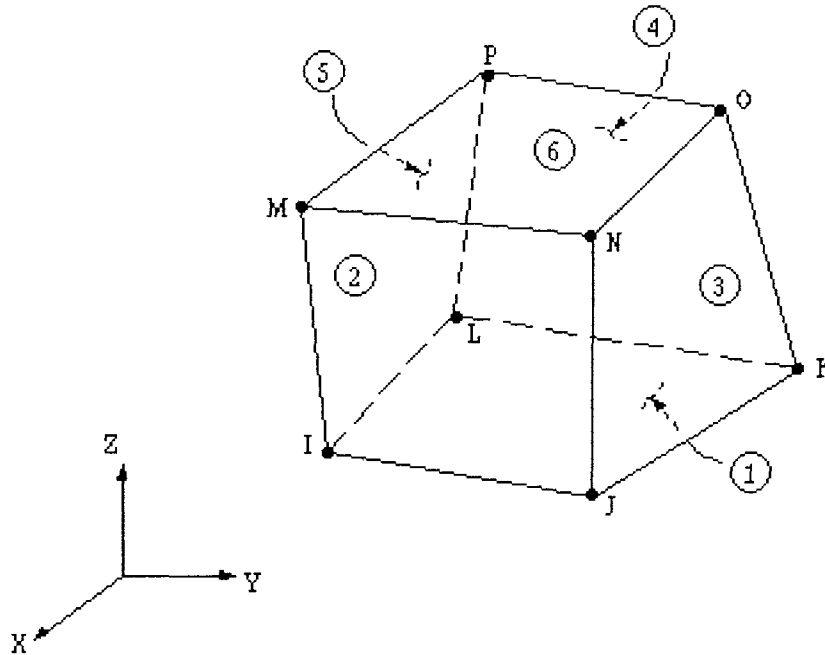


Figure 82: SOLID69 Element (Left) (Modified after ANSYS 11.0 Manual)

For structural analysis, the thermal solid element SOLID69 was converted to an equivalent structural element SOLID45. At this stage of the modeling, the given inputs were structural properties (e.g., modulus of elasticity, Poisson's ratio, and density). CONTA174 was used to represent contact and sliding between 3-D target surfaces (TARGE170) and a deformable surface, defined by this element (see Figure 83). In addition to temperature, this element has three degrees of freedom at each node (translations in the nodal x, y, and z directions). This element is located on the surfaces of 3-D solid element and has the same geometric characteristics as the element face with which it is connected. Contact occurs when the element surface penetrates in one of the

target segment elements (TARGE170) on a specified target surface. Coulomb and shear stress friction is allowed on this element.

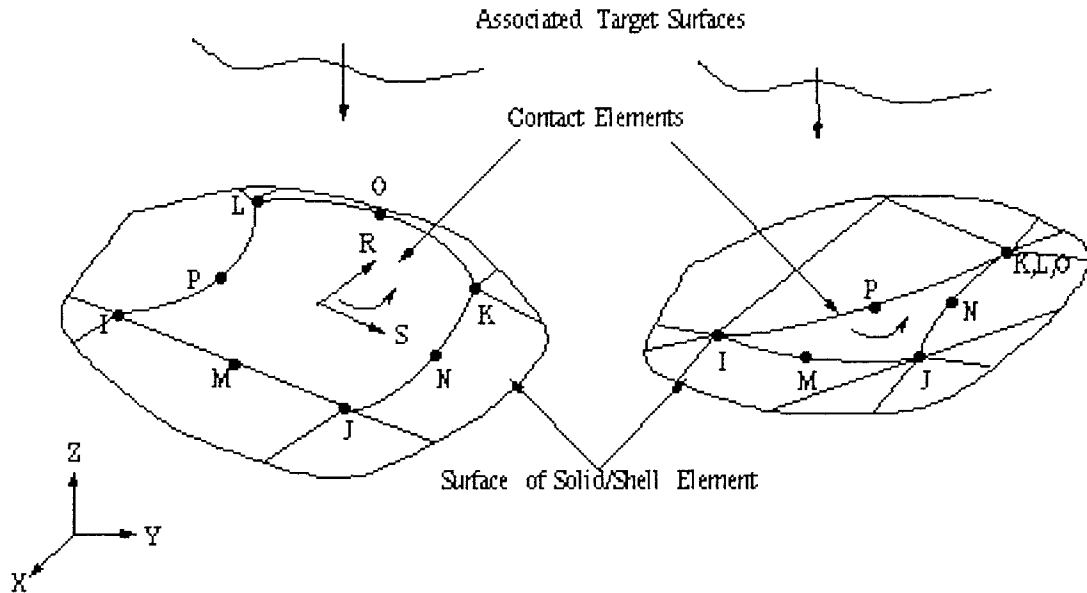


Figure 83: CONTACT174 Element (Right) (Modified after ANSYS 11.0 Manual)

The thermal analysis was performed first. Next, the thermal element was replaced with a structural element and a structural analysis was performed.

5.3 Sample Simulation with Solid Block

To get a better understanding and validate the results of the FE simulation, a small block model 30 in. long, 4 in. wide and 6 in. high was developed using the thermal, structural and contact elements listed in the previous section.

First, two blocks with a common surface were drawn in ANSYS. While the cross-sectional areas of the blocks were kept the same, the length of one block was twice the length of the other block. The smaller block was assigned the properties of steel while the

longer block was assigned the properties of aluminum (see Figure 84). Material properties (i.e., thermal and structural) of used materials are listed in Table 22.

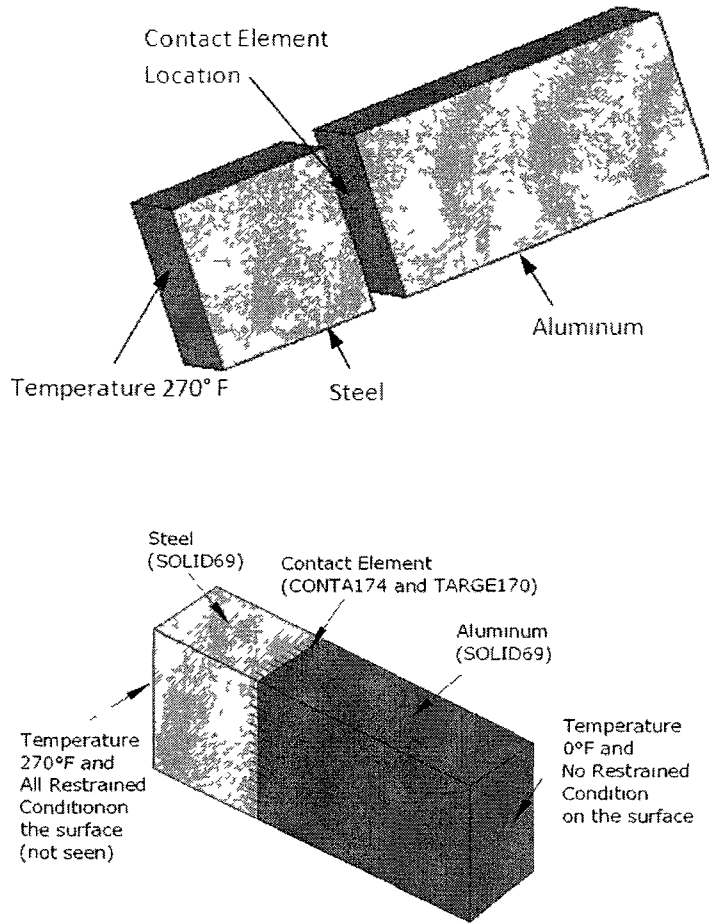


Figure 84: FE Simulation of a Block Model – Before Modeling

Table 22: Material Properties of Steel and Aluminum

Material	Modulus of Elasticity	Poisson's Ratio	Density	Specific Heat	Coefficient of Thermal Expansion	Thermal Conductivity
	psi		snail/in ³	in-lbf/snail °F*		in/in/° F
Steel	29.00e6	0.27	7.354e-4	4.33e5	6.7e-6	5.37
Aluminum	10.15e6	0.35	2.526e-4	7.72e5	13.1e-6	29.60

Next, contact elements were used on the common surface of the two blocks (i.e. two elements). Temperature load of 270° F and 0° F was applied at both ends. The surface to which 270° F was applied was restrained in all direction. The other surface was free. To compare ANSYS results with an analytical solution, the Poisson's ratio of both materials was assigned a value of zero to exclude lateral expansion due to temperature. All the side surfaces were restrained with a roller support which allowed movement in one direction only (see Figure 85).

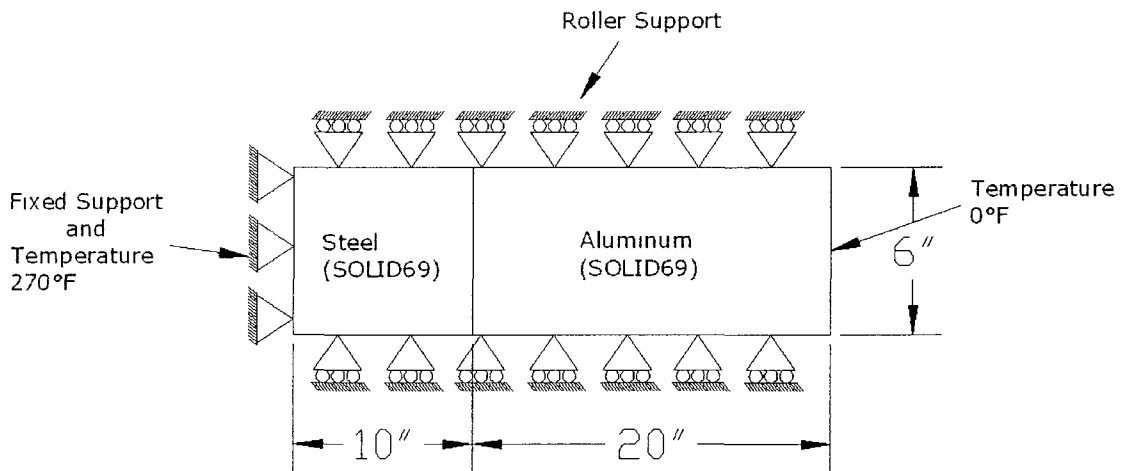


Figure 85: Restrained Condition of the Test Model

The behavior predicted by ANSYS (see Figure 86 and Figure 87) was found very close to the values given by the analytical solution. The final results are shown in Table 23.

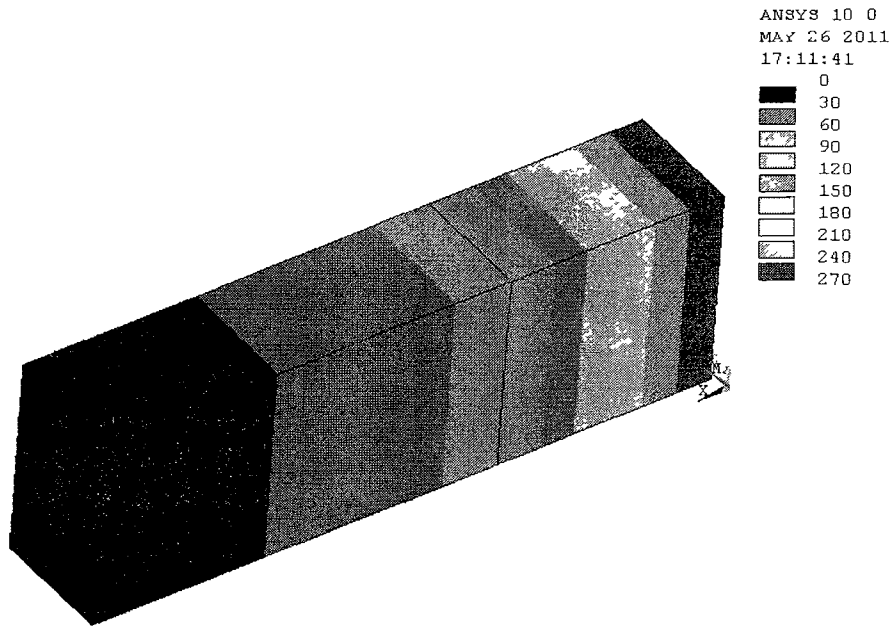


Figure 86: FE Analysis – Temperature Distribution

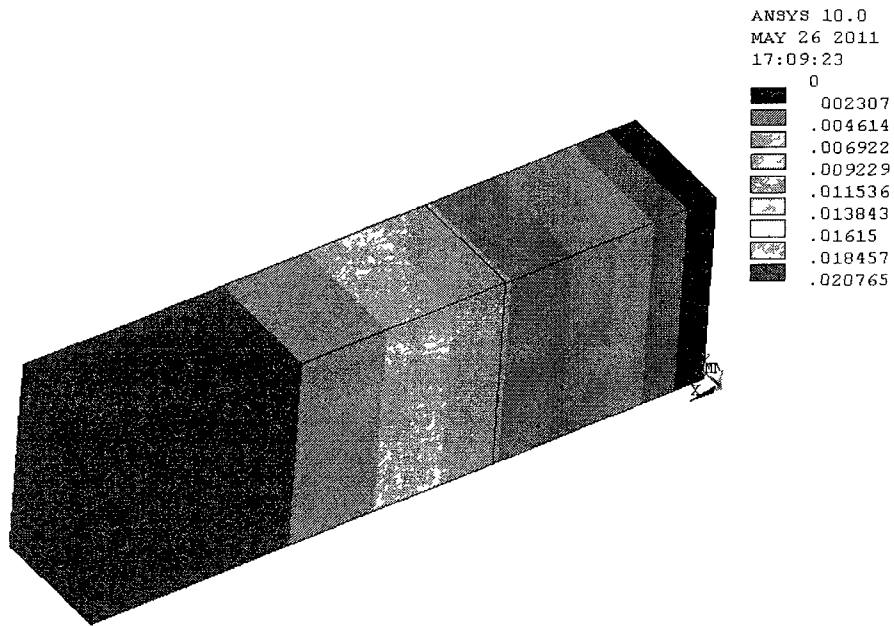
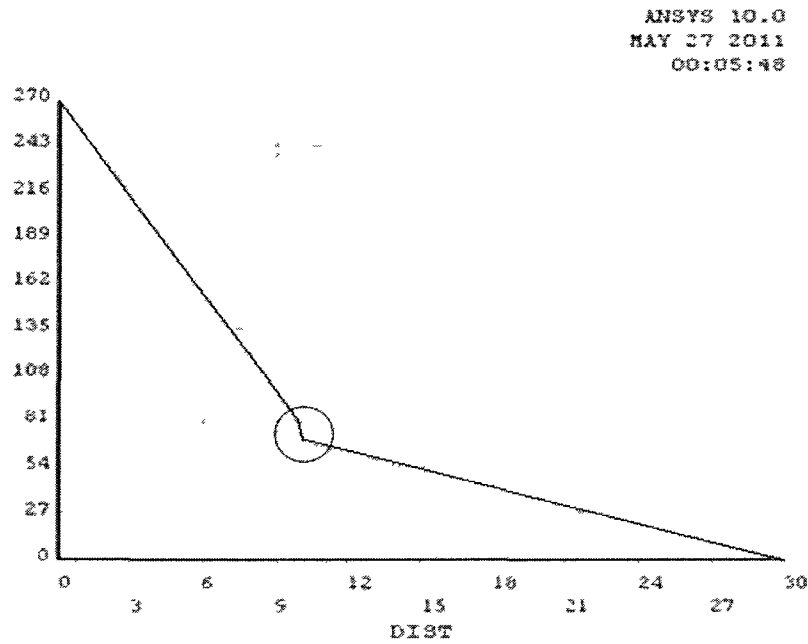


Figure 87: FE Analysis – Displacement

Table 23: Comparison of Results - FE Analysis and Analytical Solution

Method	Interface Temperature	Deflection			Deviation
		Steel	Aluminum	Total	
	$^{\circ}\text{F}$	in	in	in	%
FE Analysis	72.388	0.0117	0.009065	0.020765	0.168
Analytical Solution	71.883	0.0114	0.0094	0.0208	

The temperature gradient across the entire element and at the interface between the two blocks as predicted by ANSYS is given in Figure 88 and Figure 89. In Figure 89, the zoom view of temperature gradient (circled in Figure 88) is shown. Detail analytical calculation is given in Appendix D.

**Figure 88: Thermal Gradient for the Complete Length**

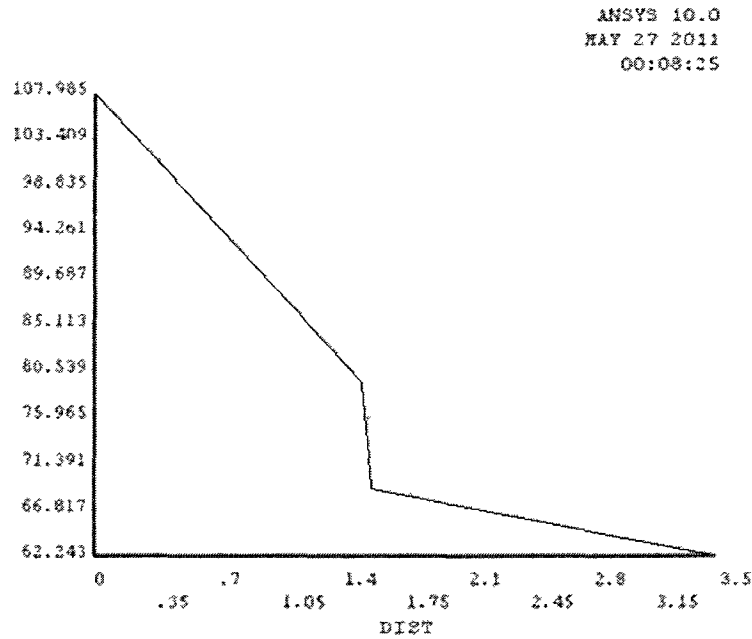


Figure 89: Thermal Gradient at the Vicinity of the Contact Surface

5.4 Steel Host Pipe and Liner – Uniform Thermal Load

The SOLID69 element was used to model the steel host pipe and liner. Contact elements (CONTA174 and TARGE170) were used at the interface of the steel pipe and the liner. The material and thermal properties are given in Table 24 and Table 25 respectively. Tests were performed on sample specimens to measure these values and later compared to values available in literatures.

Table 24: Mechanical Properties of Steel Host Pipe, Type-A and Type-C Resin

Material	Modulus of Elasticity psi	Poisson's Ratio	Density snail/in ³
Steel	29.00e6	0.27	7.354e-4
Type-A	45.69e4	0.38	1.165e-4
Type-C	44.33e4	0.45	1.122e-4

Table 25: Thermal Properties of Steel Host Pipe, Type-A and Type-C Resin

Material	Specific Heat		Coefficient of Thermal Expansion	Thermal Conductivity	
	J/kg °K	in-lbf /snail °F*		W/m°K	J/kg °K
Steel	460	3.96e5	6.7e-6	43	5.37
Type-A	1120	9.64e5	21.53e-6	0.29	0.036
Type-C	980	8.44e5	31.94e-6	0.20	0.025

For both the host-pipe and the CIPP liner, stress-strain curves (see Figure 90 and Figure 91) were provided as input data. For the first set of simulation, the thermal loading environment inside the oven was considered where both the host-pipe and the liner were subjected to similar elevated temperature. For the second set of simulations, the thermal load at the crown was assumed to be greater than that at the invert to simulate the difference in relative strain at the locations of different temperature. In the third set, simulations on a model with different temperatures at different locations were performed. For the second and third sets, the host pipe was assumed to be made of bricks.

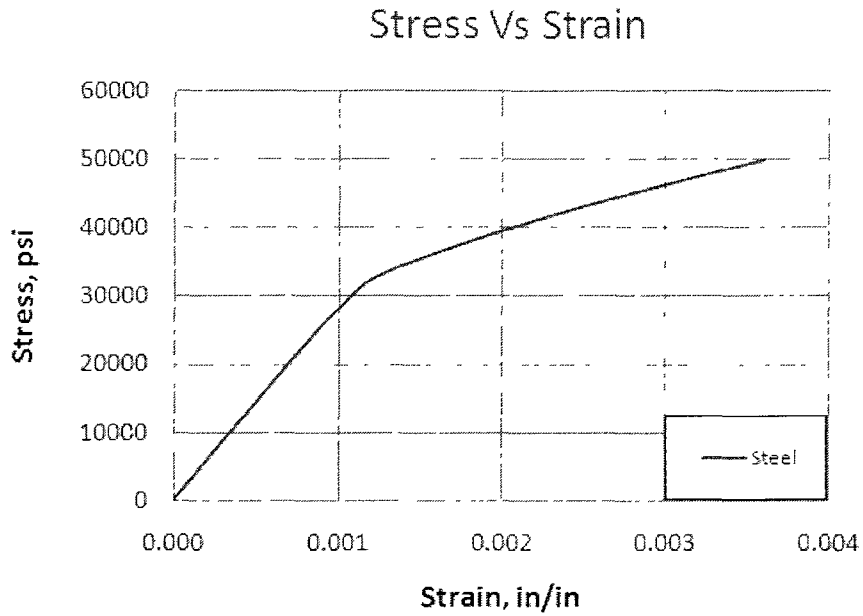


Figure 90: Stress – Strain Curve for Steel used in the FE Analysis

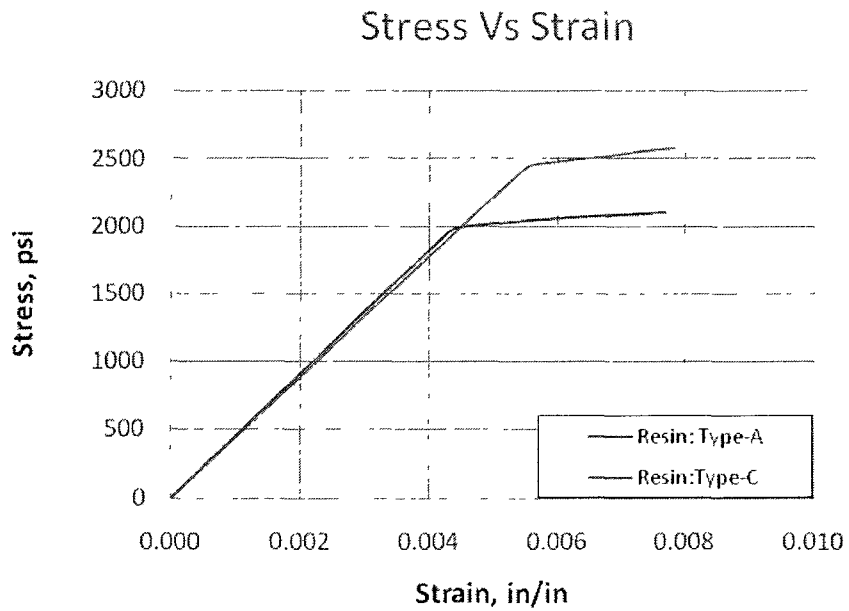


Figure 91: Stress – Strain Curve for Resins used in the FE Analysis

Total number of nodes generated in the model was 3648. Thus, results were presented for selected nodes at the crown, spring-line and invert zones. The locations of some of these nodes are shown in Figure 92 and listed in Table 26 (node numbering

depends on meshing do not follow a pattern). Change in the stress and strain at the pre-selected nodes due to thermal loading is listed in Table 27 and Table 28.

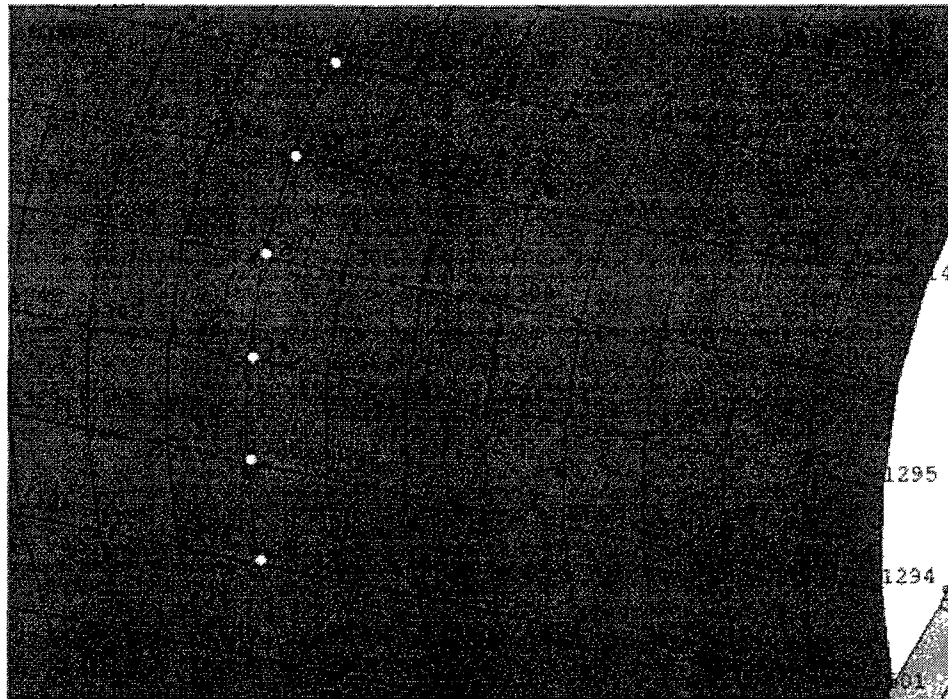


Figure 92: Location of Nodes on Spring Line

Table 26: List of the Nodes

Location	Node Number							
Crown	37	1779	1762					
Spring Line	1457	1440	1307	1343	1326	1193		
Invert	851	887	870					

Table 27: Von-Mises Stress (Equivalent Stress) in CIPP liner Containing Type-A

Location	Nodes	Von-Mises Stress at Day 1, psi						
		90° F	110° F	150° F	190° F	210° F	230° F	260° F
Crown	37	222.91	566.38	1253.3	1924.5	2005.1	2039	2069.7
	1779	222.91	566.38	1253.3	1924.5	2005.1	2039	2069.7
	1762	222.91	566.38	1253.3	1924.5	2005.1	2039	2069.7
Spring Line	1457	222.91	566.38	1253.3	1924.5	2005.1	2039	2069.7
	1440	222.91	566.38	1253.3	1924.5	2005.1	2039	2069.7
	1307	222.91	566.38	1253.3	1924.5	2005.1	2039	2069.7
	1343	222.91	566.38	1253.3	1924.5	2005.1	2039	2069.7
	1326	222.91	566.38	1253.3	1924.5	2005.1	2039	2069.7
	1193	222.91	566.38	1253.3	1924.5	2005.1	2039	2069.7
Invert	851	222.91	566.38	1253.3	1924.5	2005.1	2039	2069.7
	887	222.91	566.38	1253.3	1924.5	2005.1	2039	2069.7
	870	222.91	566.38	1253.3	1924.5	2005.1	2039	2069.7

Table 28: Von-Mises Stress (Equivalent Stress) in CIPP liner Containing Type-C

Location	Nodes	Von-Mises Stress at Day 1, psi						
		90° F	110° F	150° F	190° F	210° F	230° F	260° F
Crown	37	369.72	939.05	2071.3	2527.8	2559.9	2559.9	2559.8
	1779	369.72	939.05	2071.3	2527.8	2559.9	2559.9	2559.8
	1762	369.72	939.05	2071.3	2527.8	2559.9	2559.9	2559.8
Spring Line	1457	369.72	939.05	2071.3	2527.8	2559.9	2559.9	2559.8
	1440	369.72	939.05	2071.3	2527.8	2559.9	2559.9	2559.8
	1307	369.72	939.05	2071.3	2527.8	2559.9	2559.9	2559.8
	1343	369.72	939.05	2071.3	2527.8	2559.9	2559.9	2559.8
	1326	369.72	939.05	2071.3	2527.8	2559.9	2559.9	2559.8
	1193	369.72	939.05	2071.3	2527.8	2559.9	2559.9	2559.8
Invert	851	369.72	939.05	2071.3	2527.8	2559.9	2559.9	2559.8
	887	369.72	939.05	2071.3	2527.8	2559.9	2559.9	2559.8
	870	369.72	939.05	2071.3	2527.8	2559.9	2559.9	2559.8

From Table 27 and Table 28, it was found that, as expected, stress increased with an increase of temperature for a single cycle. Long-term performance of the liners under repeated cyclic thermal loads could not be performed at this time as limited data was available about the creep behavior of the resin material.

Summary of the stresses and corresponding strains are shown in Figure 93 and Figure 94, where it was found that Type-C resin reached its yield point at around temperature 180° F and Type-A reached the same at close to 200° F. Even then Type-A

resin was below the buckling stress of 2,500 psi. The slope of the strain Vs temperature curve for Type-C resin was higher than Type-A resin. This indicated that at the same temperature Type-C experienced greater deformation. Contour plots of Von-Mises stress at 190° F at both resins are shown in Figure 95 and Figure 96.

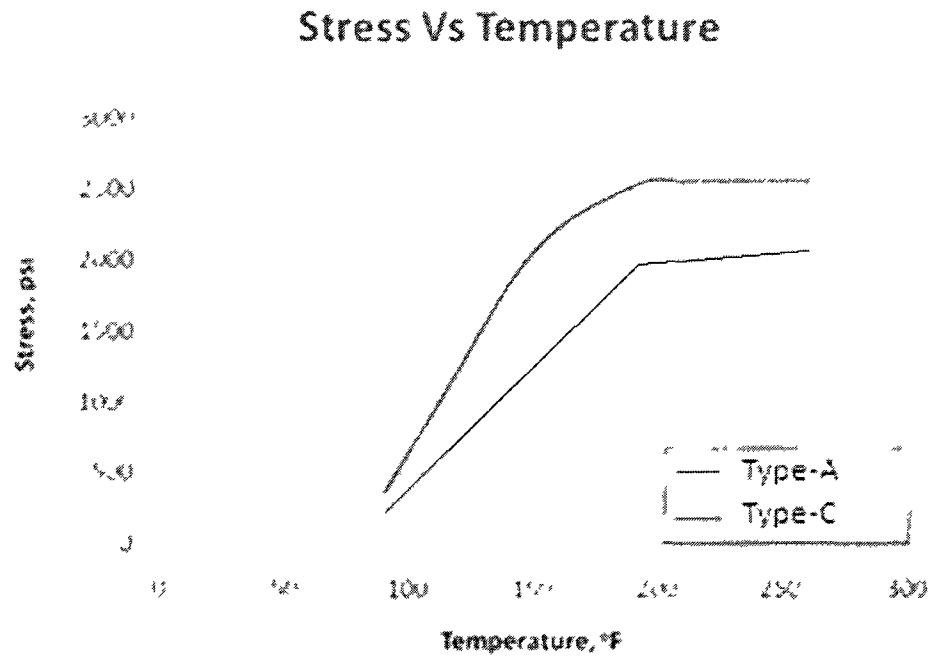


Figure 93: Change in Stress of Type-A and Type-C Resins Due to Thermal Loading

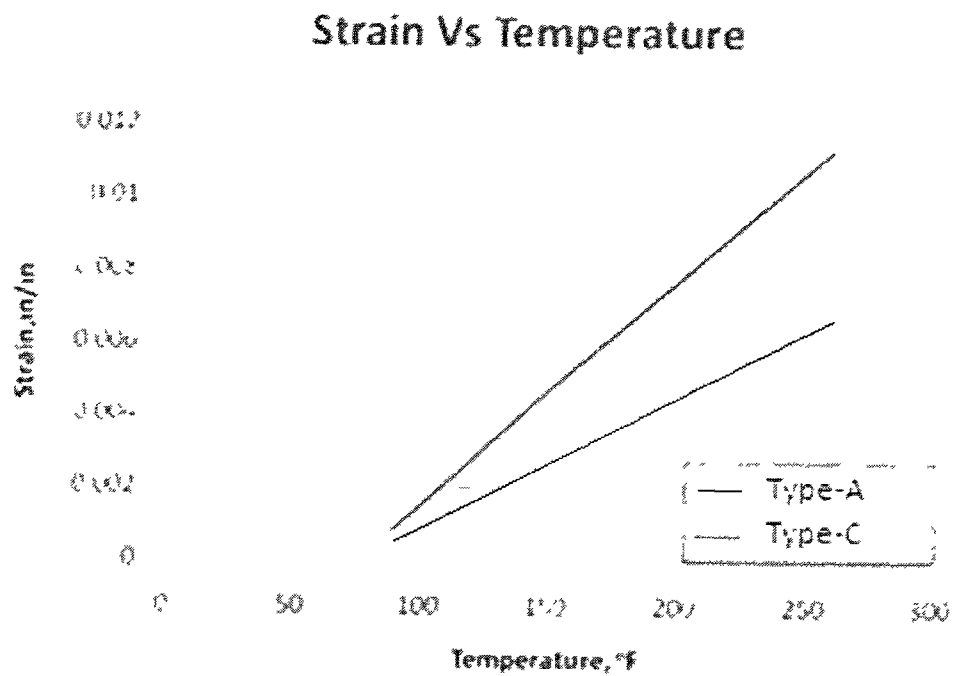


Figure 94: Change in Strains of Type-A and Type-C Resins Due to Thermal Loading

ANSYS 10.0
MAY 28 2011
23:58:36

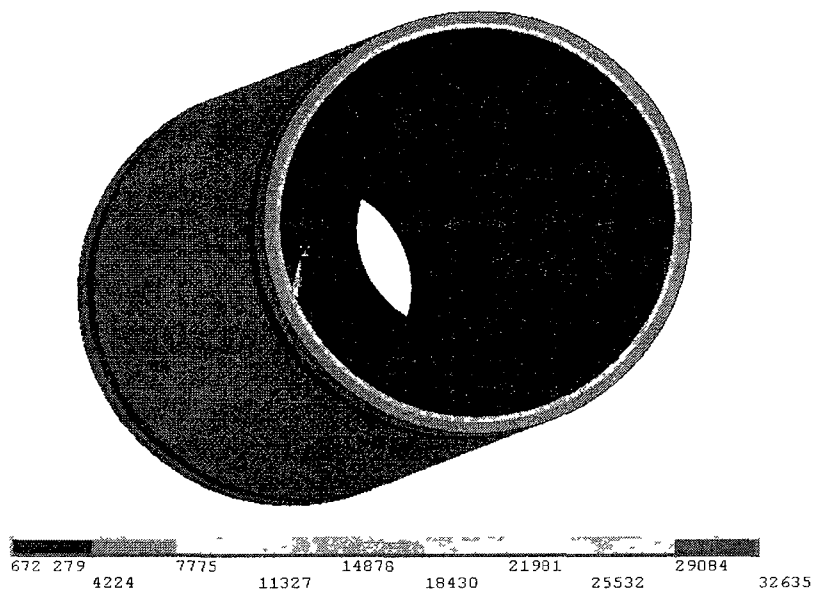


Figure 95: Contour Plot of Von-Mises Stress – Type-A Resin

ANSYS 10.0
MAY 29 2011
00:15:25

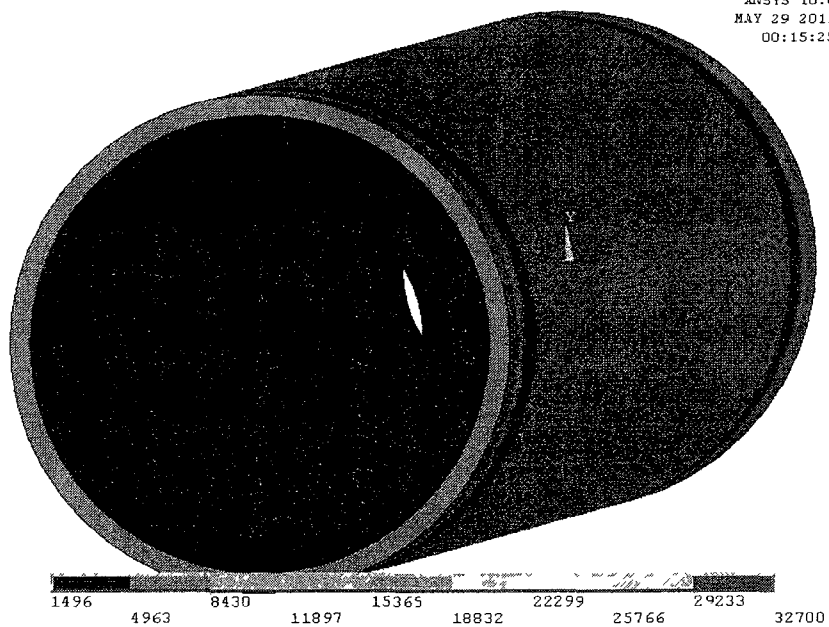


Figure 96: Contour Plot of Von-Mises Stress – Type-C Resin

5.5 Comparison between Actual and Numerical Simulation

In order to validate the model, physical tests were performed on three specimens for each temperature (i.e. 90° F, 110° F, 150° F, 190° F, 210° F, 230° F, and 260° F). Strain gauges were installed on each specimen and placed in an oven for 24 hrs. The thermal strain was monitored using the HP3497A DAQ system.

Data obtained from physical tests and numerical simulation is summarized in Table 29 and compared in Figure 97 and Figure 98. The predicted results for both Type-A and Type-C were found to follow closely the experimentally measured values.

Table 29: Thermal Stress on Resin Caused by Different Temperature

Resin	Method	Thermal Stress, psi						
		90° F	110° F	150° F	190° F	210° F	230° F	260° F
Type-A	FE Simulation	222.91	566.38	1253.3	1924.5	2005.1	2039	2069.7
	Actual Test	242.52	669.32	1222.67	1955.78	1990.37	2125.42	2080.32
	Deviation (%)	8.09	15.38	-2.51	1.60	-0.74	4.07	0.51
Type-C	FE Simulation	369.72	939.05	2071.3	2527.8	2559.9	2559.9	2559.8
	Actual Test	342.57	899.34	2122.78	2455.76	2512.37	2570.43	2680.31
	Deviation (%)	-7.93	-4.42	2.43	-2.93	-1.89	0.41	4.50

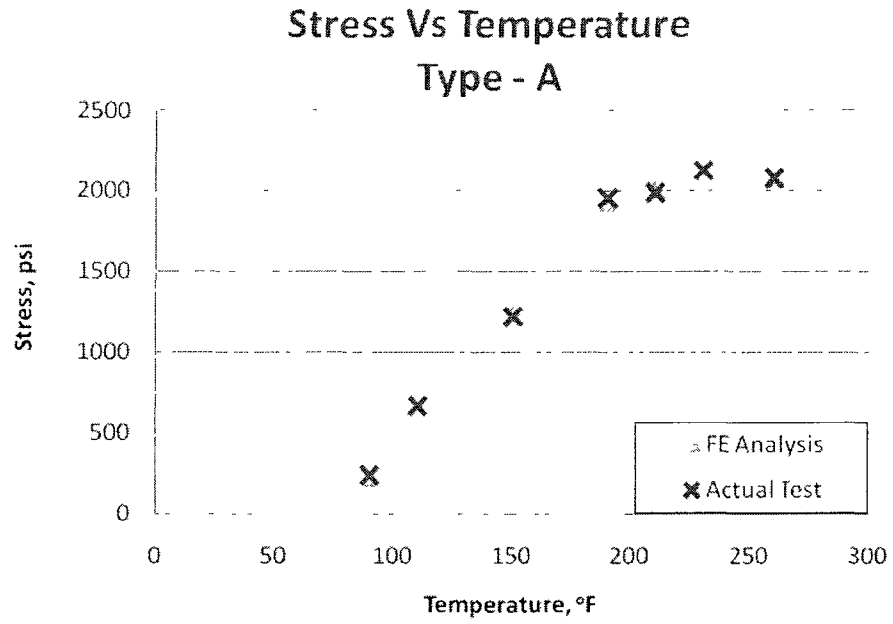


Figure 97: Thermal Stress on Resin Type-A Sample

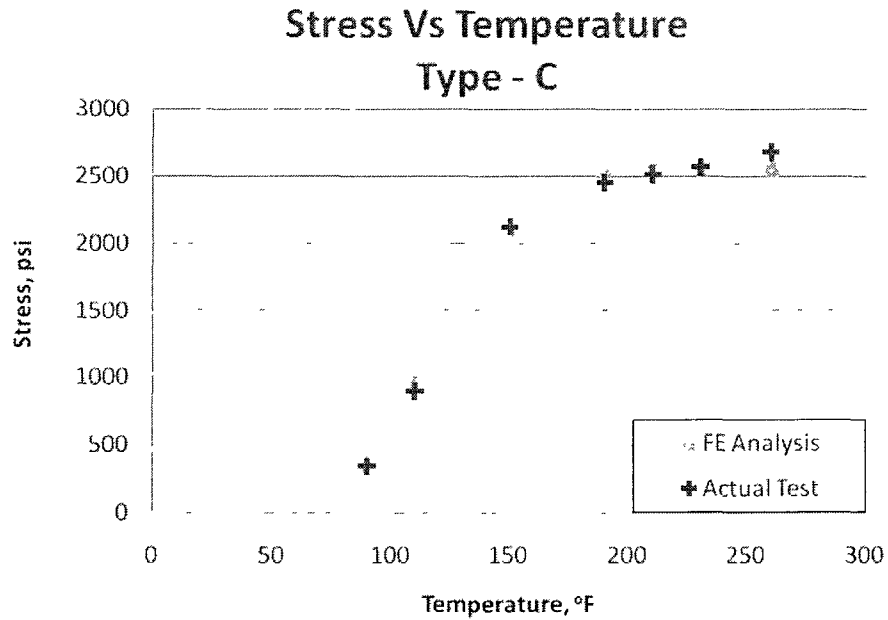


Figure 98: Thermal Stress on Resin Type-C Sample

5.6 Steel Host Pipe and Liner – Non-uniform Thermal Load

Following the validation of the model, a more realistic loading condition was utilized as non-uniform thermal load was applied to the simulated liner. In addition, the host pipe was assumed to be made of clay bricks, thus simulating the actual sewer structure scheduled for rehabilitation at Times Square. For both models, thermal load at the location spring-line to the crown ranged from 90° F to 260° F, at spring-line to invert 70° F and on the outside at 62° F. Investigation was performed again on the same nodes as mentioned in Table 26. Temperature distribution zone and selected nodes are shown in Figure 99. A temperature gradient can be noted at the spring-line locations.

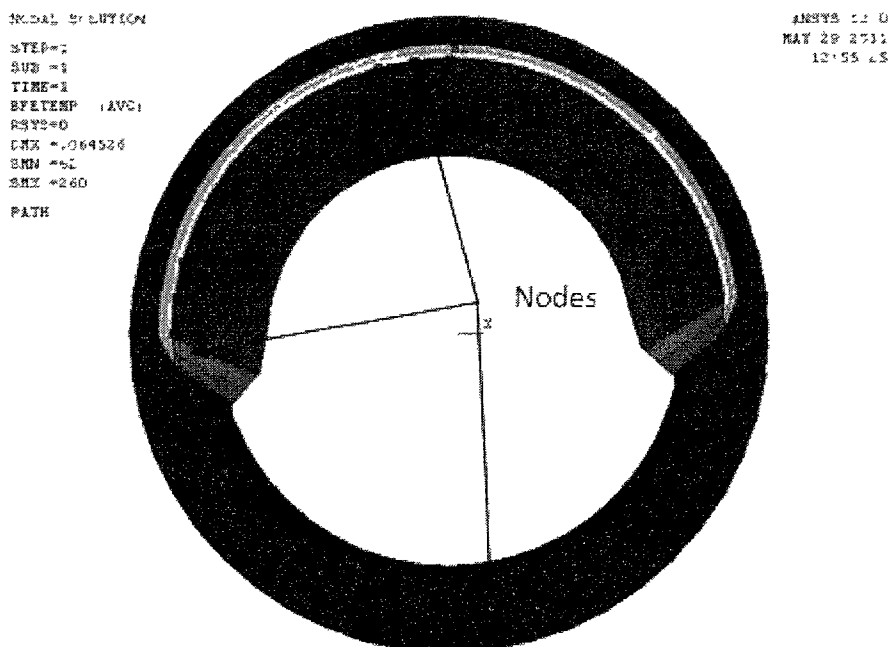


Figure 99: Thermal Gradient And Location Of The Investigated Nodes

Figure 100 shows the effect of non-uniform temperature on Type-A liner. It was found that the liner at the crown approached plastic limit stress before the liner region at the invert. As invert temperature was lower, this zone experienced lower thermal stress

and strain. Figure 101 presents the thermal strain in Resin Type-A due to change in the temperature. It can be seen that higher temperature zones exhibited higher strain. At the spring-line, where a thermal gradient existed, the strain at the higher temperatures region was more than doubled that of the lower temperature region. The magnitudes of the Von-Mises stress and strain on the mentioned nodes for Type-A resin are listed in Table 30 and Table 31.

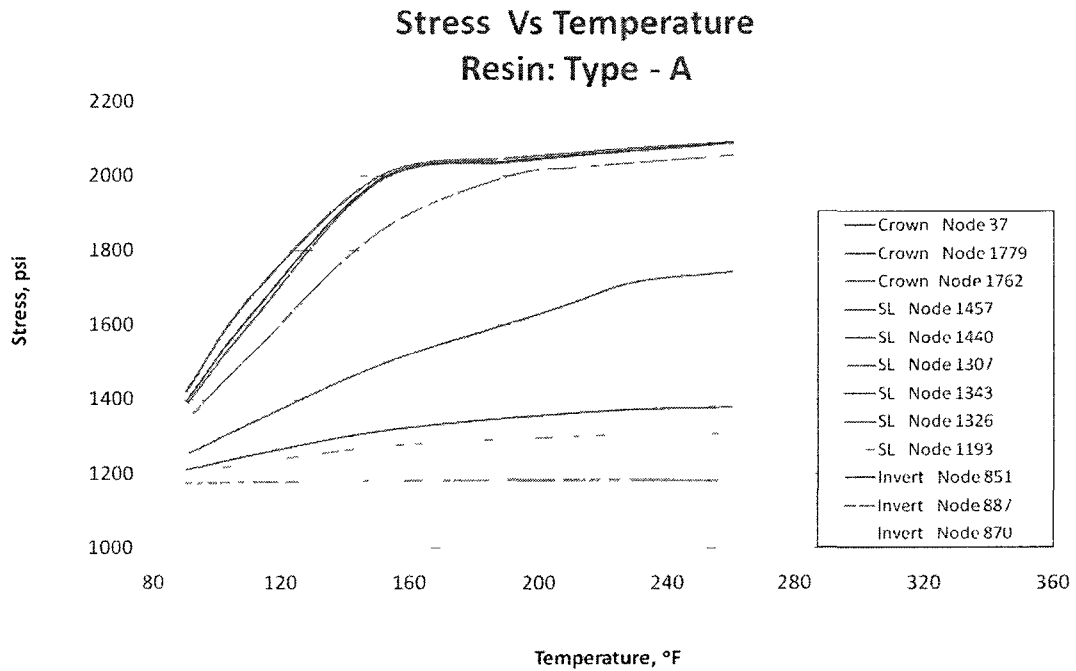


Figure 100: Thermal Stress on Liner Impregnated with Resin Type-A

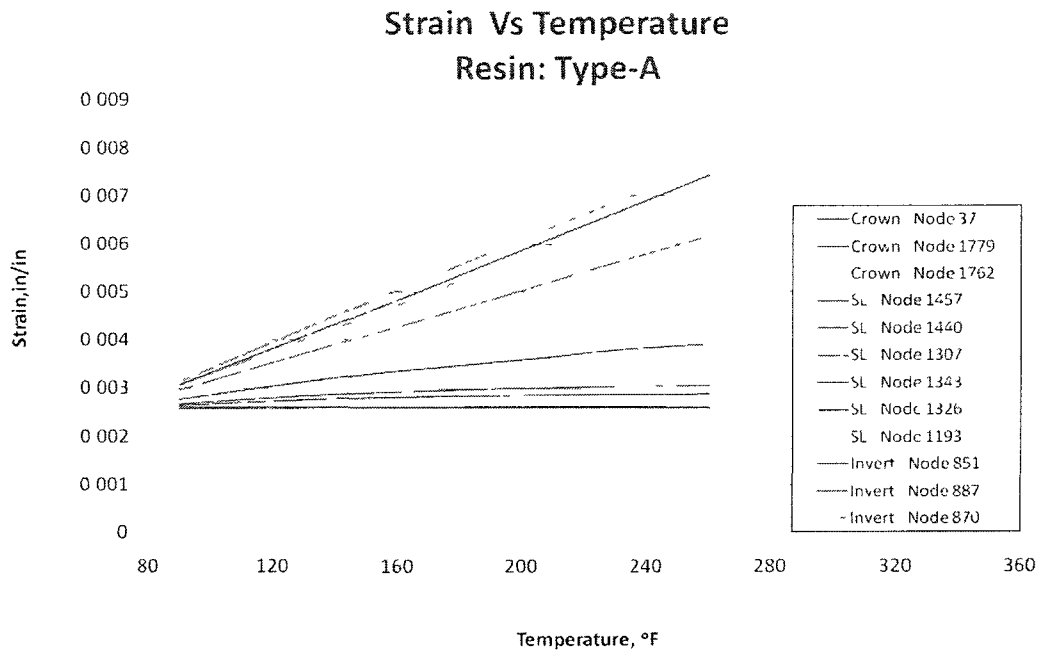


Figure 101: Thermal Strain on Liner Impregnated with Resin Type-A

Table 30: Von-Mises Stress (Equivalent Stress) at Selected Nodes in CIPP Liner Impregnated with Resin Type-A

Location	Nodes	Von-Mises Stress, psi						
		Invert 70° F and Outside 62° F						
		90° F	110° F	150° F	190° F	210° F	230° F	260° F
Crown	37	1420.5	1674.7	1999.1	2047.7	2062.3	2076.8	2091.7
	1779	1420.5	1674.7	1999.1	2047.7	2062.3	2076.8	2091.7
	1762	1420.1	1674.1	1999	2047.6	2062.2	2076.8	2091.7
Spring Line	1457	1395.1	1625.3	1989.4	2039.8	2055.9	2070.1	2091.3
	1440	1385.9	1606.5	1987.1	2036.8	2055.1	2069.3	2090
	1307	1343	1519.6	1851.4	1999.7	2023	2036.9	2056
	1343	1252.7	1337.2	1492.7	1604.7	1660.5	1716.9	1742.9
	1326	1209.5	1249.2	1314.4	1349.9	1363.3	1373.4	1379.2
	1193	1199.9	1229	1272.9	1293.3	1300.7	1306.4	1307.9
Invert	851	1174.1	1178.1	1180.3	1182.6	1183.5	1184	1180.1
	887	1174.1	1178.1	1180.3	1182.4	1183.4	1183.8	1180.2
	870	1174.5	1178.8	1181.4	1183.9	1184.8	1185.2	1181.3

Table 31: Von-Mises Strain (Equivalent Strain) at Selected Nodes in CIPP Liner Containing Type-A

Location	Nodes	Von-Mises Strain $\times 10^{-3}$ in/in						
		Spring line to Invert 70° F and Outside 62° F						
		90° F	110° F	150° F	190° F	210° F	230° F	260° F
Crown	37	3.130	3.690	4.788	5.848	6.374	6.898	7.654
	1779	3.130	3.690	4.788	5.848	6.374	6.898	7.654
	1762	3.129	3.689	4.786	5.846	6.373	6.897	7.653
Spring Line	1457	3.074	3.581	4.587	5.623	6.138	6.654	7.429
	1440	3.052	3.536	4.494	5.509	6.010	6.511	7.279
	1307	2.958	3.346	4.099	4.844	5.234	5.622	6.162
	1343	2.761	2.948	3.292	3.536	3.658	3.798	3.917
	1326	2.667	2.757	2.906	2.990	3.021	3.044	3.060
	1193	2.644	2.708	2.805	2.849	2.865	2.878	2.881
Invert	851	2.587	2.596	2.601	2.606	2.608	2.609	2.601
	887	2.587	2.596	2.601	2.606	2.608	2.609	2.601
	870	2.588	2.598	2.603	2.609	2.611	2.612	2.603

Figure 102 shows the effect of non-uniform temperature on Type-C liner. It can be seen that the liner material at the crown approached its plastic limit stress before the liner region at the invert. The liner segment at the spring-line zone was also approaching plastic limit. As invert temperature was lower, this zone exhibited lower thermal stress and strain.

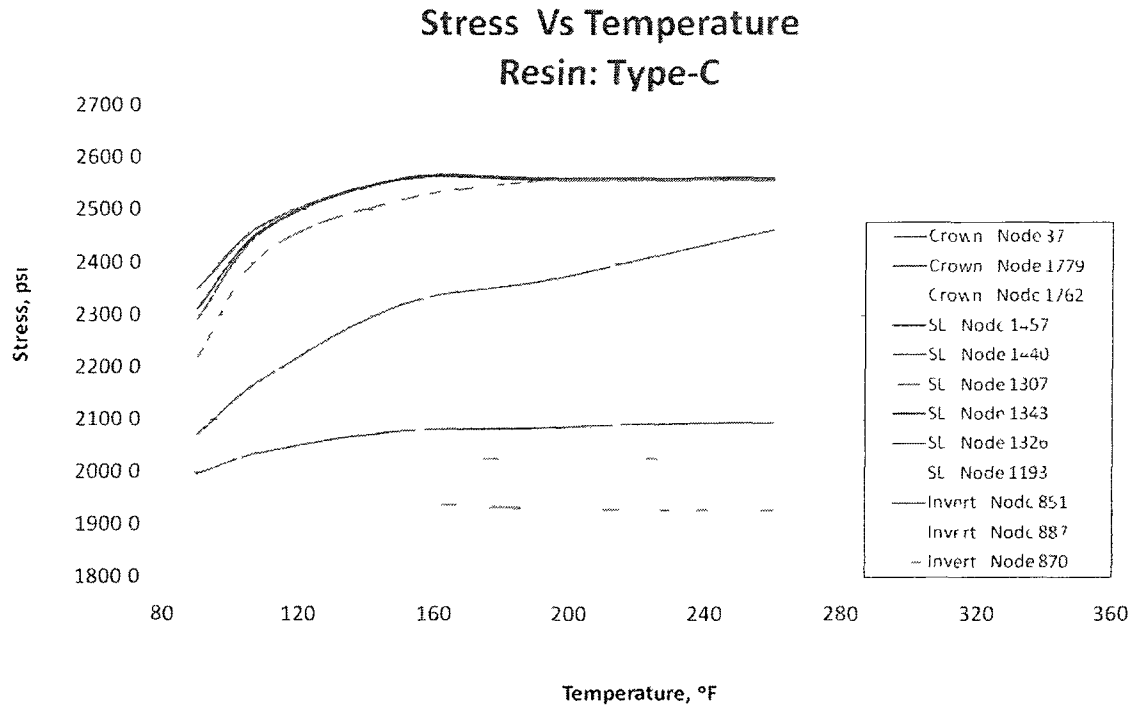


Figure 102: Thermal Stress on Liner Impregnated with Resin Type-C

Figure 103 presents the thermal strain due to the change in temperature. It is found that higher temperature zones faced more strain. At the spring-line, where a thermal gradient existed, strains at the higher temperatures region were found to be three times greater than those in the lower temperature region. The magnitudes of Von-Mises stress and strain on the mentioned nodes for Type-C resin are given in Table 32 and Table 33.

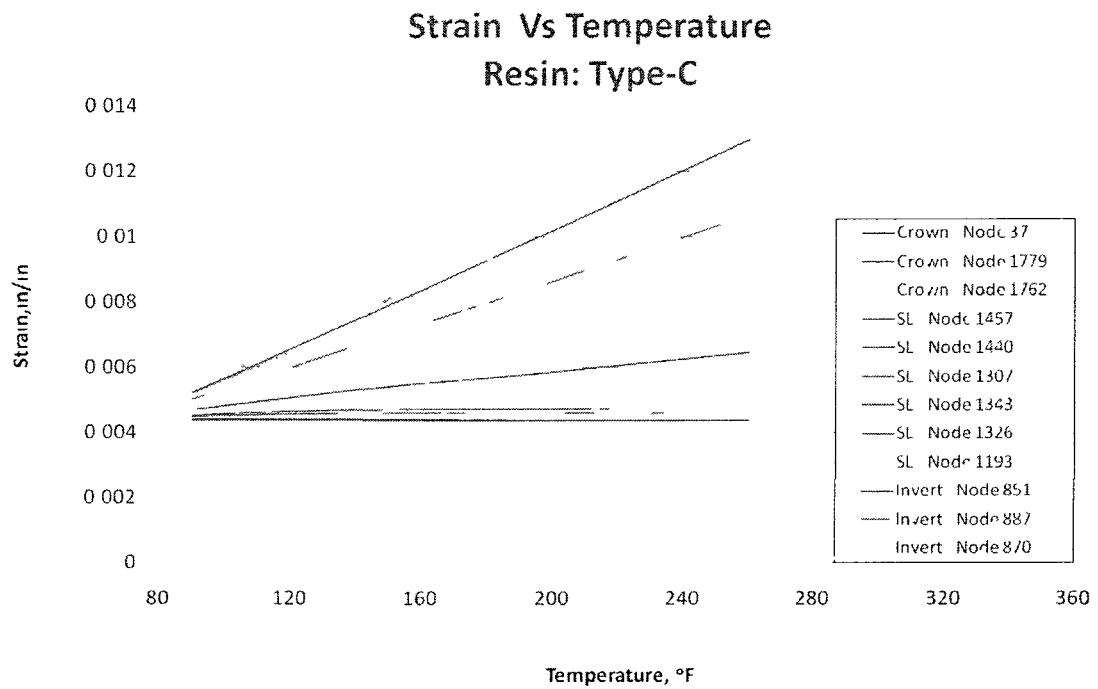


Figure 103: Thermal Strain on Liner Impregnated with Resin Type-C

Table 32: Von-Mises Stress (Equivalent Stress) at Selected Nodes in CIPP Liner Containing Type-C

Location	Nodes	Von-Mises Stress, psi						
		Invert 70° F and Outside 62° F						
		90° F	110° F	150° F	190° F	210° F	230° F	260° F
Crown	37	2350.4	2475.4	2560.2	2560.2	2560.2	2560.2	2560.2
	1779	2350.4	2475.4	2560.2	2560.2	2560.2	2560.2	2560.2
	1762	2350	2475.4	2560.2	2560.2	2560.2	2560.2	2560.2
Spring Line	1457	2311.3	2467.4	2560.3	2559.7	2559.6	2559.5	2559.5
	1440	2292.7	2464.7	2562.4	2563.1	2563.3	2563.4	2563.6
	1307	2218.7	2421.6	2521	2557.2	2560.9	2560.7	2560.5
	1343	2071.5	2180.6	2319.6	2362.5	2389.9	2419.7	2462.7
	1326	1996.9	2038.7	2078.6	2083.9	2089.4	2092.8	2094.7
	1193	1977.8	2003.8	2027.6	2023.3	2025	2025.2	2022.9
Invert	851	1938.4	1940.3	1941.2	1931	1929.1	1928.4	1927.5
	887	1938.4	1940.3	1941.2	1931	1929.1	1928.4	1927.5
	870	1938.7	1940.8	1941.8	1931.5	1929.6	1928.8	1927.8

Table 33: Von-Mises Strain (Equivalent Strain) at Selected Nodes in CIPP Liner Containing Type-C

Location	Nodes	Von-Mises Strain $\times 10^{-3}$ in/in						
		Spring line to Invert 70° F and Outside 62° F						
		90° F	110° F	150° F	190° F	210° F	230° F	260° F
Crown	37	5.337	6.276	8.132	9.922	10.836	11.754	13.127
	1779	5.337	6.276	8.132	9.922	10.837	11.755	13.128
	1762	5.336	6.275	8.131	9.922	10.836	11.754	13.129
Spring Line	1457	5.248	6.131	7.936	9.763	10.667	11.595	12.99
	1440	5.203	6.049	7.796	9.593	10.472	11.374	12.749
	1307	5.036	5.659	7.02	8.32	8.986	9.654	10.672
	1343	4.705	4.952	5.429	5.774	5.975	6.171	6.475
	1326	4.538	4.637	4.731	4.747	4.76	4.77	4.776
	1193	4.491	4.55	4.604	4.595	4.598	4.599	4.593
Invert	851	4.401	4.406	4.408	4.385	4.381	4.379	4.377
	887	4.401	4.406	4.408	4.385	4.381	4.379	4.377
	870	4.402	4.407	4.409	4.386	4.382	4.38	4.378

5.7 Case Study - Gap between Liner and Host-Pipe

The finite element simulation (see Figure 104) showed that the liner deformed more where annular space existed between the liner and host pipe in comparison to the installed liner without any annular space (see Figure 105). As the liner had some annular space, the contact element property no-bond and no-friction was used. This condition was created no force transfer situation from the liner to the host pipe. In this simulation the

temperature of the upper region was 212° F, the lower region and the outer peripheral surfaces were 160° F and 60° F respectively and the resin Type-A was simulated.

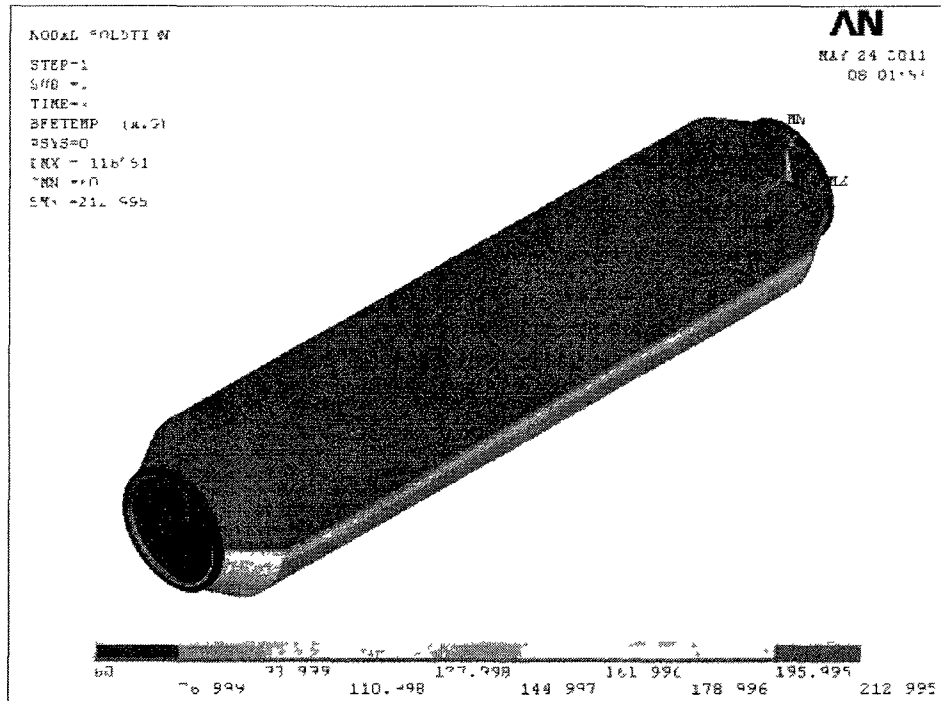


Figure 104: Change in Deformation Magnitude and Condition w/ Annular Space

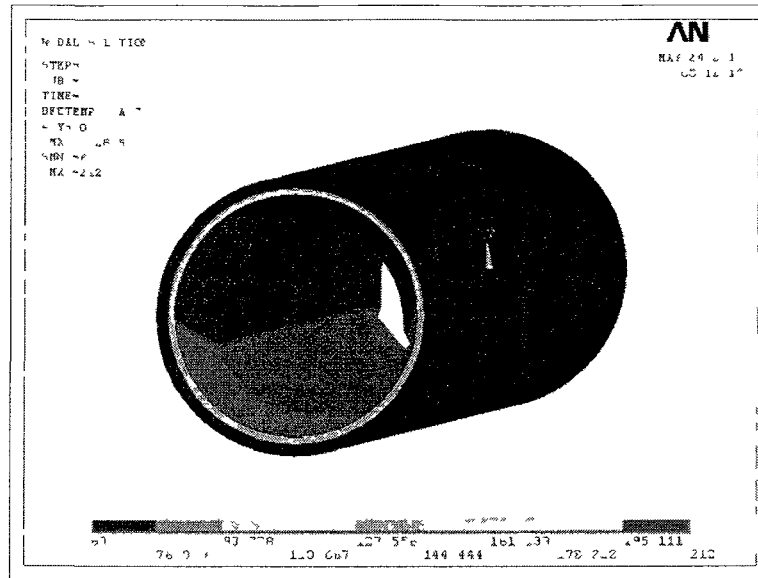


Figure 105: Change in Deformation Magnitude and Condition w/o Annular Space

Figure 106 shows the maximum deformation values with and without annular space for both resins at 212° F. It was found that the liner deflected around 2.5 to 5.0 times more where there was an annular space between the liner and host pipe compared to where there was no annular space. Therefore, the liner was shown more vulnerable to deflect under the same temperature condition.

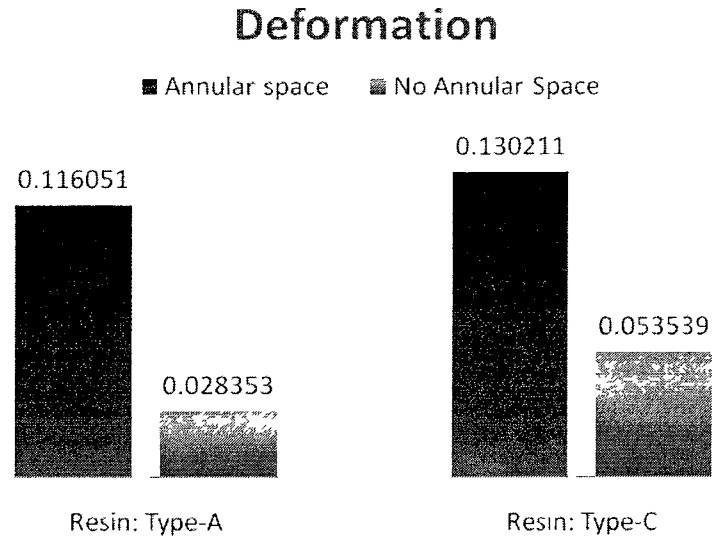


Figure 106: Maximum Deformation of the Resin at 212° F

5.8 Parametric Study – Liner Thickness

A parametric study was performed on the thickness of the liner and the Von-Mises stress value was compared to the long-term flexural strength of the liner. The temperature at the crown was kept at 200° F and that of the invert was 70° F. Peripheral temperature was assumed to be 62° F. In this case, the host pipe was assumed to be clay brick. The parametric study was performed for both Type-A and Type-C resin.

The simulation was performed on a 36 in. circular brick pipe. The pipe runs from W. 45th Street to 7th Avenue West (from M #68 to M #15) and is subjected to steam discharge. Structural and thermal properties of brick host pipe were obtained from literatures and are listed in Table 34 and Table 35.

Table 34: Material Properties of Brick Host Pipe

Material	Modulus of Elasticity	Poisson's Ratio	Density
	psi		snail/in ³
Brick	27.77e3	0.42	0.127e-3

Table 35: Physical Properties of Brick Host Pipe

Material	Specific Heat		Coefficient of Thermal Expansion	Thermal Conductivity	
	J/kg °K	in-lbf /snail ° F*	in/in/° F	W/m ⁰ K	in.lbf /in.sec. ° F *
Brick	1046.5	9.0125e5	10e-6	0.25	0.031

The Von-Mises stress values for the nodes listed in Table 26 are shown and compared with these in Table 36 and Table 37. It was observed that stresses on the crown for Type-C liner reached or exceeded the flexural strength limit in the case of the thinner liner. Views from FE analysis are shown in Figure 107 and Figure 108.

Table 36: Change in Von-Mises Stress Caused by Temperature for Different Liner Thickness (Resin: Type-A)

Location	Nodes	Von-Mises Stress, psi		
		Temperature at Crown 200° F, Invert 70° F and Outside 62° F		
		Pipe ID: 36 in., Segment Length: 5 ft.		
		Liner Thickness, mm		
		7.2	15.1	27.2
Crown	37	1566.6	1538.5	1530.0
	1779	1566.7	1538.5	1530.0
	1762	1566.6	1538.5	1529.8
Spring Line	1457	1469.6	1492.7	1447.8
	1440	1393.1	1428.6	1374.1
	1307	1184.3	1097.0	1066.8
	1343	522.84	327.08	355.22
	1326	97.782	77.753	85.086
	1193	114.89	100.98	89.862
Invert	851	138.81	141.34	142.83
	887	140.02	142.51	143.22
	870	138.79	140.99	142.05

Table 37: Change in Von-Mises Stress Caused by Temperature for Different Liner Thickness (Resin: Type-C)

Location	Nodes	Von-Mises Stress, psi		
		Temperature at Crown 200° F, Invert 70° F and Outside 62° F		
		Pipe ID: 36 in., Segment Length: 5 ft.		
		Liner Thickness, mm		
		7.2	15.1	27.2
Crown	37	2481.6	2468.4	2459.9
	1779	2481.5	2468.4	2459.9
	1762	2481.7	2468.4	2459.9
Spring Line	1457	2462.0	2462.0	2445.8
	1440	2419.8	2443.6	2360.3
	1307	2187.1	1929.1	1830.3
	1343	1073.2	601.84	624.34
	1326	144.34	101.69	113.34
	1193	187.82	155.98	134.26
Invert	851	210.41	220.81	229.40
	887	212.20	222.76	229.87
	870	210.32	220.68	228.25

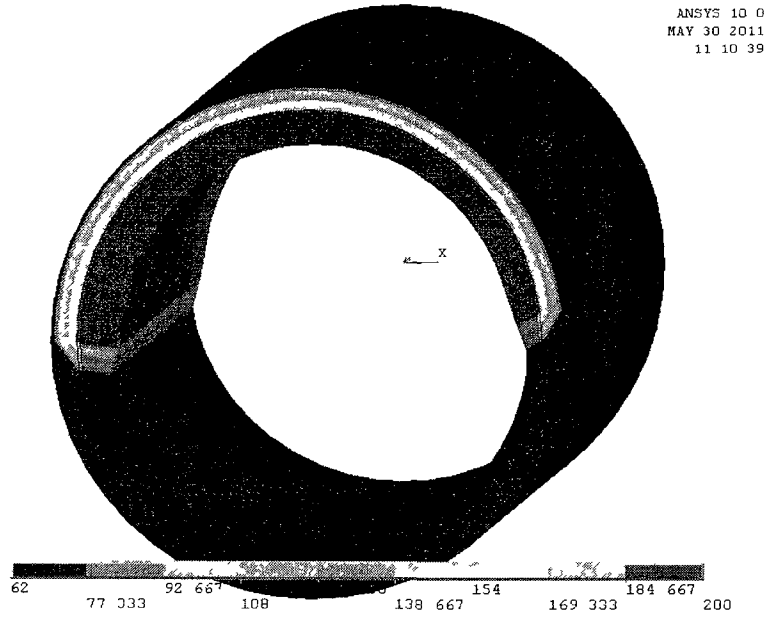


Figure 107: Temperature Distribution on the Liner

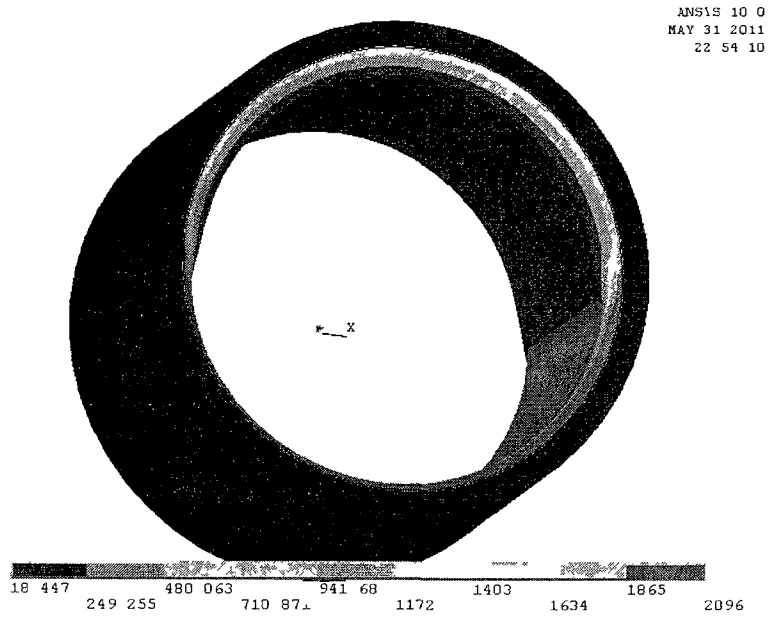


Figure 108: Von-Mises Stress Distribution on the Liner

5.9 Numerical Simulation – Projected Condition

In the projected condition, it was assumed that when the steam was injected into the sewer, the neighboring areas would experience an increase in temperature. Therefore, an uneven temperature distribution resulting in uneven stress and deformation was expected. An FE simulation was performed for three segments of brick pipes as shown in Figure 109.

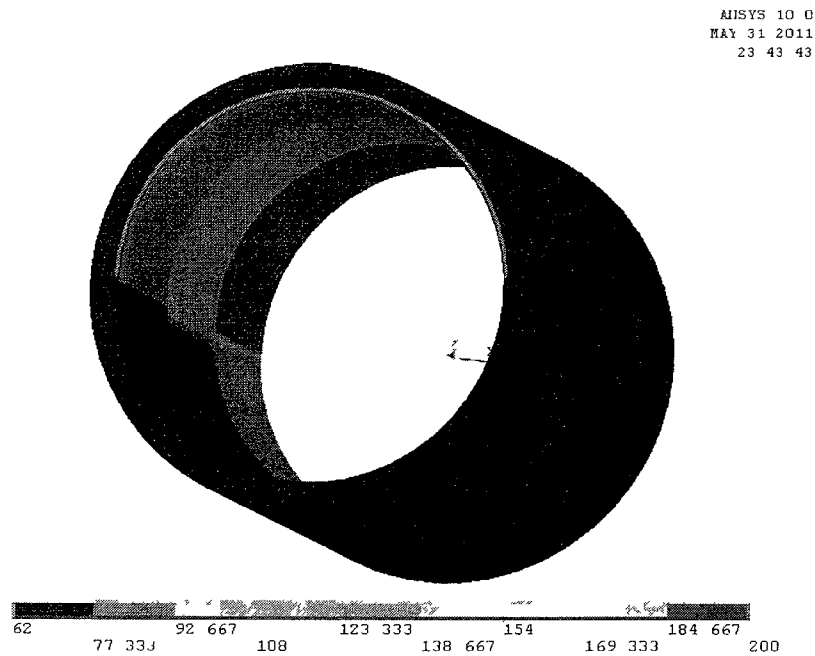


Figure 109: Temperature Distribution on the Three Segment Brick Pipe

Figure 110 shows the selected node path in the FE simulation. The node path covered from high temperature (200° F) to low temperature (80° F) regions along the crown through the entire length (100 ft) of the host pipe. Temperature distributions on the three segments are given in Table 38

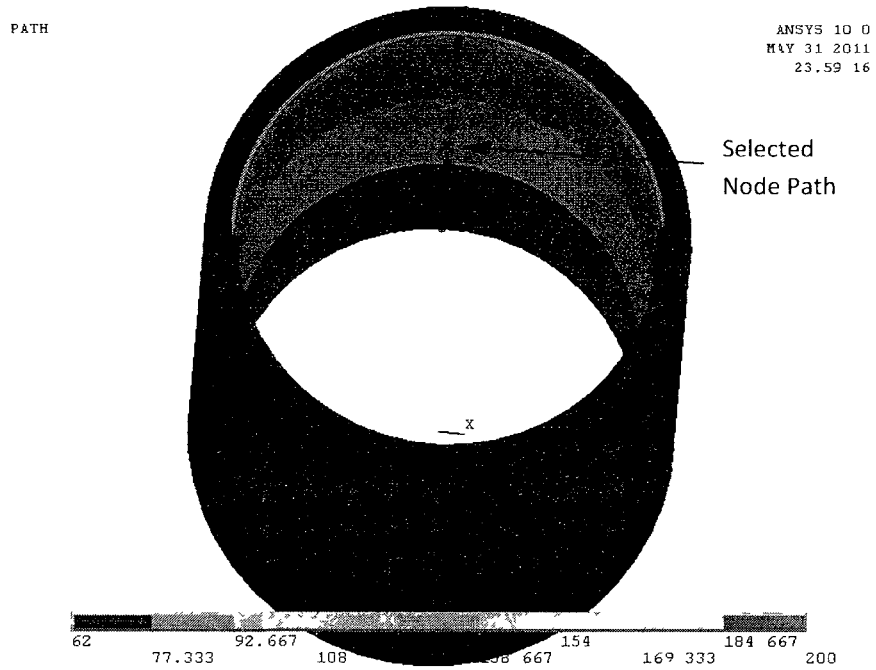


Figure 110: Selected Nodes on the Crown of the Three Segment Brick Pipe

Table 38: Temperature Value on the Three Segments of a Lined with Resin Type-A Brick Pipe

Segment	Location	Temperature, ° F
1	Crown	200
	Invert	100
2	Crown	120
	Invert	70
3	Crown	80
	Invert	70
	Outer Wall of Host Pipe	62

Figure 111 and Figure 112 show the Von-Mises stress and strain at the crown along the length of the pipe. Between the 120° F and 200° F region, stress increased around 6% while strain increased around 45%, clearly indicating a plastic behavior. In the lower temperature region (between 120° F and 80° F), increments of stress and strain were around 12% and 13%, respectively, which indicated elastic behavior.

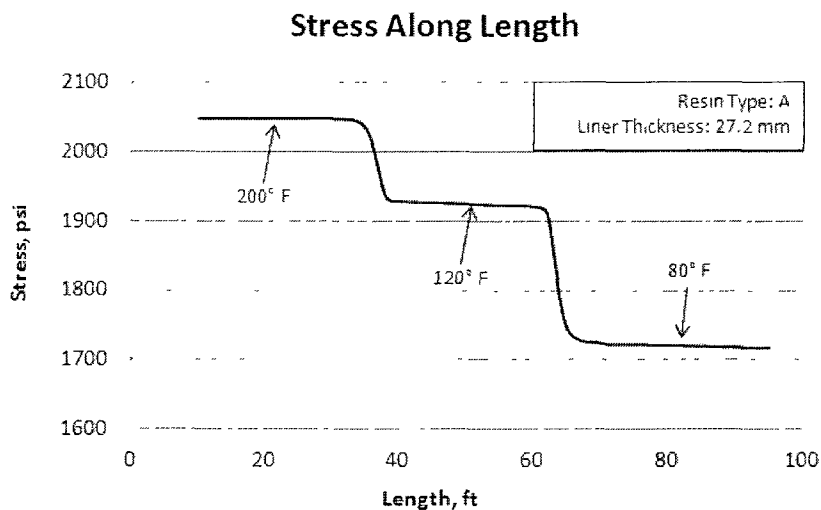


Figure 111: Von-Mises Stress along the Plotted Path on the Segments of Brick Host Pipe

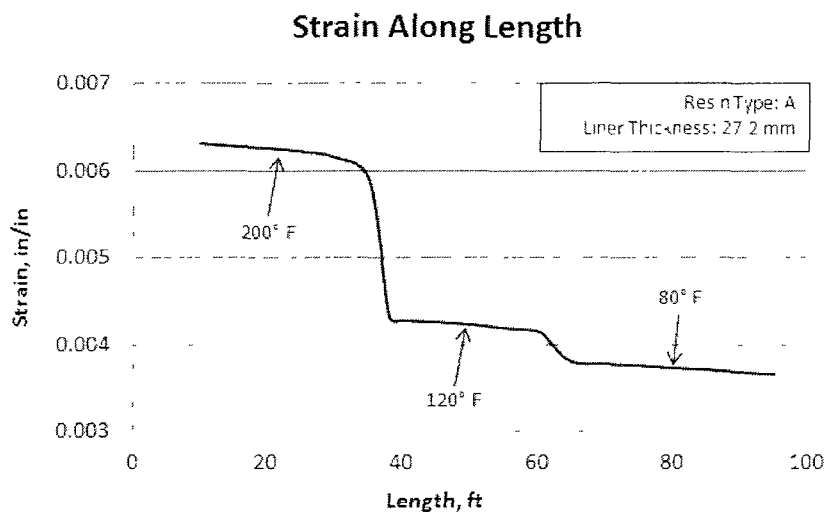


Figure 112: Von-Mises Strain along the Plotted Path on the Segments of Brick Host Pipe

5.10 Conclusion

The FE analysis revealed that the thermal gradient developed at the spring line of the CIPP liner results in strains that were three times greater above the water line than below it. The numerical analysis also suggested that liner deformation is 2.5 to 5 times greater in locations where an appreciable annular gap exists between the liner and the host pipe, compared with locations where such an annular gap was absent. Simulation of one of the brick sewers scheduled for replacement (located between W 45th St. and 7th Ave. West) revealed an increase of up to 50% in the stresses in the liner upon the introduction of the thermal load as a result of the steam. At this stage, creep data was not used in the FE model which resulted in higher stress than the plastic stress. Stresses are the highest at the spring line and the crown, and can be as high as 2500 psi. The development of such high stresses in the liner, combined with the degradation of the organic resin due to the elevated temperature, resulted in the on-set of creep, permanent deformation (due to plastic strain) and ultimately failure of the liner under repeated thermal loads.

CHAPTER 6

CONCLUSIONS, RECOMMENDATIONS, AND FUTURE WORK

6.1 Conclusions

The research demonstrated that thermal loads can initiate and accelerate creep in the liner, leading to plastic strains and permanent deformation. The thermally-induced in-plane shear strains caused bulging of the liner, ultimately leading to the formation of folds and premature failure.

In this research, three types of resin – polyester, epoxy and vinyl ester resins – were used at the bench-scale phase. Although the price of polyester resin per linear foot is the cheapest and used in most of the CIPP liner project involved with sewer rehabilitation, the results of the bench-scale experimental study revealed that polyester resin (Resin Type-D) becomes brittle after only 180 temperature cycles and is not suitable for elevated temperature application. Therefore, it was not considered for the Phase-II application where full-scale experimental study was performed.

The results of the full scale experimental study revealed that a CIPP liner impregnated with the vinyl ester resin (Resin Type-A) performed adequately after being subjected to 1,000 thermal load cycles between 90° F and 210° F and the epoxy resin (Resin Type-C), although performed better than polyester resin, exhibited premature failure under the same condition.

Extrapolating the test data collected in the course of this study, a perfectly circular CIPP liner impregnated with Resin Type-A might be able to withstand as many as 10,000 thermal cycles of 90° F to 210° F before experiencing catastrophic failure, although a more conservative value should be used for design purposes to account for geometrical imperfections and installation defects.

6.2 Recommendations

Vinyl ester and epoxy-based resins are typically more expensive than polyester resins. For the specific resins used in this study, the added cost for using a vinyl ester resin or epoxy based resin is between 25% and 30% in terms of the costs of the neat resin. In the case of an 8 in. diameter and 7 mm thick CIPP liner, approximately 2.5 lb of resin is used per linear foot, representing an increase of about \$3.50/lf in terms of material costs or \$0.0625/lf/inch diameter/mm thickness of felt. Assuming an average cost of \$25 per linear foot for an 8 in. CIPP liner (residential setting, low traffic volume), the increase in construction costs is around 14%. While this value is likely to vary as a function of different variables (pipe diameter, liner thickness, complexity of the construction project, project setting, shape of the host structure), a value between 10% and 15% can be used as a preliminary benchmark to estimate the added project cost associated with the requirement for the liner to operate in elevated temperature environments.

6.3 Future Work

The effect of elevated temperature on resin – liner combination is not considered in the current design procedures. Result obtained from this study can be used to incorporate the potential effect of thermally induced strains in the design equation (e.g. ASTM F1216, a widely accepted design practice for the rehabilitation of buried pipes

using resin impregnated tubes). This work will include the effect of elevated temperature load on the buckling stress of the liner. The existing undamaged or minimal damaged full scale sample can be used for this study.

Another future work might be to evaluate the resulting stresses from thermally induced in-plane shear strains in real sewer pipe and to examine ways in which these strains could be accounted for by the current design procedures.

Heat transfer in CIPP liners installed in sewer pipes subjected to high temperatures is generally accomplished by conduction and takes place relatively quickly. However, heat transfer into the surrounding soil is a much longer process. Therefore, temperature sensors can be installed in the vicinity of a steam trap (see Figure 113) to closely monitor real-time temperatures.

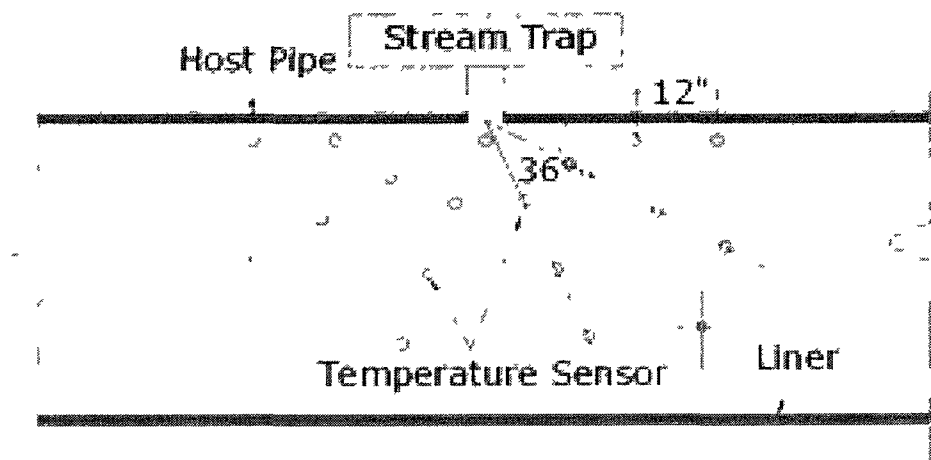


Figure 113: Proposed Installation of Distributed Thermal Sensors in the Vicinity of a Stream Trap

APPENDIX A

TENSILE AND BENDING MODULUS ELASTICITY

OF EACH DURATION SPECIMEN MADE

OF FOUR RESIN TYPES

A.1 Resin Type-A; Test Specimen; ASTM D638

0 day			
Sample	E, psi	Strain, in/in	Stress, psi
1	497107.0	0.002678	1331.25
2	507065.0	0.002874	1457.30
3	515167.0	0.002275	1172.00
4	508603.0	0.002242	1140.29
5	572726.0	0.003435	1967.31
6	535921.0	0.003076	1648.49
7	561536.0	0.003294	1849.98
8	539909.0	0.003061	1652.61
9	546619.0	0.002191	1197.72
10	564368.0	0.002757	1555.72
11	530065.0	0.003258	1726.96
12	517782.0	0.002550	1320.22
13	515454.0	0.003668	1890.82
14	541421.0	0.003230	1748.75
Mean	532410.2	0.002899	1547.10
SD	23380.5	0.000468	279.5
% Dev	4.4	16.1	18.1

7 days			
Sample	E, psi	Strain, in/in	Stress, psi
1	491624.0	0.003472	1706.919
2	450845.0	0.002827	1274.539
3	451630.0	0.002705	1221.659
4	510695.0	0.002892	1476.930
5	475214.0	0.005084	2415.988
6	501276.0	0.002746	1376.504
7	495626.0	0.003518	1743.484
8	458621.0	0.002992	1372.372
9	484717.0	0.004298	2083.339
10	489536.0	0.003005	1470.812
11	486528.0	0.004611	2243.160
12	456349.0	0.003095	1412.306
13	483492.0	0.002762	1335.402
14	503709.0	0.004282	2156.905
Mean	481418.7	0.003449	1663.59
SD	19942.8	0.000794	400.6
% Dev	4.1	23.0	24.1

14 days			
Sample	E, psi	Strain, in/in	Stress, psi
1	566392.0	0.001547	876.21
2	490422.0	0.002947	1445.27
3	488811.0	0.001821	890.12
4	522579.0	0.002863	1496.14
5	531800.0	0.004254	2262.28
6	520000.0	0.002686	1396.72
7	525146.0	0.003883	2038.93
8	546920.0	0.003348	1831.09
9	501962.0	0.001820	913.77
10	543739.0	0.002774	1508.39
11	557395.0	0.003648	2033.47
12	510723.0	0.003425	1749.01
13	501493.0	0.003178	1593.91
14	554623.0	0.003718	2061.86
Mean	525857.5	0.002994	1578.37
SD	25315.2	0.000817	454.4
% Dev	4.8	27.3	28.8

28 days			
Sample	E, psi	Strain, in/in	Stress, psi
1	479906.0	0.003107	1491.07
2	535419.0	0.001896	1015.15
3	497935.0	0.001700	846.49
4	542130.0	0.001380	748.14
5	501256.0	0.002842	1424.57
6	522797.0	0.002572	1344.63
7	485587.0	0.002090	1014.71
8	503127.0	0.002041	1026.79
9	512958.0	0.001959	1005.02
10	516420.0	0.001760	908.73
11	504557.0	0.002105	1062.09
12	480297.0	0.001905	914.98
13	493613.0	0.002110	1041.34
14	509564.0	0.001688	860.11
Mean	506111.9	0.002082	1050.27
SD	18876.2	0.000468	220.8
% Dev	3.7	22.5	21.0

2 Months			
Sample	E, psi	Strain, in/in	Stress, psi
1	597522.0	0.002289	1367.73
2	474842.0	0.005131	2436.41
3	488976.0	0.002724	1331.97
4	467832.0	0.002842	1329.58
5	510650.0	0.002611	1333.31
6	485575.0	0.003119	1514.51
7	479893.0	0.004125	1979.72
8	487587.0	0.003460	1686.87
9	480225.0	0.002488	1194.98
10	484531.0	0.003755	1819.33
11	497654.0	0.002888	1437.16
12	477679.0	0.004783	2284.87
13	495263.0	0.002677	1325.69
14	493017.0	0.004122	2032.29
Mean	494374.7	0.003358	1648.17
SD	31552.0	0.000894	398.7
% Dev	6.4	26.6	24.2

3 Months			
Sample	E, psi	Strain, in/in	Stress, psi
1	471646.0	0.002119	999.42
2	541286.0	0.005152	2788.71
3	451400.0	0.004674	2109.84
4	484936.0	0.005509	2671.51
5	477169.0	0.005349	2552.38
6	485287.0	0.004561	2213.39
7	500620.0	0.003859	1931.77
8	480843.0	0.004746	2282.24
9	518802.0	0.002519	1306.98
10	514200.0	0.002244	1153.87
11	472178.0	0.005346	2524.05
12	479484.0	0.005706	2735.81
13	478120.0	0.004419	2112.70
14	518493.0	0.005080	2633.86
Mean	491033.1	0.004377	2144.04
SD	24254.5	0.001230	598.6
% Dev	4.9	28.1	27.9

4 Months			
Sample	E, psi	Strain, in/in	Stress, psi
1	433708.0	0.005296	2296.92
2	510539.0	0.005296	2703.81
3	503571.0	0.004739	2386.42
4	505158.0	0.006166	3114.80
5	488580.0	0.006104	2982.29
6	488311.0	0.005520	2695.48
7	488466.0	0.006087	2973.29
8	488507.0	0.005533	2702.79
9	488467.0	0.005839	2852.12
10	488317.0	0.006103	2980.13
11	488532.0	0.005570	2721.15
12	488469.0	0.005668	2768.44
13	488402.0	0.005584	2727.14
14	488554.0	0.005717	2793.21
Mean	488398.6	0.005659	2764.14
SD	17524.6	0.000395	222.9
% Dev	3.6	7.0	8.1

5 Months			
Sample	E, psi	Strain, in/in	Stress, psi
1	505965.0	0.006883	3482.38
2	512095.0	0.006926	3546.72
3	495672.0	0.006021	2984.34
4	560065.0	0.006424	3597.65
5	500789.0	0.006778	3394.53
6	498688.0	0.006428	3205.43
7	515418.0	0.006382	3289.51
8	497842.0	0.006774	3372.41
9	511673.0	0.005900	3018.95
10	497820.0	0.006500	3235.65
11	502213.0	0.006521	3274.87
12	516615.0	0.005850	3022.13
13	501486.0	0.006534	3276.61
14	518001.0	0.006273	3249.63
Mean	509595.9	0.006442	3282.20
SD	16436.8	0.000342	189.2
% Dev	3.2	5.3	5.8

6 Months			
Sample	E, psi	Strain, in/in	Stress, psi
1	530189.0	0.006582	3489.67
2	560326.0	0.007652	4287.39
3	524658.0	0.006055	3176.83
4	495624.0	0.006314	3129.57
5	556452.0	0.007106	3954.38
6	535421.0	0.007271	3892.86
7	560201.0	0.006840	3831.98
8	557185.0	0.007363	4102.65
9	546575.0	0.006649	3634.29
10	514151.0	0.007088	3644.08
11	545446.0	0.006967	3799.86
12	516448.0	0.006182	3192.87
13	498348.0	0.007095	3535.92
14	531137.0	0.006329	3361.38
Mean	533725.8	0.006821	3645.27
SD	21956.5	0.000482	355.6
% Dev	4.1	7.1	9.8

A.2 Resin Type-B; Test Specimen; ASTM D638

0 day			
Sample	E, psi	Strain, in/in	Stress, psi
1	343802.0	0.006424	2208.58
2	420961.0	0.006185	2603.64
3	379386.0	0.007097	2692.50
4	394454.0	0.004694	1851.57
5	474608.0	0.002093	993.35
6	402642.0	0.005299	2133.60
7	363630.0	0.005866	2133.11
8	390929.0	0.005677	2219.32
9	438874.0	0.004994	2191.71
10	433007.0	0.004611	1996.63
11	402270.0	0.005028	2022.47
12	427048.0	0.004998	2134.51
13	437338.0	0.005037	2203.06
14	414165.0	0.005181	2145.90
15	416111.0	0.004870	2026.48
16	409409.0	0.005293	2167.19
17	425868.0	0.004707	2004.75

Continued to next page

Sample	E, psi	Strain, in/in	Stress, psi
--------	--------	---------------	-------------

18	419475.0	0.005011	2101.79
19	368877.0	0.005998	2212.36
20	426374.0	0.004959	2114.41
21	380944.0	0.005440	2072.42
22	375598.0	0.005934	2228.71
23	371062.0	0.005345	1983.15
24	387679.0	0.005041	1954.38
25	418156.0	0.004800	2007.33
26	400771.0	0.005264	2109.81
27	364360.0	0.006089	2218.55
28	432705.0	0.004617	1997.85
29	364215.0	0.005939	2162.90
30	403966.0	0.005533	2235.13
Mean	402956.13	0.005267	2104.24
SD	29170.48	0.000845	268.92
% Dev	7.24	16.04	12.78

7 days			
Sample	E, psi	Strain, in/in	Stress, psi
1	402309.0	0.003395	1365.84
2	417563.0	0.004719	1970.48
3	535065.0	0.003911	2092.64
4	449226.0	0.007357	3304.96
5	381366.0	0.006886	2626.09
6	437105.0	0.005254	2296.55
7	477198.0	0.005246	2503.49
8	469313.0	0.004498	2110.89
9	430378.0	0.005273	2269.36
10	472259.0	0.005307	2506.33
11	445263.0	0.005105	2273.15
12	427035.0	0.005654	2414.55
13	465235.0	0.004566	2124.46
14	438989.0	0.005418	2378.42
15	411631.0	0.005444	2240.79
16	445958.0	0.005154	2298.33
17	447738.0	0.005289	2367.98

Continued to next page

Sample	E, psi	Strain, in/in	Stress, psi
18	414986.0	0.003395	1365.84
19	418337.0	0.004719	1970.48
20	417601.0	0.003911	2092.64
21	419239.0	0.005822	2440.71
22	477607.0	0.004775	2280.58
23	416252.0	0.005330	2218.79
24	454729.0	0.005189	2359.38
25	409135.0	0.005415	2215.61
26	442139.0	0.004546	2009.75
27	426332.0	0.005660	2413.20
28	408541.0	0.005311	2169.90
29	444223.0	0.005660	2514.24
30	414838.0	0.004957	2056.40
Mean	437253.00	0.005285	2302.86
SD	30162.77	0.000753	301.45
% Dev	6.90	14.25	13.09

14 days			
Sample	E, psi	Strain, in/in	Stress, psi
1	375304.0	0.003395	1365.84
2	458244.0	0.004719	1970.48
3	312442.0	0.003911	2092.64
4	387786.0	0.007357	3304.96
5	443088.0	0.006886	2626.09
6	395373.0	0.005254	2296.55
7	371379.0	0.005246	2503.49
8	362114.0	0.004498	2110.89
9	384066.0	0.005273	2269.36
10	397542.0	0.005307	2506.33
11	401491.0	0.005105	2273.15
12	400803.0	0.005654	2414.55
13	410109.0	0.004566	2124.46
14	389084.0	0.005418	2378.42
15	439495.0	0.005444	2240.79
16	382733.0	0.005154	2298.33
17	393185.0	0.005289	2367.98

Continued to next page

Sample	E, psi	Strain, in/in	Stress, psi
18	367496.0	0.003395	1365.84
19	420308.0	0.004719	1970.48
20	422240.0	0.003911	2092.64
21	381033.0	0.007603	2896.94
22	382753.0	0.008795	3366.37
23	413043.0	0.007294	3012.88
24	422306.0	0.006851	2893.20
25	399358.0	0.008399	3354.15
26	400610.0	0.007768	3112.08
27	426313.0	0.006276	2675.64
28	406660.0	0.008341	3391.90
29	361136.0	0.008852	3196.71
30	365913.0	0.008614	3152.13
Mean	395780.23	0.007710	3041.62
SD	29067.71	0.001278	505.98
% Dev	7.34	16.58	16.64

28 days			
Sample	E, psi	Strain, in/in	Stress, psi
1	485083.0	0.011856	5751.14
2	441596.0	0.012658	5589.50
3	590533.0	0.005514	3256.20
4	521644.0	0.011312	5900.84
5	537030.0	0.005409	2904.80
6	515177.0	0.009350	4816.90
7	468248.0	0.007160	3352.69
8	585372.0	0.009287	5436.11
9	480533.0	0.009013	4331.20
10	555929.0	0.010169	5653.26
11	488335.0	0.008854	4323.86
12	459204.0	0.011680	5363.32
13	589152.0	0.008191	4825.67
14	454269.0	0.010945	4972.16
15	450088.0	0.012869	5792.18
16	589047.0	0.009301	5478.86
17	552361.0	0.009075	5012.74

Continued to next page

Sample	E, psi	Strain, in/in	Stress, psi
18	536559.0	0.010176	5460.20
19	544004.0	0.009258	5036.54
20	489642.0	0.011417	5590.32
21	581161.0	0.007956	4623.92
22	567892.0	0.006698	3803.60
23	526497.0	0.008617	4536.91
24	509446.0	0.010565	5382.35
25	452231.0	0.010303	4659.50
26	527562.0	0.006756	3564.45
27	485795.0	0.009778	4749.91
28	505168.0	0.009622	4860.83
29	479929.0	0.007380	3541.73
30	482882.0	0.008954	4323.59
Mean	515078.97	0.009337	4763.18
SD	46689.74	0.001919	832.49
% Dev	9.06	20.55	17.48

2 Months			
Sample	E, psi	Strain, in/in	Stress, psi
1	597522.0	0.006289	3757.82
2	474843.0	0.007131	3386.11
3	488977.0	0.010724	5243.79
4	467833.0	0.009181	4295.17
5	510650.0	0.010611	5418.51
6	485575.0	0.008787	4266.75
7	453743.0	0.009203	4175.89
8	444370.0	0.008044	3574.44
9	441943.0	0.007708	3406.48
10	481327.0	0.007451	3586.45
11	535192.0	0.006284	3363.12
12	504155.0	0.007507	3784.90
13	513829.0	0.006982	3587.44
14	471613.0	0.010550	4975.38
15	490217.0	0.010362	5079.76
16	452419.0	0.009893	4475.88
17	448621.0	0.009421	4226.55

Continued to next page

Sample	E, psi	Strain, in/in	Stress, psi
18	474470.0	0.010605	5031.57
19	513900.0	0.007378	3791.61
20	451738.0	0.010940	4941.88
21	530814.0	0.008903	4726.04
22	483551.0	0.009519	4602.71
23	462881.0	0.008070	3735.63
24	446838.0	0.010593	4733.37
25	502525.0	0.007314	3675.58
26	453777.0	0.008277	3755.85
27	503082.0	0.008096	4072.84
28	463620.0	0.008259	3829.25
29	485924.0	0.009647	4687.93
30	520770.0	0.008865	4616.46
Mean	485223.97	0.008753	4226.84
SD	34230.93	0.001395	613.28
% Dev	7.05	15.93	14.51

3 Months			
Sample	E, psi	Strain, in/in	Stress, psi
1	564798.0	0.007653	4322.40
2	548553.0	0.004894	2684.62
3	562322.0	0.017432	9802.40
4	593746.0	0.007109	4220.94
5	723545.0	0.003648	2639.49
6	598592.0	0.008147	4876.73
7	600714.0	0.008100	4865.88
8	579933.0	0.006271	3637.04
9	612829.0	0.009033	5535.95
10	598543.0	0.009476	5671.59
11	578258.0	0.009328	5393.70
12	631131.0	0.009248	5836.84
13	599285.0	0.006662	3992.61
14	555779.0	0.011956	6645.06
15	612476.0	0.008705	5331.57
16	630729.0	0.006786	4280.22
17	606592.0	0.007158	4342.05

Continued to next page

Sample	E, psi	Strain, in/in	Stress, psi
18	613808.0	0.007192	4414.53
19	569234.0	0.009435	5370.68
20	635929.0	0.008684	5522.65
21	555187.0	0.010271	5702.28
22	621050.0	0.007269	4514.52
23	596139.0	0.007269	4333.34
24	585799.0	0.009101	5331.12
25	554054.0	0.006096	3377.26
26	558560.0	0.006995	3907.24
27	640177.0	0.009454	6052.22
28	612676.0	0.005891	3609.42
29	589666.0	0.008108	4780.73
30	620939.0	0.006740	4184.84
Mean	598368.10	0.008137	4839.33
SD	35664.00	0.002428	1341.27
% Dev	5.96	29.84	27.72

4 Months			
Sample	E, psi	Strain, in/in	Stress, psi
1	457408.0	0.011581	5297.24
2	531243.0	0.007356	3907.82
3	563600.0	0.009412	5304.60
4	524793.0	0.005603	2940.42
5	558517.0	0.008199	4579.28
6	527112.0	0.008430	4443.55
7	588147.0	0.006201	3647.13
8	555718.0	0.009246	5138.03
9	590846.0	0.007570	4472.61
10	490014.0	0.007164	3510.65
11	526896.0	0.010659	5616.17
12	485390.0	0.009355	4540.78
13	561230.0	0.008796	4936.78
14	493154.0	0.010738	5295.40
15	570169.0	0.007225	4119.45
16	514213.0	0.009408	4837.80
17	563763.0	0.010042	5661.46

Continued to next page

Sample	E, psi	Strain, in/in	Stress, psi
18	538032.0	0.009045	4866.48
19	470714.0	0.007485	3523.32
20	550134.0	0.008877	4883.62
21	500545.0	0.010418	5214.86
22	494778.0	0.006430	3181.37
23	557076.0	0.006090	3392.43
24	556521.0	0.006226	3464.88
25	505249.0	0.006194	3129.46
26	519327.0	0.010834	5626.57
27	527746.0	0.009595	5063.47
28	508222.0	0.007558	3841.33
29	483480.0	0.010307	4983.37
30	509512.0	0.007597	3870.67
Mean	527451.63	0.008455	4443.03
SD	34766.23	0.001673	832.17
% Dev	6.59	19.79	18.73

5 Months			
Sample	E, psi	Strain, in/in	Stress, psi
1	509022.0	0.010740	5467.03
2	548724.0	0.009709	5327.52
3	543549.0	0.009509	5168.52
4	519932.0	0.011472	5964.70
5	471055.0	0.005496	2589.01
6	493430.0	0.006116	3017.88
7	473015.0	0.010360	4900.62
8	474160.0	0.006327	3000.15
9	435188.0	0.008479	3689.81
10	515173.0	0.010274	5292.79
11	445356.0	0.011305	5034.54
12	469175.0	0.007376	3460.57
13	492848.0	0.006781	3341.77
14	464272.0	0.011567	5370.12
15	540510.0	0.011076	5986.81
16	484395.0	0.006050	2930.81
17	521644.0	0.008266	4311.75

Continued to next page

Sample	E, psi	Strain, in/in	Stress, psi
18	462908.0	0.009495	4395.18
19	502934.0	0.011436	5751.50
20	424868.0	0.006461	2745.02
21	421000.0	0.011340	4774.16
22	551683.0	0.010219	5637.52
23	550004.0	0.006085	3346.69
24	519771.0	0.005444	2829.59
25	471799.0	0.008565	4041.02
26	525723.0	0.004844	2546.79
27	428122.0	0.013056	5589.75
28	518453.0	0.006525	3383.15
29	462229.0	0.010954	5063.46
30	457420.0	0.011956	5468.79
Mean	489945.40	0.008909	4347.57
SD	39425.70	0.002403	1161.08
% Dev	8.05	26.97	26.71

6 Months			
Sample	E, psi	Strain, in/in	Stress, psi
1	582969.0	0.008082	4711.67
2	501294.0	0.011325	5677.05
3	521339.0	0.008157	4252.65
4	573323.0	0.009308	5336.55
5	501424.0	0.008605	4314.63
6	613504.0	0.008728	5354.47
7	511785.0	0.009992	5113.87
8	508835.0	0.010025	5101.22
9	566185.0	0.007597	4301.36
10	607231.0	0.009444	5734.52
11	512814.0	0.007869	4035.10
12	539344.0	0.009281	5005.75
13	573066.0	0.007530	4315.33
14	566944.0	0.009587	5435.18
15	586998.0	0.007550	4431.95
16	584607.0	0.008558	5003.17
17	565786.0	0.006822	3859.99

Continued to next page

Sample	E, psi	Strain, in/in	Stress, psi
18	599326.0	0.008980	5382.04
19	600945.0	0.008517	5118.53
20	598424.0	0.007402	4429.32
21	547752.0	0.007213	3950.73
22	506458.0	0.010888	5514.49
23	586397.0	0.009666	5667.97
24	601274.0	0.007350	4419.19
25	605707.0	0.008314	5035.98
26	574944.0	0.008860	5093.87
27	507698.0	0.009619	4883.75
28	588840.0	0.008332	4905.96
29	541833.0	0.010376	5622.17
30	589899.0	0.007508	4429.21
Mean	562231.50	0.008716	4881.25
SD	37353.10	0.001147	557.96
% Dev	6.64	13.15	11.43

A.3 Resin Type-C; Test Specimen; ASTM D638

0 day			
Sample	E, psi	Strain, in/in	Stress, psi
1	506179.0	0.013301	6732.69
2	409210.0	0.010941	4477.17
3	479288.0	0.012216	5854.98
4	454806.0	0.004697	2136.22
5	406062.0	0.007504	3047.09
6	603748.0	0.006008	3627.32
7	505508.0	0.007871	3979.00
8	490203.0	0.010932	5359.03
9	456954.0	0.008983	4104.79
10	498922.0	0.011943	5958.70
11	457143.0	0.006945	3174.81
12	471101.0	0.006879	3240.75
13	478624.0	0.011728	5613.29
14	505566.0	0.007788	3937.44
15	469859.0	0.009757	4584.55
16	457908.0	0.013051	5976.08
17	486281.0	0.007159	3481.46

Continued to next page

Sample	E, psi	Strain, in/in	Stress, psi
18	475467.0	0.012197	5799.05
19	504046.0	0.008524	4296.46
20	455176.0	0.012331	5612.83
21	457092.0	0.010832	4951.16
22	483227.0	0.007098	3429.84
23	462906.0	0.008117	3757.27
24	506111.0	0.006053	3063.25
25	502368.0	0.007863	3950.24
26	481654.0	0.010164	4895.38
27	491396.0	0.009900	4864.70
28	491152.0	0.011695	5744.01
29	470422.0	0.007371	3467.58
30	459648.0	0.007996	3675.27
Mean	479267.6	0.009261	4426.41
SD	33968.09	0.002340	1115.80
% Dev	7.09	25.27	25.21

7 days			
Sample	E, psi	Strain, in/in	Stress, psi
1	403150.0	0.003707	1494.48
2	358913.0	0.006433	2308.89
3	375468.0	0.005703	2141.29
4	391581.0	0.006266	2453.65
5	369112.0	0.004291	1583.86
6	379644.0	0.005280	2004.52
7	365486.0	0.005149	1881.96
8	389096.0	0.004422	1720.75
9	385477.0	0.006290	2424.58
10	401633.0	0.004264	1712.58
11	364186.0	0.005709	2079.19
12	368564.0	0.006219	2292.01
13	390260.0	0.004514	1761.46
14	369353.0	0.006393	2361.14
15	385558.0	0.005573	2148.63
16	384764.0	0.005734	2206.22
17	386445.0	0.005783	2234.94

Continued to next page

Sample	E, psi	Strain, in/in	Stress, psi
18	379715.0	0.004435	1684.04
19	375009.0	0.005591	2096.79
20	384607.0	0.004349	1672.77
21	395117.0	0.004681	1849.41
22	368344.0	0.005124	1887.46
23	361418.0	0.005013	1811.94
24	389872.0	0.004447	1733.69
25	371914.0	0.004875	1812.99
26	401434.0	0.004559	1830.02
27	391304.0	0.004212	1648.17
28	359166.0	0.006243	2242.11
29	387659.0	0.005586	2165.53
30	372617.0	0.005901	2198.97
Mean	380228.9	0.005225	1981.47
SD	12637.90	0.000778	268.59
% Dev	3.32	14.88	13.56

14 days			
Sample	E, psi	Strain, in/in	Stress, psi
1	502092.0	0.005082	2551.63
2	398382.0	0.007101	2828.91
3	400495.0	0.003645	1459.80
4	364007.0	0.004756	1731.22
5	381432.0	0.006883	2625.40
6	409281.0	0.005493	2248.18
7	418918.0	0.005860	2454.88
8	409897.0	0.004969	2036.81
9	409162.0	0.005414	2215.25
10	402869.0	0.005372	2164.23
11	408491.0	0.004916	2008.24
12	399019.0	0.005283	2108.13
13	405216.0	0.005840	2366.36
14	416600.0	0.005545	2309.92
15	408039.0	0.005995	2446.13
16	419391.0	0.005458	2289.18
17	417159.0	0.005770	2406.83

Continued to next page

Sample	E, psi	Strain, in/in	Stress, psi
18	409054.0	0.005005	2047.51
19	405930.0	0.005758	2337.42
20	406223.0	0.005081	2064.12
21	409090.0	0.005450	2229.39
22	406845.0	0.005689	2314.51
23	401534.0	0.006215	2495.69
24	415819.0	0.005441	2262.46
25	413777.0	0.005939	2457.32
26	410289.0	0.005339	2190.39
27	410999.0	0.005048	2074.71
28	402102.0	0.005009	2014.29
29	400182.0	0.005676	2271.49
30	400144.0	0.005889	2356.46
Mean	408747.9	0.005497	2245.56
SD	20391.36	0.000627	258.79
% Dev	4.99	11.40	11.52

28 days			
Sample	E, psi	Strain, in/in	Stress, psi
1	537323.0	0.007995	4295.90
2	474880.0	0.007517	3569.67
3	403524.0	0.009691	3910.55
4	441276.0	0.005450	2404.95
5	397574.0	0.006938	2758.37
6	450915.0	0.007518	3389.98
7	454777.0	0.007580	3447.36
8	441550.0	0.008135	3591.99
9	452052.0	0.007978	3606.34
10	469625.0	0.007227	3393.80
11	433348.0	0.007774	3368.77
12	429853.0	0.008838	3798.90
13	425946.0	0.007816	3329.39
14	474638.0	0.006948	3297.79
15	458847.0	0.008064	3700.05
16	451592.0	0.007185	3244.75
17	471931.0	0.006829	3222.68

Continued to next page

Sample	E, psi	Strain, in/in	Stress, psi
18	466708.0	0.007210	3365.12
19	462404.0	0.007455	3447.32
20	465416.0	0.008144	3790.31
21	443013.0	0.008349	3698.60
22	436709.0	0.008415	3674.78
23	469178.0	0.007188	3372.67
24	433309.0	0.008038	3482.79
25	438749.0	0.008824	3871.67
26	448223.0	0.007638	3423.52
27	452869.0	0.007434	3366.52
28	445015.0	0.008298	3692.57
29	453190.0	0.008220	3725.02
30	464494.0	0.008055	3741.47
Mean	451630.9	0.007758	3499.45
SD	24487.91	0.000755	339.61
% Dev	5.42	9.73	9.70

2 Months			
Sample	E, psi	Strain, in/in	Stress, psi
1	423192.0	0.005829	2466.79
2	508958.0	0.009584	4877.85
3	445378.0	0.006568	2925.24
4	404207.0	0.008028	3244.97
5	512162.0	0.004226	2164.40
6	458779.0	0.006847	3141.26
7	470739.0	0.007646	3599.27
8	479818.0	0.006026	2891.53
9	431282.0	0.005974	2576.31
10	482930.0	0.005337	2577.59
11	462863.0	0.007185	3325.56
12	466129.0	0.005845	2724.59
13	469745.0	0.006586	3093.77
14	452382.0	0.005942	2688.01
15	482962.0	0.005216	2519.01
16	457869.0	0.006264	2868.06
17	475196.0	0.007698	3658.17

Continued to next page

Sample	E, psi	Strain, in/in	Stress, psi
18	457341.0	0.008025	3669.94
19	430758.0	0.006625	2853.80
20	446407.0	0.008883	3965.26
21	449495.0	0.008346	3751.57
22	476115.0	0.006057	2883.72
23	461225.0	0.008438	3891.77
24	442609.0	0.007138	3159.53
25	437051.0	0.007320	3199.41
26	430465.0	0.006358	2736.94
27	442739.0	0.005718	2531.62
28	479383.0	0.007097	3402.16
29	468052.0	0.007900	3697.71
30	457562.0	0.006088	2785.46
Mean	458793.1	0.006826	3129.04
SD	23410.42	0.001176	566.20
% Dev	5.10	17.23	18.10

3 Months			
Sample	E, psi	Strain, in/in	Stress, psi
1	409332.0	0.008009	3278.34
2	399143.0	0.008883	3545.59
3	454093.0	0.008282	3760.80
4	383540.0	0.012144	4657.71
5	380802.0	0.016677	6350.63
6	405382.0	0.010799	4377.72
7	403391.0	0.010230	4126.50
8	404894.0	0.010817	4379.88
9	401369.0	0.010042	4030.43
10	403161.0	0.010290	4148.34
11	407505.0	0.011686	4761.99
12	400196.0	0.011484	4595.99
13	405014.0	0.010564	4278.71
14	405840.0	0.010422	4229.53
15	401167.0	0.011048	4432.07
16	407860.0	0.011037	4501.36
17	408581.0	0.011057	4517.85

Continued to next page

Sample	E, psi	Strain, in/in	Stress, psi
18	402623.0	0.010076	4056.69
19	405686.0	0.010651	4320.89
20	402231.0	0.010516	4230.02
21	402969.0	0.010313	4156.01
22	407637.0	0.011334	4620.35
23	400613.0	0.010749	4306.37
24	407595.0	0.009854	4016.63
25	401110.0	0.010116	4057.80
26	404393.0	0.010943	4425.15
27	404876.0	0.011705	4738.88
28	401348.0	0.010998	4414.16
29	404728.0	0.010759	4354.28
30	405224.0	0.010617	4302.37
Mean	404410.1	0.010737	4332.43
SD	11050.97	0.001417	493.51
% Dev	2.73	13.20	11.39

4 Months			
Sample	E, psi	Strain, in/in	Stress, psi
1	433441.0	0.010484	4544.20
2	394099.0	0.009404	3706.11
3	404393.0	0.014221	5750.87
4	377957.0	0.008595	3248.54
5	484070.0	0.007712	3733.15
6	418792.0	0.010083	4222.68
7	416327.0	0.009072	3777.11
8	407561.0	0.009543	3889.21
9	430092.0	0.010622	4568.58
10	422389.0	0.010934	4618.58
11	407088.0	0.009637	3923.20
12	422362.0	0.010778	4552.16
13	431091.0	0.008705	3752.82
14	431936.0	0.010912	4713.48
15	410018.0	0.009172	3760.53
16	429565.0	0.009536	4096.15
17	418345.0	0.009460	3957.35

Continued to next page

Sample	E, psi	Strain, in/in	Stress, psi
18	420470.0	0.011442	4810.84
19	419185.0	0.011030	4623.50
20	427091.0	0.009492	4054.04
21	402174.0	0.009706	3903.39
22	406768.0	0.010003	4069.09
23	427569.0	0.009858	4214.97
24	427858.0	0.009453	4044.59
25	405759.0	0.010413	4225.25
26	402239.0	0.010930	4396.34
27	428372.0	0.009008	3858.85
28	416016.0	0.011658	4850.11
29	413457.0	0.009973	4123.22
30	430123.0	0.009770	4202.09
Mean	418886.9	0.010054	4206.37
SD	17561.28	0.001168	472.27
% Dev	4.19	11.62	11.23

5 Months			
Sample	E, psi	Strain, in/in	Stress, psi
1	425643.0	0.012321	5244.48
2	468664.0	0.009895	4637.47
3	412662.0	0.009236	3811.24
4	420745.0	0.010416	4382.46
5	406265.0	0.009820	3989.49
6	514379.0	0.009741	5010.64
7	532131.0	0.008971	4773.74
8	417942.0	0.010846	4533.12
9	504236.0	0.008728	4400.77
10	445743.0	0.009636	4295.33
11	447871.0	0.011799	5284.31
12	418526.0	0.011343	4747.31
13	521186.0	0.009997	5210.37
14	542364.0	0.008039	4360.09
15	512444.0	0.009657	4948.78
16	414069.0	0.009969	4127.81
17	492468.0	0.008096	3986.96

Continued to next page

Sample	E, psi	Strain, in/in	Stress, psi
18	453006.0	0.010106	4577.90
19	524587.0	0.007161	3756.79
20	404652.0	0.010333	4181.46
21	523201.0	0.009359	4896.73
22	460439.0	0.009313	4288.06
23	519020.0	0.008030	4167.51
24	517895.0	0.008421	4361.36
25	481027.0	0.009904	4764.18
26	469479.0	0.008239	3868.04
27	526026.0	0.008668	4559.71
28	419953.0	0.011287	4739.86
29	429047.0	0.010230	4389.05
30	437980.0	0.008771	3841.63
Mean	468788.3	0.009611	4471.22
SD	45481.61	0.001175	426.51
% Dev	9.70	12.22	9.54

6 Months			
Sample	E, psi	Strain, in/in	Stress, psi
1	506123.0	0.010159	5141.62
2	464697.0	0.010579	4915.98
3	413789.0	0.012040	4982.20
4	430949.0	0.010668	4597.30
5	443590.0	0.010922	4844.73
6	493827.0	0.010211	5042.24
7	444220.0	0.009294	4128.57
8	492628.0	0.010638	5240.50
9	432515.0	0.008174	3535.36
10	410128.0	0.011891	4876.65
11	496776.0	0.009779	4858.19
12	486202.0	0.008701	4230.26
13	426093.0	0.009649	4111.28
14	496475.0	0.008640	4289.59
15	497265.0	0.007161	3560.87
16	419213.0	0.012369	5185.08
17	467128.0	0.007437	3474.11

Continued to next page

Sample	E, psi	Strain, in/in	Stress, psi
18	503024.0	0.010054	5057.32
19	462732.0	0.009260	4284.84
20	400072.0	0.012376	4951.19
21	404664.0	0.009822	3974.47
22	496637.0	0.009040	4489.37
23	417285.0	0.010719	4472.69
24	479516.0	0.007066	3388.29
25	440552.0	0.011949	5264.12
26	421550.0	0.008032	3386.09
27	449418.0	0.009741	4377.86
28	424154.0	0.011338	4808.90
29	397181.0	0.011520	4575.68
30	446828.0	0.013039	5826.23
Mean	452174.4	0.010076	4529.05
SD	34792.98	0.001579	620.38
% Dev	7.69	15.67	13.70

A.4 Resin Type-D; Test Specimen; ASTM D638

0 day			
Sample	E, psi	Strain, in/in	Stress, psi
1	596741.0	0.006353	3791.10
2	494783.0	0.004668	2309.65
3	519840.0	0.006272	3260.44
4	423664.0	0.004052	1716.69
5	406948.0	0.003901	1587.50
6	383642.0	0.004815	1847.24
7	521702.0	0.004200	2190.89
8	432499.0	0.005216	2256.13
9	438031.0	0.003711	1625.35
10	463736.0	0.005624	2608.26
11	462672.0	0.003788	1752.62
12	506874.0	0.003229	1636.57
13	530347.0	0.004896	2596.61
14	447912.0	0.004729	2118.12
15	485593.0	0.003756	1823.97
16	466625.0	0.003712	1732.18
17	481529.0	0.004982	2399.04

Continued to next page

Sample	E, psi	Strain, in/in	Stress, psi
18	428769.0	0.004164	1785.48
19	439397.0	0.004371	1920.79
20	536165.0	0.004608	2470.41
21	524821.0	0.005247	2753.82
22	476891.0	0.006181	2947.45
23	475506.0	0.004186	1990.57
24	530585.0	0.005983	3174.53
25	436443.0	0.004828	2107.18
26	450953.0	0.003979	1794.17
27	428218.0	0.004644	1988.80
28	464411.0	0.005126	2380.76
29	430210.0	0.006604	2841.16
30	463578.0	0.006634	3075.32
Mean	471636.17	0.004815	2282.76
SD	46383.33	0.000949	568.94
% Dev	9.83	19.70	24.92

7 days			
Sample	E, psi	Strain, in/in	Stress, psi
1	1057225.0	0.001397	1476.94
2	757260.0	0.003499	2649.65
3	649661.0	0.004341	2820.18
4	646882.0	0.002454	1587.45
5	682123.0	0.003298	2249.64
6	709530.0	0.004560	3235.46
7	734191.0	0.002196	1611.98
8	683917.0	0.003880	2653.91
9	772577.0	0.002595	2004.65
10	676047.0	0.004678	3162.74
11	859331.0	0.003095	2659.95
12	851860.0	0.002103	1791.30
13	714475.0	0.003554	2538.93
14	654052.0	0.003563	2330.40
15	651933.0	0.002882	1879.19
16	664059.0	0.004086	2713.38
17	814158.0	0.002937	2390.87

Continued to next page

Sample	E, psi	Strain, in/in	Stress, psi
18	802678.0	0.003927	3152.41
19	695328.0	0.003161	2197.70
20	817918.0	0.003525	2882.85
21	900994.0	0.001927	1735.89
22	815227.0	0.003882	3164.56
23	704947.0	0.003381	2383.28
24	681230.0	0.002655	1808.40
25	813064.0	0.003425	2784.77
26	676546.0	0.002925	1978.58
27	686260.0	0.004625	3173.84
28	857472.0	0.002167	1857.83
29	681362.0	0.004121	2807.56
30	812039.0	0.003930	3191.63
Mean	750811.53	0.003292	2429.20
SD	95342.11	0.000849	554.88
% Dev	12.70	25.79	22.84

14 days			
Sample	E, psi	Strain, in/in	Stress, psi
1	382062.0	0.002463	941.02
2	1841479.0	0.001117	2056.93
3	1022761.0	0.002612	2671.45
4	765964.0	0.001774	1358.82
5	916718.0	0.003657	3352.44
6	985796.0	0.002325	2291.98
7	1426170.0	0.000778	1109.23
8	1256164.0	0.000852	1070.28
9	1312083.0	0.000948	1243.68
10	725313.0	0.002165	1570.21
11	504578.0	0.004151	2094.32
12	736066.0	0.004028	2964.96
13	769437.0	0.003361	2586.03
14	1237977.0	0.002608	3229.26
15	707904.0	0.001672	1183.76
16	1552464.0	0.001630	2530.96
17	846159.0	0.001751	1481.38

Continued to next page

Sample	E, psi	Strain, in/in	Stress, psi
18	1395359.0	0.000789	1100.51
19	919356.0	0.001839	1690.74
20	1367809.0	0.001084	1482.31
21	774389.0	0.003068	2375.70
22	1570084.0	0.000729	1144.44
23	796666.0	0.002157	1718.59
24	562600.0	0.003063	1723.48
25	433335.0	0.007387	3200.95
26	1034547.0	0.001429	1478.12
27	1444583.0	0.002264	3270.82
28	774893.0	0.003546	2747.48
29	1026729.0	0.000932	957.39
30	464641.0	0.006593	3063.37
Mean	985136.20	0.002426	1989.69
SD	379179.39	0.001601	801.54
% Dev	38.49	66.00	40.28

28 days			
Sample	E, psi	Strain, in/in	Stress, psi
1	1159911.0	0.001276	1479.82
2	Broken	Broken	Broken
3	Broken	Broken	Broken
4	1218173.0	0.001492	1817.82
5	Broken	Broken	Broken
6	Broken	Broken	Broken
7	977550.0	0.002806	2742.58
8	Broken	Broken	Broken
9	Broken	Broken	Broken
10	1491127.0	0.001989	2966.40
11	Broken	Broken	Broken
12	Broken	Broken	Broken
13	Broken	Broken	Broken
14	943977.0	0.001471	1388.67
15	Broken	Broken	Broken
16	904414.0	0.001444	1305.56
17	Broken	Broken	Broken

Continued to next page

Sample	E, psi	Strain, in/in	Stress, psi
18	Broken	Broken	Broken
19	Broken	Broken	Broken
20	Broken	Broken	Broken
21	1491865.0	0.000755	1126.90
22	Broken	Broken	Broken
23	Broken	Broken	Broken
24	Broken	Broken	Broken
25	Broken	Broken	Broken
26	Broken	Broken	Broken
27	Broken	Broken	Broken
28	Broken	Broken	Broken
29	Broken	Broken	Broken
30	Broken	Broken	Broken
Mean	1169573.86	0.001605	1832.54
SD	247588.40	0.000642	731.56
% Dev	21.17	40.03	39.92

2 Months			
Sample	E, psi	Strain, in/in	Stress, psi
1	1499028.0	0.000811	1215.53
2	Broken	Broken	Broken
3	Broken	Broken	Broken
4	Broken	Broken	Broken
5	693876.0	0.002814	1952.37
6	Broken	Broken	Broken
7	Broken	Broken	Broken
8	Broken	Broken	Broken
9	Broken	Broken	Broken
10	Broken	Broken	Broken
11	Broken	Broken	Broken
12	Broken	Broken	Broken
13	729372.0	0.001976	1441.13
14	Broken	Broken	Broken
15	Broken	Broken	Broken
16	532878.0	0.002356	1255.67
17	Broken	Broken	Broken

Continued to next page

Sample	E, psi	Strain, in/in	Stress, psi
18	Broken	Broken	Broken
19	Broken	Broken	Broken
20	Broken	Broken	Broken
21	Broken	Broken	Broken
22	Broken	Broken	Broken
23	1566268.0	0.001007	1576.77
24	Broken	Broken	Broken
25	Broken	Broken	Broken
26	Broken	Broken	Broken
27	Broken	Broken	Broken
28	Broken	Broken	Broken
29	Broken	Broken	Broken
30	Broken	Broken	Broken
Mean	1004284.40	0.001793	1488.29
SD	488556.80	0.000862	297.46
% Dev	48.65	48.11	19.99

3 Months			
Sample	E, psi	Strain, in/in	Stress, psi
1	599555.0	0.006098	3656.03
2	1742037.0	0.001673	2914.59
3	777912.0	0.004979	3873.17
4	645908.0	0.004576	2955.61
5	726905.0	0.004367	3174.44
6	533035.0	0.005915	3152.89
7	917086.0	0.003273	3001.63
8	Broken	Broken	Broken
9	704028.0	0.005138	3617.32
10	935352.0	0.003581	3349.93
11	615476.0	0.005890	3624.96
12	800172.0	0.004443	3554.99
13	762692.0	0.004980	3798.19
14	758194.0	0.003980	3017.83
15	616869.0	0.005217	3218.24
16	1040826.0	0.003647	3796.08
17	966095.0	0.003216	3106.53

Continued to next page

Sample	E, psi	Strain, in/in	Stress, psi
18	1015721.0	0.003819	3879.33
19	868795.0	0.004068	3533.95
20	678982.0	0.005431	3687.73
21	Broken	Broken	Broken
22	624175.0	0.002298	1434.55
23	925412.0	0.002260	2091.04
24	932786.0	0.001380	1287.43
25	Broken	Broken	Broken
26	995008.0	0.001777	1768.56
27	987781.0	0.001301	1285.50
28	896999.0	0.001990	1784.96
29	864283.0	0.002054	1775.37
30	669086.0	0.002094	1401.29
Mean	837080.37	0.003683	2879.34
SD	233949.51	0.001515	901.37
% Dev	27.95	41.14	31.30

4 Months			
Sample	E, psi	Strain, in/in	Stress, psi
1	938573.0	0.001736	1629.10
2	Broken	Broken	Broken
3	Broken	Broken	Broken
4	624395.0	0.003707	2314.85
5	Broken	Broken	Broken
6	Broken	Broken	Broken
7	Broken	Broken	Broken
8	779208.0	0.001627	1267.59
9	Broken	Broken	Broken
10	Broken	Broken	Broken
11	Broken	Broken	Broken
12	Broken	Broken	Broken
13	Broken	Broken	Broken
14	Broken	Broken	Broken
15	Broken	Broken	Broken
16	Broken	Broken	Broken
17	Broken	Broken	Broken

Continued to next page

Sample	E, psi	Strain, in/in	Stress, psi
18	Broken	Broken	Broken
19	611606.0	0.004627	2829.87
20	Broken	Broken	Broken
21	Broken	Broken	Broken
22	Broken	Broken	Broken
23	Broken	Broken	Broken
24	Broken	Broken	Broken
25	Broken	Broken	Broken
26	Broken	Broken	Broken
27	Broken	Broken	Broken
28	Broken	Broken	Broken
29	Broken	Broken	Broken
30	Broken	Broken	Broken
Mean	738445.50	0.002924	2010.35
SD	153632.00	0.001484	697.94
% Dev	20.80	50.76	34.72

5 Months			
Sample	E, psi	Strain, in/in	Stress, psi
1	Broken	Broken	Broken
2	Broken	Broken	Broken
3	Broken	Broken	Broken
4	Broken	Broken	Broken
5	Broken	Broken	Broken
6	Broken	Broken	Broken
7	775614.0	0.003048	2364.28
8	Broken	Broken	Broken
9	Broken	Broken	Broken
10	536131.0	0.002816	1509.71
11	Broken	Broken	Broken
12	Broken	Broken	Broken
13	Broken	Broken	Broken
14	925941.0	0.001985	1837.80
15	Broken	Broken	Broken
16	Broken	Broken	Broken
17	Broken	Broken	Broken
18	Broken	Broken	Broken
19	Broken	Broken	Broken
20	Broken	Broken	Broken

Continued to next page

Sample	E, psi	Strain, in/in	Stress, psi
21	Broken	Broken	Broken
22	Broken	Broken	Broken
23	Broken	Broken	Broken
24	482061.0	0.004712	2271.46
25	Broken	Broken	Broken
26	Broken	Broken	Broken
27	Broken	Broken	Broken
28	Broken	Broken	Broken
29	585478.0	0.00296543	1736.19
30	Broken	Broken	Broken
Mean	661045.00	0.003105	1943.89
SD	184827.69	0.000993	362.95
% Dev	27.96	31.97	18.67

6 Months			
Sample	E, psi	Strain, in/in	Stress, psi
1	580271.0	0.004142	2403.31
2	602412.0	0.002589	1559.48
3	667806.0	0.003727	2489.14
4	948369.0	0.002984	2830.03
5	719621.0	0.003932	2829.87
6	Broken	Broken	Broken
7	768977.0	0.002391	1838.76
8	514521.0	0.003795	1952.50
9	921616.0	0.002766	2548.96
10	576521.0	0.003646	2102.14
11	Broken	Broken	Broken
12	620336.0	0.004642	2879.49
13	774316.0	0.001962	1519.38
14	974802.0	0.002597	2531.20
15	840227.0	0.002545	2138.18
16	750630.0	0.003638	2730.59
17	778876.0	0.002024	1576.39
18	665300.0	0.003629	2414.08
19	993296.0	0.002155	2140.36
20	910452.0	0.002060	1875.20

Continued to next page

Sample	E, psi	Strain, in/in	Stress, psi
21	608313.0	0.002752	1674.34
22	Broken	Broken	Broken
23	612370.0	0.004250	2602.54
24	911709.0	0.002250	2051.69
25	Broken	Broken	Broken
26	990279.0	0.002364	2341.38
27	513027.0	0.004525	2321.26
28	906533.0	0.002024	1834.45
29	738417.0	0.002154	1590.65
30	709428.0	0.003955	2806.10
Mean	753785.58	0.003058	2214.67
SD	153228.08	0.000878	441.70
% Dev	20.33	28.70	19.94

A.5 Resin Type-A; Test Specimen; ASTM D790

0 day			
Sample	E, psi	Strain, in/in	Stress, psi
1	456914.0	0.004252	1942.90
2	499541.0	0.004690	2342.60
3	532004.0	0.004485	2385.78
4	533042.0	0.004853	2586.79
5	473456.0	0.005291	2505.18
6	538282.0	0.003769	2028.81
7	547358.0	0.003408	1865.60
8	476558.0	0.004069	1938.93
9	486736.0	0.004972	2419.92
10	540998.0	0.003461	1872.31
11	509489.0	0.004155	2116.70
12	464139.0	0.005280	2450.86
13	485821.0	0.004379	2127.28
14	476225.0	0.004349	2070.87
15	565598.0	0.003714	2100.50
16	494292.0	0.005046	2494.04
Mean	505028.3	0.004386	2203.1
SD	33531.4	0.000607	247.2
% Dev	6.6	13.9	11.2

7 days			
Sample	E, psi	Strain, in/in	Stress, psi
1	512162.0	0.003861	1977.635
2	500998.0	0.004293	2151.013
3	581616.0	0.003314	1927.246
4	627279.0	0.003150	1976.175
5	524431.0	0.004456	2336.989
6	488049.0	0.004006	1955.332
7	575391.0	0.004007	2305.558
8	572550.0	0.003965	2269.930
9	637160.0	0.003268	2082.299
10	596851.0	0.003009	1796.171
11	454347.0	0.004692	2132.006
12	603258.0	0.003292	1986.177
13	634259.0	0.004512	2861.642
14	511419.0	0.004787	2447.957
15	609886.0	0.003046	1857.440
16	570271.0	0.004105	2340.976
Mean	562495.4	0.003860	2150.3
SD	56753.5	0.000605	270.2
% Dev	10.1	15.7	12.6

14 days			
Sample	E, psi	Strain, in/in	Stress, psi
1	477084.0	0.003671	1751.22
2	612289.0	0.002971	1819.40
3	475925.0	0.003571	1699.66
4	487169.0	0.003281	1598.30
5	496308.0	0.003442	1708.43
6	613103.0	0.003350	2053.79
7	495301.0	0.004755	2354.92
8	526986.0	0.003031	1597.42
9	514125.0	0.003654	1878.67
10	504382.0	0.004524	2282.00
11	534277.0	0.003730	1992.95
12	498284.0	0.003307	1647.79
13	502715.0	0.004510	2267.17
14	530322.0	0.003607	1913.06
	604795.0	0.003563	2154.66
	480266.0	0.003584	1721.17
Mean	522083.2	0.003659	1902.5
SD	47135.7	0.000515	254.2
% Dev	9.0	14.1	13.4

28 days			
Sample	E, psi	Strain, in/in	Stress, psi
1	483660.0	0.004271	2065.81
2	530983.0	0.004009	2128.57
3	527460.0	0.003326	1754.32
4	498254.0	0.003487	1737.24
5	530666.0	0.003562	1890.03
6	532607.0	0.003813	2031.01
7	482443.0	0.003962	1911.38
8	538174.0	0.003516	1892.00
9	472756.0	0.003526	1667.11
10	495054.0	0.003821	1891.63
11	530218.0	0.003408	1807.17
12	519369.0	0.004023	2089.54
13	538868.0	0.003651	1967.53
14	544284.0	0.003136	1706.91
15	515009.0	0.004207	2166.80
16	503598.0	0.003741	1883.74
Mean	515212.7	0.003716	1911.9
SD	22825.9	0.000322	153.8
% Dev	4.4	8.7	8.0

2 Months			
Sample	E, psi	Strain, in/in	Stress, psi
1	494469.0	0.003706	1832.47
2	499261.0	0.003612	1803.09
3	479891.0	0.004884	2343.83
4	512725.0	0.004099	2101.45
5	522797.0	0.004316	2256.16
6	533479.0	0.003506	1870.34
7	525574.0	0.003108	1633.58
8	481312.0	0.004613	2220.50
9	513226.0	0.003969	2037.08
10	489332.0	0.004519	2211.41
11	479572.0	0.003956	1896.95
12	491014.0	0.004424	2172.04
13	523880.0	0.003740	1959.10
14	479648.0	0.004585	2198.96
15	463286.0	0.003768	1745.47
16	499567.0	0.003310	1653.79
Mean	499314.6	0.004007	1996.0
SD	20580.1	0.000512	227.0
% Dev	4.1	12.8	11.4

3 Months			
Sample	E, psi	Strain, in/in	Stress, psi
1	477043.0	0.004101	1956.17
2	494306.0	0.003661	1809.77
3	533262.0	0.002351	1253.72
4	485703.0	0.002738	1329.87
5	527255.0	0.002458	1295.79
6	530522.0	0.003099	1643.98
7	537147.0	0.004236	2275.49
8	504143.0	0.004051	2042.10
9	539450.0	0.002793	1506.55
10	491100.0	0.002934	1440.85
11	511225.0	0.002692	1376.09
12	546319.0	0.003358	1834.59
13	513467.0	0.003313	1701.36
14	523016.0	0.002989	1563.40
15	485545.0	0.003688	1790.69
16	519584.0	0.002787	1448.09
Mean	513692.9	0.003203	1641.8
SD	21836.2	0.000595	293.5
% Dev	4.3	18.6	17.9

4 Months			
Sample	E, psi	Strain, in/in	Stress, psi
1	522517.0	0.003414	1784.10
2	539448.0	0.003212	1732.44
3	466830.0	0.004197	1959.44
4	534043.0	0.003477	1857.00
5	498556.0	0.004254	2120.82
6	491992.0	0.003710	1825.25
7	525297.0	0.003889	2042.66
8	475134.0	0.004468	2122.91
9	473035.0	0.004110	1944.11
10	510597.0	0.003852	1966.74
11	529854.0	0.002743	1453.41
12	533058.0	0.004290	2286.80
13	475663.0	0.004927	2343.64
14	525454.0	0.003176	1668.78
15	520946.0	0.002932	1527.30
16	513699.0	0.003254	1671.52
Mean	508507.7	0.003744	1894.2
SD	24737.0	0.000608	254.0
% Dev	4.9	16.2	13.4

5 Months			
Sample	E, psi	Strain, in/in	Stress, psi
1	478409.0	0.003596	1720.54
2	531209.0	0.002769	1471.02
3	473373.0	0.003321	1571.98
4	468876.0	0.003088	1447.93
5	472898.0	0.003841	1816.64
6	500736.0	0.002823	1413.39
7	512789.0	0.004262	2185.64
8	471120.0	0.002745	1293.13
9	517805.0	0.003164	1638.48
10	537718.0	0.003104	1669.09
11	530145.0	0.003264	1730.51
12	527596.0	0.003257	1718.64
13	484019.0	0.002779	1345.03
14	462007.0	0.004041	1867.17
15	473425.0	0.003199	1514.62
16	508206.0	0.003294	1674.09
Mean	496895.7	0.003284	1629.9
SD	26556.5	0.000451	223.0
% Dev	5.3	13.7	13.7

6 Months			
Sample	E, psi	Strain, in/in	Stress, psi
1	542444.0	0.003344	1814.09
2	539597.0	0.003795	2047.54
3	520602.0	0.004409	2295.22
4	488729.0	0.003794	1854.18
5	478743.0	0.003820	1828.83
6	527605.0	0.003510	1852.13
7	469548.0	0.003926	1843.24
8	484227.0	0.004619	2236.45
9	544613.0	0.003185	1734.43
10	535767.0	0.003219	1724.47
11	518857.0	0.003688	1913.78
12	478747.0	0.003876	1855.45
13	493740.0	0.004537	2240.05
14	517647.0	0.003952	2045.83
15	491649.0	0.004074	2002.78
16	537003.0	0.003934	2112.36
Mean	510594.9	0.003855	1962.6
SD	26307.6	0.000424	182.9
% Dev	5.2	11.0	9.3

A.6 Resin Type-B; Test Specimen; ASTM D790

0 day			
Sample	E, psi	Strain, in/in	Stress, psi
1	531002.0	0.003160	1677.99
2	500423.0	0.003478	1740.55
3	484951.0	0.003474	1684.51
4	512353.0	0.003448	1766.46
5	498563.0	0.003320	1655.19
6	532527.0	0.003592	1913.05
7	498921.0	0.003497	1744.64
8	513583.0	0.004474	2297.88
9	500888.0	0.004252	2129.67
10	463946.0	0.005101	2366.79
11	476217.0	0.003476	1655.10
12	496973.0	0.004875	2422.80
13	458331.0	0.005114	2343.98
14	483308.0	0.004638	2241.73
15	525943.0	0.003745	1969.59
16	483192.0	0.004116	1988.63
17	501512.0	0.004442	2227.93

Continued to next page

Sample	E, psi	Strain, in/in	Stress, psi
18	468686.0	0.003617	1695.10
19	527692.0	0.004602	2428.41
20	472809.0	0.004202	1986.78
21	485231.0	0.003704	1797.41
22	465606.0	0.004619	2150.45
23	484659.0	0.004296	2082.28
24	466938.0	0.003603	1682.55
25	506317.0	0.003336	1689.22
26	468149.0	0.005197	2432.79
27	493067.0	0.003848	1897.54
28	488213.0	0.004692	2290.91
29	480023.0	0.003931	1886.78
30	467558.0	0.004598	2149.74
Mean	491252.70	0.004082	1999.88
SD	21211.67	0.000608	272.06
% Dev	4.32	14.89	13.60

7 days			
Sample	E, psi	Strain, in/in	Stress, psi
1	430417.0	0.005362	2307.74
2	519048.0	0.003218	1670.17
3	454126.0	0.003790	1721.04
4	567583.0	0.003577	2030.19
5	431331.0	0.005369	2315.69
6	491195.0	0.004609	2263.70
7	534407.0	0.003282	1753.95
8	538359.0	0.003197	1721.27
9	419745.0	0.004227	1774.36
10	472204.0	0.004975	2349.44
11	485778.0	0.003773	1832.63
12	458461.0	0.004758	2181.22
13	488772.0	0.003828	1871.21
14	492708.0	0.004220	2079.34
15	538778.0	0.003774	2033.57
16	518429.0	0.004700	2436.80
17	487577.0	0.004159	2027.68

Continued to next page

Sample	E, psi	Strain, in/in	Stress, psi
18	528549.0	0.003735	1974.20
19	430731.0	0.004602	1982.20
20	523943.0	0.004063	2128.86
21	455182.0	0.004914	2236.81
22	443923.0	0.004303	1910.31
23	586311.0	0.002828	1658.13
24	583801.0	0.003547	2070.91
25	541495.0	0.003773	2042.89
26	599876.0	0.003940	2363.66
27	499411.0	0.003865	1930.06
28	540661.0	0.004434	2397.17
29	553566.0	0.003737	2068.72
30	591881.0	0.003433	2031.65
Mean	506941.60	0.004066	2038.85
SD	52414.61	0.000639	227.42
% Dev	10.34	15.71	11.15

14 days			
Sample	E, psi	Strain, in/in	Stress, psi
1	502607.0	0.004216	2118.98
2	416636.0	0.004395	1831.14
3	456361.0	0.004465	2037.69
4	462748.0	0.003783	1750.77
5	507096.0	0.003417	1732.51
6	470539.0	0.004836	2275.72
7	478896.0	0.003789	1814.66
8	471990.0	0.004800	2265.35
9	489218.0	0.004090	2001.01
10	445171.0	0.005431	2417.77
11	525166.0	0.003514	1845.59
12	431281.0	0.004084	1761.18
13	403872.0	0.004639	1873.64
14	450489.0	0.005254	2366.76
15	461648.0	0.004182	1930.45
16	499433.0	0.004287	2141.30
17	512520.0	0.003268	1674.69

Continued to next page

Sample	E, psi	Strain, in/in	Stress, psi
18	488934.0	0.004390	2146.23
19	472168.0	0.004559	2152.76
20	508424.0	0.003285	1670.35
21	521129.0	0.003844	2003.24
22	516893.0	0.003625	1873.81
23	467015.0	0.004243	1981.55
24	511644.0	0.004057	2075.90
25	454981.0	0.004454	2026.32
26	489518.0	0.003600	1762.23
27	533289.0	0.003979	2122.22
28	411690.0	0.004465	1838.15
29	487701.0	0.004144	2021.06
30	423979.0	0.004561	1933.87
Mean	475767.87	0.004189	1981.56
SD	35465.41	0.000531	200.30
% Dev	7.45	12.68	10.11

28 days			
Sample	E, psi	Strain, in/in	Stress, psi
1	480234.0	0.004458	2140.90
2	395372.0	0.004539	1794.48
3	402621.0	0.005034	2026.84
4	400261.0	0.004153	1662.09
5	500492.0	0.004089	2046.49
6	479413.0	0.004701	2253.68
7	376329.0	0.005408	2035.31
8	412796.0	0.004623	1908.28
9	502168.0	0.004719	2369.82
10	465703.0	0.003698	1722.30
11	441715.0	0.004088	1805.76
12	472036.0	0.003934	1857.17
13	465266.0	0.005263	2448.56
14	414040.0	0.004502	1864.04
15	478504.0	0.005109	2444.63
16	495966.0	0.003506	1739.00
17	475449.0	0.003507	1667.24

Continued to next page

Sample	E, psi	Strain, in/in	Stress, psi
18	432255.0	0.005083	2197.03
19	449859.0	0.005287	2378.21
20	496487.0	0.004174	2072.21
21	422681.0	0.004962	2097.15
22	450519.0	0.004793	2159.45
23	473783.0	0.003977	1884.16
24	491590.0	0.003653	1795.84
25	481220.0	0.003746	1802.51
26	450981.0	0.005244	2365.02
27	426755.0	0.004864	2075.70
28	482335.0	0.004075	1965.57
29	409487.0	0.004851	1986.49
30	438574.0	0.004689	2056.57
Mean	452163.03	0.004491	2020.75
SD	35803.87	0.000573	232.53
% Dev	7.92	12.75	11.51

2 Months			
Sample	E, psi	Strain, in/in	Stress, psi
1	597522.0	0.004766	2847.98
2	474843.0	0.005992	2845.11
3	488977.0	0.005935	2901.99
4	467833.0	0.004490	2100.53
5	510650.0	0.005378	2746.40
6	485575.0	0.003988	1936.71
7	453743.0	0.006188	2807.61
8	444370.0	0.004336	1926.71
9	441943.0	0.006365	2812.77
10	481327.0	0.004726	2274.80
11	535192.0	0.003222	1724.61
12	504155.0	0.003937	1985.06
13	513829.0	0.004137	2125.95
14	471613.0	0.003885	1832.04
15	490217.0	0.004475	2193.56
16	452419.0	0.004374	1978.97
17	448621.0	0.004151	1862.40

Continued to next page

Sample	E, psi	Strain, in/in	Stress, psi
18	474470.0	0.004156	1971.90
19	513900.0	0.003875	1991.14
20	451738.0	0.005505	2486.70
21	530814.0	0.004444	2358.94
22	483551.0	0.005264	2545.55
23	462881.0	0.003683	1704.91
24	446838.0	0.006774	3027.10
25	502525.0	0.005462	2744.59
26	453777.0	0.004382	1988.50
27	503082.0	0.005492	2762.78
28	463620.0	0.003666	1699.55
29	485924.0	0.004247	2063.57
30	520770.0	0.005508	2868.57
Mean	485223.97	0.004760	2303.90
SD	34230.93	0.000910	431.89
% Dev	7.05	19.11	18.75

3 Months			
Sample	E, psi	Strain, in/in	Stress, psi
1	457404.0	0.004215	1927.79
2	525940.0	0.003372	1773.24
3	479801.0	0.005222	2505.51
4	543050.0	0.004367	2371.66
5	458788.0	0.004092	1877.50
6	445177.0	0.005613	2498.88
7	472167.0	0.004101	1936.38
8	455033.0	0.004573	2080.77
9	548834.0	0.004687	2572.52
10	548108.0	0.004200	2301.88
11	489414.0	0.004360	2133.82
12	553368.0	0.004295	2376.71
13	470441.0	0.005435	2556.73
14	543321.0	0.004853	2636.53
15	454636.0	0.004714	2143.09
16	503628.0	0.003365	1694.72
17	493686.0	0.004564	2253.09

Continued to next page

Sample	E, psi	Strain, in/in	Stress, psi
18	428678.0	0.005170	2216.23
19	546495.0	0.003973	2171.20
20	512886.0	0.004320	2215.69
21	440860.0	0.004040	1781.18
22	541647.0	0.003409	1846.42
23	518991.0	0.004086	2120.40
24	459108.0	0.005358	2460.02
25	497772.0	0.004693	2335.82
26	506685.0	0.003367	1705.99
27	502868.0	0.004955	2491.48
28	539453.0	0.003392	1829.84
29	484495.0	0.004415	2138.97
30	447125.0	0.004034	1803.60
Mean	495661.97	0.004375	2158.59
SD	38745.65	0.000631	287.05
% Dev	7.82	14.43	13.30

4 Months			
Sample	E, psi	Strain, in/in	Stress, psi
1	438787.0	0.005056	2218.31
2	489673.0	0.004587	2246.20
3	568152.0	0.004320	2454.50
4	553893.0	0.003269	1810.70
5	544661.0	0.003850	2096.74
6	469179.0	0.006006	2818.00
7	509990.0	0.004047	2063.70
8	542124.0	0.005221	2830.33
9	494304.0	0.004441	2195.31
10	570533.0	0.003773	2152.49
11	519299.0	0.003206	1664.99
12	510838.0	0.005468	2793.19
13	537919.0	0.003687	1983.20
14	559342.0	0.004336	2425.09
15	437649.0	0.006161	2696.29
16	503393.0	0.003683	1853.96
17	566811.0	0.003961	2245.31

Continued to next page

Sample	E, psi	Strain, in/in	Stress, psi
18	486304.0	0.005402	2626.79
19	513206.0	0.004776	2450.89
20	465734.0	0.005794	2698.46
21	474068.0	0.004174	1978.66
22	566204.0	0.003658	2070.93
23	449905.0	0.004220	1898.68
24	536066.0	0.003677	1971.03
25	495486.0	0.003884	1924.71
26	566051.0	0.003989	2257.72
27	561435.0	0.003534	1983.98
28	454482.0	0.005269	2394.75
29	506217.0	0.005074	2568.62
30	497135.0	0.004899	2435.46
Mean	512961.33	0.004447	2260.30
SD	41803.78	0.000821	325.99
% Dev	8.15	18.45	14.42

5 Months			
Sample	E, psi	Strain, in/in	Stress, psi
1	509022.0	0.003879	1974.70
2	548724.0	0.004592	2519.52
3	543549.0	0.003518	1912.12
4	519932.0	0.003647	1896.05
5	471055.0	0.005718	2693.29
6	493430.0	0.004575	2257.61
7	473015.0	0.005170	2445.32
8	474160.0	0.004970	2356.79
9	435188.0	0.005330	2319.46
10	515173.0	0.005432	2798.32
11	445356.0	0.003736	1663.80
12	469175.0	0.006007	2818.45
13	492848.0	0.005897	2906.39
14	464272.0	0.005330	2474.47
15	540510.0	0.004348	2350.17
16	484395.0	0.005307	2570.84
17	521644.0	0.004733	2469.11

Continued to next page

Sample	E, psi	Strain, in/in	Stress, psi
18	462908.0	0.004369	2022.23
19	502934.0	0.004227	2125.68
20	424868.0	0.004328	1838.92
21	421000.0	0.004124	1736.10
22	551683.0	0.005118	2823.68
23	550004.0	0.003373	1855.30
24	519771.0	0.004682	2433.56
25	471799.0	0.005951	2807.80
26	525723.0	0.004260	2239.77
27	428122.0	0.004909	2101.49
28	518453.0	0.003473	1800.40
29	462229.0	0.005500	2542.05
30	457420.0	0.004030	1843.45
Mean	489945.40	0.004684	2286.56
SD	39425.70	0.000778	372.01
% Dev	8.05	16.61	16.27

6 Months			
Sample	E, psi	Strain, in/in	Stress, psi
1	468976.0	0.005753	2697.98
2	539292.0	0.005311	2864.08
3	544877.0	0.004745	2585.33
4	550757.0	0.005122	2820.82
5	525704.0	0.003366	1769.26
6	532237.0	0.004573	2434.01
7	559621.0	0.005286	2958.12
8	444733.0	0.004697	2088.89
9	470679.0	0.006098	2870.32
10	470249.0	0.005664	2663.45
11	446957.0	0.004221	1886.65
12	555793.0	0.003584	1992.21
13	509192.0	0.003735	1902.02
14	487858.0	0.003951	1927.75
15	563428.0	0.005293	2982.12
16	552727.0	0.003159	1745.95
17	569845.0	0.004757	2710.55

Continued to next page

Sample	E, psi	Strain, in/in	Stress, psi
18	531675.0	0.005545	2948.11
19	489714.0	0.003614	1770.07
20	491638.0	0.005224	2568.41
21	508792.0	0.003853	1960.60
22	517801.0	0.003412	1766.52
23	529366.0	0.004118	2179.90
24	528301.0	0.003231	1706.91
25	430888.0	0.004317	1860.28
26	546180.0	0.005408	2953.82
27	537015.0	0.003300	1772.21
28	465308.0	0.003778	1757.91
29	484797.0	0.004946	2397.73
30	487161.0	0.005979	2912.60
Mean	511385.37	0.004535	2315.15
SD	39047.60	0.000905	479.85
% Dev	7.64	19.96	20.73

A.7 Resin Type-C; Test Specimen; ASTM D790

0 day			
Sample	E, psi	Strain, in/in	Stress, psi
1	443350.0	0.005419	2402.45
2	460850.0	0.004678	2155.89
3	522495.0	0.006562	3428.36
4	490408.0	0.007426	3641.62
5	570618.0	0.003592	2049.58
6	560003.0	0.005942	3327.55
7	488328.0	0.007563	3693.31
8	558001.0	0.004639	2588.57
9	433354.0	0.007084	3070.06
10	573067.0	0.005238	3001.79
11	482945.0	0.007618	3678.89
12	504626.0	0.005578	2814.66
13	521062.0	0.006250	3256.73
14	438371.0	0.005666	2483.93
15	470728.0	0.005076	2389.20
16	487481.0	0.004036	1967.42
17	461871.0	0.007402	3418.79

Continued to next page

Sample	E, psi	Strain, in/in	Stress, psi
18	487990.0	0.005134	2505.21
19	455426.0	0.006785	3089.98
20	552585.0	0.004923	2720.53
21	534169.0	0.004638	2477.28
22	437646.0	0.006842	2994.47
23	492577.0	0.007040	3467.68
24	493973.0	0.005967	2947.76
25	432234.0	0.005299	2290.40
26	446895.0	0.006126	2737.84
27	458890.0	0.008281	3799.95
28	561404.0	0.005837	3277.09
29	435661.0	0.007143	3111.99
30	495285.0	0.004208	2084.38
Mean	491743.1	0.005933	2895.78
SD	44445.48	0.001186	529.53
% Dev	9.04	20.00	18.29

7 days			
Sample	E, psi	Strain, in/in	Stress, psi
1	497088.0	0.004630	2301.30
2	499371.0	0.004388	2191.35
3	431285.0	0.004089	1763.66
4	427543.0	0.005826	2490.97
5	502795.0	0.003995	2008.46
6	475712.0	0.004326	2057.97
7	495095.0	0.004070	2014.95
8	440340.0	0.004486	1975.27
9	444736.0	0.006202	2758.28
10	448360.0	0.007099	3182.99
11	416765.0	0.005718	2383.17
12	434372.0	0.004213	1830.00
13	419579.0	0.004758	1996.19
14	495455.0	0.005442	2696.43
15	474729.0	0.004256	2020.28
16	405233.0	0.007196	2916.12
17	511581.0	0.003481	1780.95

Continued to next page

Sample	E, psi	Strain, in/in	Stress, psi
18	468720.0	0.004119	1930.68
19	505328.0	0.005756	2908.54
20	416843.0	0.005581	2326.39
21	412887.0	0.005651	2333.31
22	409392.0	0.005046	2065.91
23	441246.0	0.004725	2085.05
24	512286.0	0.004049	2074.43
25	508399.0	0.004769	2424.60
26	463449.0	0.004464	2068.62
27	407433.0	0.005940	2420.24
28	523405.0	0.004068	2129.36
29	420106.0	0.006398	2687.81
30	450237.0	0.004926	2217.98
Mean	458659.0	0.004989	2268.04
SD	37768.04	0.000943	354.02
% Dev	8.23	18.90	15.61

14 days			
Sample	E, psi	Strain, in/in	Stress, psi
1	510960.0	0.004333	2214.05
2	511589.0	0.004340	2220.13
3	407370.0	0.007589	3091.48
4	402243.0	0.004633	1863.42
5	453151.0	0.006006	2721.82
6	462536.0	0.004839	2238.42
7	490259.0	0.004226	2071.71
8	406957.0	0.004728	1923.92
9	472982.0	0.006571	3107.96
10	402101.0	0.007218	2902.30
11	413263.0	0.004607	1903.95
12	496856.0	0.005660	2812.42
13	461122.0	0.005079	2342.23
14	418863.0	0.005623	2355.21
15	511166.0	0.004875	2491.80
16	401945.0	0.006166	2478.27
17	408885.0	0.007940	3246.46

Continued to next page

Sample	E, psi	Strain, in/in	Stress, psi
18	422525.0	0.004639	1959.89
19	414298.0	0.005527	2290.01
20	441287.0	0.006831	3014.53
21	418363.0	0.005048	2112.05
22	508544.0	0.004599	2338.91
23	462108.0	0.006813	3148.28
24	503296.0	0.005956	2997.39
25	426969.0	0.005490	2343.97
26	420593.0	0.005894	2479.00
27	487649.0	0.004221	2058.31
28	460418.0	0.004419	2034.42
29	453341.0	0.006556	2971.92
30	497974.0	0.004930	2455.22
Mean	451653.8	0.005512	2472.98
SD	38782.44	0.001041	417.14
% Dev	8.59	18.88	16.87

28 days			
Sample	E, psi	Strain, in/in	Stress, psi
1	496368.0	0.003837	1904.65
2	515852.0	0.003969	2047.64
3	437579.0	0.006082	2661.47
4	431878.0	0.005121	2211.56
5	429976.0	0.004203	1807.36
6	532879.0	0.004591	2446.55
7	498527.0	0.006210	3095.63
8	539476.0	0.004003	2159.32
9	548541.0	0.003653	2003.99
10	530503.0	0.003486	1849.44
11	521217.0	0.003698	1927.40
12	468166.0	0.004878	2283.66
13	492288.0	0.003972	1955.40
14	459343.0	0.006020	2765.41
15	431441.0	0.005553	2395.62
16	437869.0	0.004556	1994.91
17	487196.0	0.006528	3180.22

Continued to next page

Sample	E, psi	Strain, in/in	Stress, psi
18	507635.0	0.004299	2182.21
19	510410.0	0.003899	1990.09
20	527209.0	0.003713	1957.29
21	484644.0	0.005467	2649.50
22	453296.0	0.004440	2012.72
23	492637.0	0.004709	2319.78
24	466347.0	0.006701	3125.11
25	460641.0	0.004269	1966.50
26	522829.0	0.005259	2749.50
27	458686.0	0.004618	2118.40
28	498533.0	0.006212	3097.00
29	446903.0	0.004836	2161.28
30	549012.0	0.004850	2662.64
Mean	487929.4	0.004788	2322.74
SD	36821.26	0.000920	414.23
% Dev	7.55	19.22	17.83

2 Months			
Sample	E, psi	Strain, in/in	Stress, psi
1	451585.0	0.005829	2632.29
2	521140.0	0.009584	4994.61
3	503987.0	0.006568	3310.19
4	422602.0	0.008028	3392.65
5	464650.0	0.004226	1963.61
6	487495.0	0.006847	3337.88
7	536528.0	0.006708	3599.27
8	467394.0	0.006186	2891.53
9	483015.0	0.005334	2576.31
10	439057.0	0.005871	2577.59
11	560643.0	0.005932	3325.56
12	577072.0	0.004721	2724.59
13	494813.0	0.006252	3093.77
14	439244.0	0.006120	2688.01
15	546945.0	0.004606	2519.01
16	442907.0	0.006476	2868.06
17	507230.0	0.007212	3658.17

Continued to next page

Sample	E, psi	Strain, in/in	Stress, psi
18	448270.0	0.008187	3669.94
19	446216.0	0.006396	2853.80
20	433942.0	0.009138	3965.26
21	507122.0	0.007398	3751.57
22	572473.0	0.005037	2883.72
23	464167.0	0.008384	3891.77
24	486150.0	0.006499	3159.53
25	535973.0	0.005969	3199.41
26	503315.0	0.005438	2736.94
27	561856.0	0.004506	2531.62
28	461677.0	0.007369	3402.16
29	527281.0	0.007013	3697.71
30	494120.0	0.005637	2785.46
Mean	492962.3	0.006449	3156.07
SD	43992.00	0.001299	587.20
% Dev	8.92	20.15	18.61

3 Months			
Sample	E, psi	Strain, in/in	Stress, psi
1	462900.0	0.004410	2041.57
2	563232.0	0.004893	2755.63
3	460056.0	0.006254	2877.16
4	459318.0	0.005331	2448.45
5	536250.0	0.004776	2561.08
6	558718.0	0.005466	3053.86
7	459930.0	0.005008	2303.26
8	502323.0	0.006290	3159.61
9	552545.0	0.005491	3034.25
10	479980.0	0.005819	2793.00
11	556950.0	0.003843	2140.10
12	490114.0	0.004148	2032.76
13	552498.0	0.005452	3012.47
14	486979.0	0.004238	2063.62
15	535170.0	0.004426	2368.51
16	478277.0	0.006646	3178.53
17	496111.0	0.004736	2349.58

Continued to next page

Sample	E, psi	Strain, in/in	Stress, psi
18	495507.0	0.004248	2104.73
19	521828.0	0.004355	2272.35
20	452875.0	0.006750	3056.78
21	490089.0	0.005926	2904.18
22	484363.0	0.004606	2231.20
23	501158.0	0.006309	3161.93
24	534184.0	0.004207	2247.48
25	482677.0	0.006462	3119.01
26	573442.0	0.004789	2746.44
27	486887.0	0.005117	2491.43
28	516584.0	0.005018	2592.37
29	547122.0	0.004589	2510.93
30	458080.0	0.006778	3104.80
Mean	505871.6	0.005213	2623.90
SD	36269.73	0.000864	386.90
% Dev	7.17	16.58	14.75

4 Months			
Sample	E, psi	Strain, in/in	Stress, psi
1	565105.0	0.003680	2079.62
2	524267.0	0.004882	2559.71
3	455630.0	0.004424	2015.51
4	490906.0	0.004689	2301.68
5	520049.0	0.005188	2697.99
6	468531.0	0.005892	2760.58
7	540925.0	0.004873	2635.99
8	504668.0	0.005783	2918.25
9	495000.0	0.004190	2074.25
10	519787.0	0.004404	2289.33
11	550136.0	0.004469	2458.51
12	470294.0	0.005043	2371.80
13	554360.0	0.004500	2494.60
14	573795.0	0.004059	2329.00
15	543639.0	0.004427	2406.58
16	470486.0	0.004673	2198.76
17	471874.0	0.004430	2090.51

Continued to next page

Sample	E, psi	Strain, in/in	Stress, psi
18	560751.0	0.003729	2091.08
19	564800.0	0.004977	2810.79
20	544039.0	0.004498	2447.00
21	549377.0	0.004841	2659.57
22	556919.0	0.004905	2731.80
23	509019.0	0.005377	2737.15
24	535544.0	0.004182	2239.89
25	572045.0	0.004912	2809.86
26	576398.0	0.003551	2046.88
27	489695.0	0.005197	2545.14
28	553139.0	0.004099	2267.30
29	508724.0	0.005768	2934.26
30	442843.0	0.004774	2114.24
Mean	522758.2	0.004681	2437.25
SD	38454.08	0.000580	279.38
% Dev	7.36	12.39	11.46

5 Months			
Sample	E, psi	Strain, in/in	Stress, psi
1	452508.0	0.004557	2061.87
2	424929.0	0.005187	2203.97
3	554906.0	0.004177	2318.00
4	471549.0	0.005405	2548.53
5	534961.0	0.003740	2000.86
6	506806.0	0.005806	2942.32
7	433951.0	0.005589	2425.24
8	546778.0	0.004469	2443.32
9	483516.0	0.004275	2066.89
10	531785.0	0.004219	2243.83
11	429313.0	0.006039	2592.60
12	541391.0	0.004616	2499.29
13	511621.0	0.004571	2338.71
14	550737.0	0.004090	2252.57
15	486904.0	0.004810	2342.13
16	541852.0	0.005038	2729.61
17	420222.0	0.006197	2603.94

Continued to next page

Sample	E, psi	Strain, in/in	Stress, psi
18	494309.0	0.005891	2911.73
19	529025.0	0.004763	2519.67
20	441914.0	0.006239	2756.95
21	520753.0	0.005070	2640.25
22	551088.0	0.005020	2766.47
23	546201.0	0.003873	2115.35
24	513868.0	0.005392	2770.53
25	508232.0	0.004284	2177.52
26	525940.0	0.003856	2027.80
27	469539.0	0.004662	2189.18
28	471914.0	0.005168	2439.09
29	546183.0	0.003723	2033.44
30	535720.0	0.004897	2623.59
Mean	502613.8	0.004854	2419.51
SD	42348.09	0.000720	272.01
% Dev	8.43	14.84	11.24

6 Months			
Sample	E, psi	Strain, in/in	Stress, psi
1	517457.0	0.005786	2993.87
2	495418.0	0.005536	2742.70
3	530628.0	0.006499	3448.49
4	456249.0	0.004721	2153.76
5	432448.0	0.007251	3135.82
6	492559.0	0.004632	2281.37
7	519487.0	0.005148	2674.15
8	527491.0	0.004712	2485.71
9	479290.0	0.004241	2032.64
10	459476.0	0.007285	3347.33
11	465330.0	0.005318	2474.67
12	401534.0	0.005941	2385.66
13	466272.0	0.004591	2140.74
14	541350.0	0.004149	2245.93
15	425184.0	0.007215	3067.84
16	431594.0	0.007321	3159.74
17	512361.0	0.004784	2451.38

Continued to next page

Sample	E, psi	Strain, in/in	Stress, psi
18	409972.0	0.008134	3334.83
19	405332.0	0.006762	2740.76
20	448215.0	0.005259	2357.28
21	528448.0	0.005748	3037.34
22	523134.0	0.005369	2808.95
23	423887.0	0.005487	2325.90
24	400279.0	0.006406	2564.10
25	413008.0	0.007206	2976.05
26	506036.0	0.004811	2434.62
27	433478.0	0.006747	2924.63
28	446551.0	0.006108	2727.63
29	500444.0	0.006258	3131.75
30	446129.0	0.007141	3185.89
Mean	467968.0	0.005886	2725.72
SD	44352.89	0.001069	396.09
% Dev	9.48	18.16	14.53

A.8 Resin Type-D; Test Specimen; ASTM D790

0 day			
Sample	E, psi	Strain, in/in	Stress, psi
1	527027.0	0.004430	2334.90
2	660082.0	0.004420	2917.80
3	727921.0	0.003554	2587.03
4	450921.0	0.007299	3291.10
5	777221.0	0.003289	2556.32
6	559913.0	0.004960	2777.05
7	537596.0	0.006248	3358.93
8	692773.0	0.002958	2048.93
9	430958.0	0.006248	2692.61
10	560315.0	0.003843	2153.38
11	609754.0	0.004572	2787.51
12	533667.0	0.005763	3075.39
13	461135.0	0.004745	2187.93
14	493201.0	0.004289	2115.44
15	725167.0	0.003763	2728.57
16	631213.0	0.003418	2157.76
17	696524.0	0.003600	2507.57

Continued to next page

Sample	E, psi	Strain, in/in	Stress, psi
18	631131.0	0.004660	2940.92
19	Broken	Broken	Broken
20	421809.0	0.006514	2747.62
21	540188.0	0.005341	2885.23
22	586798.0	0.004053	2378.10
23	772737.0	0.003484	2692.46
24	734533.0	0.004717	3464.86
25	648041.0	0.004814	3119.92
26	459931.0	0.006537	3006.34
27	467278.0	0.006856	3203.45
28	457707.0	0.006315	2890.60
29	442041.0	0.007045	3114.21
30	748338.0	0.003440	2574.41
Mean	585721.38	0.004868	2734.36
SD	114887.19	0.001287	392.21
% Dev	19.61	26.44	14.34

7 days			
Sample	E, psi	Strain, in/in	Stress, psi
1	628805.0	0.004014	2523.93
2	492120.0	0.006619	3257.52
3	668977.0	0.004779	3197.16
4	483164.0	0.007954	3842.90
5	592670.0	0.004182	2478.28
6	530447.0	0.007167	3801.62
7	603691.0	0.004888	2950.57
8	757964.0	0.002560	1940.03
9	597047.0	0.004421	2639.42
10	410682.0	0.008723	3582.57
11	669137.0	0.004306	2881.22
12	573377.0	0.004664	2673.98
13	570808.0	0.004622	2638.26
14	723057.0	0.005196	3756.86
15	767537.0	0.004881	3746.64
16	414748.0	0.007160	2969.64
17	517778.0	0.006374	3300.22

Continued to next page

Sample	E, psi	Strain, in/in	Stress, psi
18	601333.0	0.005305	3190.12
19	448287.0	0.004760	2134.02
20	681935.0	0.004130	2816.72
21	451309.0	0.007671	3462.01
22	765097.0	0.004259	3258.75
23	719991.0	0.003604	2594.81
24	568672.0	0.004809	2734.87
25	751227.0	0.004837	3633.69
26	723775.0	0.005262	3808.32
27	423218.0	0.008754	3704.86
28	711622.0	0.003477	2474.18
29	731448.0	0.002697	1972.97
30	743885.0	0.003810	2834.11
Mean	610793.60	0.005196	3026.67
SD	117161.86	0.001639	564.74
% Dev	19.18	31.54	18.66

14 days			
Sample	E, psi	Strain, in/in	Stress, psi
1	532429.0	0.005020	2672.86
2	797792.0	0.003828	3054.07
3	700480.0	0.003321	2326.06
4	574063.0	0.005362	3078.08
5	637933.0	0.004351	2775.35
6	437718.0	0.007327	3207.20
7	463226.0	0.005630	2608.11
8	532674.0	0.004301	2290.93
9	876619.0	0.002833	2483.59
10	665911.0	0.004062	2704.61
11	666513.0	0.005824	3881.84
12	665777.0	0.005746	3825.43
13	635538.0	0.003798	2413.69
14	691187.0	0.003374	2331.90
15	820046.0	0.004652	3814.85
16	679125.0	0.005807	3943.40
17	409459.0	0.008126	3327.24

Continued to next page

Sample	E, psi	Strain, in/in	Stress, psi
18	690688.0	0.002858	1973.72
19	638480.0	0.003457	2207.02
20	652067.0	0.003795	2474.82
21	616625.0	0.004183	2579.36
22	599772.0	0.003528	2116.12
23	481197.0	0.007360	3541.82
24	683217.0	0.002842	1941.86
25	742770.0	0.005045	3747.52
26	670688.0	0.004136	2774.05
27	854249.0	0.003028	2586.87
28	571342.0	0.005450	3114.07
29	727865.0	0.004817	3506.17
30	765562.0	0.003914	2996.13
Mean	649367.07	0.004592	2876.62
SD	116096.15	0.001378	601.91
% Dev	17.88	30.00	20.92

28-day			
Sample	E, psi	Strain, in/in	Stress, psi
1	476799.0	0.007319	3489.71
2	576060.0	0.007361	4240.4
3	Broken	Broken	Broken
4	643506.0	0.003562	2292.01
5	554873.0	0.005675	3148.7
6	954461.0	0.003330	3178.7
7	862317.0	0.005154	4444.66
8	Broken	Broken	Broken
9	Broken	Broken	Broken
10	937037.0	0.004305	4034.38
11	Broken	Broken	Broken
12	Broken	Broken	Broken
13	Broken	Broken	Broken
14	533697.0	0.004931	2631.65
15	Broken	Broken	Broken
16	646929.0	0.005892	3811.53
17	Broken	Broken	Broken

Continued to next page

Sample	E, psi	Strain, in/in	Stress, psi
18	Broken	Broken	Broken
19	Broken	Broken	Broken
20	Broken	Broken	Broken
21	873720.0	0.002474	2161.56
22	Broken	Broken	Broken
23	Broken	Broken	Broken
24	Broken	Broken	Broken
25	Broken	Broken	Broken
26	633142.0	0.003306	2093.2
27	889943.0	0.002835	2522.8
28	Broken	Broken	Broken
29	Broken	Broken	Broken
30	Broken	Broken	Broken
Mean	715207.00	0.004679	3170.77
SD	174549.32	0.001659	836.00
% Dev	24.41	35.46	26.37

2 Months			
Sample	E, psi	Strain, in/in	Stress, psi
1	935027.0	0.004564	4267.90
2	Broken	Broken	Broken
3	Broken	Broken	Broken
4	Broken	Broken	Broken
5	467506.0	0.004267	1994.67
6	Broken	Broken	Broken
7	Broken	Broken	Broken
8	Broken	Broken	Broken
9	Broken	Broken	Broken
10	Broken	Broken	Broken
11	Broken	Broken	Broken
12	Broken	Broken	Broken
13	550881.0	0.004462	2458.26
14	Broken	Broken	Broken
15	Broken	Broken	Broken
16	723648.0	0.005976	4324.34
17	Broken	Broken	Broken

Continued to next page

Sample	E, psi	Strain, in/in	Stress, psi
18	Broken	Broken	Broken
19	Broken	Broken	Broken
20	Broken	Broken	Broken
21	Broken	Broken	Broken
22	Broken	Broken	Broken
23	644416.0	0.006937	4470.07
24	Broken	Broken	Broken
25	Broken	Broken	Broken
26	Broken	Broken	Broken
27	Broken	Broken	Broken
28	Broken	Broken	Broken
29	Broken	Broken	Broken
30	Broken	Broken	Broken
Mean	664295.60	0.005241	3503.05
SD	179445.27	0.001165	1179.14
% Dev	27.01	22.23	33.66

3 Months			
Sample	E, psi	Strain, in/in	Stress, psi
1	745339.0	0.003616	2695.20
2	868979.0	0.003750	3258.99
3	472265.0	0.005730	2705.99
4	607906.0	0.006228	3785.91
5	932392.0	0.004109	3830.96
6	439149.0	0.007911	3474.10
7	841206.0	0.003830	3221.73
8	968691.0	0.002395	2320.4
9	663747.0	0.005715	3793.28
10	358725.0	0.010200	3658.84
11	721651.0	0.005749	4148.87
12	560299.0	0.006907	3869.95
13	895833.0	0.002766	2477.51
14	863968.0	0.003016	2605.82
15	460117.0	0.004442	2044.05
16	404452.0	0.008572	3467.02
17	Broken	Broken	Broken

Continued to next page

Sample	E, psi	Strain, in/in	Stress, psi
18	Broken	Broken	Broken
19	Broken	Broken	Broken
20	Broken	Broken	Broken
21	Broken	Broken	Broken
22	Broken	Broken	Broken
23	Broken	Broken	Broken
24	Broken	Broken	Broken
25	Broken	Broken	Broken
26	Broken	Broken	Broken
27	Broken	Broken	Broken
28	Broken	Broken	Broken
29	Broken	Broken	Broken
30	Broken	Broken	Broken
Mean	675294.94	0.005308	3209.91
SD	207085.89	0.002238	647.34
% Dev	30.67	42.17	20.17

4 Months			
Sample	E, psi	Strain, in/in	Stress, psi
1	672261.0	0.002878	1934.57
2	482434.0	0.005237	2526.69
3	897103.0	0.002340	2099.37
4	943792.0	0.002047	1932.05
5	739964.0	0.003628	2684.38
6	757695.0	0.005845	4428.96
7	887484.0	0.002602	2308.85
8	770447.0	0.003592	2767.10
9	521057.0	0.005199	2708.87
10	834031.0	0.003728	3109.22
11	807260.0	0.002373	1915.98
12	532505.0	0.008067	4295.98
13	391663.0	0.008408	3292.98
14	533024.0	0.004960	2643.99
15	Broken	Broken	Broken
16	Broken	Broken	Broken
17	Broken	Broken	Broken

Continued to next page

Sample	E, psi	Strain, in/in	Stress, psi
18	Broken	Broken	Broken
19	Broken	Broken	Broken
20	Broken	Broken	Broken
21	Broken	Broken	Broken
22	Broken	Broken	Broken
23	Broken	Broken	Broken
24	Broken	Broken	Broken
25	Broken	Broken	Broken
26	Broken	Broken	Broken
27	Broken	Broken	Broken
28	Broken	Broken	Broken
29	Broken	Broken	Broken
30	Broken	Broken	Broken
Mean	697908.57	0.004350	2760.64
SD	176256.60	0.002045	801.25
% Dev	25.25	47.01	29.02

5 Months			
Sample	E, psi	Strain, in/in	Stress, psi
1	899483.0	0.005521	4966.08
2	363476.0	0.006290	2286.38
3	929918.0	0.003496	3250.95
4	528670.0	0.004340	2294.39
5	731789.0	0.006794	4972.08
6	392437.0	0.012899	5061.98
7	670137.0	0.004560	3056.02
8	427986.0	0.006586	2818.92
9	767030.0	0.003209	2461.04
10	839290.0	0.003722	3123.44
11	717424.0	0.002732	1959.85
12	690673.0	0.002843	1963.29
13	615304.0	0.004475	2753.76
14	726174.0	0.005612	4075.55
15	828148.0	0.003349	2773.09
16	476264.0	0.005013	2387.43
17	853720.0	0.003156	2694.36

Continued to next page

Sample	E, psi	Strain, in/in	Stress, psi
18	773162.0	0.003128	2418.39
19	Broken	Broken	Broken
20	Broken	Broken	Broken
21	Broken	Broken	Broken
22	Broken	Broken	Broken
23	Broken	Broken	Broken
24	Broken	Broken	Broken
25	Broken	Broken	Broken
26	Broken	Broken	Broken
27	Broken	Broken	Broken
28	Broken	Broken	Broken
29	Broken	Broken	Broken
30	Broken	Broken	Broken
Mean	679504.72	0.004874	3073.17
SD	175866.27	0.002396	1016.17
% Dev	25.88	49.16	33.07

6 Months			
Sample	E, psi	Strain, in/in	Stress, psi
1	398356.0	0.013047	5197.41
2	669140.0	0.003671	2456.44
3	536110.0	0.007535	4039.84
4	719675.0	0.005532	3981.42
5	651838.0	0.007311	4765.31
6	840011.0	0.0	4414.2
7	646421.0	0.004235	2737.79
8	807455.0	0.003886	3138.13
9	664313.0	0.004802	3189.80
10	948797.0	0.003889	3689.43
11	757813.0	0.0	2261.2
12	611915.0	0.004079	2496.11
13	483232.0	0.007953	3843.04
14	386767.0	0.006554	2534.99
15	813134.0	0.003464	2816.52
16	742393.0	0.006032	4478.09
17	754304.0	0.003076	2320.17

Continued to next page

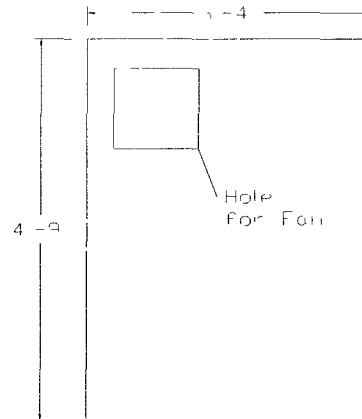
Sample	E, psi	Strain, in/in	Stress, psi
18	613521.0	0.004411	2705.94
19	631847.0	0.003679	2324.62
20	427947.0	0.009536	4080.72
21	792960.0	0.002648	2099.72
22	Broken	Broken	Broken
23	Broken	Broken	Broken
24	Broken	Broken	Broken
25	Broken	Broken	Broken
26	Broken	Broken	Broken
27	Broken	Broken	Broken
28	Broken	Broken	Broken
29	Broken	Broken	Broken
30	Broken	Broken	Broken
Mean	661807.10	0.005408	3312.90
SD	151095.52	0.002546	942.23
% Dev	22.83	47.07	28.44

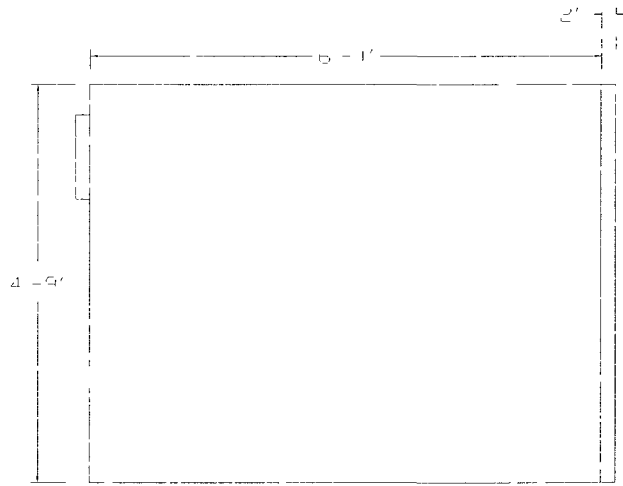
APPENDIX B

CAD DRAWING OF THE OVEN FRAMES

AND POWER SUPPLY CIRCUIT

DIAGRAM TO THE OVENS

B.1 Front View and Rear View of Custom Built Oven**Figure A. 114: Oven Front View****Figure A. 115: Oven Rear View**

B.2 Side Views of Custom Built Oven**Figure A. 116: Left Side View****Figure A. 117: Right Side View**

B.3 View of Frame of Custom Built Oven

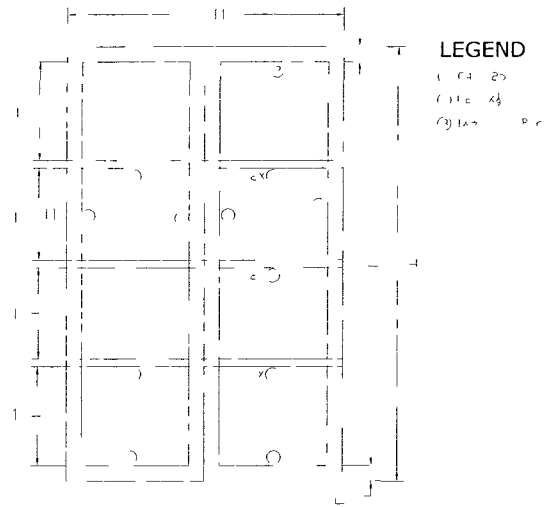


Figure A. 118: Front View of Door Frame

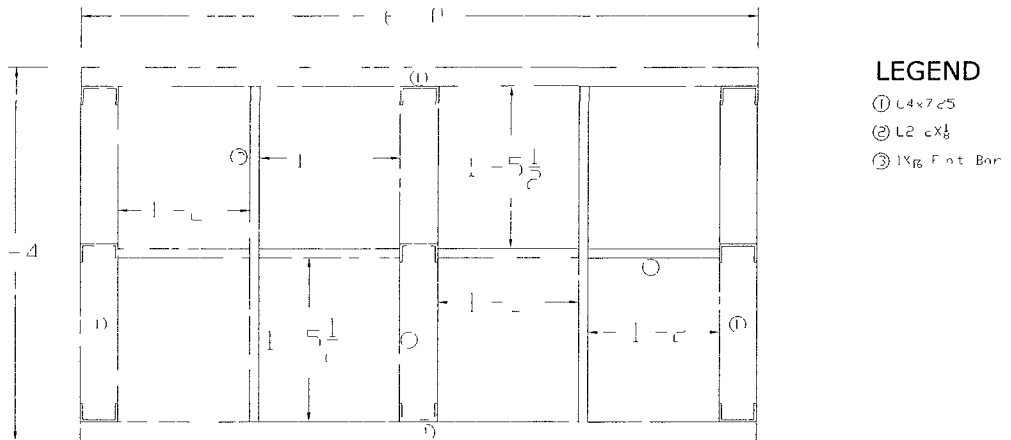


Figure A. 119: Bottom View of Frame

B.4 Top View and Side View of Frame of Custom Built Oven

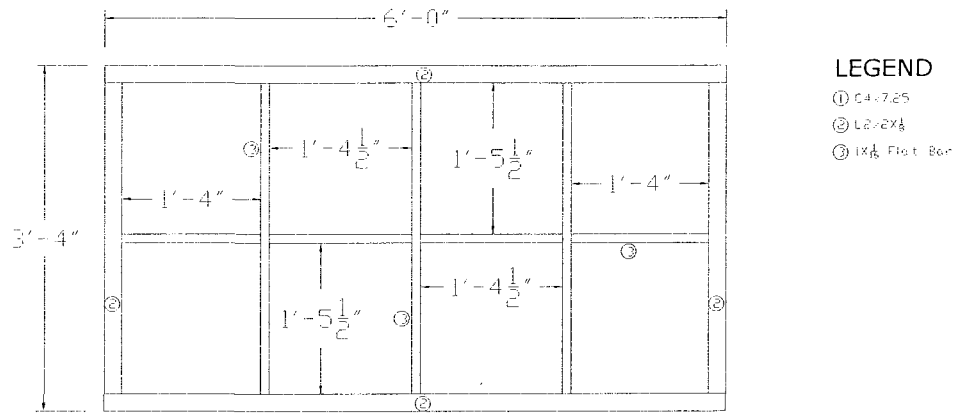


Figure A. 120: Top View of Frame

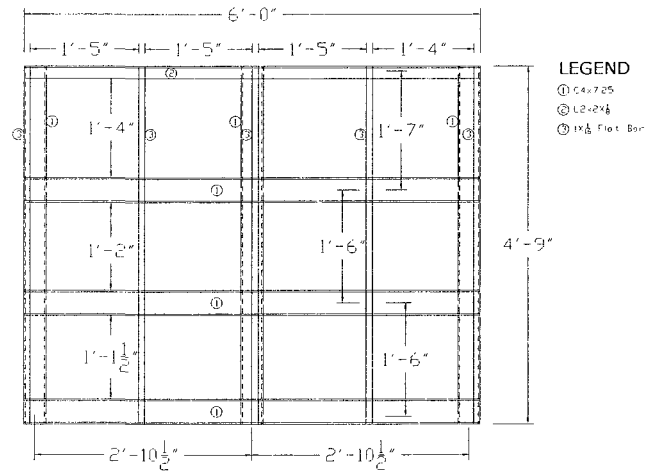


Figure A. 121: Side View of Frame

B.5 View of Rear Frame and Front Frame of Custom Built Oven

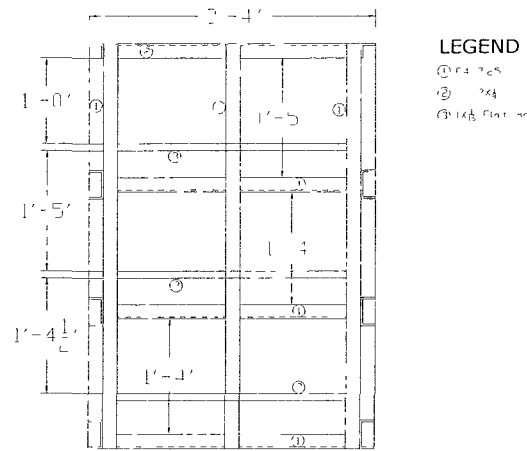


Figure A. 122: View of Rear Frame

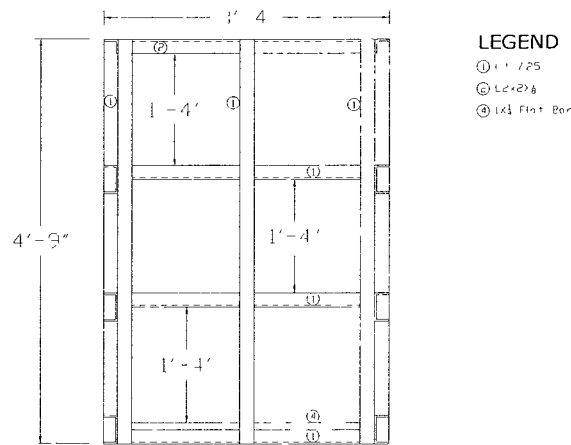


Figure A. 123: View of Front Frame

B.6 View of Middle Frame of Custom Built Oven

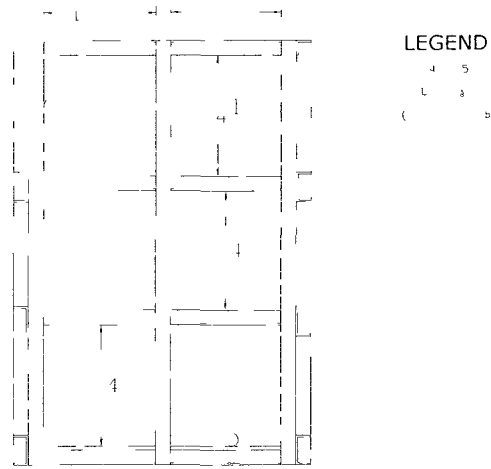


Figure A. 124: View of Middle Frame

B.7 Power Circuit Diagram of the Oven

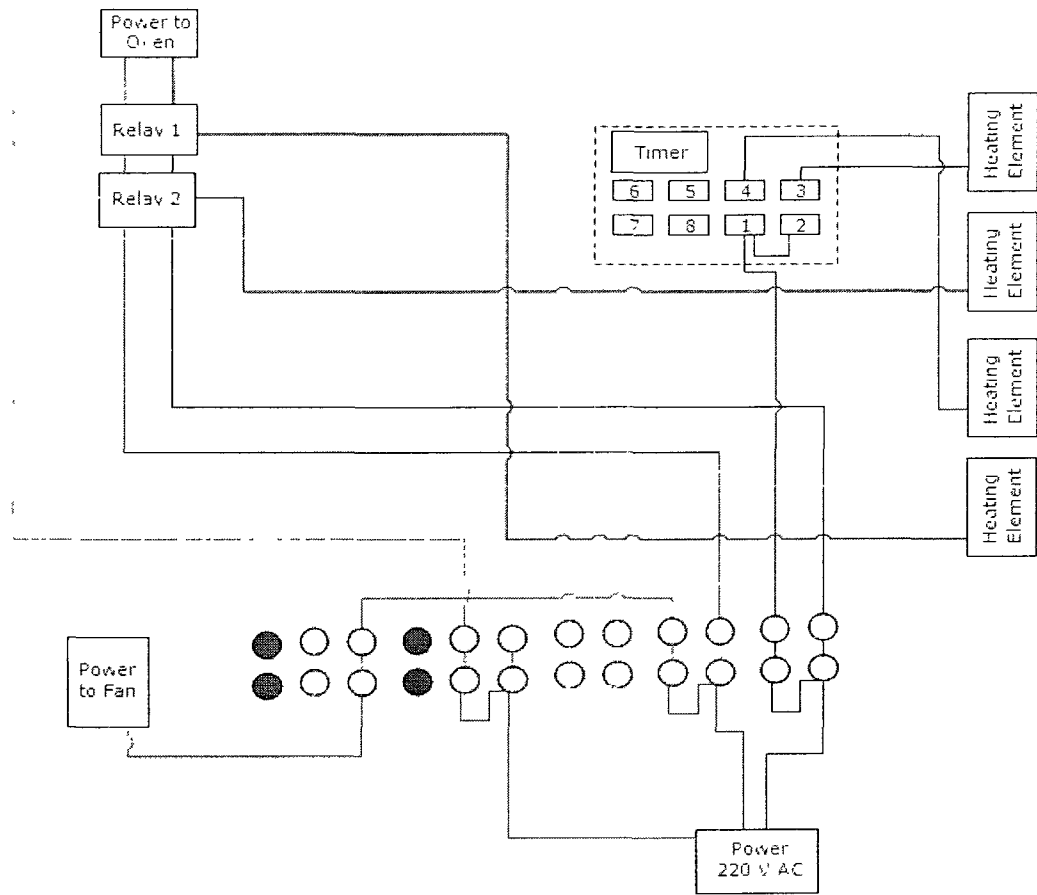


Figure A. 125: Power Circuit Diagram

APPENDIX C

**LABEL OF THE STRAIN GAGES AND STRAIN
ROSETTES FOR EACH OVEN**

C.1 Oven 1 – Resin Type A – Full Scale Sample # 1

Pipe Designation	Location	Type	Wire Color	Direction	Location on Liner	DAQ
A-1	Front	SG	Black	Long.	SL	101
			Green	Long.	SL	
A-1	Front	SR	Green	Long.	Crown	102
			Black	Long.	Crown	
A-1	Front	SR	Red	Circum.	Crown	103
			White	Circum.	Crown	
A-1	Back	SR	Green	Long.	Invert	104
			Black	Long.	Invert	
A-1	Back	SR	Red	Circum.	Invert	105
			White	Circum.	Invert	

C.2 Oven 1 – Resin Type C – Full Scale Sample # 3

Pipe Designation	Location	Type	Wire Color	Direction	Location on Liner	DAQ
C-3	Front	SG	Red	Long	SL	211
			White	Long	SL	
C-3	Front	SR	Green	Long	Crown	212
			Black	Long	Crown	
C-3	Front	SR	Red	Circum	Crown	213
			White	Circum	Crown	
C-3	Back	SR	Green	Long	Invert	214
			Black	Long	Invert	
C-3	Back	SR	Red	Circum	Invert	215
			White	Circum	Invert	

C.3 Oven 1 – Temperature Sensor

Location on Liner	Wire Color	DAQ
Front	Red	116
	White	
Rear	Red	117
	White	

C.4 Oven 2 – Resin Type A – Full Scale Sample # 3

Pipe Designation	Location	Type	Wire Color	Direction	Location on Liner	DAQ
A-3	Front	SG	Black	Long	SL	111
			Green	Long	SL	
A-3	Front	SR	Green	Long	Crown	112
			Black	Long	Crown	
A-3	Front	SR	Red	Circum	Crown	113
			White	Circum	Crown	
A-3	Back	SR	Green	Long	Invert	114
			Black	Long	Invert	
A-3	Back	SR	Red	Circum	Invert	115
			White	Circum	Invert	

C.5 Oven 2 – Resin Type C – Full Scale Sample # 2

Pipe Designation	Location	Type	Wire Color	Direction	Location on Liner	DAQ
C-2	Front	SG	Green	Long	SL	206
			Black	Long	SL	
C-2	Front	SR	Green	Long	Crown	207
			Black	Long	Crown	
C-2	Front	SR	Red	Circum	Crown	208
			White	Circum	Crown	
C-2	Back	SR	Green	Long	Invert	209
			Black	Long	Invert	
C-2	Back	SR	Red	Circum	Invert	210
			White	Circum	Invert	

C.6 Oven 2 – Temperature Sensor

Location on Liner	Wire Color	DAQ
Front	Red	216
	White	
Rear	Red	217
	White	

C.7 Oven 3 – Resin Type A – Full Scale Sample # 4

Pipe Designation	Location	Type	Wire Color	Direction	Location on Liner	DAQ
A-4	Front	SG	Red	Long.	SL	301
			White	Long.	SL	
A-4	Front	SR	Green	Long.	Crown	302
			Black	Long.	Crown	
A-4	Front	SR	Red	Circum.	Crown	304
			White	Circum.	Crown	
A-4	Back	SR	Green	Long.	Invert	305
			Black	Long.	Invert	
A-4	Back	SR	Red	Circum.	Invert	306
			White	Circum.	Invert	

C.8 Oven 3 – Resin Type A – Full Scale Sample # 2

Pipe Designation	Location	Type	Wire Color	Direction	Location on Liner	DAQ
A-2	Front	SG	Red	Long.	SL	106
			White	Long.	SL	
A-2	Front	SR	Green	Long.	Crown	107
			Black	Long.	Crown	
A-2	Front	SR	Red	Circum.	Crown	108
			White	Circum.	Crown	
A-2	Back	SR	Green	Long.	Invert	109
			Black	Long.	Invert	
A-2	Back	SR	Red	Circum.	Invert	110
			White	Circum.	Invert	

C.9 Oven 3 – Resin Type C – Full Scale Sample # 4

Pipe Designation	Location	Type	Wire Color	Direction	Location on Liner	DAQ
C-4	Front	SG	Green	Long	SL	307
			Black	Long	SL	
C-4	Front	SR	Green	Long	Crown	308
			Black	Long	Crown	
C-4	Front	SR	Red	Circum	Crown	309
			White	Circum	Crown	
C-4	Back	SR	Green	Long	Invert	310
			Black	Long	Invert	
C-4	Back	SR	Red	Circum	Invert	311
			White	Circum	Invert	

C.10 Oven 3 – Resin Type C – Full Scale Sample # 1

Pipe Designation	Location	Type	Wire Color	Direction	Location on Liner	DAQ
C-1	Front	SG	Red	Long	SL	201
			White	Long	SL	
C-1	Front	SR	Green	Long	Crown	202
			Black	Long	Crown	
C-1	Front	SR	Red	Circum	Crown	203
			White	Circum	Crown	
C-1	Back	SR	Green	Long	Invert	204
			Black	Long	Invert	
C-1	Back	SR	Red	Circum	Invert	205
			White	Circum	Invert	

C.11 Oven 3 – Temperature Sensor

Location on Liner	Wire Color	DAQ
Front	Red	216
	White	
Rear	Red	217
	White	

APPENDIX D

ANALYTICAL CALCULATION OF THE SAMPLE

SOLID BLOCK

D.1 Temperature Change Calculation at the Interface

According to Fourier's law, $\frac{dQ}{dt} = KA \frac{dT}{dx}$.

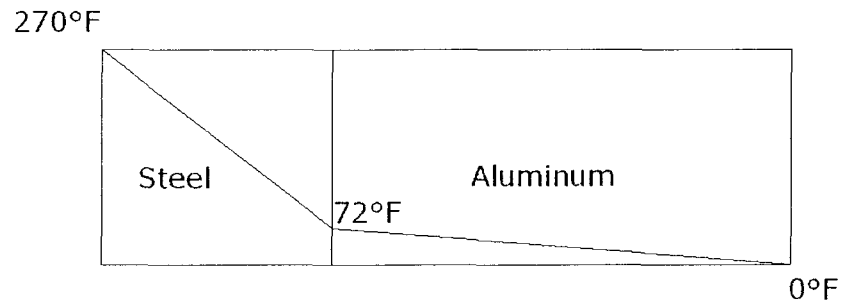


Figure A. 126: Temperature Gradient on the Steel and Aluminum Block

At the interface, temperature is equal at ideal condition (i.e. no contact thermal resistance). Therefore, heat transfer rate (dQ/dT) should be constant at any transverse section. After calculation the temperature at the interface of two metals was got 71.883° F.

D.2 Deflection Calculation due to Temperature

Table A. 39: Mechanical Properties of Steel and Aluminum

Material	Modulus of Elasticity psi	Poisson's Ratio	Density snail/in³
Steel	2.90E+07	0.27	7.35E-04
Aluminum	1.02E+07	0.35	2.53E-04

Table A. 40: Thermal Properties of Steel and Aluminum

Material	Specific Heat in-lbf/snail ° F	Coefficient of Thermal Expansion in/in/° F	Thermal Conductivity in-lbf/in sec ° F
Steel	4.33E+05	6.70E-06	5.37
Aluminum	7.72E+05	1.31E-05	29.6

D.3 Calculation for Elongation of Steel

Highest Temp	270		
Lowest Temp	71.883		
Length	10		
Division	10		
Element Length	1		
	270	260.09415	0.001743
	250.1883	240.28245	0.001610
	230.3766	220.47075	0.001477
	210.5649	200.65905	0.001344
	190.7532	180.84735	0.001212
	170.9415	161.03565	0.001079
	151.1298	141.22395	0.000946
	131.3181	121.41225	0.000813
	111.5064	101.60055	0.000681
	91.6947	81.78885	0.000548
End Surface Temperature	71.883		
Elongation due to thermal effect			0.011453

D.4 Calculation for Elongation of Aluminum

Highest Temp	71.883		
Lowest Temp	0		
Length	20		
Division	10		
Element Length	2		
	71.883	68.28885	0.001789
	64.6947	61.10055	0.001601
	57.5064	53.91225	0.001413
	50.3181	46.72395	0.001224
	43.1298	39.53565	0.001036
	35.9415	32.34735	0.000848
	28.7532	25.15905	0.000659
	21.5649	17.97075	0.000471
	14.3766	10.78245	0.000283
	7.1883	3.59415	0.000094
End Surface Temperature	8.88178E-15		
Elongation due to Thermal Effect			0.009417
Total Elongation, in			0.020870

APPENDIX E

LONGITUDINAL AND CIRCUMFERENTIAL STRESS

AT 53, 79,181 AND 241 DAYS

E.1 Oven 1

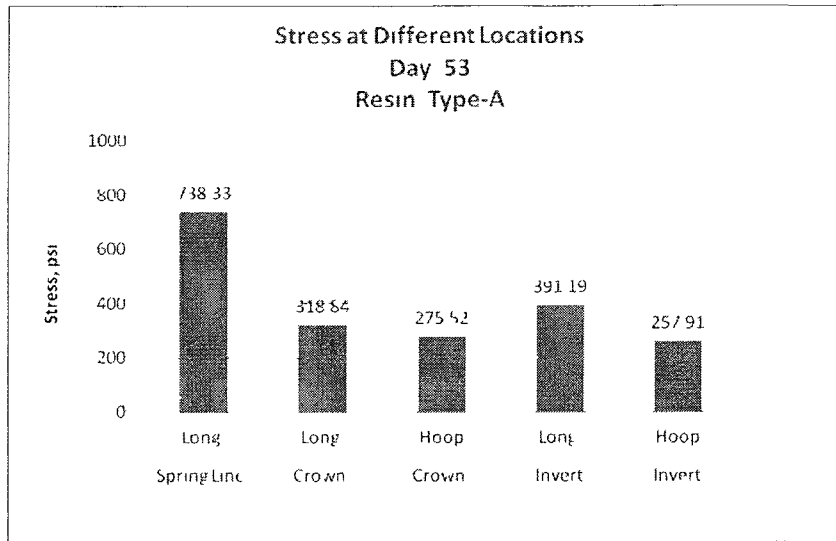


Figure A. 127: Longitudinal and Hoop Stress Due to Thermal Loading on Day 53 for Resin Type-A (Temperature Range 110° F-260° F)

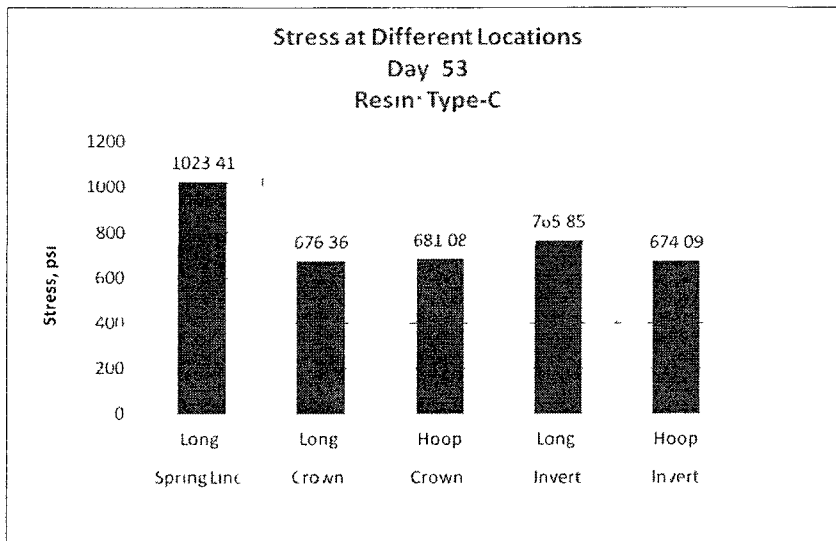


Figure A. 128: Longitudinal and Hoop Stress Due to Thermal Loading on Day 53 for Resin Type-C (Temperature Range 110° F-260° F)

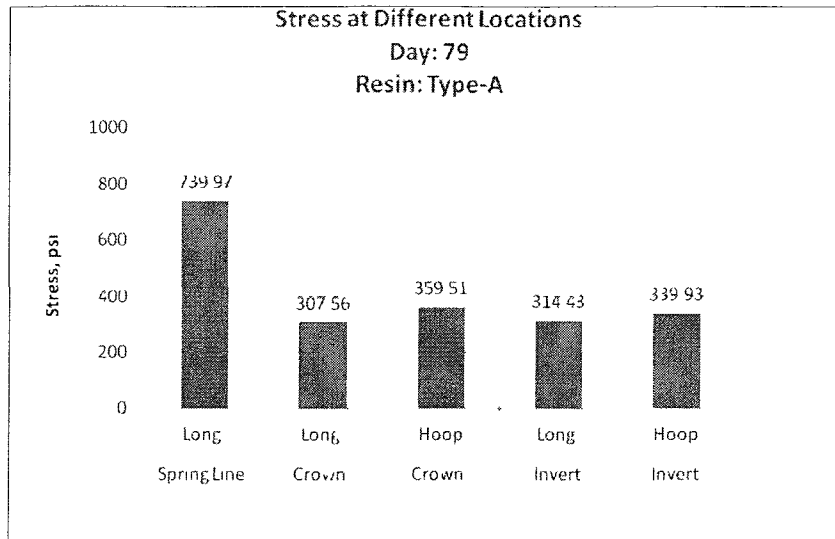


Figure A. 129: Longitudinal and Hoop Stress Due to Thermal Loading on Day 79 for Resin Type-A (Temperature Range 110° F-260° F)

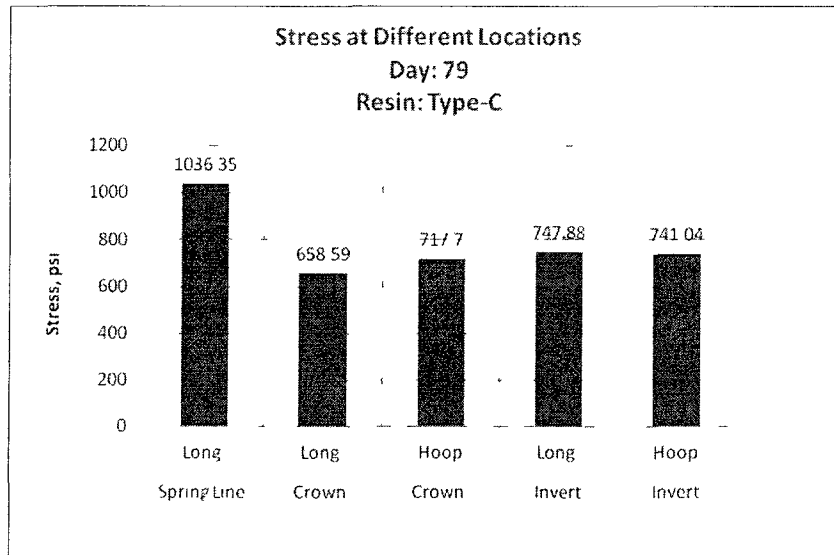


Figure A. 130: Longitudinal and Hoop Stress Due to Thermal Loading on Day 79 for Resin Type-C (Temperature Range 110° F-260° F)

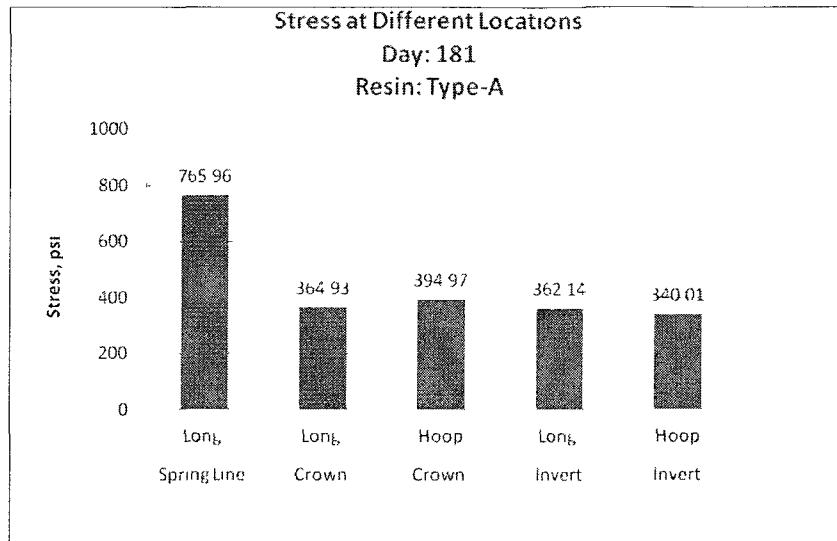


Figure A. 131: Longitudinal and Hoop Stress Due to Thermal Loading on Day 181 for Resin Type-A (Temperature Range 110° F-260° F)

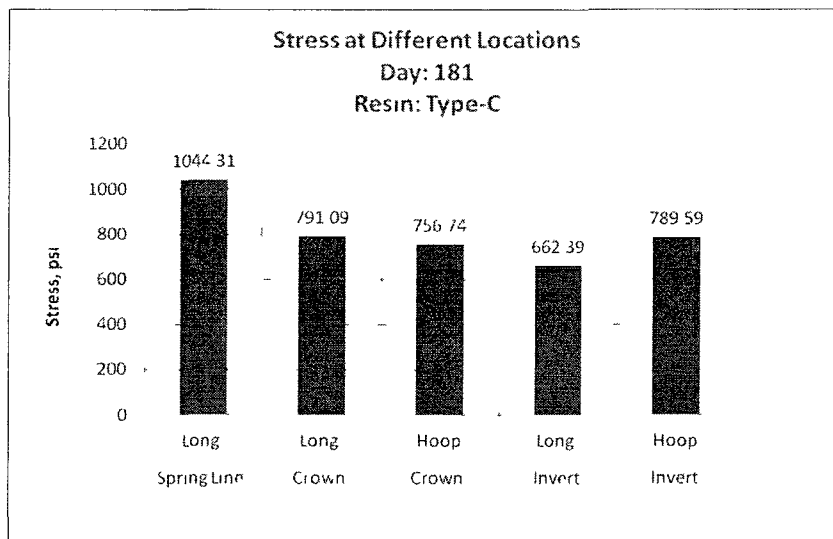


Figure A. 132: Longitudinal and Hoop Stress Due to Thermal Loading on Day 181 for Resin Type-C (Temperature Range 110° F-260° F)

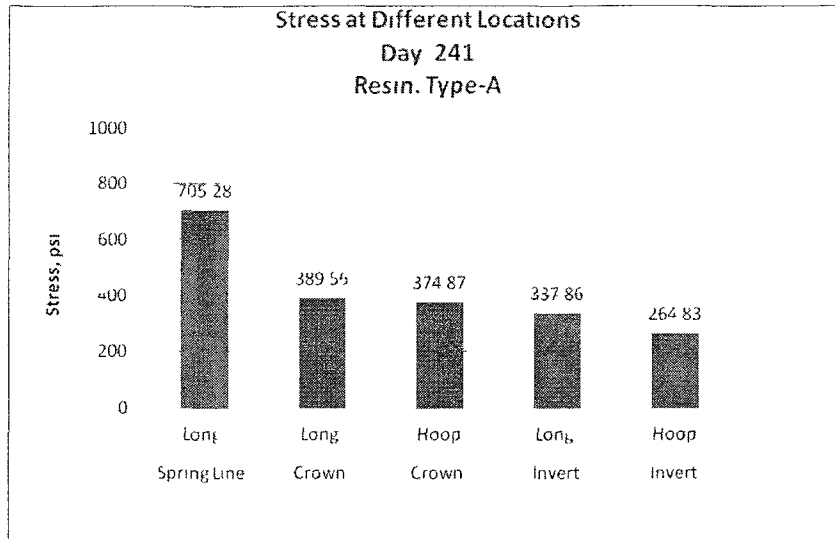


Figure A. 133: Longitudinal and Hoop Stress Due to Thermal Loading on Day 241 for Resin Type-A (Temperature Range 110° F-260° F)

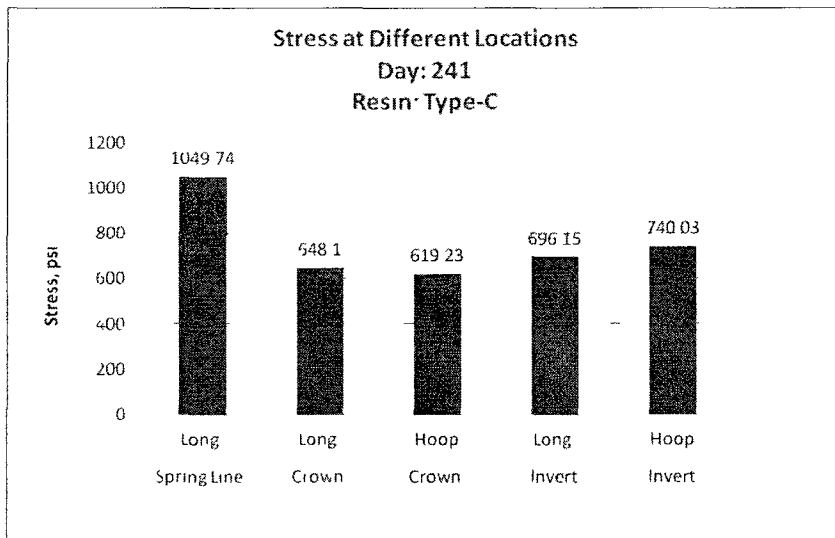


Figure A. 134: Longitudinal and Hoop Stress Due to Thermal Loading on Day 241 for Resin Type-C (Temperature Range 110° F-260° F)

E.2 Oven 2

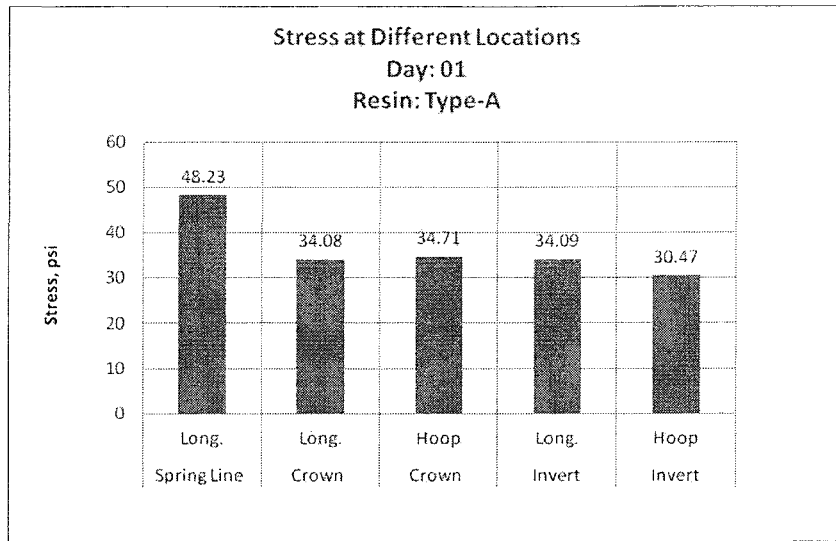


Figure A. 135: Longitudinal and Hoop Stress Due to Thermal Loading on Day 1 for Resin Type-A (Temperature Range 90° F-210° F)

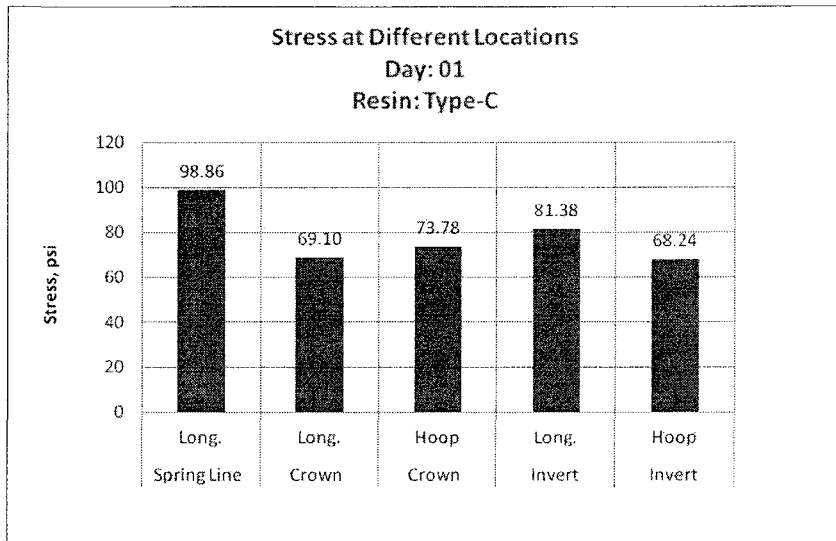


Figure A. 136: Longitudinal and Hoop Stress Due to Thermal Loading on Day 1 for Resin Type-C (Temperature Range 90° F-210° F)

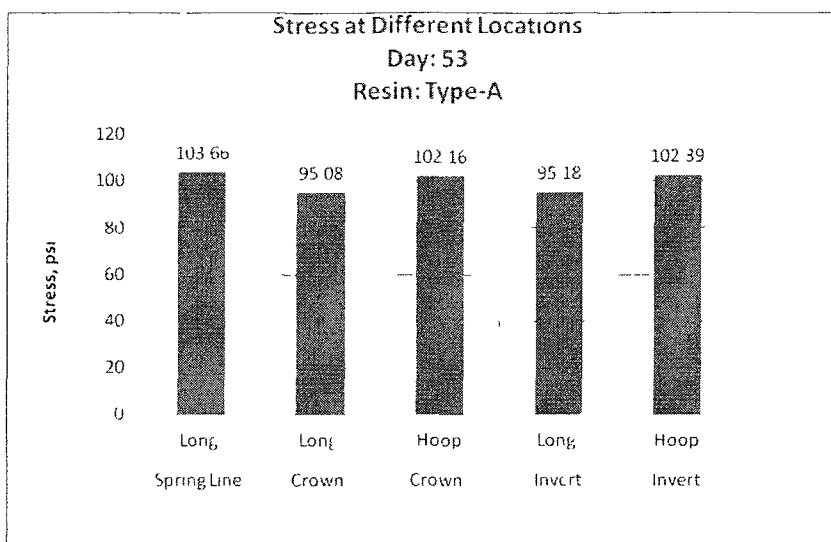


Figure A. 137: Longitudinal and Hoop Stress Due to Thermal Loading on Day 53 for Resin Type-A (Temperature Range 90° F-210° F)

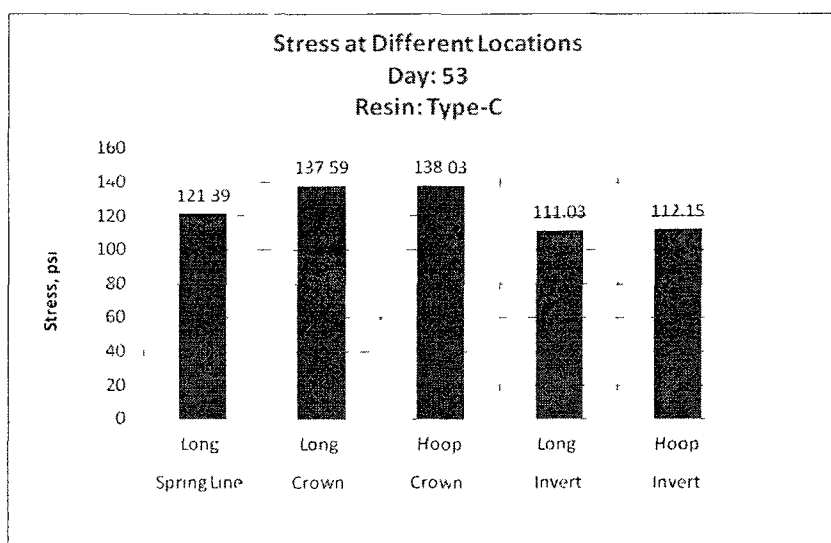


Figure A. 138: Longitudinal and Hoop Stress Due to Thermal Loading on Day 53 for Resin Type-C (Temperature Range 90° F-210° F)

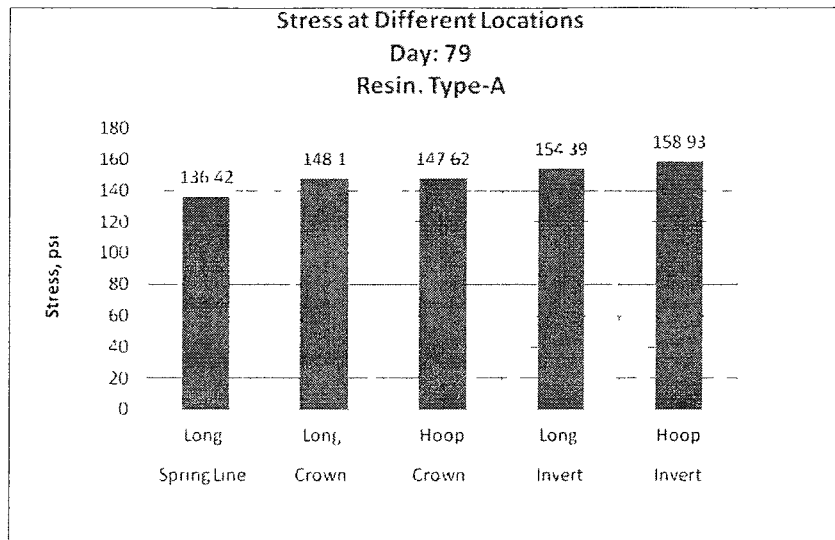


Figure A. 139: Longitudinal and Hoop Stress Due to Thermal Loading on Day 79 for Resin Type-A (Temperature Range 90° F-210° F)

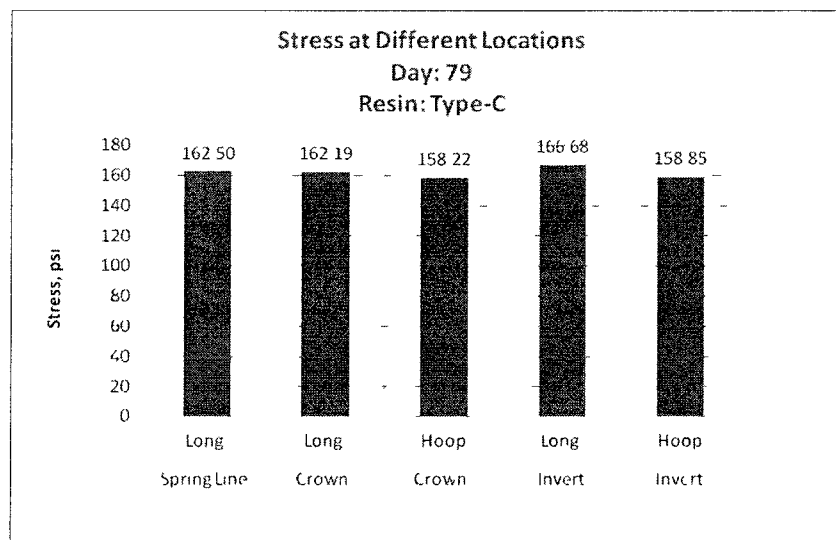


Figure A. 140: Longitudinal and Hoop Stress Due to Thermal Loading on Day 79 for Resin Type-C (Temperature Range 90° F-210° F)

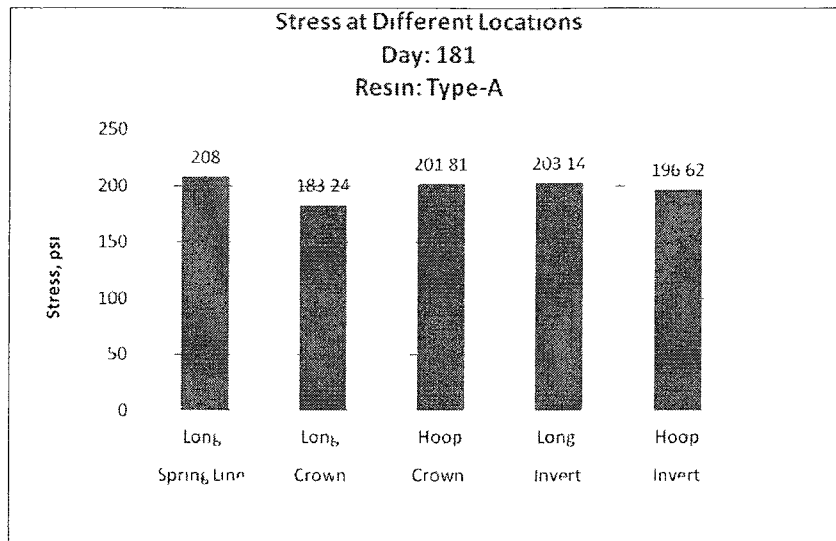


Figure A. 141: Longitudinal and Hoop Stress Due to Thermal Loading on Day 181 for Resin Type-A (Temperature Range 90° F-210° F)

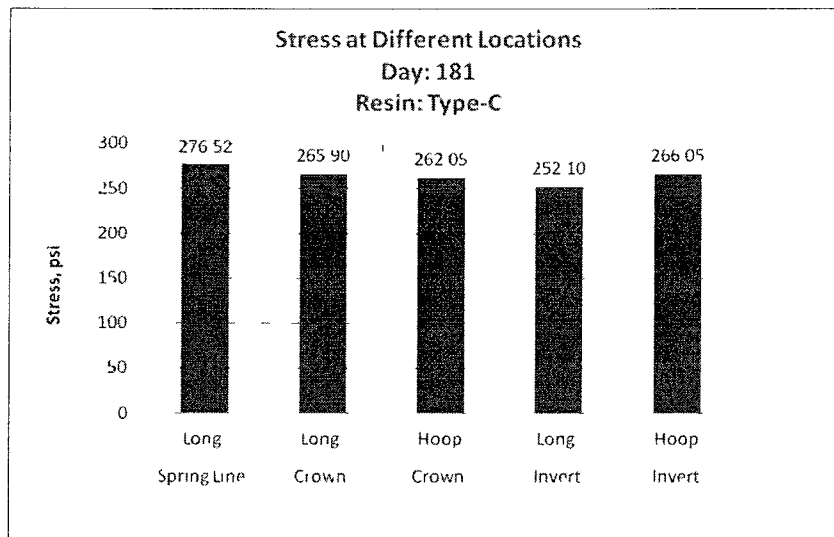


Figure A. 142: Longitudinal and Hoop Stress Due to Thermal Loading on Day 181 for Resin Type-C (Temperature Range 90° F-210° F)

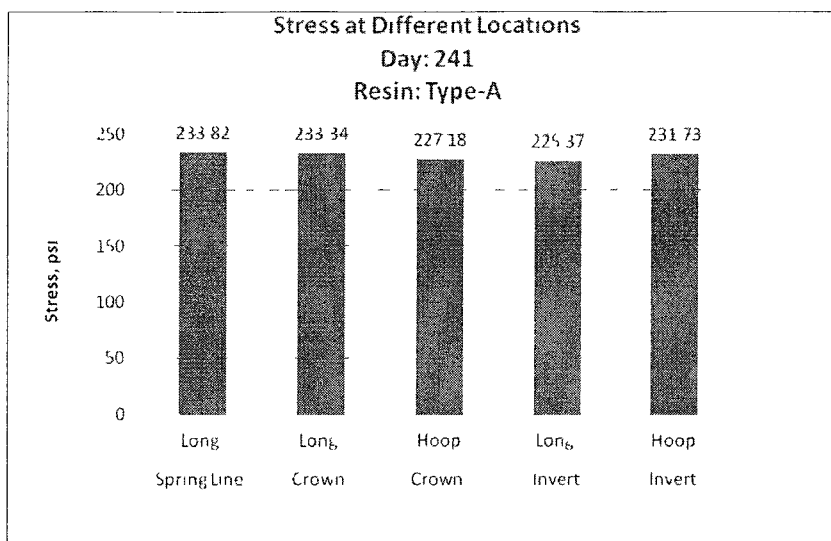


Figure A. 143: Longitudinal and Hoop Stress Due to Thermal Loading on Day 241 for Resin Type-A (Temperature Range 90° F-210° F)

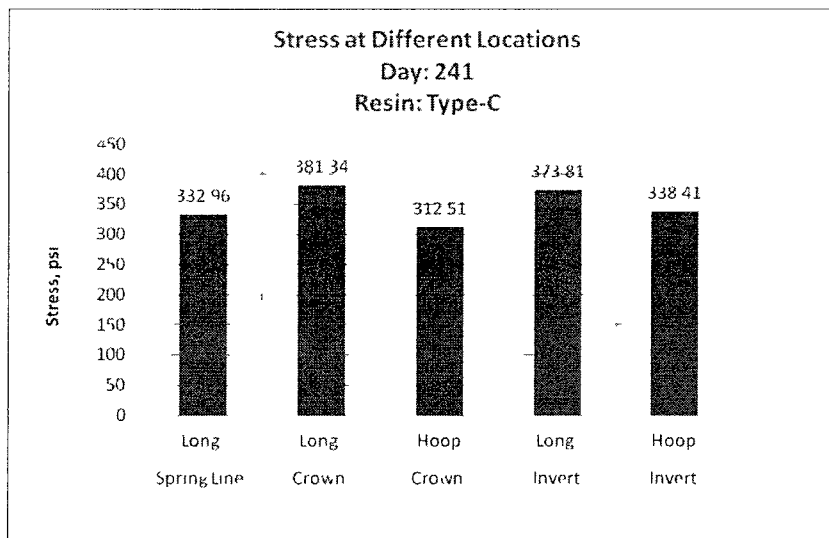


Figure A. 144: Longitudinal and Hoop Stress Due to Thermal Loading on Day 241 for Resin Type-C (Temperature Range 90° F-210° F)

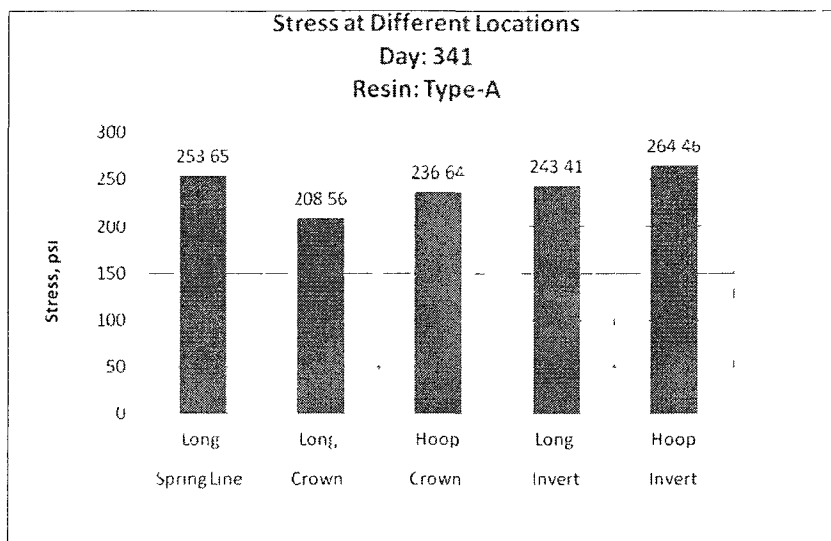


Figure A. 145: Longitudinal and Hoop Stress Due to Thermal Loading on Day 341 for Resin Type-A (Temperature Range 90° F-210° F)

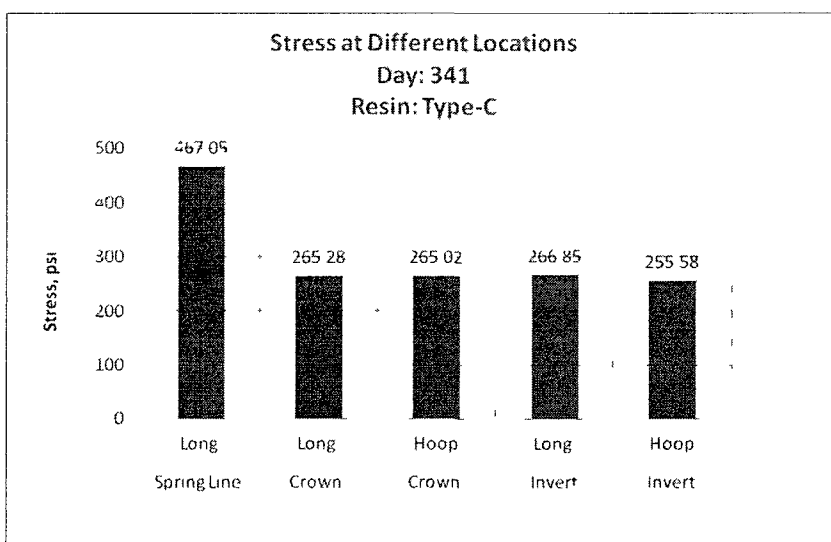


Figure A. 146: Longitudinal and Hoop Stress Due to Thermal Loading on Day 341 for Resin Type-C (Temperature Range 90° F-210° F)

E.3 Oven 3

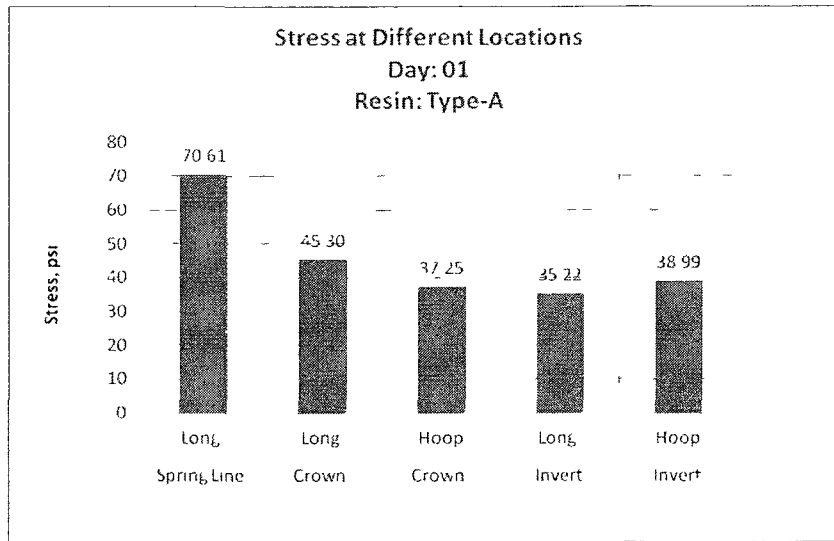


Figure A. 147: Longitudinal and Hoop Stress Due to Thermal Loading on Day 1 for Resin Type-A (Temperature Range 100° F-150° F)

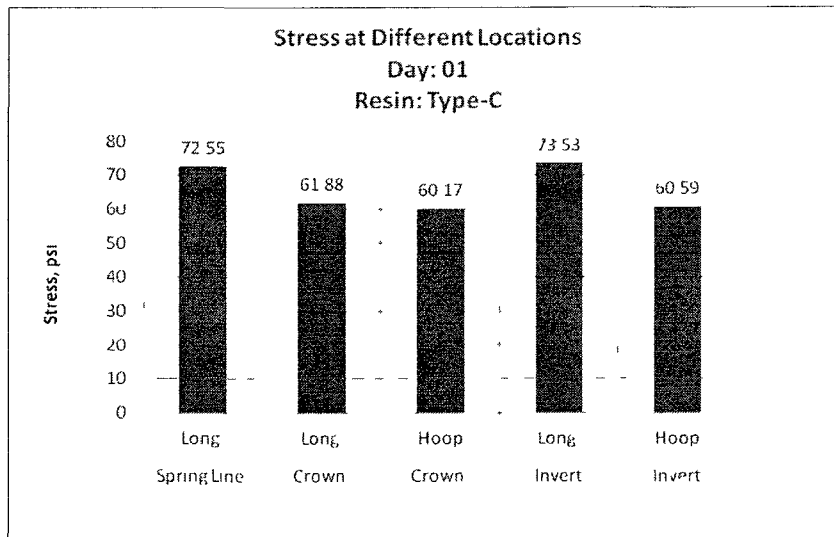


Figure A. 148: Longitudinal and Hoop Stress Due to Thermal Loading on Day 1 for Resin Type-C (Temperature Range 100° F-150° F)

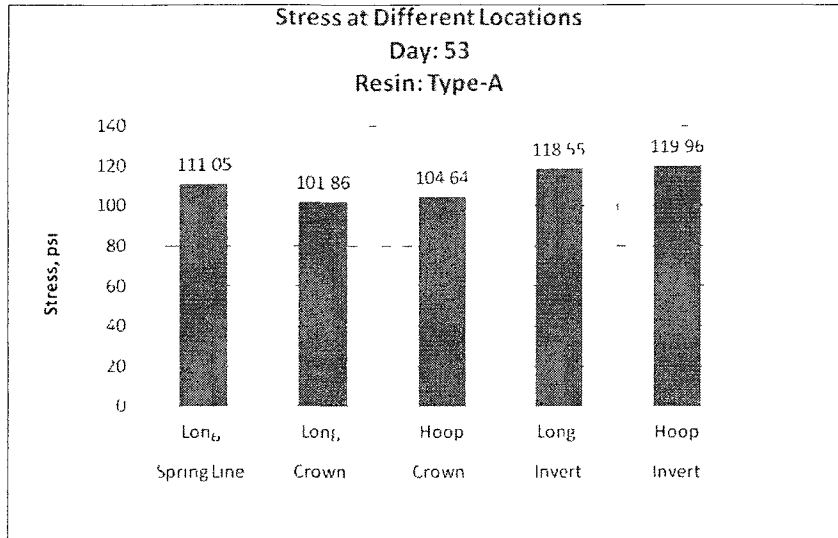


Figure A. 149: Longitudinal and Hoop Stress Due to Thermal Loading on Day 53 for Resin Type-A (Temperature Range 100° F-150° F)

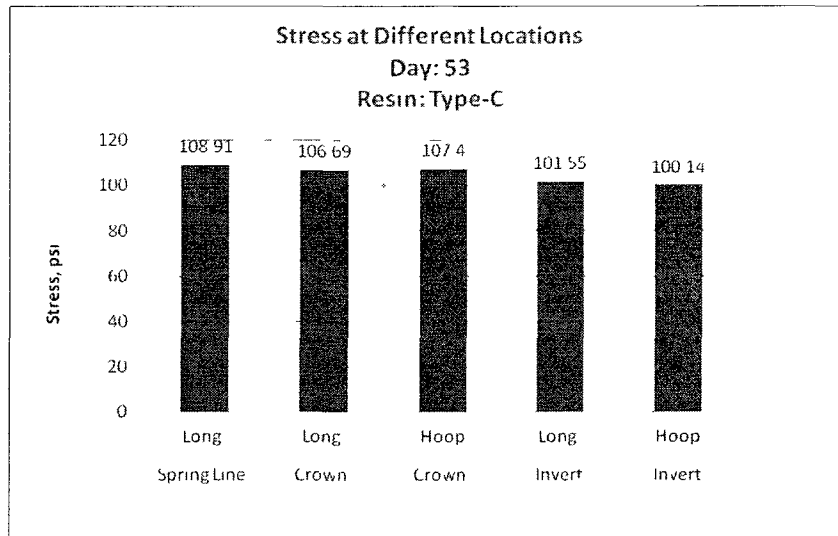


Figure A. 150: Longitudinal and Hoop Stress Due to Thermal Loading on Day 53 for Resin Type-C (Temperature Range 100° F-150° F)

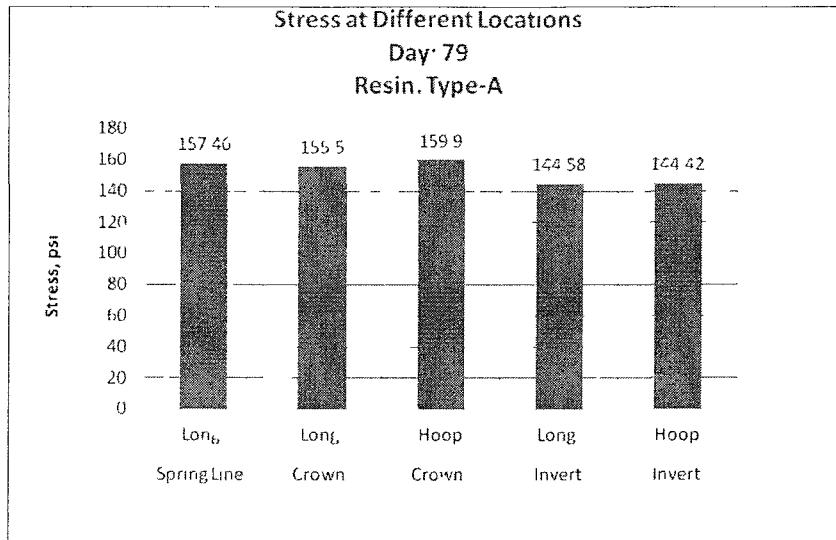


Figure A. 151: Longitudinal and Hoop Stress Due to Thermal Loading on Day 79 for Resin Type-A (Temperature Range 100° F-150° F)

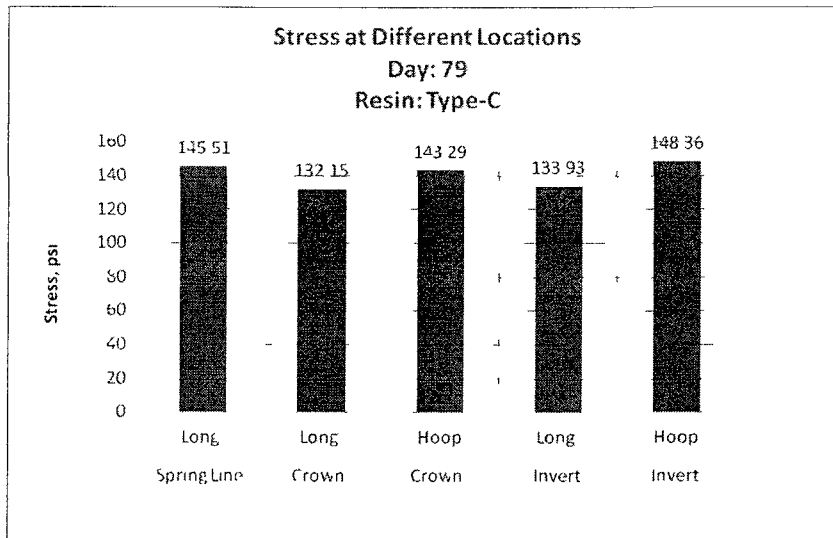


Figure A. 152: Longitudinal and Hoop Stress Due to Thermal Loading on Day 79 for Resin Type-C (Temperature Range 100° F-150° F)

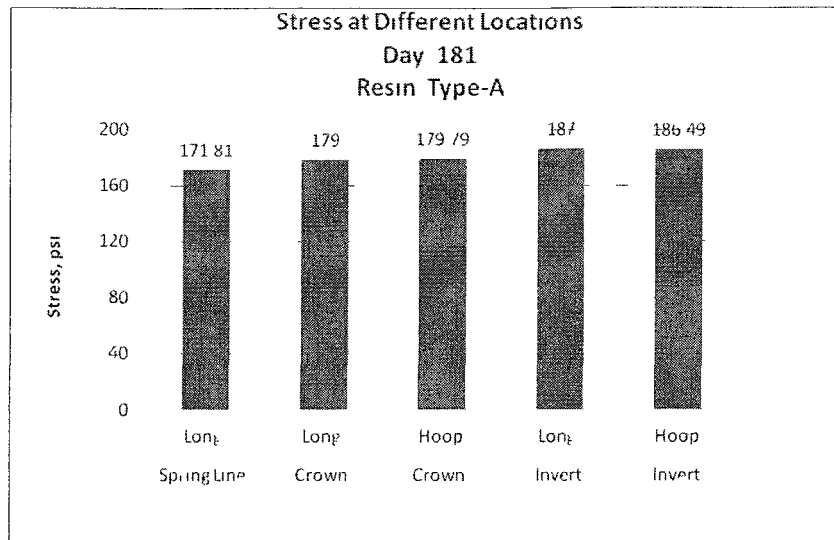


Figure A. 153: Longitudinal and Hoop Stress Due to Thermal Loading on Day 181 for Resin Type-A (Temperature Range 100° F-150° F)

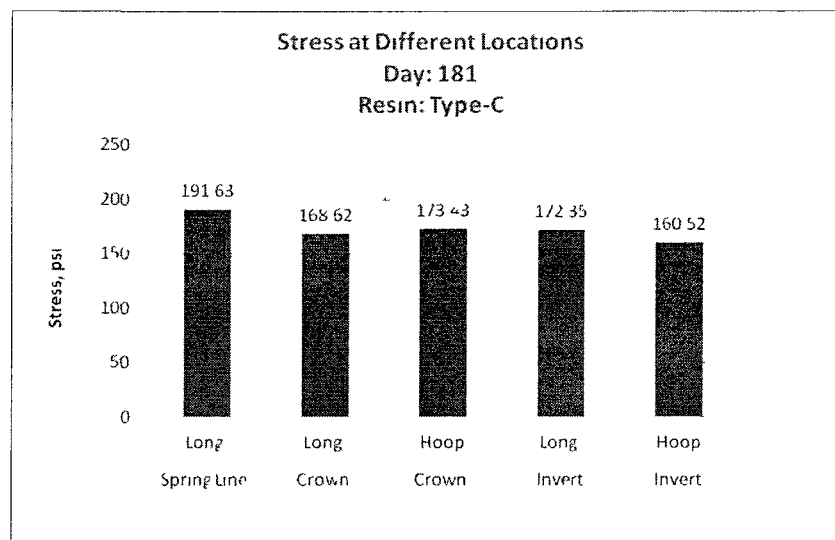


Figure A. 154: Longitudinal and Hoop Stress Due to Thermal Loading on Day 181 for Resin Type-C (Temperature Range 100° F-150° F)

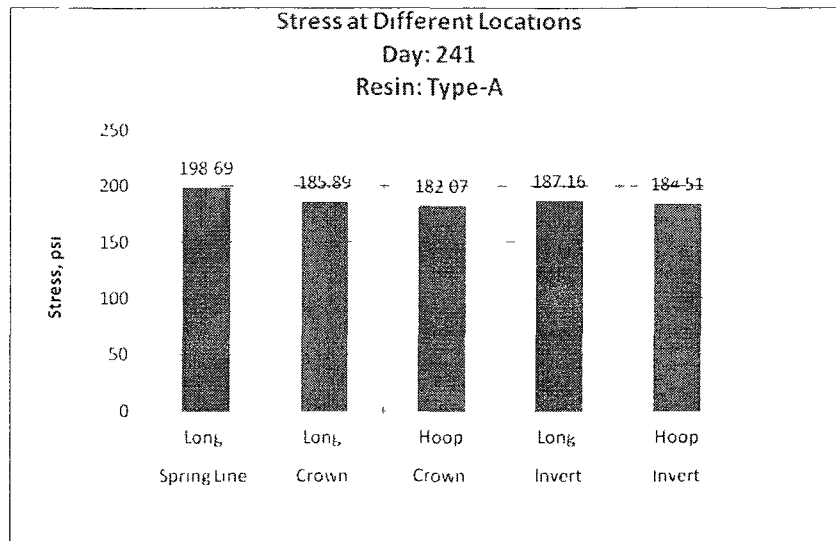


Figure A. 155: Longitudinal and Hoop Stress Due to Thermal Loading on Day 241 for Resin Type-A (Temperature Range 100° F-150° F)

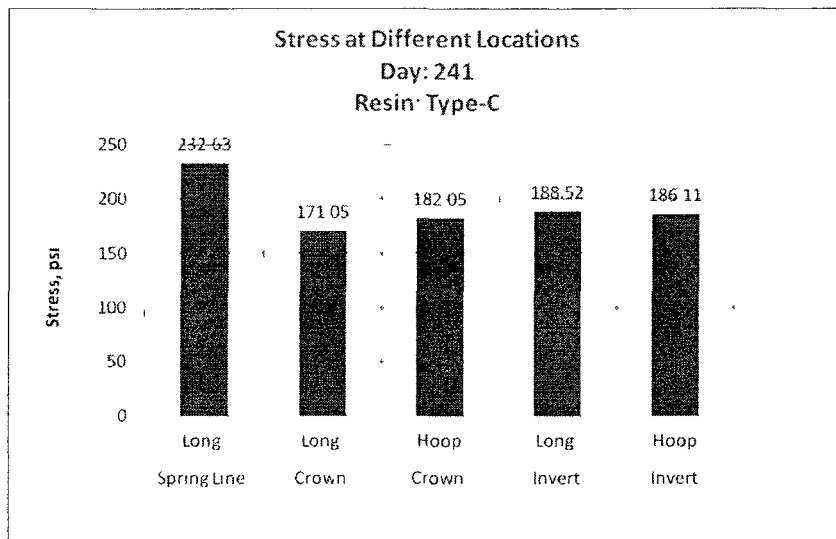


Figure A. 156: Longitudinal and Hoop Stress Due to Thermal Loading on Day 241 for Resin Type-C (Temperature Range 100° F-150° F)

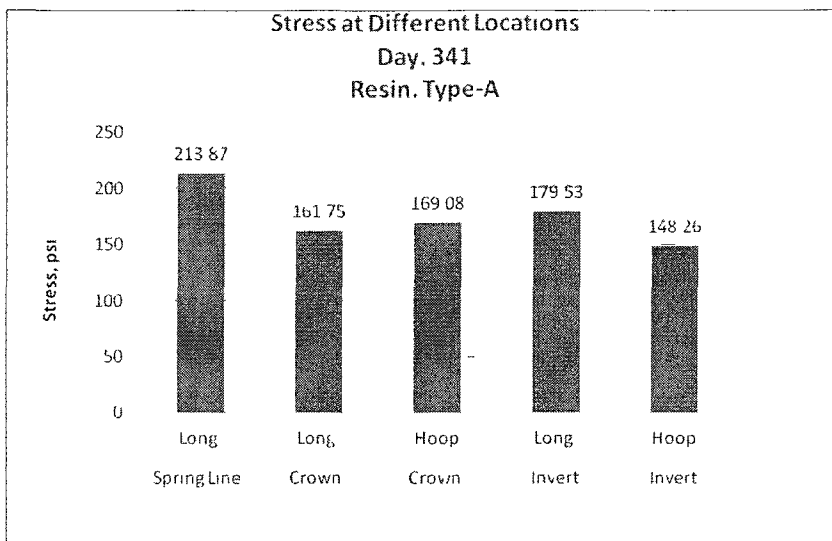


Figure A. 157: Longitudinal and Hoop Stress Due to Thermal Loading on Day 341 for Resin Type-A (Temperature Range 100° F-150° F)

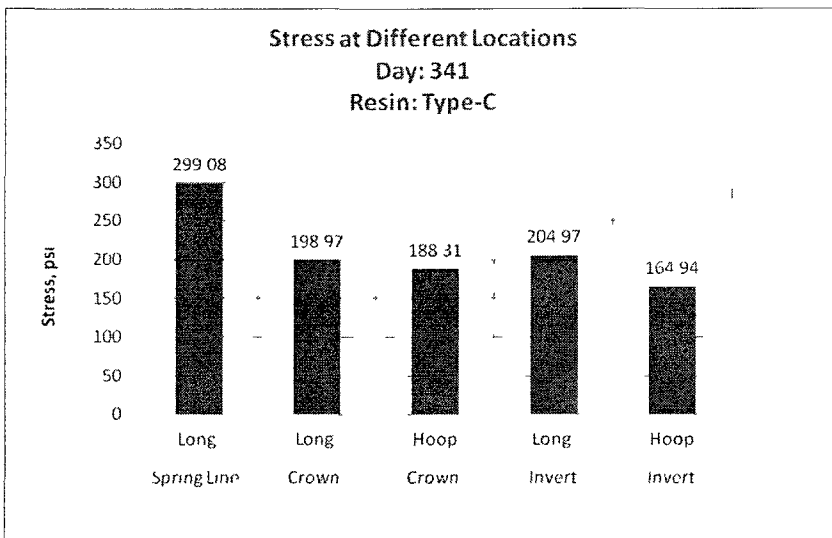


Figure A. 158: Longitudinal and Hoop Stress Due to Thermal Loading on Day 341 for Resin Type-C (Temperature Range 100° F-150° F)

REFERENCES

- ASTM D 638, Standard Test Method for Tensile Properties of Plastics, 2010.
- ASTM D 790, Standard Test Methods for Flexural Properties of Unreinforced and Reinforced Plastics and Electrical Insulating Materials, 2010.
- ASTM D2990, Standard Test Methods for Tensile, Compressive, and Flexural Creep and Creep-Rupture of Plastics, 2009.
- ASTM F 1216, Standard Practice for Rehabilitation of Existing Pipelines and Conduits by the Inversion and Curing of a Resin-Impregnated Tube, 2009.
- Boot J.C., Welch A.J. Creep buckling of thin-walled polymeric pipe linings subject to external ground water pressure. *Thin Walled Structure*; Vol. 24,191–210,1996.
- Boot J.C. Elastic buckling of cylindrical pipe linings with small imperfections subject to external pressure. *Trenchless Technology Research*; Vol. 12, No.1 – 2, 3–15, 1997.
- Boot J.C., Javadi AA. The structural behaviour of cured-in-place pipe linings, *Plastic Pipes X, Proceedings of International Conference, Gothenberg, 369 – 378, September, 1998.*
- Bruzzone A.A.G., Leonardo P.M., Diverio G., DIPTTEM, University of Genoa, Italy. *Experimental characterization of Cured In Place Pipes (CIPP)*, 1987.
- Dino Y. P. Ng, P.E. Associate Commissioner, City of New York, Department of Design and Construction, *New York City Times Square Lining Project: Challenges and Approaches.*

- Falter B. Structural analysis of sewer linings. *Trenchless Technology Research*; Vol. 11, No. 2, 27–41, 1996.
- Glock, D. Post-critical Behaviour of a Rigidly Encased Circular Pipe Subject to External Water Pressure and Temperature Rise. *Der Stahlbau*, Vol. 46, No.7, 212 – 217, 1977.
- Gumbel J.E. Structural design of pipe linings — review of principles, practice and current developments worldwide. In: *Proceedings of the International No-Dig 97*, Taipei, 1997.
- Hall, D.E.; Zhu, M.: Creep induced contact and stress evolution in thin-walled pipe liners. *Thin-Walled Structures*; Vol. 39, No. 11, 939 – 959, 2001.
- Lauire Goodstein, *Washington Post*, *Star Tribune* November 24, 1989.
- Leslie K. Guice and J.Y. Li. *Buckling Models and Influencing Factors for Pipe Rehabilitation Design*, Louisiana Tech University, Ruston, LA, 1994.
- McKim R. A., D. Meyer, and Alejandro Doble. *Thermal Aspects of Designing a CIPP Liner to Rehabilitate a CIPP Liner*. *First CISTT Colombian Underground Infrastructure and No-Dig Show*, 2010.
- Moore, I.D. and El Sawy, K., *Buckling Strength of polymer liners used in sewer rehabilitation*. *Transportation Research Record* 1541, 127 – 132, 1996.
- Moore, I.D., *Tests for liner stability: What we can and cannot learn*. Paper presented at *North American No-Dig '98*, Albuquerque, NM, April, 1998.
- Oliver Thépot. *Structural design of oval shaped sewer linings*. SAGEP, 9 – 11 rue Berthollet, 91100 Corbeil, France, 2001.
- Oliver Thépot. *International comparison of methods for the design of sewer linings*. *3R International* 8 – 9/2004.

- Robert D.Bennett, Dr. Leslie K. Guice, Salam Khan, Kimberlie Staheli. Trenchless Construction: Evaluation of methods and materials to install and rehabilitate underground utilities. TTC Technical Report # 400, July, 1995.
- Seemann, R.K., Hall, D.E. & Straughan, W.T. .Buckling experiments for CIPP liners installed in ovalized host pipes., TTC Research Report, Louisiana Tech Univ., Ruston LA, 2001.
- S.M.Seraj, U.K.Roy, M.N.Pavlović. Structural design of closely packed horse-shoe shaped sewer linings during installation. Thin walled structures; Vol. 33, 19 – 48, 1999.
- The New York Times. Steam Pipe Explosion Jolts Midtown; One Person Is Confirmed Dead. July 18, 2007.
- Timoshenko, S.P., and Gere, J.M., Theory of Elastic Stability, 2nd ed., McGraw-Hill, New York, 1961.
- Trenchless Technology Research Colloquium, Rehabilitation Group Communique. Structural performance of close-fit non-bonded flexible linings for nominally circular gravity systems: Agreed basis for a rational design methodology, <http://www.latech.edu>, 2000.
- Watkins K.R., Anderson L.R. Structural mechanics of buried pipes. New York: CRC Press, 2000.
- WRc/WAA. Sewerage rehabilitation manual. UK Water Research Center/Water Authorities Association, 1994.
- Water Research Centre. Sewerage Rehabilitation Manual. Swindon, 1983.
- Wood E., 1977, Method of lining a pipe, US patent US4009063.